Recapitulating Parkinson's disease pathology in a three-dimensional neural cell culture model

Teresa Rachel Taylor-Whiteley

A thesis submitted in partial fulfilment of the requirements of Sheffield Hallam University Degree of Doctor of Philosophy

Faculty of Health and Wellbeing

September 2019

Candidate's Statement

I hereby declare that:

1. I have not been enrolled for another award of the University, or other academic or professional organisation, whilst undertaking my research degree.

2. None of the material contained in the thesis has been used in any other submission for an academic award.

3. I am aware of and understand the University's policy on plagiarism and certify that this thesis is my own work. The use of all published or other sources of material consulted have been properly and fully acknowledged.

4. The work undertaken towards the thesis has been conducted in accordance with the SHU Principles of Integrity in Research and the SHU Research Ethics Policy.

The word count of the thesis is 50,000.

Name	**Teresa Rachel Taylor-Whiteley**
Date	**September 2019**
Award	**PhD**
Faculty	**Health and Wellbeing**
Director(s) of Studies	**Dr David Smith**

Dedication

This thesis is dedicated to the memory of

Martyn Whiteley

1963-2018

Dad,

I hope you found the peace you were searching for

Love always,

Your daughter,

Teresa

Acknowledgements

I would like to acknowledge the Biomolecular Sciences Research Centre at Sheffield Hallam University for the funding of this project.

I would like to express my gratitude to the people who have supported me throughout the past four years. First of all, thank you to all my supervisors: Dr David Smith, Dr Caroline Dalton, Prof. Christine Le Maître and Dr James Duce. Thank you for all the help and support you have all offered throughout the completion of this PhD. A special thanks to David, I've never had much self-esteem, but you have always believed in me and I just wanted to say how grateful I am for all you have done for me throughout the past four years.

To friends at work, a special thank you to Sophie, Lauren, Kirstie, Rachel, Emma, Alex, Becky and Cristina for not only providing help and support on PhD-related topics but also sharing good times throughout.

Millie, Hannah and Dr Joseph Michael Hufton, thank you for your help and encouragement during these last 8 years throughout undergrad/placement/PhD.

To my husband, Scott. You and your family are nothing but supportive of everything I do, and you make me smile every day. I am so proud of everything you've achieved and hope you are proud of me. Love you Pooks and I can't wait to meet our little boy soon.

Abstract

Parkinson's disease (PD) is the second most common neurodegenerative disorder, after Alzheimer's disease (AD), occurring at a rate of 0.1%-0.2% of the population. The incidence of PD increases with advancing age, affecting 1% of the population over the age of 65. Extensive loss of dopaminergic neurons and aggregation of the protein α-synuclein (α-syn) into ubiquitin-positive Lewy bodies (LBs) represents a major neuropathological hallmark of PD. The impact of LB pathology on the disease pathogenesis is still largely unknown, with evidence suggesting small soluble oligomeric assemblies that precede LB development are the causative agent in PD. At present, the generation of large nuclear-associated LBs from endogenous wild-type α-syn, translationally regulated under its own promoter in human cell culture models, requires costly and time-consuming protocols.

The primary objective of this thesis was to develop a more physiologically relevant cell culture model of PD that recapitulates the development of LB inclusions. Using a cell culture model of fully differentiated human SH-SY5Y neuroblastoma cells grown in three-dimensions (3D), cells were shown to develop LB-like pathology upon exposure to exogenous α-syn species. In contrast to most cell- and rodent based PD models, which exhibit multiple diffuse α-syn aggregates throughout the cytoplasm, a single large nuclear inclusion that is immunopositive for α-syn and ubiquitin is rapidly obtained in our model. However, phosphorylation of α-syn within these inclusions was not observed. This was achieved without the need for overexpression of α-syn or genetic modification of the cell line.

To further explore the mechanism of LB formation the recently discovered programmed cell death pathway ferroptosis was investigated. Ferroptosis is an iron-dependent cell death pathway that shares similar pathogenic features with PD including elevated iron concentration, GSH depletion, lipid peroxidation and increased ROS. However, there are currently no studies that have explored whether α-syn is involved in ferroptotic cell death.

Viability assays within the 3D cell culture model following treatment with ferroptosis and apoptosis inducers and qPCR of ferroptotic targets demonstrated resistance to this mechanism of programmed cell death. Nevertheless, treatment with iron was associated with some features of ferroptosis including increased ROS, some lipid peroxidation and reduced levels of glutathione peroxidase 4 (GPX4). Phosphorylation of α-syn at serine 129 (S129) was increased upon iron treatment and reduced following treatment with a ferroptosis inhibitor, liproxstatin-1. These results demonstrate the potential implications of iron exposure, α-syn aggregation, and ferroptosis in the pathogenesis of PD.

The system described in this thesis provides an ideal tool to screen compounds to intervene therapeutically in LB formation, and to investigate the mechanisms involved in disease progression in synucleinopathies.

Dissemination

Scientific Publications:

Taylor-Whiteley, T. R., Le Maitre, C. L. Duce, J. A., Dalton, C. F. and Smith, D. P. (2019) 'Recapitulating Parkinson's disease pathology in a three-dimensional human neural cell culture model' Disease Models and Mechanisms 12: dmm038042. doi:10.1242/dmm.038042 (a copy of which can be found in Chapter 8)

Conference Presentations:

Parkinson's UK Research Conference 2016 (Leeds, UK). **Whiteley, T. R.**, Duce, J. A., Dalton, C. F. and Smith, D. S. 'Establishing a Three-Dimensional Human Neural Cell Culture Model to Investigate the Intracellular Aggregation of α-synuclein'- Poster presentation.

International Society for Neurochemistry 2017 (Paris, France). **Whiteley, T. R.**, Duce, J. A., Dalton, C. F. and Smith, D. S. 'Establishing a Three-Dimensional Cell Culture Model of Parkinson's disease'- Poster presentation.

Glial symposium 2016/2017 (University of Sheffield/Sheffield Hallam University). **Whiteley, T. R.**, Duce, J. A., Dalton, C. F. and Smith, D. S. 'A Three-Dimensional Cell Culture Model of Parkinson's disease'- Talk.

List of Figures

List of Tables

List of Abbreviations

2D	Two-dimensional
3D	Three-dimensional
4-HNE	4-hydroxynonenal
µM	Micromolar
Aβ	Amyloid-β
ACD	Accidental cell death
AD	Alzheimer’s disease
AFM	Atomic force microscopy
ALS	Autophagy-lysosomal system
APAF1	Apoptosis peptidase activating factor-1
APS	Ammonium persulphate
α-syn	α-synuclein
AuD	Autosomal dominant
AuR	Autosomal recessive
BAK	BCL2 antagonist/killer 1
BAX	BCL2 associated X, apoptosis regulator
BCA	Bicinchoninic acid

BDNF	Brain-derived neurotrophic factor
BOK	BCL2 family apoptosis regulator
BSA	Bovine serum albumin
BSE	Bovine spongiform encephalopathies
cAMP	Cyclic adenosine monophosphate
CJD	Creutzfeldt-Jakob disease
CMA	Chaperone-mediated autophagy
CNS	Central nervous system
CYCS	Cytochrome c somatic
DAT	Dopamine transporter
DBH	Dopamine-β-hydroxylase
dH_2O	Distilled water
DLB	Dementia with Lewy bodies
DOPAC	Dihyroxyphenylacetic acid
E. coli	*Escherichia coli*
ECM	Extracellular matrix
ELISA	Enzyme-linked immunosorbent assay
ESCs	Embryonic stem cells
Fe^{2+}	Ferrous iron

Fe^{3+}	Ferric iron
FFI	Fatal familial insomnia
GBA	Glucocerebrosidase
GDNF	Glial-derived neurotrophic factor
GPx	Glutathione peroxidase
GPX4	Glutathione peroxidase 4
GSH	Reduced glutathione
GSS	Gerstmann-Straüssler-Scheinker disease
GSSG	Oxidised glutathione
H + E	Haematoxylin + Eosin
hr/hrs	Hour/hours
HSC70	70-kDa heat shock cognate
HT	Huntingtin's disease
IHC	Immunohistochemistry
iPSCs	Inducible pluripotent stem cells
LB	Luria-Bertani broth
LBs	Lewy bodies
LDH	Lactate dehydrogenase
L-DOPA	Levodopa

LIP	Labile iron pool
LNs	Lewy neurites
LOOH/LOO·	Lipid hydroperoxides/Lipid peroxide radical
LRRK2	Leucine rich repeat kinase 2
MAO	Monoamine oxidase
MAO B	Monoamine oxidase type B
MIM	Mitochondrial inner membrane
mins	Minutes
MLKL	Mixed lineage kinase domain like pseudokinase
mM	Millimolar
MOM	Mitochondrial outer membrane
MOMP	Mitochondrial outer membrane permeabilisation
MPP^+	1-methyl-4-phenylpyridinium
MPTP	1-methyl-4-phenyl-1, 2, 3, 6,-tetrahydropyridine
MRI	Magnetic resonance imaging
mRNA	Messenger RNA
MSA	Multiple system atrophy
NA	Noradrenaline
NAC	N-acetylcysteine

NFM	Non-fat milk
NTA	Nitrilotriacetic acid trisodium salt
OMM	Outer mitochondrial membrane
p-α-syn	Phosphorylated α-syn (specifically at S129)
P/S	Penicillin/streptomycin
PBS	Phosphate buffered saline
PBS-T	Phosphate buffered saline with Tween-20
PCD	Programmed cell death
PD	Parkinson’s disease
PET	Positron emission tomography
PFFs	Pre-formed fibrils
PK	Proteinase K
PLK2	Polo-like kinase 2
PMCA	Protein misfolded cyclic amplification
PRNP	Gene encoding prion protein
PrP	Prion protein
PrP^{C}	Normal cellular prion protein
PrP^{SC}	Disease-associated prion protein
PTMs	Post-translational modifications

PTP	Permeability transition pore
PUFAs	Polyunsaturated fatty acid
PVDF	Polyvinylidene fluoride
qPCR	Quantitative real-time polymerase chain reaction
RFU	Relative fluorescence units
ROS	Reactive oxygen species
RSL3	Ras-selective lethal small molecule-3
RT	Room temperature
S129	α-Syn phosphorylated at serine 129
SDS-PAGE	Sodium dodecyl sulphate- polyacrylamide gel electrophoresis
SMAC	Second mitochondrial activator of caspases
SN	*Substantia nigra*
SNARE	Soluble NSF attachment protein receptor
SNPc	*Substantia nigra pars compacta*
SOD1	Superoxide dismutase 1
TBS	Tris buffered saline
TBS-T	Tris buffered saline with Tween-20
TEMED	N, N, N', N'-Tetramethylethylene-Diamine

TFR	Transferrin receptor
TFR2	Transferrin receptor 2
TH	Tyrosine hydroxylase
ThT	Thioflavin T
TNFR-1	Tumour necrosis factor-receptor-1
TNTs	Tunnelling nanotubes
TPA	12-*O*-tetradecanoyl-phorbol-13 acetate
TPS	Total Protein Stain
TRKB	Tropomyosin receptor kinase B
TUBB3	βIII-tubulin
TSEs	Transmissible spongiform encephalopathies
UK	United Kingdom
UPS	Ubiquitin-proteasome system
vCJD	Variant Creutzfeldt-Jakob disease
VMAT2	Vesicular monoamine transporter-2

Contents Page

Chapter 1 : General Introduction

1.1 Protein aggregation in disease

Protein aggregation and accumulation is associated with a wide range of disease states, termed amyloidoses. In these conditions, misfolded protein assembles into misfolded amyloid cross-β conformations that are deposited mainly in the extracellular space of tissues (Sipe *et al.*, 2014). Non-pathogenic amyloid formations that have a normal, physiological role have been discovered in mammalian tissue as well as lower-order organisms, such as *Escherichia coli* (*E. coli*) (Fowler *et al.*, 2006; Li *et al.*, 2012; Biesecker *et al.*, 2018). Amyloid formation has been implicated in over 30 human diseases, with many proteins determined to be amyloidogenic at least *in vitro* (Sipe *et al.*, 2014, 2016). Systemic amyloidoses in which amyloid fibrils are deposited throughout the body is related to proteins such as immunoglobulin light chain (AL), (Apo) serum amyloid A (AA) and transthyretin, among others (Wechalekar, Gillmore and Hawkins, 2016) (Table 1.1). Amyloidosis can also affect single organs and has been associated with type 2 diabetes in the case of accumulation of islet amyloid polypeptide (IAPP) in the Islets of Langerhans (Andisheh and Marie, 2013). An amyloid fibril protein is defined by the Nomenclature Committee of the International Society of Amyloidosis as: ‘a protein that occurs in body deposits and exhibits affinity for Congo red and green, yellow or orange birefringence when the Congo red-stained deposits are viewed with polarised light’ (Howie and Brewer, 2009; Sipe *et al.*, 2014, 2016). The process of amyloidogenesis has also been linked to several neurodegenerative diseases including Alzheimer’s disease (AD; amyloid-β and tau in amyloid plaques and neurofibrillary tangles), Parkinson’s disease (PD; α-syn in LBs), prion diseases (amyloid plaques) and Huntington’s disease (PolyQ expanded huntingtin in inclusion bodies) (Klatzo, Gajusek and Zigas, 1959; Macdonald *et al.*, 1993; Stelzmann, Schnitzlein and Murtagh, 1995; Spillantini *et al.*, 1997; Sipe *et al.*, 2016).

Fibril protein	Associated disease	Target organs
Immunoglobulin light/heavy chain†	Primary amyloidosis; associated with plasma cell dyscrasia and multiple myeloma	All organs, except CNS
Serum amyloid A†	Secondary systematic amyloidosis; Associated with chronic infections and inflammatory diseases	All organs except CNS
β2-Microglobulin	Dialysis-associated amyloidosis	Wild type: musculoskeletal system Variant: autonomic nervous system
Apolipoprotein A I, II, IV†	Cardiovascular disease	I: Heart, liver, kidney, testis, larynx, skin II: Kidney IV: Kidney medulla and systemic
Apolipoprotein C II, III	Cardiovascular disease	II: Kidney III: Kidney
Lysozyme	Lysozyme systemic amyloidosis	Kidney
Aβ † and Tau*	AD, inclusion body myositis, fronto-temporal dementia, Pick's disease, progressive supranuclear palsy	Aβ and Tau: CNS
α-syn*	PD, multiple system atrophy (MSA), dementia with LBs (DLB), LB variant of AD	CNS
Prion protein†	CJD, Kuru, Gerstmann-Straüssler-Scheinker syndrome, fatal insomnia	CNS
Islet amyloid polypeptide†	Type 2 diabetes	Islets of Langerhans, insulinomas

Table 1.1-1. *Amyloid proteins and their associated diseases in humans.* Table adapted from Sipe *et al.* 2016 and Uversky 2008. * Protein aggregates are found intracellularly as well as extracellularly. † Amyloid fibril proteins also found to cause disease in animals. *Abbreviations:* Aβ, amyloid-beta; α-syn, α-synuclein; CNS, central nervous system; DLB, dementia with Lewy bodies; LB, Lewy body; MSA, multiple system atrophy

1.2 Parkinson's disease

1.2.1 Pathophysiology of Parkinson's disease

PD is the second most common neurodegenerative disorder after AD in the UK, affecting approximately 1% of the population over the age of 65 with increasing prevalence with advancing age (Bousset *et al.*, 2013; Parkinson's UK, 2018). First described nearly 200 years ago in 'An Essay on the Shaking Palsy' authored by James Parkinson, PD is a complex and currently incurable neurodegenerative

disease. Although clinically heterogeneous, PD is characterised by the cardinal motor symptoms of tremor at rest, bradykinesia, postural instability, and rigidity. In later stages of the disease, motor symptoms are accompanied by autonomic disturbances and, in up to 80% of patients, cognitive impairment (Chaudhuri and Schapira, 2009; Lees, Hardy and Revesz, 2009; Sveinbjornsdottir, 2016). The disease has distinct neuropathology, characterised by the progressive loss of dopaminergic neurons in the *substantia nigra pars compacta (SNPc)* region of the midbrain and the presence of proteinaceous inclusions in neurons termed LBs and Lewy neurites (LNs) comprised mainly of an aggregated form of the protein α-syn (Fig. 1.1) (Spillantini *et al.*, 1997; Takeda *et al.*, 1998; Langston *et al.*, 2015).

LB pathology in surviving neurons is synonymous with the neuropathology of PD and other synucleinopathies including DLB and MSA. These proteinaceous inclusions are mainly comprised of an abnormal misfolded form of α-syn in association with other proteins such as ubiquitin, neurofilament protein, and heat shock proteins but may also contain the microtubule-associated tau protein and neurofibrillary tangles commonly associated with AD (Ueda *et al.*, 1993a; Spillantini, Divane and Goedert, 1995; Goedert *et al.*, 2013). LBs are present as amorphous protein inclusions in the cell body of neurons in contrast to LNs which are spindle, thread-like aggregates typically present in neurites. Although the involvement of LBs in the development and progression of PD is still largely unknown, alongside details as to their formation, the immunoreactivity of α-syn in these inclusions has since garnered attention as the protein implicated in the pathogenesis of PD, DLB and MSA (Milber *et al.*, 2012). Mutations in the *SNCA* gene that encodes α-syn, including genomic duplications, triplications, and point mutations, are typically associated with an early-onset and more aggressive form of PD, implicating α-syn in the development of the disease (Polymeropoulos *et al.*, 1997; Spillantini *et al.*, 1997).

Catecholaminergic and serotoninergic neurons can also be affected as the disease progresses, disrupting connectivity in a large number of brain regions (Wirdefeldt *et al.*, 2011; Berman *et al.*, 2016). The Braak hypothesis identifies six neuropathological stages that consist of α-syn-containing inclusions confined to the medulla oblongata/pontine tegmentum and olfactory bulb/anterior olfactory nucleus (stage 1 and 2) progressing to the *SNPc* and other nuclei of the midbrain and forebrain (stage 3 and 4), culminating in the neocortex (stage 5 and 6) in which clinical symptoms

arise as the stages progress (Del Tredici *et al.*, 2002; Wolters and Braak, 2006; Rey *et al.*, 2013). Motor symptoms are not experienced in patients until approximately 50-60% of the *SNPc* neurons are depleted, resulting in a dopamine deficit of 80-85% which is partially rescued by supplementation of the dopamine precursor, levodopa (L-DOPA) (Oertel and Schulz, 2016). In the development of this staging model, Braak and colleagues proposed the 'dual-hit' hypothesis (Hawkes and Braak, 2007) in which a pathological insult initiates the progression of PD subsequently spreading to vulnerable regions in a potential ‘prion-like’ spread.

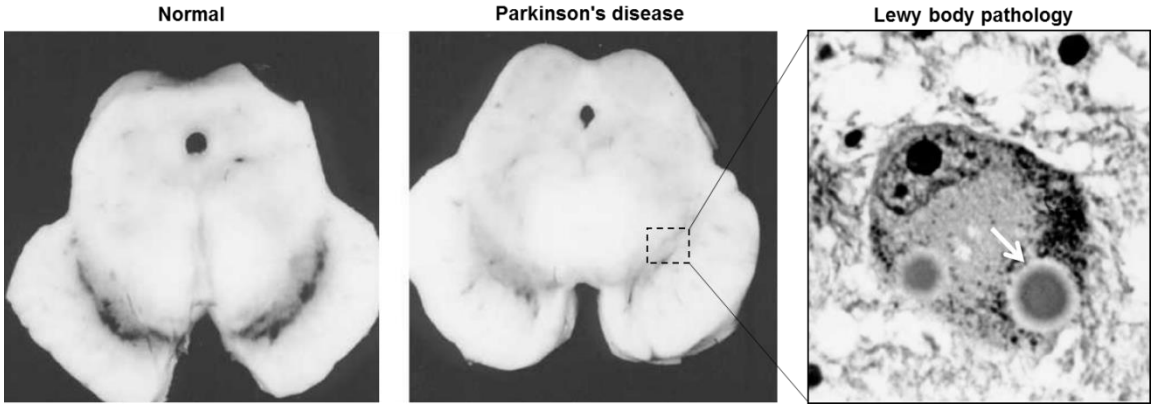

Figure 1.1. *Pathology of Parkinson's disease.* Horizontal midbrain sections from normal (*left*) and Parkinson's disease brains (*middle*) demonstrate the loss of pigmented neurons from the *SNPc* in disease. Classical Haematoxylin and Eosin (H&E) staining of LBs in neurons of the *SNPc* highlight the presence of spherical, intracytoplasmic inclusions measuring between 8 and 30 µm in diameter with an eosinophilic hyaline core and pale staining peripheral halo (*right, arrow*). Image adapted from Mackenzie, 2001.

The significant loss of neuromelanin-pigmented neurons in the *SNPc* and the subsequent dopamine deficit of the nigrostriatal system represents the most important hallmark of PD. Braak and colleagues (2003) in the seminal, yet debated, study relating α-syn immunoreactivity of LBs and LNs in post-mortem brain samples of both clinically-diagnosed PD and incidental Lewy pathology highlighted a potential spread of pathology. In this study, the spread of pathology occurs in a predictable sequential pattern resulting in progression from either the brainstem or olfactory centres along vulnerable neuronal subsets, culminating in degeneration of neurons of the *SNPc* (Braak *et al.*, 2003). Although the Braak staging scheme is largely accepted by scientists and clinicians, not all the observations made in patients with LB pathology are represented in this staging scheme (Burke, Dauer and Vonsattel, 2008; Jellinger, 2019). For example, the Braak staging scheme suggests the spread of pathology and thus clinical symptoms of parkinsonism develop as the staging progresses from 1 through to 6 (McCann, Cartwright and Halliday, 2016). However,

patient symptoms do not necessarily represent the staging scheme, with only ~51% of patients conforming to Braak staging in some studies (Zaccai *et al.*, 2008; Beach *et al.*, 2009; Jellinger, 2009). There are reported individuals with a Braak staging of only 2 with clinical PD symptoms, in contrast to individuals with Braak staging of 6 without observable symptoms (Ahlskog, 2007; Zaccai *et al.*, 2008; Jellinger, 2019). Taken together, the Braak staging scheme may not be appropriate for all types of PD. In addition, patients presenting with DLB were omitted from the original Braak staging scheme (Burke, Dauer and Vonsattel, 2008). This is important as patients that present with an initial diagnosis of DLB may progress to develop a condition indistinguishable from PD (Lippa *et al.*, 2007; Jellinger and Korczyn, 2018).

1.2.2 Aetiology and pathogenesis of Parkinson's disease

The aetiology of PD is complex and not completely understood, but is hypothesised to involve the interplay between genetic, environmental and lifestyle factors as well as the presence of pre-existing medical conditions and previous infections (McCulloch *et al.*, 2008; Wirdefeldt *et al.*, 2011). Mechanisms in which these factors contribute to the pathogenesis of idiopathic PD are likely linked, with multiple themes emerging including mitochondrial dysfunction, oxidative stress, inflammation, proteasomal and lysosomal impairment (Fig. 1.2) (Khan *et al.*, 2019).
Epidemiological studies have consistently associated environmental factors including exposure to pesticides such as rotenone and 1-methyl-4-phenyl-1, 2, 3, 6,-tetrahydropyridine (MPTP) as risk factors in the development of the disease, linked to human exposure through contaminated food products, drinking water and occupational exposure related to agricultural working (Lai *et al.*, 2002). Illicit drug use in the 1980s of 'synthetic heroin' containing MPTP was clinically linked to the development of L-DOPA-responsive acute parkinsonism and MPTP is commonly used to induce PD pathology in various animal models (Langston *et al.*, 1983, 1984). Both MPTP and rotenone-based animal models have enabled researchers to delineate key aetiologic pathways associated with PD including impaired mitochondrial function and free radical generation, although this model does not fully recapitulate PD disease processes, due to the absence of LB formation (Przedborski and Jackson-Lewis, 1998; Shimoji *et al.*, 2005; Perier and Vila, 2012). Rotenone has been demonstrated to down-regulate the protective chaperone protein HSC70 (70-kDa heat shock cognate), involved in the catabolism of α-syn which effectively

fragments α-syn fibrils into non-toxic monomers, suggesting a critical role of this protein in preventing PD (Sala *et al.*, 2016). Occupational exposure to manganese induced parkinsonian symptoms determined to be clinically distinct from PD. However, the presence of altered levels of transition metals in the *SNPc* of PD patients has indicated altered metal homeostasis in the development of the disease (Gorell *et al.*, 1997; Jankovic, 2005; Lan *et al.*, 2016). In contrast, and typically with a larger sample size than previous epidemiological studies regarding metal exposure in PD patients, van der Mark *et al.* (2015) didn't observe any statistically significant associations in the development of PD due to occupational exposure to metals or aromatic/chlorinated solvent exposure (van der Mark *et al.*, 2015). One caveat of the study reveals that specific metals were not able to be analysed separately, therefore the effects of single metals may be masked in the results (van der Mark *et al.*, 2015). PD has also been related to head trauma and exposure to previous infection, suggesting an inflammatory mechanism, substantiated by the presence of activated microglial cells and inflammatory cytokines of the *SNPc* in both post-mortem samples and models of PD (Lieberman, 1996; Gagne and Power, 2010; Panicker *et al.*, 2015; Ransohoff, 2016). Ageing is the strongest risk factor, although there is a small percentage of patients with an early-onset form of the disease (Reeve, Simcox and Turnbull, 2014). This association is largely attributed to mitochondrial dysfunction and oxidative stress, key themes in ageing and specifically in relation to neurodegeneration (Federico *et al.*, 2012). An increased incidence of PD in the male population is potentially explained by increased occupational exposure to toxins, the protective role of oestrogens and recessive susceptibility genes on the X chromosome (Inestrosa, Marzolo and Bonnefont, 1998; Baldereschi *et al.*, 2000; Wooten *et al.*, 2004; Moisan *et al.*, 2016). Lifestyle factors such as smoking and caffeine consumption are inversely correlated with the risk of PD, suggesting these activities have a protective effect on PD risk, by delaying disease onset yet with no impact on disease progression (Ascherio *et al.*, 2001; Kandinov, Giladi and Korczyn, 2007, 2009; Moccia *et al.*, 2016). In the case of smoking, cigarettes contain a multitude of compounds, such as nicotine and hydroquinone, which have been shown to inhibit the formation of α-syn fibrils potentially stabilising soluble oligomeric forms of α-syn and thus preventing the formation of a toxic species (Hong, Fink and Uversky, 2015).

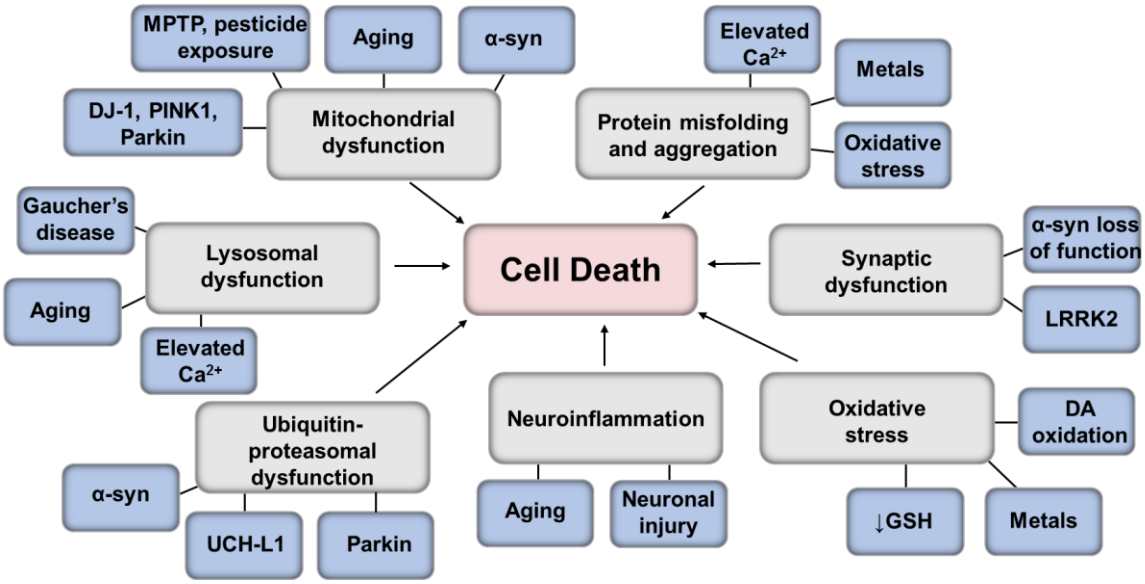

Figure 1.2. *Pathogenesis of PD.* Some of the key features of PD pathogenesis (grey) include protein misfolding and aggregation, synaptic/ lysosomal/ ubiquitin-proteasomal/mitochondrial dysfunction and oxidative stress. Highlighted in blue are some of the contributors to disease pathogenesis, with many converging across the different molecular features of PD including aging and α-syn.

The pathogenesis of PD involves a cascade of events leading to cellular death (Fig. 1.2). Cell loss, although predominant in the *SNPc*, is not restricted to this region of the brain and instead includes many other non-dopaminergic regions of the brain including the noradrenergic locus coeruleus, the cholinergic nucleus basalis of Meynert, and the autonomic nervous system (Heiko Braak, Tredici, *et al.*, 2003). The selective vulnerability of dopaminergic neurons, in particular, has been the subject of intense investigation given that as much as 70% of dopaminergic cell loss accompanies the diagnosis of PD (Giguère, Nanni and Trudeau, 2018). Intracellular aggregates of α-syn and the propagation of these aggregates are discussed further in Chapter 4.

1.2.3 Genetics of Parkinson's disease

PD is usually sporadic; however, familial forms of PD account for approximately 10% of all cases and have either autosomal dominant (AuD) or autosomal recessive (AuR) modes of inheritance (Table 1.2) (Pchelina, Emel'ianov and Usenko, 2014). AuD forms of PD are associated with a toxic gain-of-function phenotype attributed to mutations in the leucine-rich repeat kinase 2 *(LRRK2) (PARK8)*, SNCA *(PARK1), PARK3,* omi/HtrA2 *(PARK13)* and ubiquitin-carboxy-terminal hydrolase L1 *(UCH-L1) (PARK5)* genes. AuR genes that cause a loss-of-function phenotype include *parkin (PARK2), PINK1 (PARK6), DJ-1 (PARK7), ATP13A2 (PARK9), PLA2G6 (PARK14)*

Gene	Protein	Mode of inheritance	Function and possible role in PD
***SNCA* (*PARK1*)**	α-syn	AuD	Function: Involved in dopamine metabolism, SNARE vesicle trafficking and as a cellular ferrireductase (Davies, Moualla and Brown, 2011; Huang *et al.*, 2019). Role in PD: The major component in LBs, α-syn is thought to contribute to cellular toxicity and spread of disease (Spillantini, Divane and Goedert, 1995). Missense mutations (A53T, A30P, E56K, H50Q) associated with increased propensity to form toxic oligomeric species (Ostrerova-Golts *et al.*, 2000; Greenbaum *et al.*, 2005; Bharathi, Indi and Rao, 2007; Porcari *et al.*, 2015).
***LRRK2* (*PARK8*)**	LRRK2	AuD	Function: LRRK2 phosphorylates a subgroup of RAB GTPases, regulating vesicular trafficking and immune responses, protecting against pathogenic infection (Alessi and Sammler, 2018). Mounting evidence suggests LRRK2 phosphorylates tau, important given the pathological accumulation of tau in PD patients and the accumulation of tau in LBs (Ishizawa *et al.*, 2003; Bailey *et al.*, 2013). Role in PD: The most common mutation, G2019S, is associated with two to three-fold increase in LRRK2 kinase activity, potentially associated with defects in lysosomal function and enhancing neuronal transmission of tau (Phu *et al.*, 2018).
***PARKIN* (*PARK2*)**	Parkin	AuR	Function: Encodes the E3 ubiquitin ligase targeting several proteins for proteasomal degradation, including mitochondria (Arkinson and Walden, 2018). Role in PD: Dysfunction in mitochondrial clearance leading to the accumulation of damaged mitochondria (Arkinson and Walden, 2018). Alteration in E3 ligase activity leads to the accumulation of Parkin substrates and subsequent impairment of autophagy-lysosomal pathways (Wallings *et al.*, 2019).
***DJ-1* (*PARK7*)**	DJ-1	AuR	Function: Several functions of including regulating mitochondrial integrity, ROS scavenging (e.g. deglycase function), metal ion binding, transcriptional regulation, chaperone-mediated autophagy regulator (Andres-mateos *et al.*, 2007; Björkblom *et al.*, 2013; Richarme *et al.*, 2015; Xu *et al.*, 2017; Andreeva *et al.*, 2019) Role in PD: PD-related mutations result in the loss of structure of DJ-1, increased degradation and/or dimerisation (Malgieri and Eliezer, 2008). Oxidation of DJ-1 at Cys-106 functions as a ROS scavenger and the loss of this activity contributes to increased oxidative stress (Andres-mateos *et al.*, 2007; Lev *et al.*, 2013). DJ-1 deficiency is associated with reduced expression of LAMP2A, the receptor required for CMA-mediated α-syn degradation, therefore leading to the accumulation of α-syn (Xu *et al.*, 2017). In addition, DJ-1 acts as a binding partner for α-syn which can influence the aggregation process of pathological forms of α-syn. Taken together, DJ-1 function acts to reduce levels of α-syn to prevent the formation of toxic protein aggregates (Shendelman *et al.*, 2004; Zondler *et al.*, 2014).

GBA	GCase	AuR	Function: Associated with the lysosomal storage disorder, Gaucher's disease (Wong and Krainc, 2016). GCase is an intermediate enzyme in glycolipid metabolism which cleaves a glucose moiety from glucosylceramide (Hruska *et al.*, 2008). Role in PD: Associated with GBA1 mutations, with an estimated 7-12% patient with PD carrying this mutation (Sidransky *et al.*, 2009; Do *et al.*, 2019). Loss of GCase activity by various factors (loss of GCase function, increased storage of intermediates, decreased transport of GCase from the ER/CMA disruption) facilitates accumulation of α-syn (Mazzulli *et al.*, 2011; Do *et al.*, 2019). GCase appears to be important in maintaining levels of monomeric levels of α-syn within the cell, therefore preventing the development of potentially toxic α-syn aggregates (Mazzulli *et al.*, 2011; Gruschus, 2015). GBA1 mutations can alter the ratio of α-syn tetramers to monomers *in vivo*, preferring the latter, potentially inducing aggregation of α-syn into toxic multimers (Kim *et al.*, 2018)
PINK1 **(*PARK6*)**	PINK1	AuR	Function: PINK1 contains a mitochondrial targeting sequence, which facilitates recruitment of the protein to damaged and aged mitochondrial. Binding of PINK1 to mitochondria is associated with the recruitment of cytosolic Parkin, promoting the autophagic degradation of mitochondria via mitophagy (Valente *et al.*, 2004; Narendra *et al.*, 2008). Role in PD: Loss of function mutations in PINK1 (along with Parkin) are the most common causes of AuR early-onset PD (Valente *et al.*, 2004). Loss of function of both PINK1 and Parkin alter several important mitochondrial processes including the maintenance of mitochondrial integrity, mitophagy, regulating fission/fusion dynamics, and regulating local translation of mitochondrial genes (Arkinson and Walden, 2018; Ge, Dawson and Dawson, 2020). In addition to mitochondrial dysfunction, loss of PINK1 may alter the immune response via alteration of glial activation, contributing to an overreactive immune response and subsequent cellular damage (Sun *et al.*, 2018).

Table 1-2 . *Genetics of Parkinson's disease.* Abbreviations: α-syn, α-synuclein; AuD, autosomal dominant; AuR, autosomal recessive; CMA; chaperone-mediated autophagy; GBA, glucosylceramidase; GCase, glucocerebrosidase; GlcCer, glucosylceramide; GlcSph, glucosylsphingosine; LRRK2, leucine-rich repeat kinase 2; PINK1, PTEN induced putative kinase 1; SNARE, soluble NSF attachment protein receptor.

and *FBXO7 (PARK15)* (Wirdefeldt *et al.*, 2011; Cookson, 2012). A large-scale genome-wide meta-analysis identified 28 independent risk variants across 24 loci for PD (Nalls *et al.*, 2015).

The first mutation linked to PD was mapped to chromosome 4q21-q23 in the *SNCA* gene which encodes α-syn, the major protein component of LBs (Polymeropoulos *et al.*, 1997; Spillantini *et al.*, 1997). *SNCA* gene mutations include genomic duplications, triplications and point mutations and are typically associated with an early-onset of PD, implicating the role of α-syn in the development of PD (Singleton *et al.*, 2003; Farrer *et al.*, 2004; Kara *et al.*, 2015; Konno *et al.*, 2016). Duplications and triplications of the *SNCA* correlate with a toxic gain-of-function phenotype, suggesting that the overexpression of α-syn is toxic (Singleton *et al.*, 2003; Chartier-Harlin *et al.*, 2004). Patients with triplications rather than duplications of *SNCA* typically present with a more severe form of the disease, both with earlier onset and faster disease progression (Lesage and Brice, 2009). Five rare missense (point) mutations, A53T (Polymeropoulos *et al.*, 1997), A30P (Kruger *et al.*, 1998), E46K (Zarranz *et al.*, 2003), H50Q (Appel-Cresswell *et al.*, 2013; Proukakis *et al.*, 2013) and G51D (Lesage *et al.*, 2013) have all been linked to early-onset. A53T, A30P, and E46K mutant proteins have a higher propensity to accelerate α-syn to form oligomers, in comparison to wild-type (WT) protein; with A53T and E46K enhancing fibrillisation *in vitro* and *in vivo* (Conway, Harper and Lansbury, 1998; O. M. A. El-Agnaf *et al.*, 1998; Kahle *et al.*, 2000; Li, Uversky and Fink, 2001; Greenbaum *et al.*, 2005). The A53T mutation destabilises the α-helical domain of α-syn, thus facilitating the adoption of the β-sheet conformation (Biere *et al.*, 2000) whereas the E46K mutation is thought to increase intermolecular interactions, accelerating dimerisation and generation of oligomers (Rospigliosi *et al.*, 2009). It is interesting to note that A53T, A30P, and E46K mutants activate microglia more strongly than WT α-syn, suggesting a role of mutant protein in inducing a pro-inflammatory response, potentially exacerbating the disease process (Hoenen *et al.*, 2016).

Meta-analyses have identified genes that are associated with an increased susceptibility to develop PD. A genetic predisposition may, therefore, increase the likelihood of developing the disease. *LRRK2 (PARK8)* mutations account for 10% of AuD familial and 3.6% of sporadic PD, with over 40 different variants found, including the missense mutation Gly2019Serine (G2019S) (Berg *et al.*, 2005; Lesage and

Brice, 2009). Mutations in *LRRK2 (PARK8)* are linked to mitochondrial impairment through compromised oxidative phosphorylation and mitochondrial dynamics leading to a loss of mitochondrial function in neuronal cells (Sanders *et al.*, 2014). Recently, identification of an AuD disease-linked mutation in the *TMEM230* gene which encodes a synaptic vesicle transmembrane protein has implicated impaired synaptic vesicle trafficking in the disease pathogenesis (Deng *et al.*, 2016). Gaucher's disease, caused by mutations in the glucosylceramidase (*GBA)* gene, encoding a lysosomal membrane protein, also represents a higher genetic risk factor in the development of disorders of α-syn aggregation (Sardi, Cheng and Shihabuddin, 2015). Patients with the *GBA1* mutation associated with lysosomal trafficking defects and impaired calcium homeostasis are estimated to have an increased risk in the development of PD of up to 30% at 80 years of age, accounting for approximately 5-10% of all PD patients (Schöndorf *et al.*, 2014; Sardi, Cheng and Shihabuddin, 2015; Schapira, 2015; Wong and Krainc, 2016).

1.2.4 The potential role of iron in Parkinson's disease

PD, AD, MSA, DLB, amyotrophic lateral sclerosis, Huntington's disease, PSP, and frontotemporal dementia are all neurodegenerative diseases where insoluble protein aggregates co-localise with iron (Arawaka *et al.*, 1998; Dickson *et al.*, 1999; Kwan *et al.*, 2012; Chen *et al.*, 2013; Jenkins *et al.*, 2014; Lee *et al.*, 2017; Sheelakumari *et al.*, 2017). Iron accumulation has therefore been implicated as a common theme in neurodegeneration, given the pathologically distinct iron accumulation and clinically different disease presentation.

The loss of pigmented neurons of the *SNPc* represents the major pathological feature of PD. In addition to dopaminergic cell loss from the *SNPc*, surviving neurons contain abnormally aggregated forms of α-syn and elevated iron concentrations (Dexter *et al.*, 1987; Gorell *et al.*, 1995). An additional risk factor for the development of PD is the association of aging and increased iron levels across brain regions (Zecca *et al.*, 2001; Acosta-cabronero *et al.*, 2016; Wang *et al.*, 2016). Deposits of iron have been observed in animal models, post-mortem brains of patients and *in vivo* using iron-sensitive MRI imaging of PD patients (He *et al.*, 1996; Luigi Zecca *et al.*, 2004; Dixon *et al.*, 2012; Rowe *et al.*, 2014; Wang *et al.*, 2016; Ayton *et al.*, 2017).

Under normal physiological conditions, the redox recycling activity of iron between ferrous (Fe^{2+}) and ferric (Fe^{3+}) makes this metal important in many reactions within the brain. However, when intracellular iron levels are dysregulated, this can lead to oxidative stress. Iron is essential in the synthesis and metabolism of neurotransmitters, for generating ATP by electron transport in mitochondria and the synthesis of lipid components for myelination. Specifically for dopaminergic neurons, iron plays an important role as a co-factor for the enzyme tyrosine hydroxylase (TH) (Goodwill, Sabatier and Stevens, 1998; L. Zecca *et al.*, 2004; Richardson *et al.*, 2010). TH catalyses the reaction of L-tyrosine to L-DOPA, a fundamental step in the production of dopamine (Molinoff and Axelrod, 1971). Dopamine is packaged in vesicles at acidic pH to prevent autoxidation into harmful reactive quinone species (dopamine-*o*-quinone), hydrogen peroxide and superoxide (Graham, 1978; Zucca *et al.*, 2015; Umek *et al.*, 2018). Within certain environments, including in the presence of divalent metals, dopamine can be enzymatically deaminated by monoamine oxidase (MAO) to create dihyroxyphenylacetic acid (DOPAC) and H_2O_2 along with hydroxyl radicals, contributing to an oxidative stress environment (Maker *et al.*, 1981; Linert *et al.*, 1996). Iron accumulation has been shown to be protective by detoxification of excess dopamine (*o*-quinones and aminochromes) into melanin that precedes neuromelanin biosynthesis (Izumi *et al.*, 2005).

The catecholaminergic neurons that comprise the *SNPc* have a pronounced blackened appearance due to the presence of neuromelanin, a cytoplasmic insoluble pigment comprised of dopamine, dopamine metabolites, proteins, lipids and metal ions (iron, copper, and zinc) (Wakamatsu *et al.*, 2003; Izumi *et al.*, 2005). Iron is the most abundant metal ion stored within the neuromelanin (at ~ 10 μg/mg of neuromelanin pigment) in dopamine neurons of the *SNPc*, the sequestration of iron, therefore, prevents Fenton's reaction and the subsequent formation of ROS (Zecca *et al.*, 2001; L. Zecca *et al.*, 2004). Neuromelanin can bind iron with either high or low affinity (B_{max} 3.27 and 16.62 nmol/mg melanin, respectively), and in cases of iron overload, high-affinity sites within neuromelanin become saturated (Double *et al.*, 2003). When saturated, iron binds to low-affinity sites leading to reactive/toxic forms becoming available. This process is known to occur in PD leading to oxidative stress within the neurons affected (Faucheux *et al.*, 2003; Zecca, Casella, *et al.*, 2008). Although neuromelanin is neuroprotective, the release of neuromelanin by dying

neurons induces neurodegeneration through activation of microglia in the CNS, as previously reported in PD patients. In addition, the MPTP-induced model of PD whereby extracellular melanin is situated close to activated microglia is associated with neurodegeneration (Langston *et al.*, 1999; Zecca, Wilms, *et al.*, 2008; Viceconte *et al.*, 2015).

The ROS environment of the *SNPc* due to high concentrations of iron and dopamine is therefore proposed as a crucial mediator in the pathogenesis of PD (Jenner *et al.*, 1992). Further to the increased levels of iron, decreased levels of GSH and lipid peroxidation have been demonstrated to affect the *SNPc* in patients (Dexter *et al.*, 1989; Sian *et al.*, 1994; de Farias *et al.*, 2016). A link between increased dietary (non-heme) iron has been shown to dramatically increase the risk of PD by ~30% (Logroscino *et al.*, 2008). Mutations in genes relating to iron homeostasis and metabolism are also linked to PD, and other neurodegenerative disorders including AD (Rhodes and Ritz, 2013; Fan *et al.*, 2018). For example, hereditary haematochromatosis, a genetic disorder defined by abnormal iron handling and excessive iron accumulation in systemic tissues has been linked to PD (Costello *et al.*, 2004). Mutations in the *PLA2G6 (PARK14)* gene, which encodes a calcium-dependent phospholipase A2, are associated with L-DOPA responsive dystonia/parkinsonism and also characterised by high levels of brain iron (Gregory *et al.*, 2008; Ferese *et al.*, 2018). Ferroptosis, an iron-dependent cell death pathway, has been linked to the mechanism of cell death in PD and is discussed further in Chapter 5 (Dixon *et al.*, 2012; Do Van *et al.*, 2016).

1.3 α-Synuclein is associated with Parkinson's disease

1.3.1 Structure and function of α-synuclein

α-Syn is a 140-residue protein encoded by the *SNCA* (*PARK1)* gene located on chromosome 4 and has since garnered attention as the protein implicated in the pathogenesis of PD (Fig. 1.3) (Spillantini, Divane and Goedert, 1995). The NAC domain of α-syn was identified as a component of β-amyloid plaques in patients with AD and later as the major immunoreactive component in LBs and Lewy neurites (Ueda *et al.*, 1993b; Spillantini *et al.*, 1997; Takeda *et al.*, 1998). Although there are several physiological roles designated to α-syn, the precise function of the protein remains poorly understood. A vast amount of experimental data, both from animal

and cell models, indicate α-syn has roles in several physiological processes including; regulation and trafficking of synaptic vesicles through lipid interactions (Cabin *et al.*, 2002; Zaltieri *et al.*, 2015); neuronal plasticity (Rasia *et al.*, 2005; Liu *et al.*, 2007; Burré *et al.*, 2011; Cremades *et al.*, 2012; Lashuel, Overk, Abid Oueslati, *et al.*, 2013; Burré, Sharma and Südhof, 2014); neurotransmitter release (Burré *et al.*, 2011); dopamine biosynthesis (Tavassoly *et al.*, 2014); microtubule organisation (Cartelli *et al.*, 2016); metal homeostasis (Tavassoly *et al.*, 2014); mitochondrial function, and as a ferrireductase (Davies, Moualla and Brown, 2011).

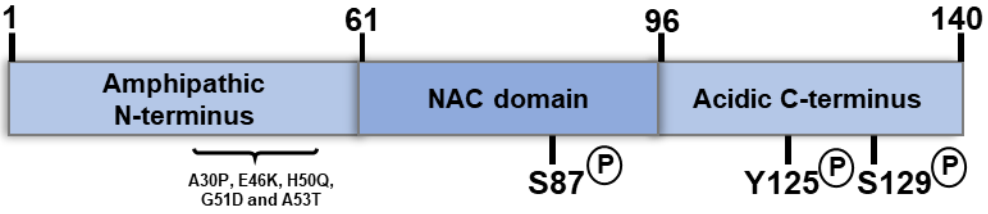

Figure 1.3. *Structure of α-syn*. α-syn is a 14kDa, 140-residue protein with three distinct regions; a highly conserved N-terminal, NAC region and an acidic C-terminal. The N-terminus has a series of imperfect KTKEGV repeat motifs involved in lipid binding and prone to forming amphipathic helixes (Davidson et al., 1998; Bussell and Eliezer, 2003). Missense mutations associated with familial PD are located in this region. The central (non-amyloid-β component) NAC region confers β-sheet potential, and is prone to aggregation and misfolding (Giasson *et al.*, 2001). The acidic C-terminal is largely unfolded and slightly negatively charged region that acts as both a chaperone for other proteins and inhibiting α-syn assembly by interfering with molecular interactions of the NAC region (Murray *et al*., 2003; Halliday and McCann, 2008).Phosphorylation of serine at position 129 is the most common posttranslational modification associated with α-syn, corresponding to approximately 90% of α-syn found in Lewy bodies (Walker et al., 2013). Lipid-interactions of α-syn (bottom diagram, image credit: (Gallegos *et al*., 2015) recruits an α-helical conformation in the N-terminus in contrast to the unstructured nature of the C-terminus (Ulmer and Bax, 2005; Plotegher *et al.,* 2014).

1.3.2 α-Syn as a functional tetramer

There is controversy as to whether α-syn exists functionally as 'natively unfolded' monomer that acquires α-helical content following binding to lipid structures or whether the protein is present as a function tetramer *in vivo* (Davidson *et al.*, 1998; Ulmer and Bax, 2005; Bartels, Choi and Selkoe, 2011). Principally, data from protein conformation studies uses the expression of high concentrations of protein either *in vitro* or *in vivo* and preparation via denaturing samples using heat and/or chemical denaturation, all which have been found to abolish potential tetrameric structure formation (Bartels, Choi and Selkoe, 2011; Pochapsky, 2015). The suggestion of a tetrameric structure of α-syn was initially suggested in a seminal study by Bartels and colleagues (Bartels, Choi and Selkoe, 2011). *In vivo* cross-linking experiments

revealed the presence of a tetrameric species of α-syn with a mass of ~55-60 kDa in erythrocytes, human cell lines (M17D, HeLa, HEK293, and COS-7), and mammalian brain tissue. Other investigations by two-dimensional gel analysis, scanning transmission electron microscopy (STEM) with particle analysis, and sedimentation equilibrium analytical ultracentrifugation (SE-AUC) also suggested a tetrameric conformation. The capture of α-syn images using STEM under non-denaturing conditions yielded a homogenous distribution of spherical particles measuring ~3.0-3.5 nm in diameter, with a size distribution at ~55 kDa when analysed by unbiased automatic sampling. SE-AUC investigations, a technique used to establish the native state of proteins independent of their conformations, yielded an average molecular weight of 57.8 kDa. These investigations provide several independent lines of evidence to suggest the native structure of α-syn, at least in erythrocytes and the cell lines investigated, is a tetramer with a MW ~58 kDa (Bartels, Choi and Selkoe, 2011). Interestingly, this tetramer formation resists aggregation into ThT-positive aggregates when compared to recombinant α-syn over a time course sufficient to induce fibril formation, suggesting therapeutic potential (Bartels, Choi and Selkoe, 2011; Dettmer *et al.*, 2015). A subsequent study characterised a soluble tetramer of α-syn recombinantly expressed in *E.coli*, with characteristics of WT α-syn derived from erythrocytes (Bartels, Choi and Selkoe, 2011; Wei Wang *et al.*, 2011). In the latter study, tetrameric α-syn does not form pores in membranes, is not toxic when added to cells in culture, resists aggregation, increased cellular concentrations shift the cellular equilibrium towards monomer, and disease-associated mutants (A30P, A53T, and E46K) render the protein more disordered when compared to WT protein (W. Wang *et al.*, 2011). The tetramer model for α-syn structure rationalises the localisation of mutations known to bring on early-onset PD, including A53T, A30P, and E46K mutations (Bartels, Choi and Selkoe, 2011; W. Wang *et al.*, 2011; Dettmer *et al.*, 2015). The location of the A53T, A30P, and E46K mutations in the N-terminal domain of α-syn result in the destabilisation of tetrameric structure resulting in a significantly decreased tetramer:monomer ratio in cells (between 10-40% depending on cell type). This finding strongly suggests destabilisation of a tetrameric structure facilitates subsequent pathological aggregation of monomer into disease-associated structures (Dettmer *et al.*, 2015).

Follow-up studies disputing this finding, have again suggested the normal cellular structure of α-syn exists as an intrinsically disordered monomeric protein (Binolfi, Theillet and Selenko, 2012; Fauvet *et al.*, 2012; Burré *et al.*, 2013; Araki *et al.*, 2016; Theillet *et al.*, 2016). These studies provide several lines of evidence for the presence of a monomeric structure of α-syn in living cells and when purified under non-denaturing conditions, again in various cell and tissue types including erythrocytes, mammalian cells, and *E. coli* (Fauvet *et al.*, 2012; Theillet *et al.*, 2016). Using in-cell nuclear magnetic resonance (NMR) imaging, α-syn was shown to maintain a disordered conformation in the cell, which upon molecular crowding, became slightly more compact than in free solution (Theillet *et al.*, 2016). The presence of a soluble tetramer in the study by Bartels *et al.* has since been suggested to be dependent on the oxidative environment of the erythrocyte in which much of the biochemical characterisation was undertaken (Killinger *et al.*, 2019). α-Syn is highly expressed in erythrocytes and haemoglobin in erythrocytes oxidatively catalyses the formation of intramolecular dityrosine bonds resulting in populations of dimers and tetramers of α-syn (Barbour *et al.*, 2008; Elhadi *et al.*, 2019). The latter of which is hypothesised to occur rapidly during purification of α-syn from erythrocytes (Killinger *et al.*, 2019). In conjunction with the presence of α-syn bound to vesicles in erythrocytes, the purification of α-syn from erythrocytes may preferentially produce a tetrameric structure bound to vesicle membranes. Therefore, it is likely the aggregate-resistant tetramer described is stabilised via oxidative crosslinking due to the oxidative environment of erythrocytes (Killinger *et al.*, 2019). This, however, does not suggest no tetrameric structure *in vivo* but instead that the assembly of a tetrameric structure is highly dependent on the cell type and biochemical factors during purification. For example, tetrameric populations are most prevalent have in human erythroid leukaemia cells and absent from gastrointestinal neuronal cells (Dettmer *et al.*, 2013; Corbille, Neunlist and Derkinderen, 2016).

1.3.3 The physiological role of α-syn

α-, β-, and γ-synucleins are highly expressed throughout the brain, with the expression of α- and β-synuclein associated with the presynaptic terminal of neurons (Galvin *et al.*, 2001). Neuronal expression of α-syn is heterogeneous throughout the CNS, with high expression of α-syn in the *SNPc*, caudate nucleus, putamen, and ventral pallidum nuclei (Galvin *et al.*, 2001; Taguchi *et al.*, 2016). These regions

closely follow vulnerable regions affected in PD (H. Braak *et al.*, 2003; Hawkes and Braak, 2007). The location of α-syn within presynaptic terminals, its interaction with synaptic vesicles and vesicle-associated membrane protein 2 (VAMP2/synaptobrevin-2), SNARE (soluble *N*-ethylmaleimide-sensitive-factor attachment protein receptor)-complex chaperoning activity, and high expression levels of the protein in areas requiring synaptic modifications (e.g. song-learning in the zebra finch) support a role for α-syn in neurotransmitter storage and release within the synapse (Clayton and George, 1999; Kahle *et al.*, 2000; Murphy *et al.*, 2000; Burré *et al.*, 2011). Mechanisms of dopamine compartmentalisation in the storage pool and readily releasable pool maintain an important role in neurotransmission. For exocytosis of synaptic vesicles, and release of dopamine to the synaptic cleft, SNARE proteins on the plasma membrane (syntaxin and synaptosome-associated protein 25) interact with SNARE proteins on synaptic vesicles (SVs; VAMP2) to allow fusion to the membrane following stimulation (Lautenschläger, Kaminski and Schierle, 2017). α-Syn can induce vesicle-vesicle interactions associated with SVs through its lipid-binding functionality and interaction with VAMP2. The amphipathic helix of monomeric α-syn acts as a curvature-sensing and stabilizing protein, able to insert into the lipid surface of membranes with negatively charged lipids, most notably of which is present in synaptic vesicles (Pranke *et al.*, 2011; Westphal and Chandra, 2013). Cholesterol in the SV membrane promotes a double-anchor mechanism of SV clustering, wherein upon binding to cholesterol in SV membranes, α-syn undergoes a conformation change to expose the NAC region (Fig. 1.3) (Fusco *et al.*, 2017a). This interaction promotes the clustering of SVs, through the interaction of bound α-syn and other SVs (Man *et al.*, 2020). The direct interaction of α-syn and VAMP2 on the surface of SVs, independent of the NAC region, maintains close contact of VAMP2 with t-SNAREs to promote SV clustering at the plasma membrane and neurotransmitter release (Haberman *et al.*, 2012; Ninkina *et al.*, 2012; Sun *et al.*, 2019). There are several lines of evidence for a role of α-syn as a molecular chaperone in SNARE-complex activity. α-syn shares structural and functional homology with 14-3-3 and cysteine-string protein α (CSPα) chaperone proteins (Ostrerova *et al.*, 1999; Perez *et al.*, 2002; Bronk *et al.*, 2012). Knockout of the cochaperone, CSPα, in a murine model results in lethal neurodegeneration, which is rescued upon expression of α-syn and associated with chaperoning assembly of SNARE-complexes (Burré *et al.*, 2011;

Ninkina *et al.*, 2012). Moreover, depletion of α-syn is associated with increased 14-3-3 protein expression (Greten-Harrison *et al.*, 2010).

Synthesis of dopamine by the enzyme TH, the storage of dopamine in vesicles, and the subsequent release of dopamine as a neurotransmitter is critical to the function of dopaminergic neurons. α-syn can interact to modulate dopamine production through interaction with proteins involved in dopamine homeostasis. Firstly, α-syn can inhibit the production of dopamine through interaction with the enzyme TH (Perez *et al.*, 2002). Under normal circumstances, 14-3-3 protein binds phospho-TH to enhance the activity of TH, thus promoting conversion of L-tyrosine to L-DOPA by TH. L-DOPA is subsequently converted to dopamine via aromatic L-amino acid decarboxylase. On the other hand, α-syn interacts with TH to inhibit its activity by reducing TH phosphorylation (Perez *et al.*, 2002). In addition, as a protein involved in iron homeostasis, α-syn can regulate the availability of iron required for TH activity (Wu *et al.*, 2011). Secondly, α-syn interacts with VMAT2 and DAT to modulate the storage and reuptake of DA following release to the synaptic cleft (Yavich, Tanila and Vepsa, 2004). Overexpression of α-syn disrupts storage of dopamine through the inhibition of VMAT2 activity, resulting in increased cytosolic dopamine levels and significantly enhanced presence of intracellular reactive oxygen species (Guo *et al.*, 2008).

Interaction between α-syn and metals have been investigated extensively and have allowed us to elucidate a function for α-syn in the homeostasis of metals. As discussed in Section 1.2.4, dyshomeostasis of metals and toxic accumulation of metals, specifically iron, is associated with the pathogenesis of PD and other neurodegenerative disorders (Li *et al.*, 2017). Iron regulation is tightly controlled by the binding of iron regulatory protein (IRP) to iron-responsive elements (IREs) in the mRNA of proteins responsible for iron import, export, and storage of iron (Fig.1.4) (Sipe, Lee and Beutler, 2002; Rouault, 2013). For example, in physiological conditions of low levels of cellular iron, binding of IRP to the IRE in 5’ untranslated region (UTR) of the mRNA of the iron storage protein ferritin, prevents translation of the protein. Reduced levels of ferritin subsequently increase the concentration of bioavailable Fe^{2+} in the LIP by preventing the storage of iron. In situations of abundant cellular iron, IRPs bind cellular iron preventing binding to the IRE in the mRNA of ferritin, resulting in the translation of ferritin. To store iron, ferritin oxidises

Fe^{2+} from the LIP to Fe^{3+} (Muhoberac and Vidal, 2019). With a predicted iron-response-element (IRE) in a 46 nucleotide stretch within the 5' UTR region of α-syn, similar to IREs of ferritin and other proteins in iron regulation, α-syn is hypothesised to function in the regulation of cellular iron (Friedlich, Tanzi and Rogers, 2007). The receptor-mediated uptake of TfR via clathrin-coated endocytosis is hypothesised to involve interaction between α-syn and dynamin, directly influencing Fe^{3+} import by the cell. In support of this, ablation of α-syn expression in a transgenic murine model alters the cellular iron levels by altering the expression of ferritin and transferrin (TfR) (Baksi, Tripathi and Singh, 2016). In dopaminergic neurons, regulation of cellular levels of Fe^{2+} and Fe^{3+} is important to reduce the formation of ROS via Fenton's chemistry, whilst enabling utilisation of Fe^{2+} for dopamine biosynthesis (cofactor for TH) and other cellular processes. Indeed, ratios of Fe^{2+} and Fe^{3+} are altered in PD patient brains, highlighting the importance of iron regulation to the survival of dopaminergic neurons. α-syn, as a metal-binding protein, acts as a cellular ferrireductase to maintain levels of Fe^{2+} in cells in the presence of copper (II) ions (Davies, Moualla and Brown, 2011).

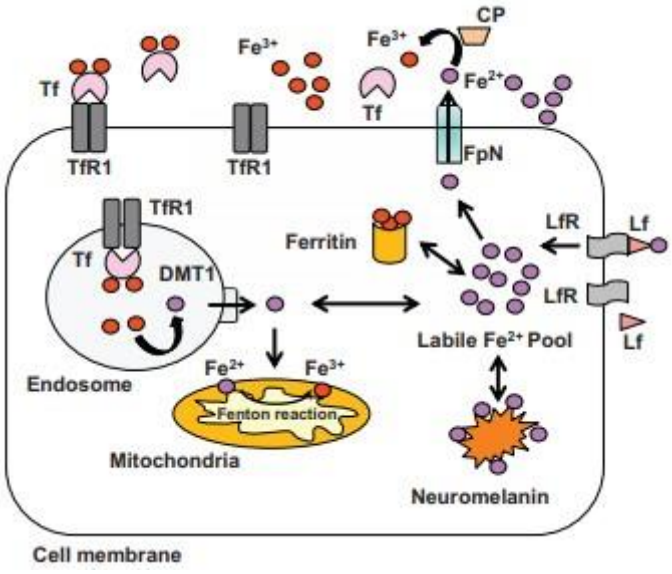

Figure 1.4. *Schematic of brain iron homeostasis.* Binding of Fe^{3+}-loaded transferrin (Tf) to transferrin receptor 1 (TfR1) results in the internalisation of this complex to the endosomal component whereby Fe^{3+} is reduced to Fe^{2+} by acidification to aid in release of Fe^{3+} from bound transferrin and the actions of the ferrireductase Steap3 (Ohgami *et al.*, 2005). Fe^{2+} is transported out of the endosome to the cytosol via divalent metal transporter 1 (DMT1). Fe^{2+} is associated with a transitionary pool of chelatable of redox-active iron known as the labile iron pool (LIP) (Kakhlon and Cabantchik, 2002). Iron in this pool is available for utilisation in various cellular processes, exported out of the cell by ferroportin (FpN), or stored in a complex with ferritin or neuromelanin (in *SNPc* neurons). Reprinted by permission from Elsevier: License Number 4816461364330. Elsevier, Free Radical Biology and Medicine, Targeting dysregulation of brain iron homeostasis in Parkinson's disease by iron chelators, Orly Weinreb,Silvia Mandel,Moussa B.H. Youdim,Tamar Amit et al. Sept. 1, 2013 (Weinreb *et al.*, 2013).

The ferrireductase activity of α-syn was initially determined using recombinant human α-syn generated from *E. coli* with a Vmax of 2.72, 2.52, 2.37, and 2.62 nmol/min/mg for wildtype, E46K, A30P, and A53T, respectively. Overexpression of α-syn in a human neural cell line resulted in both the increase in cellular Fe^{2+} and increased ferrireductase activity when compared to cell lines without this genetic modification (Davies, Moualla and Brown, 2011). More recently, *in vivo* ferrireductase activity of α-syn has been determined in an AAV6-α-syn-overexpressing rat model and reduced levels of α-syn correlate with reduced ferrireductase activity in post-mortem PD striatum (McDowall *et al.*, 2017). The data generated by McDowall *et al.* (2017) highlight the active form of α-syn with ferrireductase activity as a tetramer associated with membranes in SH-SY5Y cells overexpressing α-syn (Mcdowall *et al.*, 2017). In disease, the loss of function of α-syn as a ferrireductase may contribute to an accumulation of Fe^{2+} with pathological consequences associated with ROS due to Fenton chemistry and initiation of cell loss in relation to ferroptosis (Do Van *et al.*, 2016).

1.3.4 Post-translational modifications of α-synuclein

α-Syn undergoes several post-translational modifications (PTMs) including acetylation, phosphorylation, oxidation, nitration, ubiquitination and truncation that modulates the structure and function of the protein (Fig. 1.4). In LBs, α-syn has been reported to contain the PTMs of phosphorylation (at S129; referred to as p-α-syn), ubiquitination (K12, 21 and 23), truncation (N115, D122, Y133 and D135) and ubiquitous N-terminal acetylation (Anderson *et al.*, 2006). This pattern of phosphorylation, truncation, ubiquitination and acetylation is also observed in the detergent-insoluble fraction of patients with familial PD (A53T mutation) and MSA, suggesting a common pathogenic pathway in synucleinopathies (Anderson *et al.*, 2006).

Several phosphorylation sites in α-syn are known and are located in the C-terminal domain on the amino acids tyrosine, threonine or serine (Y125, S129, Y133 and Y136) (Oueslati, Fournier and Lashuel, 2010). Ninety percent of α-syn within deposits is phosphorylated at S129 in PD patients compared to 4% in controls, suggesting accumulation of p-α-syn over a certain threshold leads to the formation of LBs (Fujiwara *et al.*, 2002; Chen and Feany, 2005; Anderson *et al.*, 2006; Freichel *et*

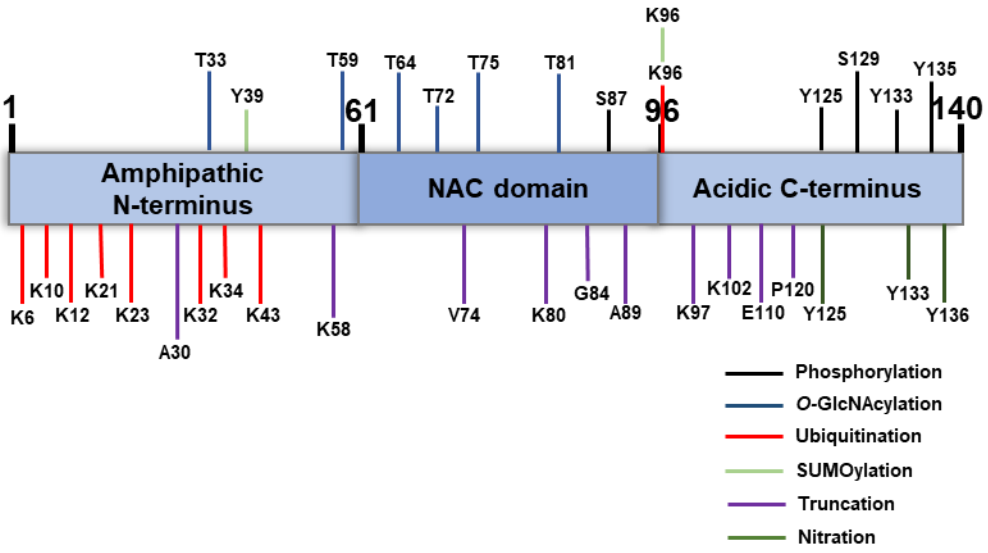

Figure 1.5. *Major post-translational modifications on α-syn*. Image adapted from (Zhang, Li and Li, 2019).

al., 2007). Additionally, the presence of this PTM in the soluble fractions of normal and diseased brains highlights a role of α-syn S129 in normal cellular metabolism (Anderson *et al.*, 2006; Muntané, Ferrer and Martinez-Vicente, 2012). Phosphorylation at S129 modulates the capacity of α-syn to bind biological membranes, culminating in an inhibitory effect, whereby a decrease in the affinity of α-syn with phospholipids is observed (Visanji *et al.*, 2011; Nübling *et al.*, 2014). Overexpression of the main kinase responsible for phosphorylation of α-syn (polo-like kinase 2; PLK2) enhances the turnover of α-syn and the significantly shorter half-life of p-α-syn (54.9 ± 6.4 min compared to >240 min in non-phosphorylated αsyn) demonstrates p-α-syn is selectively targeted for degradation by the ubiquitin-proteasome and autophagy-lysosomal pathways (Chau *et al.*, 2009; Machiya *et al.*, 2010; Oueslati *et al.*, 2013). Although 90% of α-syn is phosphorylated at this position in LBs, phosphorylation at S129 is not required for the development of LB-like aggregates (Anderson *et al.*, 2006; Luk *et al.*, 2009; Arawaka *et al.*, 2017). Using an S129 mutant, S129A, LB-like aggregates developed in the absence of phosphorylation, suggesting phosphorylation occurs after LB formation (Luk *et al.*, 2009; Volpicelli-Daley *et al.*, 2011). In support of this, several phosphorylation kinases (CK2, GRK5 and LRRK2) located in association with α-syn in LBs are able to efficiently phosphorylate aggregated forms of α-syn (Arawaka, 2006; Ryu *et al.*, 2008; Qing *et al.*, 2009; Waxman and Giasson, 2011). In patients with PD, accumulation of insoluble p-α-syn is thought to be a late-stage event disease due to

the positive correlation of p-α-syn and severity of disease (Beach *et al.*, 2009; Walker *et al.*, 2013).

More than 90% of eukaryotic proteins are acetylated (Arnesen *et al.*, 2009). Acetylation represents the major PTM of α-syn, with 15 putative acetylation sites located in the N-terminal region of the protein (Fig. 1.4) (Anderson *et al.*, 2006; Fauvet *et al.*, 2012; de Oliveira *et al.*, 2017). α-Syn is constitutively N-terminally acetylated in its normal physiological state, specifically on lysine residues 6, 34, 45 and 96 (Bartels *et al.*, 2010). N-terminal acetylation of α-syn is important for the interaction of α-syn with lipids by increasing α-helical content and preventing the ability of the protein to aggregate by destabilising the oligomerisation state of α-syn, thus protecting against toxicity (Bartels *et al.*, 2014; Bu *et al.*, 2017).

Ubiquitin, a 76-amino acid protein, is responsible for marking proteins for degradation and subsequent targeting of proteins to large protease complexes including the 26S proteasome (Swatek and Komander, 2016). Ubiquitin is conjugated to proteins through the action of three enzymes: ubiquitin-activating enzyme (E1), ubiquitin-conjugating enzyme (E2) and ubiquitin-ligating enzyme (E3) (Schulman and Harper, 2009; Ye and Rape, 2009; Callis, 2014). In addition to a role in degradation of substrates, other regulatory functions of ubiquitin have been described including the regulation of protein activity and control of cellular localisation of proteins (Ronai, 2016). In the normal function of α-syn, it is postulated that ubiquitination controls vesicle fusion in presynaptic terminals (Goedert *et al.*, 2013). The association of PD-linked mutations to ubiquitin signalling (e.g. *PARKIN*, *PINK1*) and the presence of mono-, di- and tri-ubiquitinated α-syn in LBs suggest the involvement of α-syn ubiquitination in disease (Sampathu *et al.*, 2003; Walden and Muqit, 2017). Ubiquitination of α-syn at K6, K12 and K21 moderately inhibit the formation of fibrils, whereas residues K32, K34 and K96 showed a strong inhibitory effect (Rott *et al.*, 2008; Hejjaoui *et al.*, 2011; Meier *et al.*, 2012). In contrast, residues at K10 and K23 can readily form fibrils (Meier *et al.*, 2012).

1.3.5 Normal degradation of α-synuclein

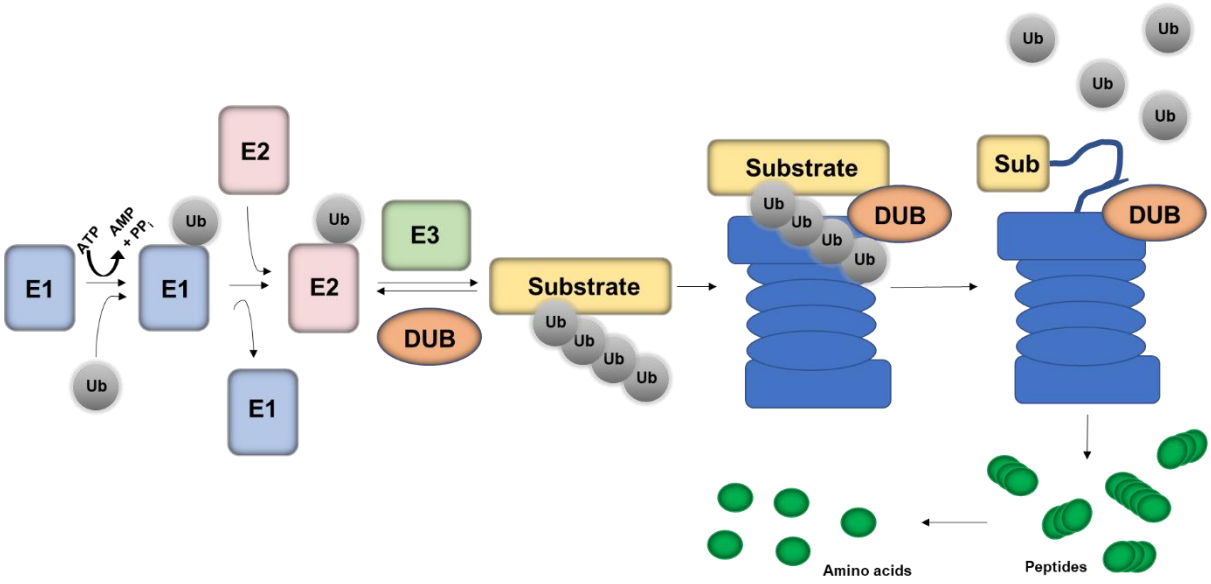

Figure 1.6. *Schematic representation of the ubiquitin-proteasome pathway.* The ubiquitin-activating enzyme (E1) activates ubiquitin (Ub) prior to binding of Ub to E1. Ub is transferred from E1 to a ubiquitin-conjugating enzyme (E2). A ubiquitin ligase (E3) recruits Ub-E2 and transfers Ub to the substrate. Successive rounds of Ub conjugation results in the formation of lysine 48-linked polyubiquitin chains on substrates. Following substrate recognition by the 19S regulatory subunit of the 26S proteasome, deubiquitylating enzymes (DUBs) remove ubiquitin molecules from substrates before degradation (Clague, Coulson and Urbé, 2012). Targeted degradation by β1, β2, and β5 proteolytic subunits of the 20S core particle degrades the substrate into corresponding short peptide sequences. Peptides are further degraded by aminopeptidases (APPs) into amino acids (Rousseau and Bertolotti, 2018). Free Ub molecules generated by DUBs are recycled for further use in targeting substrates for degradation. Image adapted from (Eldridge and Brien, 2010).

In the cell, two main systems are responsible for the degradation of intracellular proteins; the ubiquitin-proteasome system (UPS) and autophagy-lysosome system (ALS). The UPS targets the clearance of short-lived, damaged, and misfolded proteins in the cell via ubiquitylation and subsequent proteasomal degradation to ensure turnover of proteins to maintain amino acid homeostasis (Fig. 1.6) (Suraweera et al., 2012; Rousseau and Bertolotti, 2018). Proteins tagged with ubiquitin, usually as 48-linked polyubiquitin chains attached to lysine residues of proteins, and presence of an unstructured region in proteins serves as a signal for degradation (Prakash et al., 2004; Finley, 2012; Yu and Matouschek, 2017). Typically, longer proteins (>150 residues) require the addition of a polyubiquitin tag to promote efficient proteolysis by the proteasome whereas proteins with <150 residues can be degraded following monoubiquitylation (Shabek *et al.*, 2012). Once ubiquitylated, substrates are targeted to the proteasome (Ronai, 2016). The 26S proteasome is a multi-subunit enzyme consisting of both a regulatory (19S) and core (20S) unit (Yoshimura et al., 1993; Collins and Goldberg, 2017). The 19S subunit has crucial mechanisms to control function of the proteasome through substrate

recognition, deubiquitination of polyubiquitin chains, and unfolding of protein substrates before degradation of proteins in the narrow proteolytic chamber of the 20S core unit (Smith *et al.,* 2005; Lander *et al.,* 2012). The 20S core unit comprises both α- and β-subunits, forming four stacked heteroheptameric rings (Unno *et al.,* 2002; Kunjappu, Hochstrasser and Wolf, 2014). α- Subunits function as a gate mechanism to prevent unwanted access to the proteolytic chamber (Latham, Sekhar and Kay, 2014). β-Subunits function as the catalytic mechanism for the degradation of substrates. Of the seven β-subunits, only the β1, β2, and β5 units have proteolytic activity, known as caspase-like, trypsin-like, and chymotrypsin-like activity, respectively (Groll et al., 1999; Kunjappu, Hochstrasser and Wolf, 2014). The resulting peptides leave the proteasome and are further broken down to their constituent amino acids by the action of aminopeptidases (Saric, Graef and Goldberg, 2004).

Autophagy, meaning ‘self-eating’ in Greek, targets longer-lived macromolecules and dysfunctional organelles to the lysosome for clearance (Fig. 1.7) (Galluzzi *et al.*, 2018). The ALS serves two major functions with the cell: removal of deleterious intracellular components, and recycling of macromolecules to ensure proteome renewal (Lawrence and Zoncu, 2019). In normal cellular conditions, autophagy occurs at constitutively low levels but can be altered in conditions of cellular stress. Cellular stress, including presence of protein aggregates and cellular ROS, causes activation of autophagy processes (He *et al.*, 2017). The ALS consists of three subtypes, differing on how targets are delivered to the lysosome; chaperone-mediated autophagy (CMA), microautophagy, and macroautophagy (Kaushik and Cuervo, 2018). For CMA, proteins in the cytosol are targeted for degradation to the lysosome through the interactions of the chaperone protein HSC70, LAMP2A, and substrates targeted for degradation (Cuervo and Dice, 1996; Agarraberes and Dice, 2001; Schneider, Suh and Cuervo, 2014). The chaperone protein HSC70 recognises a KFERQ motif on targeted substrates and delivers it to the lysosomal surface protein LAMP2A (Bandyopadhyay *et al.*, 2008; Kirchner *et al.*, 2019). Interaction of HSC70 and the substrate with the cytosolic region of LAMP2A results in the formation of a LAMP2A-transmembrane pore, allowing for the translocation of substrates to the lysosomal lumen (Cuervo and Dice, 1996; Rout *et al.*, 2014). In microautophagy, lysosomes directly engulf cytosolic material through membrane

invagination to the lysosomal lumen (Sattler and Mayer, 2000). In a similar mechanism of substrate translocation in CMA, a KFERQ motif on a cytosolic protein substrate is recognised and delivered to the lysosome via interaction with HSC70 (Tekirdag and Cuervo, 2018). In contrast to CMA, microautophagy does require interaction with LAMP2A on the lysosomal membrane to introduce the substrate to the lysosomal lumen but instead involves lysosomal membrane invagination (Kaushik and Cuervo, 2018). Macroautophagy requires the fusion of another organelle, the autophagosome, with the lysosome in order to degrade target substrates. Briefly, formation of a double-membraned organelle, the autophagosome, sequesters proteins for degradation before fusion with lysosomes (Nakamura and Yoshimori, 2017). For all types of autophagy, once in the lysosomal lumen, substrates are degraded by the actions of hydrolases capable of degrading proteins, DNA, RNA, polysaccharides, and lipids (Yim and Mizushima, 2020).

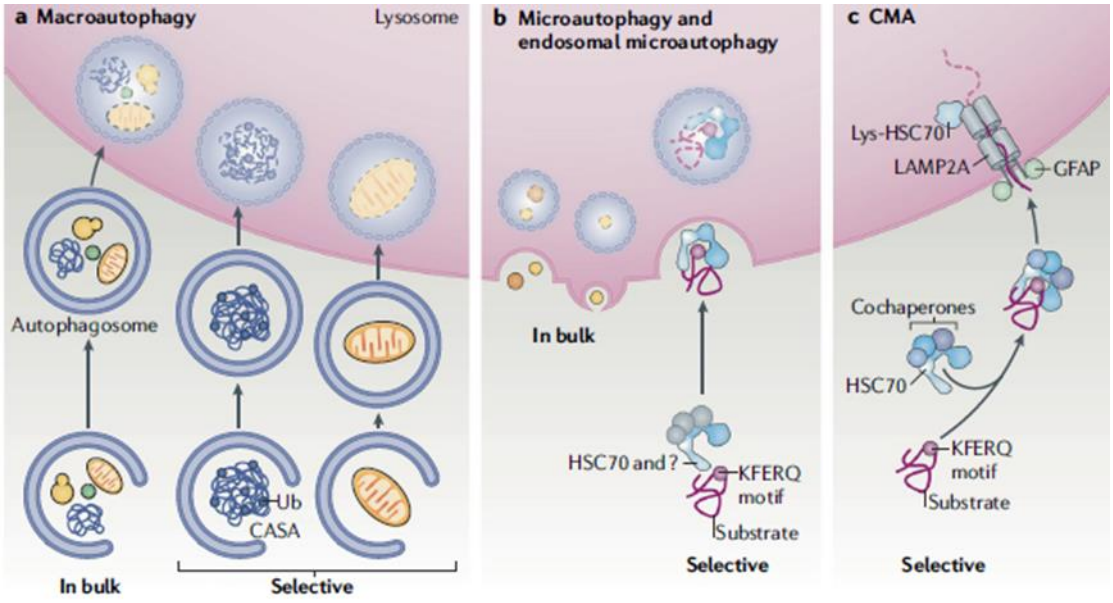

Figure 1.7. *Autophagic pathways.* Three types of autophagy have been identified as microautophagy, chaperone-mediated autophagy (CMA) and macroautophagy (Li, Li and Boa, 2012; Cuervo and Wong, 2013; Feng et al., 2013). Autophagy operates under tight transcriptional and post-transcriptional regulation and typically mediates cryoprotective effects (Wani et al., 2015). Five key stages of macroautophagy are: (1) phagophore formation or nucleation; (2) Atg5-Atg12 conjugation and interaction with Atg16L and multimerisation at the phagophore; (3) LC3 processing and insertion into the extending phagophore membrane; (4) capture of random or selective targets for degradation; and (5) fusion of the autophagosome with the lysosome, resulting in proteolytic degradation by lysosomal proteases (Glick, Barth and Macleod, 2010; Gong et al., 2013). For microautophagy, substrates are targeted to the lysosome via KFERQ and HSC70. At the lysosome, invagination of the lysosomal membrane results in the delivery of substrates to the lysosomal lumen. In CMA, the KFERQ motif on targets for degradation are recognised by the chaperone protein HSC70 and delivered to the lysosomal membrane. At the lysosomal membrane, interaction of cytosolic substrates and HSC70 with the lysosomal surface protein LAMP2A results in the formation of a transmembrane pore in the lysosomal membrane, capable of translocating substrates to the lysosomal lumen. In the lumen, hydrolase enzymes degrade substrates (Yim and Mizushima, 2020). Reprinted by permission from Springer Nature: License Number 4658831389575, Springer Nature, Nature Reviews Molecular Cell Biology, The coming of age of chaperone-mediated autophagy, Susmita Kaushik et al. Apr 6, 2018 (Kaushik and Cuervo, 2018).

Both the ALS and the UPS are involved in the normal degradation and clearance of α-syn (Webb *et al.*, 2003). Initial studies suggested that α-syn is principally degraded by the proteasome. In one of the first studies of proteasomal inhibition, using the chemicals *n*-acetyl-leu-leu-norleucinal, lactacystin, or MG132, the formation of α-syn-positive inclusions were seen in cultured neurons suggesting degradation of the protein occurs via a proteasome-dependent mechanism (Bennett *et al.*, 1999; Mclean, Kawamata and Hyman, 2001). Later studies also indicated a role for the proteasome in α-syn degradation, including in a murine model of PD where nigral proteasome inhibition led to increased levels of p-α-syn (at S129) and motor deficits (Webb *et al.*, 2003; Emmanouilidou, Stefanis and Vekrellis, 2010; Ebrahimi-fakhari *et al.*, 2011; Bentea *et al.*, 2015). However, not all studies demonstrated a similar accumulation of α-syn following proteasomal inhibition (Martín-Clemente *et al.*, 2004; Emmanouilidou, Stefanis and Vekrellis, 2010). Using both murine and cell models, Martín-Clemente and colleagues (2004) suggest overexpression of α-syn was not associated with altered proteasome function. The differences in these studies have been suggested to involve experimental differences in the presence or absence of epitope tags, stable or transient expression of α-syn, and cell-specific effects (Emmanouilidou, Stefanis and Vekrellis, 2010; Stefanis *et al.*, 2019). These studies did not characterise the species of α-syn degraded, however, it was determined an intermediate soluble oligomeric species to be selectively targeted to and degraded by the 26S proteasome (Emmanouilidou, Stefanis and Vekrellis, 2010). Instead, lysosomal inhibition led to the increase of all species of α-syn examined, suggesting a role for ALS in the normal degradation of α-syn species (Emmanouilidou, Stefanis and Vekrellis, 2010; Batelli *et al.*, 2011).

For ALS degradation of α-syn, CMA and macroautophagy have been suggested as the autophagic pathways responsible for degradation of α-syn (Paxinou *et al.*, 2001a; Cuervo *et al.*, 2004; Vogiatzi *et al.*, 2008; Stefanis *et al.*, 2019). α-Syn contains the KFERQ sequence required for CMA degradation systems and overexpression of WT α-syn in murine models results in the upregulation of both LAMP2A and HSC70 critical to the function of the CMA pathway (Mak *et al.*, 2010; Kirchner *et al.*, 2019). A more complex picture of α-syn degradation pathways emerge given how upon inhibition of one proteolytic system, the other can be activated to promote degradation. For example, in PC12 cells overexpressing A53T mutant α-syn, the

addition of a proteasomal inhibitor MG132 is sufficient to induce increased numbers of autophagosomes associated with macroautophagy, highlighting the activation of ALP to promote clearance of α-syn (Lan *et al.*, 2015).

1.3.6 Aggregation of α-synuclein

Monomeric α-syn exists as a natively unstructured protein at physiological pH due to its low intrinsic hydrophobicity and high net charge (Eliezer *et al.*, 2001; Fauvet *et al.*, 2012; Theillet *et al.*, 2016). α-Syn undergoes aggregation into cross-β-sheet rich amyloid fibrils akin to filaments found in LBs (Fig. 1.5) (Uversky *et al.*, 2002; Fauvet *et al.*, 2012). *In vitro*, α-syn aggregation follows a nucleation-dependent sigmoidal growth curve as measured by Thioflavin T (ThT) kinetic assays. Monitoring the aggregation kinetics by fluorescence demonstrates sigmoidal growth associated with three distinct phases: lag phase, the signal remains constant due to lack of fibrillar species and lack of nucleation centre for the development of fibrils; elongation phase, ThT fluorescence rapidly increases as monomers aggregate to form fibrillar species; stationary phase, ThT fluorescence reaches its maximum intensity as fibril structures formed remain in thermodynamic equilibrium with soluble proteins (Wood *et al.*, 1999; Wördehoff and Hoyer, 2018). Various factors contribute to the increased propensity for α-syn aggregation including temperature, lowering pH, ligand binding, presence of familial α-syn mutations and metals such as iron and copper (Wood *et al.*, 1999; Uversky, Li and Fink, 2001; Winner *et al.*, 2011; Buell *et al.*, 2014; Xiao *et al.*, 2018). Oligomers populated during the lag phase of fibril formation are thought to be a key pathological species implicated in the toxicity in PD and other neurodegenerative diseases such as AD and may help explain the discrepancy with the Braak staging scheme (Zhang *et al.*, 2014; Ingelsson, 2016).

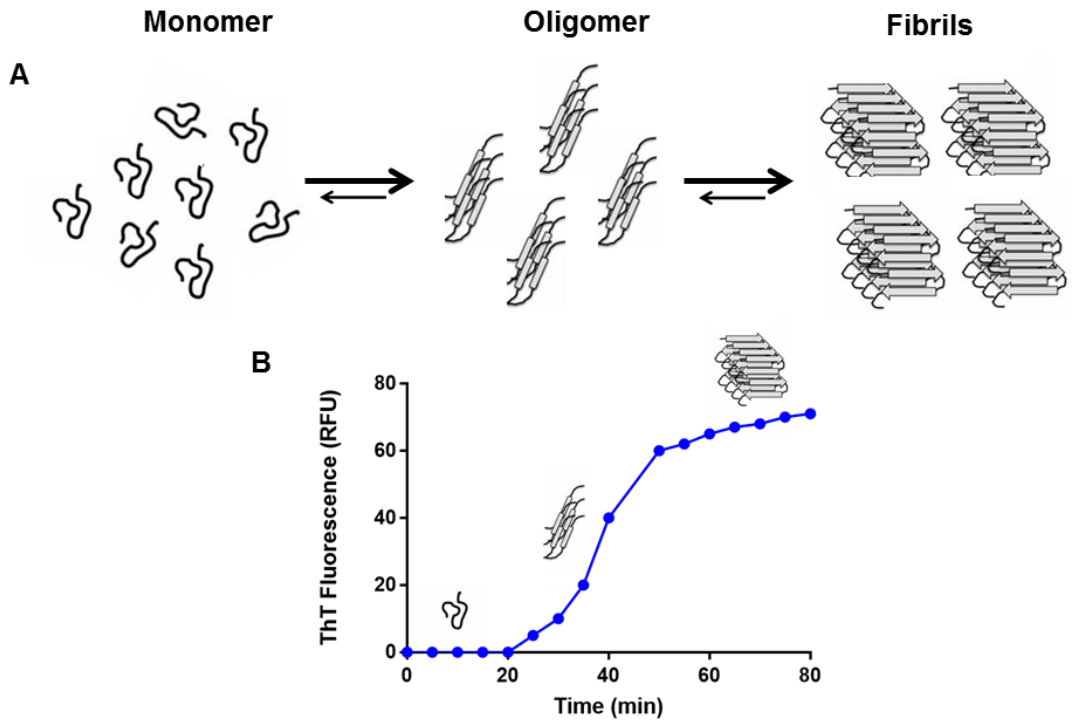

Figure 1.7. *Aggregation kinetics of amyloid*. **(A)** Simplified diagram highlighting primary nucleation events in α-syn fibrillogenesis. Several species populate the pathway to fibril formation including dimers, soluble oligomers, β-sheet-rich intermediates, small fibrils in addition to monomer, oligomers and larger fibrils. **(B)** Representative ThT fluorescence aggregation kinetics of fibril formation over time and the species that occupy these regions. Monomeric α-syn populates the lag phase (nucleation phase) which is characterised by low ThT fluorescence. In the elongation phase (fibril growth phase), oligomers are formed and ThT fluorescence increases. ThT fluorescence intensity increases upon binding of ThT to fibrillar species formed in the stationary phase. Figure adapted from (Ghosh *et al.*, 2017).

In vitro, under physiological conditions, α-syn assembles into fibrillar structures akin to the insoluble, fibrillar structure found within LBs through a series of intermediate species, known as oligomers and protofibrils (Brown *et al.*, 2018). The term 'oligomer' does not correspond specifically to a particular multimeric species of α-syn but designates a multimer that has not acquired fibrillar structure (Danzer *et al.*, 2007). 'On-pathway' soluble oligomers precede the formation of insoluble fibrils through a series of oligomeric and protofibrillar structures (Brown *et al.*, 2018). 'Off-pathway' oligomers are multimeric α-syn species arrested in an oligomeric structure and do not form fibrils (Winner *et al.*, 2011; Fagerqvist *et al.*, 2013). Toxicity of α-syn has been designated to both 'on-pathway' and 'off-pathway' oligomers by various mechanisms of action. Despite strong evidence that α-syn oligomers are the toxic species associated with PD, the heterogeneity of oligomer preparations and the ability of fibrils and oligomer to aggregate/disaggregate prevents a definitive mechanism of toxicity in disease (Cremades *et al.*, 2012).

Oligomers of α-syn can be produced through the interaction of various ligands present in neurons of the *SNPc* including dopamine, lipids, iron, copper and hydrogen peroxide (Ostrerova-Golts *et al.*, 2000; Cappai *et al.*, 2005; Smith *et al.*, 2008; Xu *et al.*, 2015; Mason *et al.*, 2016; Han, Choi and Kim, 2018). The interaction of α-syn with metal ions (e.g. iron) leads to a conformational change resulting in abnormal protein folding (Uversky, Li and Fink, 2001). Recombinant protein studies have identified specific metal-binding sites in the monomeric α-syn sequence that induce the formation of oligomers (PAIK *et al.*, 1999; Binolfi *et al.*, 2006a, 2012). Fe^{3+} has a higher affinity for α-syn binding at D121, N122 and E123 (1.2×10^{13} M^{-1}) compared to Fe^{2+} (5.8×10^{3} M^{-1}) (Binolfi *et al.*, 2006a). Phosphorylation at S129 or Y125 increases the binding affinity of α-syn for Fe^{2+} at residues 107-140 (Lu *et al.*, 2011). Binding of Fe^{3+} accelerates the aggregation of both WT and mutant and can lead to the formation of stable oligomers (in lipid membranes) (Bharathi, Indi and Rao, 2007; Schmidt *et al.*, 2012).

The exact nature of a pathological α-syn species capable of propagating throughout brain regions *in vivo* is unknown. Oligomers and fibrils can be produced *in vitro* through a variety of different methods and are likely to exert different biological functions. Oligomeric species can be produced by various protocols that differ in morphologies, including spherical, chain-like and annular oligomers. For example, incubation of monomeric protein for a shorter time period and lower temperature than fibrils followed by centrifugation has been shown to produce a species of annular oligomer capable of cell-to-cell transmission (Danzer *et al.*, 2007; Illes-Toth *et al.*, 2015). Importantly, not all oligomeric species are capable of seeding (Danzer *et al.*, 2007; Fagerqvist *et al.*, 2013). Danzer *et al.* (2007) initially described protocols that produce two distinct types of oligomers: a seeding type (Type B and Type C) and a pore-forming membrane capable of inducing neuronal cell death (Type A). Additionally, it is difficult to study the conformations of α-syn that relate to spreading of pathology due to the inability to experimentally reproduce protocols in which cells only form one type of oligomeric species, as highlighted by the identification of varying proportions of multimers in experimental models (Dettmer *et al.*, 2013; Corbille, Neunlist and Derkinderen, 2016). This experimental caveat has prevented the identification of oligomeric conformations responsible for cell-to-cell transmission in a physiological conformation (Grozdanov and Danzer, 2018).

1.4 Cellular toxicity associated with α-synuclein

Numerous studies have investigated the cellular toxicity associated with α-syn and have highlighted both gain-of-function and loss-of-function mechanisms in which α-syn modulates toxicity (Fig. 1.8). If the normal conformation of α-syn exists as an aggregation-resistant tetramer, the loss of this structure would result in the loss of ferrireductase activity within the cell. The loss of ferrireductase activity in the cell would result in dyshomeostasis of iron (Fe^{3+}/Fe^{2+}) and accumulation of the ROS-associated Fe^{2+}. In this sense toxicity would be secondary to the loss of α-syn function, with ROS-modification of cellular components and subsequent initiation of cell death pathways attributed to excess Fe^{2+} (McDowall *et al.*, 2017; Sian and Peter, 2020). In a gain-of-function mechanism, α-syn can gain a toxic conformation capable of interacting with various cellular components resulting in cellular dysfunction (Sian and Peter, 2020). Several *in vitro* and *in* vivo studies have implicated α-syn aggregation, principally the generation of prefibrillar oligomeric species, as the toxic species responsible for neurodegeneration in PD (Kahle *et al.*, 2000; Danzer *et al.*, 2007; Outeiro *et al.*, 2008; Karpinar *et al.*, 2009; Choi *et al.*, 2013, 2015). The intracellular and extracellular neurotoxic effects of oligomers have been described as toxic consequences of the interaction between α-syn oligomers and cells both *in vitro* and *in vivo*. During the course of fibril formation, α-syn oligomers have been shown to have a high affinity for binding lipids (Smith *et al.*, 2008). The highly lipophilic oligomers promote strong membrane interactions and are able to insert into the bilayer due to the presence of an oligomeric core rich in β-sheet structures (Fusco *et al.*, 2017b). Binding of α-syn oligomers to cellular membranes has been shown to disrupt cellular membrane integrity resulting in calcium influx and subsequent cell death (Volles *et al.*, 2001; Danzer *et al.*, 2007; Tsigelny *et al.*, 2012; Illes-Toth *et al.*, 2015). The interaction of α-syn oligomers with mitochondrial membranes leads to fragmentation of mitochondria and complex I impairments, leading to an accumulation of cellular ROS and mitochondrial l defects resulting in cell death (Ludtmann *et al.*, 2018). Distinguishing the mechanism of α-syn toxicity is difficult, given the heterogeneity of α-syn aggregation products and the likely interaction of cellular pathways that mediate stress responses and subsequent cell death. Some of the mechanisms in which aggregated species of α-syn interacts with cellular components to induce toxic effects are described in the following sections.

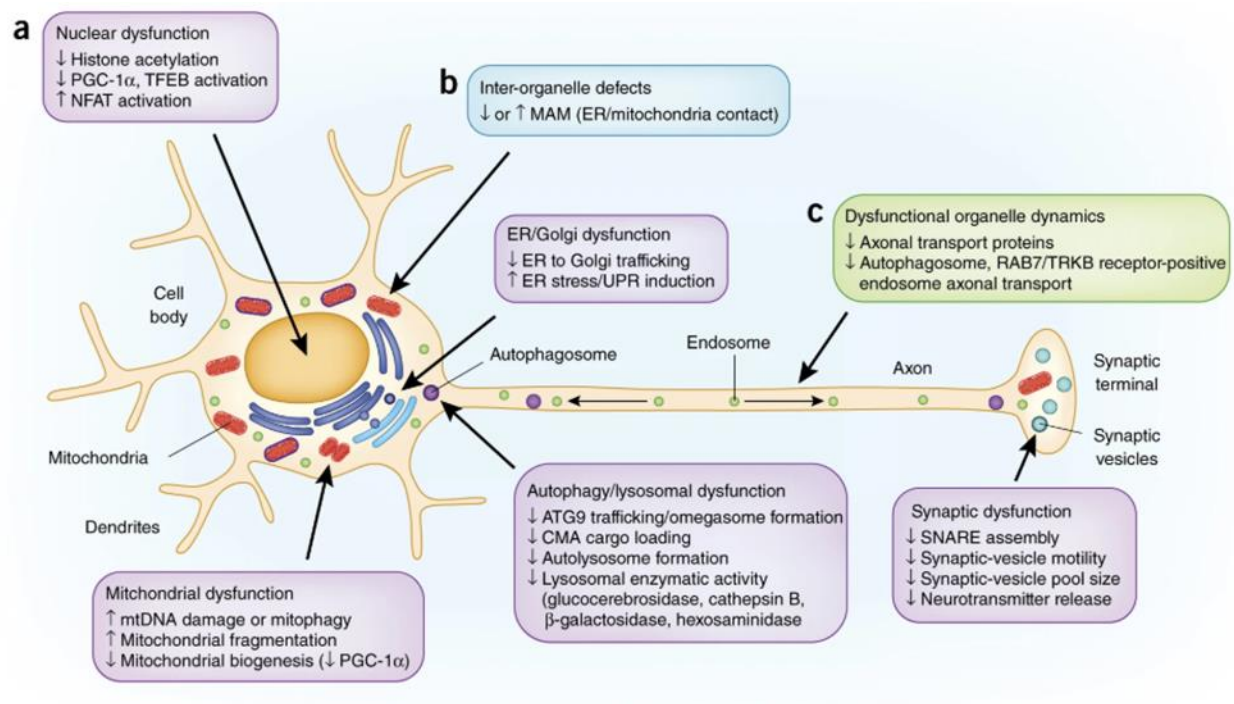

Figure 1.8. *Pathways implicated in α-syn-induced cellular toxicity.* α-Syn interacts with various cellular pathways. In disease, α-syn interacts with these pathways to induce cellular dysfunction and cellular toxicity. These interactions result in organelle dysfunction **(A)**, defects in inter-organelle contacts **(B)**, and dysfunctional organelle dynamics **(C)** which contribute to cellular dysfunction and subsequent cell death. Reprinted by permission from Elsevier: License Number 4820860567834. Springer Nature, Nature Medicine, α-synuclein toxicity in neurodegeneration: mechanism and therapeutic strategies, Yvette C Wong et al. Feb. 7, 2017 (Wong and Krainc, 2017).

1.4.1 Pore-forming and calcium influx

One of the most studied cytotoxic effects of α-syn-mediated toxicity is the interaction of α-syn species with cellular membranes. Formation of pores in biological membranes, produced as a consequence of α-syn lipid interactions is consistent with the diameter of annular and tubular protofibrils (Lashuel *et al.*, 2002), leading to membrane perturbation that results in calcium (Ca^{2+}) influx and subsequent cell death (Furukawa *et al.*, 2006; Danzer *et al.*, 2007; Gallegos *et al.*, 2015; Illes-Toth *et al.*, 2015; Angelova *et al.*, 2016). The N-terminal region of the protein is important for promoting strong membrane interactions and thus subsequent cellular toxicity (Bartels *et al.*, 2010; Fusco *et al.*, 2017a). Ellipsometry analysis of fragmented fibril structures on natively-derived SH-SY5Y cell membranes demonstrates increased membrane disruption, highlighting a toxic gain-of-function mechanism, in contrast to fibrillar structures found in amyloid plaques that exert minimal biological activity (Smith *et al.*, 2015). Continuous Ca^{2+} influx in *SNPc* neurons is important to modulate the physiological release of dopamine, therefore the pace-making activity of *SNPc* neurons is finally modulated by Ca^{2+}(Dryanovski *et al.*, 2013). Alterations in

Ca^{+} signalling by α-syn by either interfering with Ca^{2+} channels and/or altering of Ca^{2+} influx/efflux generate metabolic stress and mitochondrial damage (Ronzitti *et al.*, 2014; Guzman *et al.*, 2018).

1.4.2 Mitochondrial dysfunction

Many genes associated with the onset of familial forms of PD converge on mitochondrial function (e.g. *DJ-1*, *PINK1* etc.), thereby highlighting the crucial role of the organelle in the pathogenesis of PD (Cieri, Brini and Calì, 2017). The endogenous expression of α-syn has been reported to be required for the normal activity of mitochondria given the localisation of α-syn to mitochondria in various experimental models (Li *et al.*, 2007; Nakamura *et al.*, 2008; Di Maio *et al.*, 2016; Devoto *et al.*, 2017; Miraglia *et al.*, 2018). Mitochondria in the *SNPc* of post-mortem PD patient samples reveal the accumulation of α-syn (X. Wang *et al.*, 2019). The lipid-binding capabilities of α-syn, including the specific binding to the mitochondria-specific phospholipid cardiolipin, associates the protein with mitochondrial membranes and mitochondria-associated membranes (MAMs) (Devi *et al.*, 2008; Parihar *et al.*, 2009; Martin *et al.*, 2014; Dudek, 2017; Paillusson *et al.*, 2017).

α-Syn-induced toxicity of mitochondria has been associated with several processes including mitochondrial protein import (Devi *et al.*, 2008; Di Maio *et al.*, 2016), Ca^{2+} signalling in mitochondria (Oueslati, Fournier and Lashuel, 2010; Surmeier and Schumacker, 2013), mitochondrial fusion/fission (Nakamura *et al.*, 2011; Xie and Chung, 2012), mitophagy (Lahiri and Klionsky, 2017), impairment of complex I and energy defects (Devi *et al.*, 2008; Ludtmann *et al.*, 2018; Martínez *et al.*, 2018). The high energy demands of dopamine neurons of the *SNPc* require the continuous production of ATP from mitochondria (Bolam and Pissadaki, 2012; Surmeier, Obeso and Halliday, 2017). Impairment of complex I by α-syn can lead to energy deficits and the production of toxic cellular ROS (Reeve *et al.*, 2015a). Recently, oligomeric α-syn was shown to impair complex I respiration through the selective oxidation of ATP synthase, leading to mitochondrial lipid peroxidation and cell death (Ludtmann *et al.*, 2018). Using a *SNCA* triplication-bearing iPSC model, the aggregation of α-syn from monomeric protein into oligomeric species was shown to associate with the mitochondrial membrane (Reeve *et al.*, 2015b; Ludtmann *et al.*, 2018). This interaction of soluble β-sheet-rich oligomers with the mitochondrial membrane directly induced the opening of the permeability transition pore (PTP) (Ludtmann *et*

al., 2018). β-sheet-rich structures of oligomers interact with inner mitochondrial membrane proteins (ATP synthase) and act to inhibit complex I, which in turn, generates ROS and produces bio-energetically compromised mitochondria (Ludtmann *et al.*, 2018).

1.4.3 Synaptic dysfunction

Given the localisation of α-syn within synaptic vesicles and its suggested function as a chaperone protein in SNARE-vesicle trafficking and DAT modulation, α-syn is important for maintaining normal synaptic function (Iwai *et al.*, 1995; Totterdell, Hanger and Meredith, 2004; Burré *et al.*, 2011; Butler *et al.*, 2015). In addition, α-syn interacts with other synaptic proteins, including synapsin III, to modulate synaptic function in dopaminergic neurons through the organisation of synaptic vesicles (Zaltieri *et al.*, 2015; Atias *et al.*, 2019). Supporting the function of α-syn in synaptic regulation, knockout mouse models of α/β-syn result in altered synaptic features including synaptic structure, synaptic plasticity, neurotransmitter release and decreased dopamine levels (Chandra *et al.*, 2004; Greten-Harrison *et al.*, 2010; Oaks *et al.*, 2013).

Synaptic dysfunction is thought to be one of the early changes in PD, before the loss of dopaminergic neurons (Chesselet and Richter, 2011; Kordower *et al.*, 2013; O'Keeffe and Sullivan, 2018). Overexpression of α-syn in the rat midbrain reveals significant synaptic disruption *in vivo* as analysed by positron emission tomography (PET) radioligand to vesicular monoamine transporter-2 (VMAT2) and animals displaying progressive motor impairment (Kirik *et al.*, 2002; Phan *et al.*, 2017a). Importantly, elevated expression of α-syn induced synaptic dysfunction in the absence of neuronal loss, but with the accompanying pathological accumulation of insoluble p-α-syn (Phan *et al.*, 2017b). Moderate overexpression of α-syn results in the aggregation of α-syn found selectively at presynaptic terminals in a mouse model of PD (Kramer and Schulz-Schaeffer, 2007; Spinelli *et al.*, 2014). Under these conditions, aggregates are not observed in cell bodies and this is associated with a significant decrease in the presynaptic protein synapsin. Taken together, α-syn aggregation in presynaptic terminals is related to changes in synapse transmission (through reduction in synapsin protein), ultimately leading to a 'dying back' of axonal processes (Yasuda *et al.*, 2013; Spinelli *et al.*, 2014). In cell culture models, abnormal accumulation of α-syn aggregates is linked to interfering of axonal

transport of synaptic proteins or inhibition of synaptic vesicle reclustering leading to reduced neurotransmitter release (Nemani *et al.*, 2010; Scott *et al.*, 2010).

1.4.4 Autophagy-lysosomal/proteasomal impairment

The ALP is critical to the normal degradation of monomeric, soluble oligomeric species, and aggregated forms of α-syn. Impairment of the ALP in pathological conditions is therefore associated with the accumulation of α-syn species, which can interact with essential cellular processes or be released to the extracellular environment. Although deficiency in ALP function will result in accumulation of α-syn, α-syn itself can have detrimental effects to the function of the ALP by a 'dual loop' effect (Arotcarena, Teil and Dehay, 2019). Overexpression of WT α-syn impairs lysosomal activity and autophagosome function (Winslow *et al.*, 2010). Interestingly, dopamine-modified α-syn is associated with inhibitory effects on ALP function by several mechanisms (Martinez-vicente *et al.*, 2008). These mechanisms include forming oligomeric species at the lysosomal membrane, binding to the LAMP-2A protein on the lysosomal membrane, and preventing translocation of substrates to the lysosomal lumen, therefore blocking the degradation of CMA cellular substrates (Ho *et al.*, 2020). In both idiopathic PD patients and an iPSC model expressing WT α-syn, α-syn is capable of altering the hydrolase activity of enzymes associated with the lysosomal lumen, including Cathepsin B, GCase, β-galactosidase, or β-hexosamidase (Mazzulli *et al.*, 2011, 2016). Rather than altering total levels of hydrolases, α-syn altered the location of Rab1, a key regulator of ER-Golgi trafficking, therefore preventing trafficking and subsequent maturation of hydrolases in the Golgi (Mazzulli *et al.*, 2016).

The presence of mono-, di- and tri-ubiquitinated α-syn in LBs of patients with PD, highlight the dysfunction of the UPS in disease (McNaught and Jenner, 2001; McNaught *et al.*, 2003; Walden and Muqit, 2017). The UPS is a proteolytic complex responsible for maintenance of cellular protein homeostasis through cleavage of ubiquitinated polypeptide chains into short peptides to aid in cellular clearance. Impairment of the proteasome prevents degradation of proteins, resulting in the formation of intracellular protein aggregates (Lindersson *et al.*, 2004). α-Syn is degraded by the proteasome when the protein is in its monomeric form (Webb *et al.*, 2003; Mo *et al.*, 2012). In contrast, aggregated forms of α-syn have a longer half-life, which is degraded by the lysosomal pathway (Mo *et al.*, 2012). Alterations in either of

these pathways could lead to dysfunction of the other, leading to the accumulation of α-syn ultimately leading to degeneration and death of dopaminergic neurons (Wang *et al.*, 2015).

Triggering of the unfolded protein response and persistent endoplasmic reticulum stress by the accumulation of misfolded proteins, including α-syn, has been demonstrated to lead to activation of the cell death cascade and subsequent apoptosis (Smith *et al.*, 2005; Ogen-Shtern, Ben David and Lederkremer, 2016). Proteasomal impairment and oxidative stress are continuing themes in neurodegeneration, attributing to altered biochemical functions within cells. Overexpression of A53T α-syn in PC12 cells increased cell death through the inhibition of proteasome function as well as producing a significant increase in the intracellular level of ROS (Smith *et al.*, 2005).

1.5 α-Synuclein is a prion-like protein

1.5.1 Prion hypothesis

Transmissible spongiform encephalopathies (TSEs), or prion disorders, are a curious class of fatal neurodegenerative disorders caused by infectious prion protein. TSEs are characterised by the accumulation of β-sheet-rich protein aggregates and substantial neurodegeneration (Aguzzi and Lakkaraju, 2016). In humans, prions are associated with Creutzfeldt-Jakob disease (CJD), Gerstmann-Straüssler-Scheinker (GSS) disease, familial fatal insomnia (FFI), Kuru and variant CJD (vCJD). In animals, prions are associated with bovine spongiform encephalopathy (BSE), commonly known as 'mad cow disease' in cattle, scrapie in sheep and goats and chronic wasting disease of the Cervidae family in nonhumans (Collinge, 2001). Pathological features of TSEs include brain vacuolation, astrogliosis, neuronal apoptosis and accumulation of abnormal PrP isoforms in the CNS, a feature common to prion disorders in other mammalian species, including scrapie in sheep. Attempts to classify the infective agent associated with TSEs led scientists to conclude a slow virus was responsible for the disease following epidemiological evidence of a long lag phase of over 30 years in some cases (Alper *et al.*, 1967; Rudge *et al.*, 2015). Experimental attempts to inactivate the scrapie agent using formalin, UV and ionising radiation, extreme heat and high pressure suggested a virus substantially different from any previously discovered (Pattison, 1965; Alper *et*

al., 1967; Prusiner, 1982). The controversial 'protein-only' hypothesis, first indicated by Alper and Griffith in 1967, and later expanded upon by Prusiner in 1982 describes prions as infectious protein particles devoid of nucleic acids, instead able to encipher infectivity through the propagation of misfolded protein (Alper *et al.*, 1967; Prusiner *et al.*, 1982).

The normal cellular prion protein (PrP^{C}) is a natively unfolded glycosylphosphatidylinositol- variably N-glycosylated anchored membrane glycoprotein encoded by the highly conserved *PRNP* gene (Bolton, Meyer and Prusiner, 1985; Basler *et al.*, 1986; Stahl *et al.*, 1987). Conversion of the mainly α-helical PrP^{C} to the β-sheet rich disease-associated isoform, PrP^{SC}, is the key pathogenic event associated with prion disorders although this is mechanism is not completely understood. Spectroscopic studies demonstrated PrP^{SC} is biochemically distinct to PrP^{C}, with specific differences in the biophysical structure associated with the change in conformation from α-helices to β-sheets (Pan *et al.*, 1993; Riek *et al.*, 1996; Vázquez-Fernández *et al.*, 2016). The PrP^{SC} conformation was originally determined to be resistant to proteinase K (PK) digestion, denoted as PrP^{RES}, although it should be noted that PK resistance is a relative concept that depends critically on various factors including PK concentration and the prion strain (McKinley *et al.*, 1991; Weissmann, 2004). Classically, identification of PrP^{SC} involves removal of PrP^{C} by PK digestion and subsequent characterisation of electrophoretic bands indicative of the prion strain detected by anti-PrP antibodies (Kuczius and Groschup, 1999; Shan *et al.*, 2016); however, it has become apparent PK-sensitive PrP^{SC} is related to infectivity and conversion of PrP^{C}, therefore, PK digestion does not always correlate PrP^{SC} conformations to diseased states (Silveira *et al.*, 2005; Pastrana *et*

al., 2006).

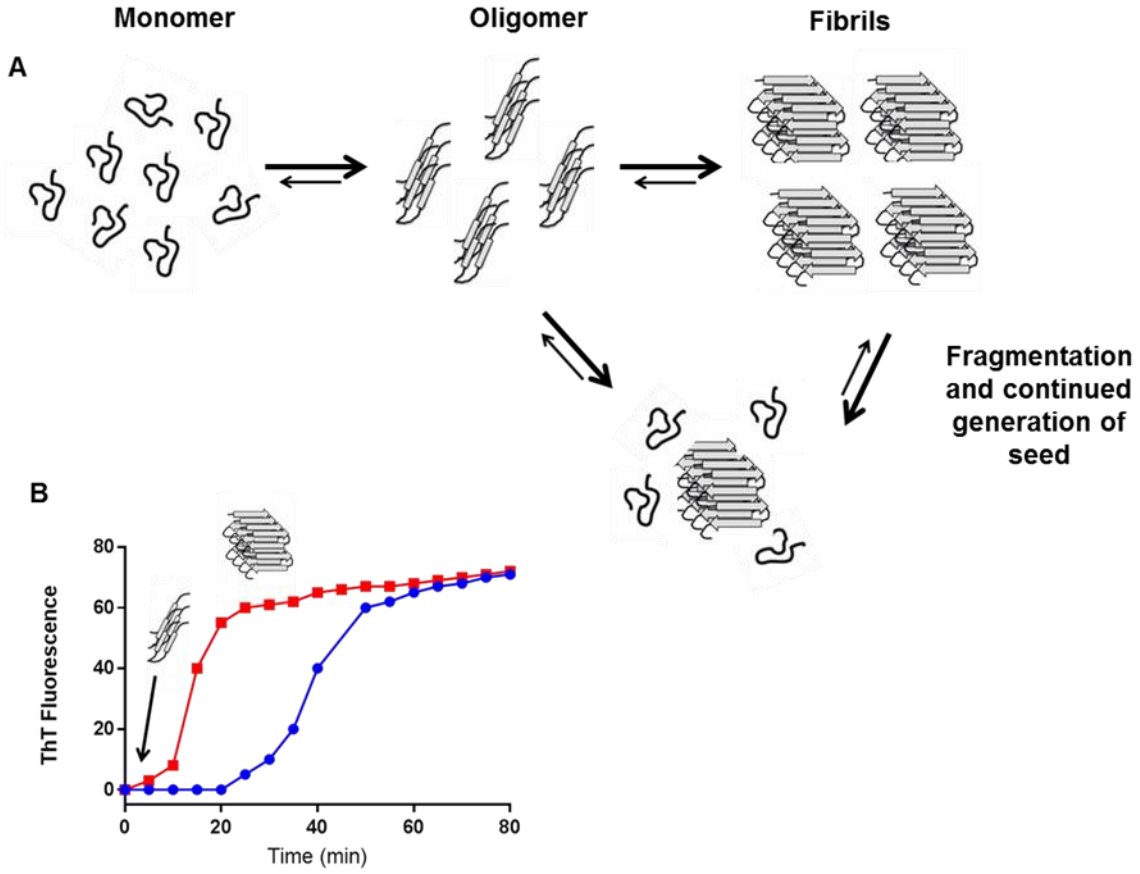

Figure 1.9. *Secondary nucleation events associated with continued generation of seed in PrP^{SC}*. **(A)** Secondary nucleation events associated with continued generation of seed in PrP^{SC} (and other amyloidogenic proteins). Fragmentation of fibrils allows for secondary nucleation points for the interaction of monomeric protein and subsequent oligomer/fibril formation. **(B)** Representative ThT fluorescence kinetics of fibril formation following the addition of an oligomeric/fibrillar seed. Lag phase is shortened due to the presence of nucleation surface for the recruitment of monomer. Time taken to reach stationary phase is reduced as fibrils are produced quicker in the presence of seeds. Co-factors may aid in the propagation of prions by a) catalyst for induction of PrP^{SC} from interaction with PrP^{C}; b) interact to stabilise PrP^{SC}; c) interaction with oligomeric structure to produce alternative strains; d) generation of infective seed through fragmentation of fibrillar structures. Image adapted from (Ghosh *et al.*, 2017).

In vitro conversion of PrP^{C} to PrP^{SC} has been demonstrated in cell-free systems and the few permissive cell lines which maintain PrP^{SC} infectivity over several passages, including the murine neuroblastoma line (N2a), the rat adrenal phaeochromocytoma (PC12) and hypothalamic neuronal line (GT1) (Supattapone, 2004; Weber *et al.*, 2006; Castilla *et al.*, 2008). From these models, it is understood PrP^{SC} catalyses the accumulation of misfolded protein in a nucleation-polymerisation reaction akin to crystal growth and fragmentation (Jarrett and Lansbury, 1993; Knowles *et al.*, 2009). In this sense, PrP^{SC} acts as a seed that enciphers its structure onto the natively expressed PrP^{C} based on the stoichiometry of the molecule, allowing for the growth of oligomeric/protofibrillar structures present in the plaques associated with TSEs

including Kuru, consistent with the observation that *PRNP*$^{o/o}$ knockout mice do not propagate PrP^{SC} (Bueler *et al.*, 1992; Nishina *et al.*, 2006). A secondary nucleation event, aggregate fragmentation, is crucial to the propagation and infectivity associated with prion infections (Fig. 1.6), thus enabling the production of seeds for PrP^{SC} to elongate and multiply, demonstrated in non-Mendelian heritability of the yeast prions *URE3* and *PSI*$^{+}$ and protein misfolded cyclic amplification (PMCA) reactions (Wickner, 1994; Saborio, Permanne and Soto, 2001; Bieschke *et al.*, 2004; Liebman and Chernoff, 2012).

1.4.1.1 Cell-to-cell propagation of PrP^{SC}

PrP^{SC} molecules can spread *in vitro* and *in vivo* vertically, to progeny, and horizontally, to neighbouring cells, providing production of prions overcomes protein quality control mechanisms (Deriziotis *et al.*, 2011). Vertical transmission of prions in mammalian cells is modulated by cell division (Ghaemmaghami *et al.*, 2007) and is hypothesised to aid in prion propagation through the production of secondary nucleation events which occur following mechanical sheering during cell division (Knowles *et al.*, 2009). Vertical transmission may be important in the spreading of prions in the periphery, where PrP^{SC} replicates in the lymphoreticular system (McCulloch *et al.*, 2011; Srivastava *et al.*, 2015), in contrast to the post-mitotic cells of the CNS which may impede vertical transmission. The most common laboratory method to administer PrP^{SC} into experimental animals is intracerebral inoculation, however, ingestion of prions is the most common mechanism for the spread of the disease in nature. Speculatively, change in transmission from vertical to horizontal (which is generally less efficient) (Ghaemmaghami *et al.*, 2007) may represent the long lag phase associated with neuroinvasion in the pathogenesis of natural prion diseases, which is partially circumvented using experimental animal models of prion diseases. Therefore, in the CNS, horizontal transmission of prions may be central to disease progression, resulting from PrP^{SC} hijacking of methods of cell-to-cell to communication such as exosomes and tunnelling nanotubes (TNTs) to facilitate intercellular spread in conjunction with direct cell-to-cell contact (Kanu *et al.*, 2002; Paquet *et al.*, 2007; Victoria *et al.*, 2016).

Exosomal transmission of PrP^{SC} is well documented as a method of pathogen transfer and stimulating release of exosomes increases the intracellular transfer of prions (Guo, Bellingham and Hill, 2016). These small (50-200 nm) membrane-bound

extracellular vesicles are found in most biological fluids and are determined to be generated by the trafficking of multivesicular bodies from the cytosol to the cell surface (Harding, Heuser and Stahl, 1983; Johnstone *et al.*, 1987). Following secretion from cells, exosomes are taken up by other cells by one of three pathways: 1) captured by neighbouring cells; 2) internalised by cells at a certain distance or; 3) taken up by cells of distant tissues by utilising the systemic circulation (Pant, Hilton and Burczynski, 2012; De Toro *et al.*, 2015). Exosomes are reported to function in cell-to-cell communication and modulation of the immune response (Basso and Bonetto, 2016), however, these vesicles, along with other multivesicular bodies such as microvesicles and apoptotic cell bodies, are becoming increasingly linked to disease pathogenesis and progression in a variety of disorders, including neurodegeneration, cancer, HIV and others (Madison and Okeoma, 2015; Zhang *et al.*, 2015). It is interesting to note over 11,000 proteins have been identified in exosomes along with mRNA, miRNA and lipids and most are not associated with disease (Mathivanan *et al.*, 2012). Various cell types secrete PrP^{C} and PrP^{SC}, in association with exosome-like vesicles including glial cells (Fevrier *et al.*, 2004); activated platelets (Robertson *et al.*, 2006); primary cultured cortical neurons (Fauré *et al.*, 2006); neuroblastoma cells (Alais *et al.*, 2008; Veith *et al.*, 2009) and monocytes (Wang *et al.*, 2010). There is increasing evidence to suggest PrP^{SC} transmission in the blood and plasma is associated with exosomes (Saá *et al.*, 2014; Properzi *et al.*, 2015). In addition to the transfer of PrP alone, evidence suggests that exosomes may be important in the transfer of cofactors required for prion conversion, in particular lipids and RNA (Wang *et al.*, 2007, 2010; Deleault *et al.*, 2012; Srivastava and Baskakov, 2015) or by the association of PrP to lipid rafts in exosomal membranes are thought to play a role in PrP^{SC} conversion (Taylor and Hooper, 2006; Marijanovic *et al.*, 2009). Furthermore, exosomal packaging may represent alternative processing of PrP which may aid in infectivity following the observation of N-terminally distinct exosomal-derived PrP (Vella *et al.*, 2007; Wik *et al.*, 2012; Guo, Bellingham and Hill, 2015). Although the size and conformation of PrP^{SC} have not consistently been identified, a study by Coleman *et al.* (2012) demonstrated prion infectivity in exosomes at a maximum of 150 nm in diameter, suggesting PrP^{SC} or the infectious entity to be inherently small (Coleman *et al.*, 2012). Aβ neurotoxicity was reduced by exosomal PrP^{C} enhancing Aβ fibrillisation,

highlighting a protective effect of exosomal PrP in molecular mechanisms of AD (Falker *et al.*, 2016).

TNTs represent another method of cell-to-cell communication that assists in intercellular transfer of PrP^{SC} (Gousset *et al.*, 2009). TNTs are F-actin-based structures with diameters of 50 to 200 nm and a length of several cell diameters observed in a variety of cell types, forming complex cellular networks that enable the transfer of organelles and other material between cell types (Rustom *et al.*, 2004; Wang and Gerdes, 2015). Combining both vesicle transport and TNTs, these dynamic structures have been shown to traffic PrP^{SC} aggregates through TNTs in endosomal vesicles (Zhu *et al.*, 2015). Taken together, these data suggest prions utilise several routes for efficient intercellular spreading, but it is unclear whether these differences represent PrP^{SC} strain types or potentially varying culture conditions.

1.5.2 Insights into the prion-like nature of α-synuclein from *in vitro* cell culture models

Although there are several mechanistic similarities between the proteins involved in neurodegeneration such as α-syn (in PD), tau and A-β (in AD), huntingtin (in Huntingtin's disease) and superoxide dismutase (SOD1 in ALS) and PrP, there is reluctance to use the term 'prion' to describe these diseases. There is no evidence of transmissibility of disease between individuals in contrast to the highly infective nature of prion diseases (Cersosimo, 2015; Jaunmuktane *et al.*, 2015; Abbott, 2016). Instead, a series of terms including 'prion-like', 'propagon', 'prionoid' has been used to describe the proteins related to these protein-misfolding diseases where some, but not all, of the molecular features of prion diseases exist (Harbi and Harrison, 2014; Aguzzi and Lakkaraju, 2016). Recent research, utilising *in vitro* cell culture models of α-syn aggregation and propagation highlight intriguing similarities of PrP, these are listed below.

1.4.5.1 Seeding and cell-to-cell propagation of α-synuclein

The staging of α-syn-immunopositive pathology through post-mortem observations by Braak and colleagues suggested a predictable pattern of disease propagation following long unmyelinated axons of known anatomical pathways (Fig. 1.7) (Heiko Braak, Del Tredici, *et al.*, 2003; Hawkes and Braak, 2007). The 'dual-hit' hypothesis

suggests the spread of pathology initiated by an unknown neurotrophic pathogen/virus via olfactory and gastric routes of entry (Hawkes and Braak, 2007; Manfredsson *et al.*, 2018; Uemura *et al.*, 2018). The neurotrophic agent was speculated to 'possess unconventional prion-like properties' and potentially consist of misfolded α-syn fragments that induce the spread of PD pathology (H. Braak *et al.*, 2003; Dagher and Zeighami, 2018). The discovery of LBs immunopositive for α-syn and ubiquitin in graft neurons 11-18 years following the transplantation of dopaminergic neurons in the striatum of individuals with PD, has propelled the idea of α-syn as a 'prion-like' protein (Jeffrey H Kordower *et al.*, 2008; Jeffrey H. Kordower *et al.*, 2008; Li *et al.*, 2008). In this context, the 'prion-like' capacity of α-syn enabled the spread of α-syn from diseased neurons to the relatively young, newly implanted graft neurons (Jeffrey H Kordower *et al.*, 2008; Jeffrey H. Kordower *et al.*, 2008; Li *et al.*, 2008). The development of LB pathology was shown to be a progressive process (e.g. whole LBs do not move from cell to cell) suggesting the transfer of a seed that could initiate the development of pathology in transplanted neurons (Chu and Kordower, 2010; J.-Y. Li *et al.*, 2010). Application of oligomeric/fibrillar species to both cultured cells and animal models provide a 'seed' or nucleation site for the recruitment of monomeric protein in the process of nucleation-dependent fibrillisation leading to the development of cellular inclusions reminiscent of LB pathology (Paula Desplats *et al.*, 2009; Iljina *et al.*, 2016).

Although α-syn does not contain a classical secretory signal for extracellular release, both soluble and aggregated forms of the protein have been detected in culture media (secreted by living neurons), brain interstitial fluid, CSF, saliva and plasma (Lee, 2005; Paleologou *et al.*, 2009; Emmanouilidou *et al.*, 2010; Hansson *et al.*, 2014). Given the detection of a normally cytoplasmic protein found in the extracellular milieu, mechanisms of cellular clearance of α-syn are important mediators of seeding and propagation (Lee, 2005). Extracellular α-syn release depends on several factors including rate of proteasomal degradation (Bennett *et al.*, 1999; Webb *et al.*, 2003; Zondler *et al.*, 2017); the rate of lysosomal degradation (Paxinou *et al.*, 2001b; Alvarez-Erviti *et al.*, 2011; Wong and Krainc, 2016); post-translational modifications of the protein (e.g. phosphorylation, ubiquitination, SUMOylation); intracellular levels of α-syn (Reyes *et al.*, 2015); the mutated form of the protein (e.g. A30P, A53T etc.) (Conway *et al.*, 2006; Lázaro *et al.*, 2014);

potential release of α-syn upon the death of neurons (Omar M.A. El-Agnaf *et al.*, 1998; Ulusoy *et al.*, 2015); accumulation of misfolded/damaged proteins (Jang *et al.*, 2010) and export in exosomes (Emmanouilidou *et al.*, 2010; Danzer *et al.*, 2012; Marie *et al.*, 2015). In an inducible pluripotent stem cell (iPSC)-derived neuronal model, high levels of intracellular α-syn through the expression of an *SNCA* gene triplication results in high levels of secreted α-syn (Reyes *et al.*, 2015). This is important when considering aging is the greatest risk factor for the development of disease and presumed to be associated with higher levels of α-syn (Tyson, Steiner and Brundin, 2016). In addition, an increase in oligomeric species is associated with an aging brain (Chen *et al.*, 2015). Mechanisms to degrade released α-syn can potentially prevent the transmission of pathology, through the removal of the pathological conformation of the protein. However, in the aging brain, these mechanisms may have declined in the natural aging process leading to the accumulation of aggregated species that evade clearance and subsequently spread pathology to neighbouring cells.

The uptake of α-syn by recipient cells allows for the perpetuation of pathological spread and can occur through several mechanisms. Extracellular α-syn can be taken up by neighbouring cells by various mechanisms including passive diffusion through the plasma membrane (Jiang *et al.*, 2017); internalisation by endocytic processes (pinocytosis and phagocytosis) (Lee, 2005; Paula Desplats *et al.*, 2009); interaction through TNTs (Gousset *et al.*, 2009; Nath *et al.*, 2012; Abounit *et al.*, 2016) and exposure of cells to exosomes containing α-syn as cargo (Guo, Bellingham and Hill, 2016). Uptake of extracellular α-syn by passive diffusion through the plasma membrane was shown to occur by monomeric protein but not oligomeric or aggregated structures (Grozdanov and Danzer, 2018). In contrast, aggregated α-syn is preferentially taken up by receptor-mediated endocytosis through the interaction of surface receptors such as the α3+-subunit of Na+/K+ - ATPase, LAG3 and neurexin-1 (Shrivastava *et al.*, 2015; Mao *et al.*, 2016). Following endocytosis aggregated α-syn species can induce lysosomal membrane rupture and subsequent release of pathological species into the cytoplasm (Freeman *et al.*, 2013). Evasion of

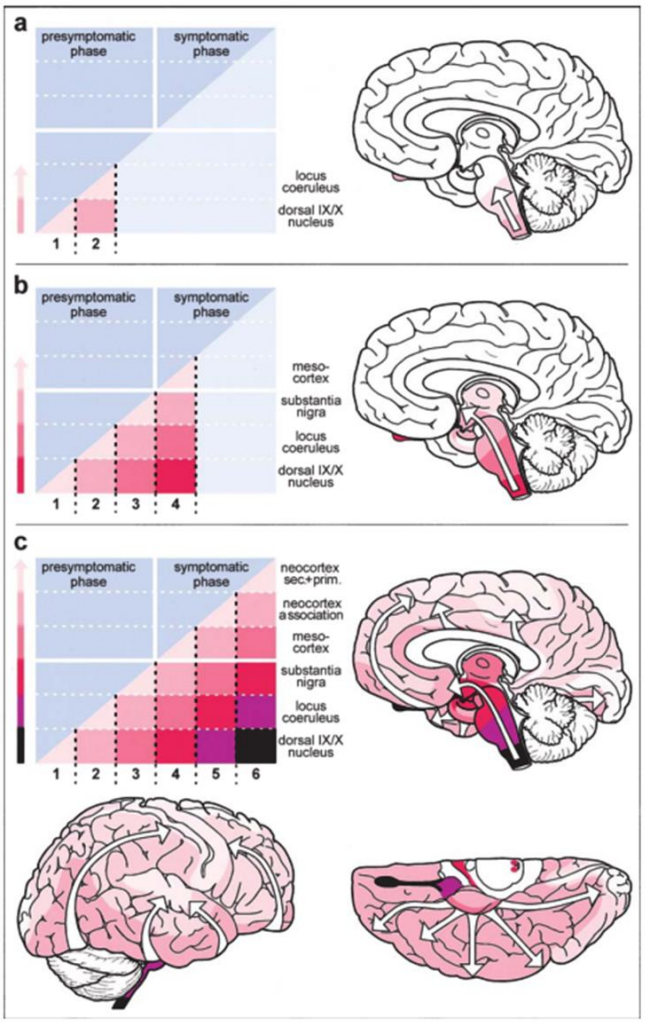

Figure 1.10. *Progression of α-syn-immunopositive pathology as described in the Braak hypothesis of α-syn spread of pathology*. **(A)** Stage 1-2: In the presymptomatic phase of disease progression, the earliest lesions are associated with the olfactory bulb and dorsal IX/X motor nucleus (stage 1), followed by lesions appearing in the caudal raphe nuclei, reticular nucleus and locus coeruleus (stage 2). **(B)** Stage 3-4: Pathology steadily moves upwards into the mesencephalic tegmentum and portions of the prosencephalon, with lesions in the substantia nigra pars compacta. Cortical involvement is evident with lesions in the temporal mesocortex and allocortex. **(C)** Stage 5-6: Areas of high order sensory association in areas of the neocortex and prefrontal neocortex develop lesions plus pathology of previous stages (stage 5). In the final stage (stage 6) pathology extends further into first order sensory association areas and occasionally primary sensory and motor fields. Impaired cognition is commonly associated with this final phase of PD progression, related to the damage in the neocortex (Heiko Braak, Tredici, *et al.*, 2003; Watson and Leverenz, 2010). Image reference: (Braak *et al.*, 2003)

degradation mechanisms of the endo-lysosomal vesicles by aggregated α-syn allows for access of the pathological protein to the cytoplasm of cells and acts as a seed to recruit normal cellular protein (Victoria and Zurzolo, 2015). Exosomes have been demonstrated to efficiently transport oligomeric species into recipient cells (Danzer *et al.*, 2012; Stuendl *et al.*, 2016). Delenclos *et al.* (2017) demonstrate the preparation of cell-produced α-syn oligomers results in a small proportion of exosome-associated α-syn, in contrast to free α-syn oligomers that are not efficiently internalised by the cells. However, exosomes were readily internalised inside recipient cells in contrast to free α-syn oligomers (Bliederhaeuser *et al.*, 2016; Delenclos *et al.*, 2017). The increased propensity of α-syn to aggregate by exosomes could provide an environment favourable for the oligomerisation process and subsequent spreading of pathology (Delenclos *et al.*, 2017).

1.6 Aims and objectives

Overall aim:

The hypothesis was that 3D cell culture can be used to model the templated propagation of α-syn. Building on the recent publications describing a specific species of oligomeric α-syn able to induce aggregation of intracellular α-syn in a traditional 2D cell culture model and the demonstration that 3D cell culture increases development of aggregate formation in an AD disease model, we sought to develop a PD-relevant 3D culture system to investigate the propagation of these previously described species (Danzer *et al.*, 2007; Choi *et al.*, 2014, 2016; Illes-Toth *et al.*, 2015).

The specific goals were:

- To develop a human-relevant cell culture model of PD, utilising the human neuroblastoma SH-SY5Y cell line.
- To develop methods for assessing the intracellular aggregation of α-syn in the 3D model.
- Characterise the formation of α-syn aggregates in the 3D model and determine whether these aggregates recapitulate traditional 2D cell culture systems.
- Investigate the impact of the newly discovered cell death pathway, ferroptosis, on the intracellular aggregation of α-syn in the 3D model.
- Characterise the action of ferroptosis inhibitors on the development of α-syn aggregates.

Chapter 2 : Materials and Methods

2.1 Cell culture

2.1.1 SH-SY5Y cell culture

All cell manipulations were undertaken in sterile conditions in a Grade II laminar flow hood. SH-SY5Y human dopaminergic neuroblastoma cells (Cat. No. 94030304, ECACC, Public Health England, Salisbury, UK) were maintained at 37^{o}C, 5% CO_2 in high glucose Dulbecco's modified Eagle's GLUTAMAX^{TM} medium (DMEM; Cat. No. 61965026, Gibco, ThermoFisher Scientific, Warrington, UK) supplemented with 10% (v/v) foetal bovine serum (FBS, batched, Cat. No. 10500-064, Gibco) and 1% (v/v) penicillin-streptomycin (P/S, Gibco). To subculture, the culture medium was removed, and cells were washed in phosphate-buffered saline (PBS, Gibco) to remove traces of serum before incubation with trypsin. 3 mL trypsin-EDTA (0.05% (v/v), Gibco) per 75 cm^2 flask was incubated with the cells for approximately 2-3 mins at 37^{o}C, or until cells were visibly detached from the culture flask. Trypsin-EDTA was inactivated following the addition of an equal volume of culture medium with 10% (v/v) FBS added. The resulting cell suspension was counted using a haemocytometer and the cell density was adjusted for use in experiments or subculture. Cells were purchased at passage 11 and used until passage 21, to prevent loss of neuronal characteristics as per ECACC culture guidelines.

2.1.1.1 Cryopreservation of SH-SY5Y cells

Cells were grown in culture flasks until 70-80% confluency before cryopreservation. Cells were trypsinised and resuspended in 3 mL DMEM supplemented with 10% (v/v) FBS and 1% P/S (v/v). Cell viability was determined by counting cells using a haemocytometer and trypan blue cell stain (0.4%, Gibco). Only cell populations with a percentage viability >90% were frozen to achieve a good recovery after freezing. Cells were centrifuged at 1,000 rpm for 5 mins before resuspension in freezing medium (90% FBS: 10% DMSO) at a concentration of 2 x 10^6 cells/mL. One mL aliquots of freezing medium and cells in cryoprotective ampules were placed inside a Nalgene Mr Frosty™ container filled with isopropyl alcohol and placed in a -80^{o}C freezer to gradually freeze at 1^{o}C/minute overnight. Frozen ampules were transferred to the vapour phase of liquid nitrogen.

2.1.1.2 Differentiation of SH-SY5Y cells

Differentiation of SH-SY5Y cells into a more neuronal phenotype was undertaken using three different protocols and their suitability for adaptation into a 3D culture system was assessed. The following protocols were used: all-*trans*-retinoic acid (RA; Cat. No. R2625, Sigma-Aldrich, Dorset, UK) alone, sequential treatment with RA and aphidicolin (Cat. No. 10583155 Fisher Scientific, Leicestershire, UK) and sequential treatment with RA and brain-derived neurotrophic factor (BDNF; Cat. No. 450-02, Peprotech, London, UK). For differentiation with RA alone, cells were cultured in 10 µM RA for 5-14 days in DMEM supplemented with either 1% (v/v) or 10% (v/v) FBS. For differentiation with RA and aphidicolin (0.1 µM, 0.3 µM or 0.5 µM aphidicolin), cells were cultured in 10 µM RA for 5 days. After 5 days, the culture medium was replaced with aphidicolin-containing culture medium and incubated for a further 9 days. For differentiation with RA and BDNF, Cells were seeded at an initial density of 15,000/cm^2 in DMEM media supplemented with 10% (v/v) FBS, 1% (v/v) P/S and the addition of 10 µM RA. After 5 days in the presence of RA, cells were washed with serum-free DMEM, trypsinised and transferred to Matrigel-coated (Matrigel™ growth-factor-reduced phenol-red free, Cat. No. 356231, Lot: 7086009, Corning, UK) 8-well chamber slides (Nunc Lab-Tek® Chamber Slide™, ThermoFisher) in serum-free DMEM with 50 ng/mL BDNF. After 7 days in BDNF-supplemented serum-free DMEM cells were ready for experimentation (Encinas *et al.*, 2000).

2.1.1.3 3D cell culture

Cells were pre-differentiated with RA in uncoated T75 flasks for 5 days before seeding into 3D Matrigel™ cultures. Matrigel™ was diluted to 6 mg/mL total protein with ice-cold serum-free DMEM and vortexed with cell pellets for 10 s, to a final cell concentration of approximately 7.5 x 10^6 cells per mL of diluted Matrigel™. Using pre-chilled pipettes, Matrigel™/cell mixtures were transferred to either pre-warmed 8-well chamber slides or tissue culture inserts (ThinCerts, 0.4 µm pore size, Cat. No. 662641, Greiner Bio-One, Gloucestershire, UK), at 100 µL and 300 µL volumes respectively, and incubated at 37^{o}C for 1 h to form a gel. Following solidification of the 3D gels, pre-warmed serum-free DMEM supplemented with 50 ng/mL BDNF was added to the cultures and cells differentiated for a further 7 days. Media was changed every 3-4 days. After 7 days in 3D, cultures were treated with either oligomers or metals for 24 h.

2.1.1.4 Treatment with oligomers/iron (II) chloride

When treating with oligomers, 10% (v/v) oligomers were added alongside cultures treated with 10% (v/v) solvent (sodium phosphate buffer + 20% ethanol), 10% (v/v) monomeric α-syn and media-only control for 24 hrs. Preparation of oligomers is stated in section 2.10.3. For metal treatments, 1000 µM iron (II) chloride was added to 3D cultures alongside 200 µM (II) chloride, solvent-only control (NTA only) and media-only control for either 24 or 72 hrs (Fig. 2.1). The “continual stress” group was subjected to fresh treatments of iron (II) chloride (and controls) every 24 hrs for a total of 72 hrs before cellular analysis, in contrast to a singular treatment of iron (II) chloride (and controls) (Fig. 2.1).

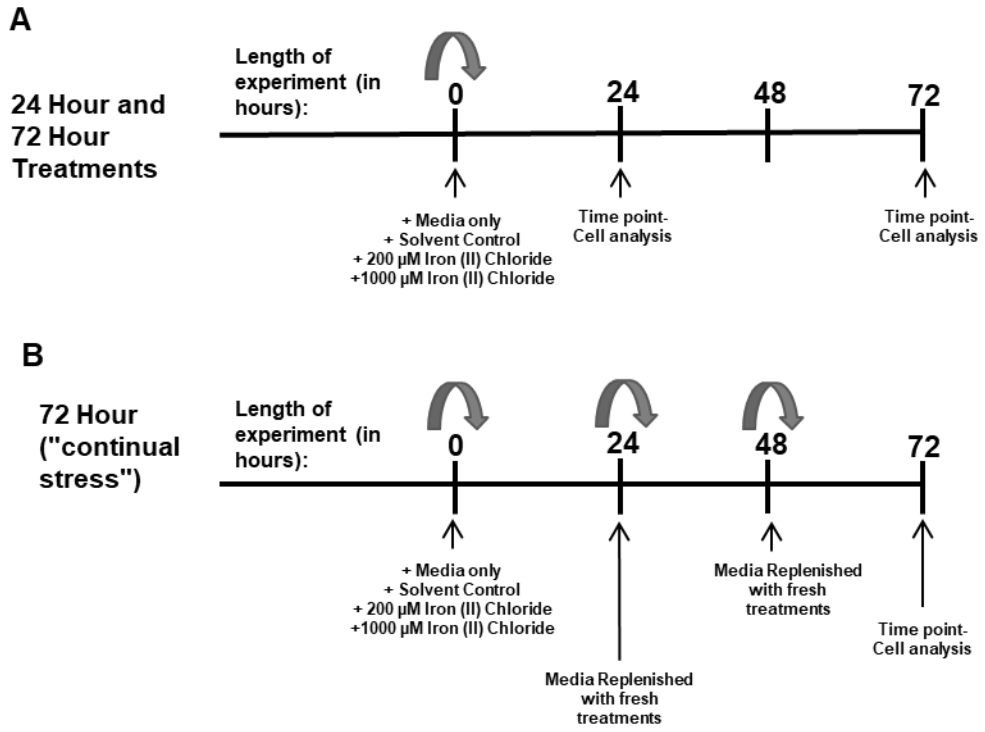

Figure 2.1. *Schematic representation of cell culture treatments*. **(A)** Cells were treated with either media only, solvent control, 200 µM iron (II) chloride and 1000 µM iron (II) chloride **once** for the duration of the experiment at time 0, followed by analysis at either 24 or 72 hrs. **(B)** Cells were treated with either media only, solvent control, 200 µM iron (II) chloride and 1000 µM iron (II) chloride **three times** during the course of the experiment (at 0, 24 and 48 hrs), followed by analysis at 72 hrs from initial iron treatment.

2.1.2 LUHMES cell culture

The Lund human mesencephalic cell line (LUHMES) was purchased from ATCC® (Cat. No. CRL-2927, Virginia, USA). For LUHMES culture, cell culture flasks and multi-well plates pre-coated with 50 µg/mL poly-L-ornithine and 1µg/mL fibronectin (Cat. Nos. P3655 and F0895, Sigma-Aldrich) dH_2O were used, to aid in adhesion of

neuronal cells to culture surfaces. Flasks were coated with 50 µg/mL poly-L-ornithine overnight at room temperature (RT). After removal of the coating solution, culture vessels were washed twice in dH_2O and left to air dry prior to coating with 1µg/mL fibronectin for 3 hrs at RT. Removal of the coating was followed by a further wash with dH_2O and air-dried before cell seeding.

LUHMES cells were grown at 37^oC in a humidified 95% air, 5% CO_2 atmosphere. Proliferating LUHMES cells were grown in proliferation medium consisting of Advanced Dulbecco's modified Eagle's medium/F12 without L-glutamine (DMEM/F12; Cat. No. 10-090-CV, Corning), 1x N-2 supplement (Cat. No. 17502048, Invitrogen), 1x GlutaMAX™ (Cat. No. 35050061, Gibco), 40 ng/mL recombinant basic fibroblast growth factor (bFGF; Cat. No. 100-18B, Peprotech) and 1% (v/v) P/S. For passaging (at 85% confluency), cells were washed with PBS and incubated with 4 mL trypsin (0.05% trypsin-EDTA) for approximately 5 mins at 37^oC, whilst monitoring cell detachment under an inverted microscope. Twelve mL of pre-warmed wash medium (DMEM/F12 + 1% (v/v) P/S) was added to each flask and cells aspirated by pipetting over the flask. The cell suspension was centrifuged at 300 x g for 5 mins at 18^oC and the supernatant was discarded. Cell pellets were resuspended in 3 mL wash media and counted before seeding into pre-coated T75 flasks. Three million cells were seeded for 2-day maintenance. Two million cells were seeded for 3-day maintenance. Ten mL of proliferation media was used per flask.

2.1.2.1 Cryopreservation of LUHMES

Cells were grown in culture flasks until 80-90% confluency prior to cryopreservation. Cells were trypsinised and resuspended in 3 mL DMEM/F12 supplemented with 20% (v/v) FBS and 1% (v/v) P/S. Cell viability was determined by counting cells using a haemocytometer and trypan blue cell stain. Only cell populations with a percentage viability >90% were frozen in order to achieve a good recovery after freezing. Cells were centrifuged at 300 x g for 5 mins at 18^oC before resuspension in freezing medium (proliferation media supplemented with 20% (v/v) FBS and 10% (v/v) DMSO) at a concentration of 3 x 10^6 cells/mL. One mL aliquots of freezing medium and cells in cryoprotective ampules were placed inside a Nalgene Mr Frosty container filled with isopropyl alcohol and placed in a -80^oC freezer to gradually

freeze at 1°C/minute overnight. Frozen ampules were transferred to the vapour phase of liquid nitrogen.

2.1.2.2 Differentiation of LUHMES

For differentiation, LUHMES were seeded at $2x10^6$ cells per T75 flask and left to adhere and expanded for 2 days in proliferation media. After 48 hrs of proliferation (on Wednesday), media was changed to differentiation media (Day 0) consisting of Advanced Dulbecco's modified Eagle's medium/F12 without L-glutamine, 1x N-2 supplement, 1x GlutaMAX™, 1 mM di-butyryl adenosine 3′, 5′-cyclic monophosphate sodium salt (cAMP; Cat. No. SC-201567B, Santa Cruz Biotechnology, Germany), 1 µg/mL tetracycline hydrochloride (Cat. No. T7660, Sigma-Aldrich), 20 ng/mL glial-derived neurotrophic factor (GDNF; Cat. No. 450-10, Peprotech) and 1% (v/v) P/S. At Day 2 of differentiation, cells were harvested and seeded into pre-coated plates/flasks in differentiation media. Cells were left to differentiate for 72 hrs.

2.2 Neurite length analysis

For neurite length analysis, phase-contrast images of undifferentiated SH-SY5Y or differentiated SH-SY5Y with 10 µM RA or sequential treatment with 10 µM RA and BDNF were analysed using ImageJ (Fig. 2.2) (US National Institutes of Health, Bethesda, MD, USA). This was performed by first setting the scale using the image scale bar in ImageJ then manually measuring randomly picked neurites. Two hundred neurites were measured per biological repeat and all data is displayed.

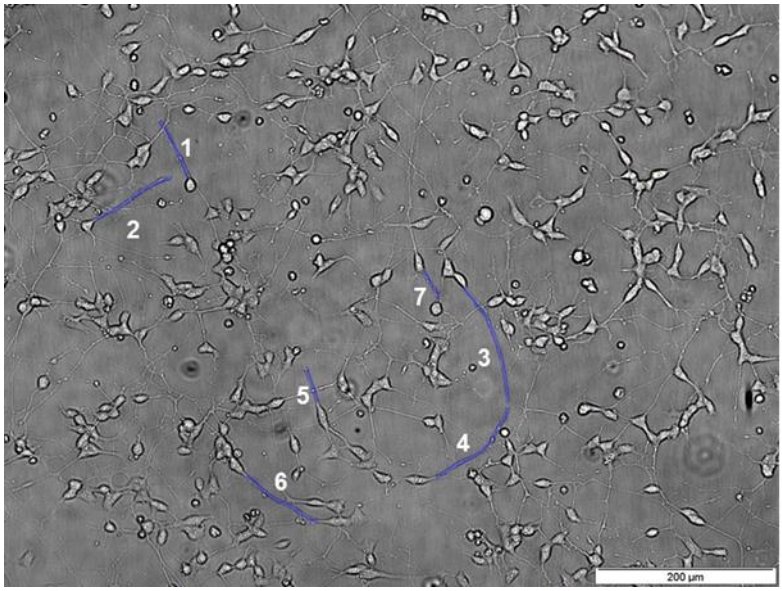

Selection Number	Length (µm)
1	76
2	100
3	145
4	122
5	40.5
6	101
7	37.6

Figure 2.2. *Example neurite length analysis using ImageJ.* Neurite length is indicated by the table on the right hand side and numbered on the image on the left hand side. Scale bar represents 200 µm.

2.3 Immunocytochemistry

2D cultures were fixed with ice-cold methanol for 15 mins at -20ºC followed by washing with PBS solution containing 0.1% (v/v) Tween-20 (PBS-T). After washing, unspecific binding sites were blocked with a solution containing PBS and 1% (w/v) bovine serum albumin (BSA, Sigma-Aldrich) for 1 hr at RT under gentle continuous shaking. After blocking, cells were washed in PBS-T before incubation with the primary antibody in blocking solution for 1 hr at RT under gentle continuous shaking. Following primary antibody incubation, cells were washed with PBS-T and incubated with secondary antibodies for 1 hr at RT in the dark (Table 2.1). Nuclei were counterstained with 0.1 µg/mL 4', 6-diamidino-2-phenylindole, dihydrochloride (DAPI, Sigma-Aldrich) for 5 mins, followed by 3 x washes with PBS-T. Slides were mounted with immersion oil, sealed with nail varnish and left to cure overnight at 4ºC in the dark prior to image capture using an Olympus BX60 bright field/fluorescence microscope. Evaluation of immunofluorescence staining was performed by counting 200 cells per repeat, with immunopositive cells expressed as a percentage of the total count.

2.3.1 Corrected Total Cell Fluorescence Calculations

To quantify total fluorescence per cell, fluorescent images were analysed using the image analysis software ImageJ using the corrected total cell fluorescence (CTCF) calculation were the background fluorescence in a selected area is subtracted from the fluorescence value of a measured area, using the calculation:

$$CTCF = \frac{(Integrated\ Density - (Mean\ Fluorescence\ Reading\ of\ Background\ X\ Area\ of\ Selection)}{Cell\ Number}$$

Three independent biological repeats were performed in total.

2.3.2 Quantification of inclusion area

α-Syn-positive-inclusions were selected at random and quantification of inclusion area was performed in ImageJ. This was achieved by first setting the scale in ImageJ using the image scale bar and manually measuring randomly picked aggregates within the field of view. Measurements were obtained from three independent experiments with 50 inclusions measured per repeat.

Target Antibody	Supplier and Catalogue Number	Clonality	Optimal Dilution	Secondary Antibody
α-synuclein syn211	Fisher: AFMA112874	Mouse monoclonal	1:2000	Goat anti-mouse (Texas Red™)
Amyloid fibrils OC	Millipore: AB2286	Rabbit monoclonal	1:1000	Goat anti-rabbit (Texas Red™)
Ubiquitin	Abcam: ab7780	Rabbit polyclonal	1:1000	Goat anti-rabbit (AlexaFluor® 488)
βIII-Tubulin	Sigma-Aldrich: SDL3D10	Mouse monoclonal	1:500	Goat anti-rabbit (Texas Red™)
Nestin	Sigma-Aldrich: N5413	Rabbit polyclonal	1:200	Goat anti-rabbit (Texas Red™)
Tyrosine hydroxylase	Sigma-Aldrich: T1299	Mouse monoclonal	1: 7500	Goat anti-mouse (Texas Red™)
NF200	Abcam: ab82259	Mouse monoclonal	1:100	Goat anti-mouse (Texas Red™)
Dopamine	Abcam: ab6427	Rabbit polyclonal	1:200	Goat anti-rabbit (Texas Red™)
Ki67	Abcam: ab16667	Rabbit monoclonal	1:200	Goat anti-rabbit (Texas Red™)
Texas Red™ Goat anti-mouse secondary Ab	Invitrogen: T6390	Goat polyclonal	1:1000	N/A
Texas Red™ Goat anti-rabbit secondary Ab	Invitrogen: T2767	Goat polyclonal	1:1000	N/A
AlexaFluor® 488 Goat anti-rabbit secondary Ab	Abcam: ab150077	Goat polyclonal	1:1000	N/A

Table 2.1. *Antibody information used for immunofluorescence staining of 2D cultures.* All antibodies diluted in 1% w/v BSA in 1 x TBS.

2.4 Staining and immunohistochemistry of 3D sections

2.4.1 Processing, paraffin embedding and sectioning

Three-dimensional cultures were fixed with 4% (w/v) PFA, 1% (v/v) glutaraldehyde (ThermoFisher) at RT overnight. The fixed Matrigel was then transferred to a plastic mould, pre-loaded with liquefied Histogel™ (Cat. No. HG-4000-012, ThermoFisher). The fixed Matrigel was positioned in the centre of the mould and encapsulated with liquefied Histogel. The Matrigel/Histogel complex was fixed with 4% (w/v) PFA, 1% (v/v) glutaraldehyde overnight before being processed in sequential changes of 50% IMS, 70% IMS, 100% IMS 3x and Sub-X followed by infiltration by paraffin wax (Leica TP1020 semi-enclose benchtop tissue processor, Milton Keynes, UK). The paraffin blocks were cut into 10 µm sections (Leica microtome), mounted onto X-tra adhesive glass slides (Leica) and incubated at 45^{o}C overnight for Haematoxylin and Eosin (H+E) staining and 1 week for immunohistochemistry (IHC) staining.

2.4.2 Cryosectioning of 3D cultures

For cryostat sectioning, 3D cultures were fixed by snap-freezing in isopentane over liquid nitrogen and stored at -80^{o}C before sectioning. Ten µm Matrigel sections were cut using Leica CM3050S cryostat at -25^{o}C and mounted on X-tra adhesive glass slides. Sections were stored at -80^{o}C until stained.

2.4.3 Haematoxylin and Eosin staining

Following sectioning, the 10 µm sections were oven-dried for 24 hrs before staining with H + E (Leica). For the H + E stain, dried slides were subjected to three changes of Sub-X for 5 mins, three changes of IMS for 5 mins, stained in Haematoxylin for 5 mins, blued in running tap water for 5 mins, stained in Eosin for 5 mins, three changes of IMS for 5 mins, three changes of Sub-X for 5 mins before mounting in Pertex (Leica). Slides were viewed using an Olympus BX60 bright field/fluorescent microscope.

2.4.4 Immunohistochemistry for 3D cultures

For IHC, 10 µm frozen sections from 3D thick-layer cultures were fixed with 1:1 methanol and ice-cold acetone. Staining with anti-α-syn monoclonal antibody was performed using the Mouse on Mouse Polymer IHC Kit according to the manufacturer's protocols (Cat. No. ab127055; Abcam, Cambridge, UK). Briefly, following fixation, slides were washed in TBS-T before incubation in Hydrogen

Target Antibody	Supplier and Catalogue Number	Clonality	Optimal Dilution	Secondary Antibody
α-synuclein syn211	Fisher: AFMA112874	Mouse monoclonal	1:100	Goat anti-mouse
α-synuclein (phospho S129)	Abcam: ab59264	Rabbit polyclonal	*1:10, 1:25, 1:50, 1:100	Goat anti-rabbit
Ubiquitin	Abcam: ab7780	Rabbit polyclonal	1:50	Goat anti-rabbit
βIII-Tubulin	Sigma-Aldrich: SDL3D10	Mouse monoclonal	1: 500	Goat anti-rabbit
NF200	Abcam: ab82259	Mouse monoclonal	1:100	Goat anti-mouse
Dopamine	Abcam: ab6427	Rabbit polyclonal	1:200	Goat anti-rabbit
Ki67	Abcam: ab16667	Rabbit monoclonal	1:200	Goat anti-rabbit
B**iotinylated goat anti-rabbit secondary**	Abcam: ab6720	Goat polyclonal	1:500	N/A
Biotinylated goat anti-rabbit secondary	Abcam: ab6788	Goat polyclonal	1:500	N/A

Table 2.2. *Antibody information used for immunohistochemistry protocols on 3D sections*. All antibodies diluted in 1% BSA in 1 x TBS. *Unable to detect any staining at the following dilutions, therefore no optimal dilution was determined.

Peroxide Block (provided in the kit) for 10-15 mins at RT. Slides were washed in TBS-T and subsequently incubated in Rodent Block for 30 mins. After blocking, slides were washed in TBS-T and primary antibody added for overnight incubation at 4^{o}C (Table 2.2). Slides were washed in TBS-T and Mouse on Mouse HRP Polymer was incubated for 15 mins at RT. 0.08 % (v/v) hydrogen peroxide in 0.65 mg/ml 3, 3-diaminobenzidine tetrahydrochloride (DAB; Cat. No. D5905, Sigma-Aldrich) in TBS was added to sections prior to counterstaining with Mayer's haematoxylin (section 2.4.3).

Staining with anti-ubiquitin rabbit primary antibodies was performed using the following method. Following blocking, endogenous peroxidases were blocked with 0.3% H_2O_2 in methanol for 30 mins at RT. Slides were washed with TBS-T and non-

specific binding sites were blocked at RT for 2 hrs with 25% (v/v) normal goat serum (Fisher Scientific) and 1% (w/v) BSA in TBS. Sections were incubated with primary antibody overnight at 4ºC (Table 2.2). Slides were washed in TBS before incubation with secondary antibodies for 30 min at RT (Table 2.2). Binding of the secondary antibody was detected using a streptavidin–biotin complex (Vector Laboratories, Peterborough, UK) technique with. Sections were counterstained with Mayer's haematoxylin (section 2.4.3).

2.4.4.1 Antigen Retrieval Methods

To unmask antigens in α-syn S129 IHC, both heat-mediated and enzymatic antigen retrieval methods were undertaken on sections. For enzyme-mediated antigen retrieval, sections were incubated in α-chymotrypsin from bovine pancreas (Sigma; 0.1% (w/v) α-chymotrypsin in TBS, 46.8 mM calcium chloride dihydrate, pH 7.5) for 30 min at 37ºC. For heat-mediated antigen retrieval, sections were incubated in sodium citrate buffer (10 mM sodium citrate, 0.05% (v/v) Tween-20, pH 6.0) in a water bath at 60ºC overnight.

2.4.5 Immunocytochemistry for 3D cultures

For immunofluorescence staining of thin-layer 3D cultures in 8-well glass-bottomed chamber slides, cultures were fixed with 4% PFA at RT overnight. The fixed cells were washed with TBS-T (TBS buffer containing 0.1% (v/v) Tween-20) three times before permeabilisation and blocking. For permeabilisation and blocking, 3D cultures were incubated in permeabilisation buffer (TBS-T containing 0.5% (v/v) Triton X-100 and 4% (v/v) goat IgG) for 1 hr at RT followed by incubation with blocking solution (TBS-T containing 1% (v/v) BSA, 0.1% (w/v) gelatin, 0.3 M glycine and 4% (v/v) goat IgG) for 12 hrs at 4ºC with gentle shaking. After washing with TBS-T once for 10 mins, the 3D cultures were incubated with the primary antibody in the blocking solution for 24 hrs at 4ºC with gentle shaking. Following primary antibody incubation, 3D cultures were washed with TBS-T three times for 10 mins, followed by overnight incubation in TBS-T at 4ºC and final 10 min TSB-T incubation. After washing, cultures were incubated with Alexa Fluor secondary antibodies for 5 hrs at RT. A drop of ProLong™ Gold Antifade (Cat. No. P10144, ThermoFisher) was added to each well to prevent fluorescence quenching. Stained 3D cultures were imaged immediately using an Olympus IX51 inverted microscope. The following antibody dilutions were used in this study: anti-βIII tubulin antibody (1:500, Cat. No. SDL3D10,

Sigma-Aldrich,) and goat anti-mouse AlexaFluor488 secondary antibody (1:500, Cat. No. AB150113, Abcam).

For immunofluorescence staining of sections, sections were processed as per section 2.4.4. Fluorescent secondary antibodies were used in the place of HRP-conjugated antibody. Nuclei were counterstained with 0.1 µg/mL DAPI for 5 mins at RT, with immersion oil, sealed with nail varnish and left to cure overnight at 4^{o}C in the dark. Image capture was undertaken using an LSM 800 confocal microscope with Zen Blue software. All samples were imaged using a 40 X plan-apochromat oil objective. To image DAPI staining a 405 nm diode laser with a maximum output of 5 mW was used. For imaging of fluorophores excited to 488 nm, a diode laser with a maximum output of 10 mW was used.

2.5 Cell viability assays

2.5.1 Resazurin reduction assay

A 3 mg/mL stock solution of resazurin (Cat. No. R7017, Sigma-Aldrich) was prepared in cell culture media and further diluted to 10 µg/mL. Following treatment with oligomeric or monomeric species and appropriate solvent controls, media was removed and 100 µL of culture media with 10 µg/mL resazurin was incubated with the cells for 2 hrs. Fluorescence (Ex530 nm /Em590 nm) was measured on a CLARIOstar® plate reader (BMG LABTECH, Buckinghamshire, UK). Culture media was incubated with resazurin in parallel as a blank control. As a positive control, cells were incubated with 1% (v/v) Triton X-100. Cell viability was calculated as a percentage of live cells normalised to negative controls minus relative fluorescence intensity (RFU) of blank wells.

2.5.2 Lactate dehydrogenase assay

Lactate dehydrogenase (LDH) assay was undertaken to quantitatively measure LDH released from damaged cells as a biomarker for cell viability to determine cell viabilities of 3D cultures at various cell densities (1 x 10^6 to 2 x 10^7 cells/mL) within the 3D matrix. LDH released was assayed by measuring extracellular LDH in culture media by using the Pierce^{TM} LDH Cytotoxicity Assay Kit according to the manufacturer's protocols (Cat. No. 88953, Pierce, ThermoFisher). Briefly, 50 µL media from 3D cultures was transferred to a 96-well plate in duplicate and incubated with 50 µL of the reaction mixture (0.6 mL Assay Buffer with 11.4 mL Substrate Mix)

for 30 mins at RT. 50 µL of stop reaction was added to each well and the plate was read at 490 nm (background) and 680 nm. Data were analysed by subtracting media-only control and background from the instrument (value at 490 nm) from average values of each duplicate. Percentage live cells were calculated by normalising to positive controls (same cell density treated with 0.1% (v/v) Triton-X-100).

2.5.3 LIVE/DEAD viability/cytotoxicity assay

LIVE/DEAD assay was undertaken to determine cell viability and distribution of cells with the 3D matrix. The LIVE/DEAD viability/cytotoxicity assay kit for mammalian cells was undertaken according to the manufacturer's instructions (Cat. No.: L3224, Invitrogen, ThermoFisher). Stock solutions of 2 µM calcein AM and 4 µM EthD-1 were made up in sterile PBS prior to addition to differentiated 3D cultures. Three hundred µL of calcein/EthD-1 solution was added per well of thin layer 3D cultures and incubated for 45 mins at RT. Cultures were visualised immediately using an IX51Inverted fluorescence microscope (Olympus).

2.6 Sodium dodecyl sulphate-polyacrylamide gel electrophoresis (SDS-PAGE) and western blotting

2.6.1 Protein extraction

2.6.1.1 Protein extraction from 2D cultures

Culture medium was removed from monolayer cultures and cells washed twice with sterile PBS. Protein was extracted using lysis buffer (CellLytic M™, 1 mM phenylmethylsulphonyl fluoride (PMSF) and 1x protease inhibitor cocktail) at 4^{o}C under gentle shaking for 15 mins. Following lysis, cells were scraped and centrifuged at 15,000 x g for 10 mins to separate protein from cellular debris. The resultant supernatant containing protein was frozen at -80^{o}C until further use.

2.6.1.2 Protein extraction from 3D cultures

For general protein extraction, 3D cultures were harvested from cell culture inserts by cutting round (but not completely) the ThinCert membrane, placing onto a centrifuge tube and spinning at 1,000 x g to collect Matrigel™-cell pellet. Samples were frozen at this point at -80^{o}C for future analysis. For protein extraction, Matrigel™-cell pellet was thawed on ice for 10 mins. An equal volume of 2x extraction buffer (1 x TBS, pH 7.4, 2 x protease inhibitor tablets, 100 mM sodium

orthovanadate, 100 mM sodium fluoride and 20 mM PMSF) was added to Matrigel™-cell pellet and homogenised using a rotor-driven homogenizer before sonication. The homogenised solution was centrifuged at 15, 000 x g for 10 mins to separate cellular debris. The resultant supernatant containing protein was frozen at -80^{o}C until further use.

2.6.1.3 TBS/SDS/Formic acid extraction of thick-layer 3D cultures

For TBS/SDS/Formic acid extraction of thick-layer 3D cultures, the protein was harvested from Matrigel™-cell pellets as section 2.6.1.2, prior to centrifugation. Following sonication, centrifugation was performed at 100,000 x g (~48,000 rpm using a TLA-55 fixed angle rotor) for 1 hr at 4^{o}C using a benchtop Beckman Coulter Optima™ MAX ultracentrifuge (Beckman Coulter, UK). The supernatant was then TBS-soluble fraction and was frozen at -20^{o}C. The cell pellet remaining was homogenised with 50 µL of 1 x SDS extraction buffer (2% (w/v) SDS, 1% (v/v) Triton X-100, 1 x TBS/EDTA, pH 7.4, 2 x protease inhibitor tablets, 100 mM sodium orthovanadate, 100 mM sodium fluoride and 20 mM PMSF) then sonicated before centrifugation at 100,000 x g for 1 hr at 4^{o}C. The supernatant was saved as the TBS-insoluble/2% SDS-soluble fractions and stored at -20^{o}C. The cell pellet was washed with 100 µL 1x SDS extraction buffer and 10 µL of 70% (v/v) formic acid were added before centrifugation at 100,000 x g for 1 hr at 4^{o}C. The supernatant was the TBS-insoluble/2% SDS-insoluble/formic-acid-soluble fraction. Fractions were used for western blotting or ELISA analysis.

2.6.2 BCA assay for protein determination

Protein concentration was determined using the manufacturer's protocols for the Bicinchoninic Acid Protein Assay Kit (BCA, Sigma-Aldrich). Briefly, 25 µL sample or standard was added to 200 µL of working BCA reagent (19 mL BCA and 0.38 mL 4% (w/v) copper sulphate) in a 96-well plate incubated at 37^{o}C for 30 mins. In order to produce a standard curve, protein standards were made using bovine serum albumin (BSA) in distilled water (dH_2O) at concentrations of 0, 0.1, 0.2, 0.4, 0.6, 0.8, 1.0 and 2.0 mg/mL. The absorbance at 570 nm was measured and protein concentration was determined using the equation of the standard curve.

2.6.3 SDS-PAGE electrophoresis

Glass plates were used to cast gels according to the manufacturer's protocols (1.5 mm thickness, Bio-Rad). The resolving gel was cast first and allowed to polymerise with the addition of 200 µL isopropanol to the top of the gel (Table 2.3). Following polymerisation, isopropanol was removed and stacking gel added on top of the resolving gel. A well-comb was added (10 or 15 wells) for the formation of wells.

For electrophoresis, cell lysates were prepared to known protein concentrations (from BCA assay) at 30-50 µg protein in 20 µL samples followed by the addition of 4x loading buffer. 10 mL of 4x loading buffer contained: 2 mL 1M Tris-HCl pH 6.8, 0.8g SDS, 4 mL 100% glycerol, 0.4 mL 14.7 M β-mercaptoethanol, 1 mL 0.5 M EDTA and 8 mg bromophenol blue. 10x running buffer (5 mM Tris-HCl, 250 mM glycine, pH 8.3, 0.1% (w/v) SDS) in 1 L ultrapure water) was diluted 1:10 in ultrapure water prior to addition to gels. Samples were loaded into wells in addition to a broad molecular weight prestained protein ladder (10-245 kDa, Cat. No.: ab116028, Abcam). Proteins were resolved at 120 V for 1-2 hrs before either staining gels with Instant Blue (Cat. No.: 1SB1L, Expedeon, Cambridge, UK) to visualise proteins or proceeded with western blotting.

	Gel component	Volume added for resolving gel	Volume added for stacking gel
12% gel	1.5 M Tris-HCl, pH 8.8	2 mL	-
	0.5 M Tris-HCl, pH 6.8	-	1.25 mL
	Ultrapure water	3.4 mL	2.9 mL
	40% acrylamide	2.4 mL	0.75 mL
	10% (w/v) SDS	80 µL	50 µL
	10% (w/v) APS	80 µL	50 µL
	TEMED	8 µL	5 µL
15% gel	1.5 M Tris-HCl, pH 8.8	2 mL	-
	0.5 M Tris-HCl, pH 6.8	-	1.25 mL
	Ultrapure water	2.8 mL	2.9 mL
	40% acrylamide	3 mL	0.75 mL
	10% (w/v) SDS	80 µL	50 µL
	10% (w/v) APS	80 µL	50 µL
	TEMED	8 µL	5 µL

Table 2.2-1. *Components for 12% and 15% SDS-PAGE gel recipes.*

2.6.4 Western blotting

Resolved protein was transferred onto a 0.45 µm polyvinylidene fluoride (PVDF) membrane (Amersham Hybond 0.45 µm, Cat. No.: 10600023, GE Healthcare Life Sciences, Buckinghamshire, UK) for either 90 mins at 75 volts (GPX4) or 120 mins at 100 volts (α-syn/phosphorylated α-syn). For improved immunodetection of α-syn/phosphorylated α-syn on membranes, the membrane was fixed using 4% (w/v) PFA/0.1% (v/v) glutaraldehyde for 30 mins at RT (Lee and Kamitani, 2011; Sasaki *et al.*, 2015). Membranes were rinsed briefly in water before proceeding with staining of total protein with REVERT™ Total Protein Stain Kit (P/N 926-11010; LI-COR Biosciences, UK) and subsequent immunodetection.

As an alternative for housekeeping proteins to normalise target proteins, normalisation of the target protein to loaded sample was undertaken using the REVERT™ Total Protein Stain Kit. For total protein staining, membranes were washed following transfer with dH_2O and incubated in 5 mL of REVERT™ Total Protein Stain solution for 5 mins with gentle shaking. After staining, the membrane was rinsed two times for 30 seconds with 5 mL wash solution and rinsed briefly in dH_2O before imaging immediately in the 700 nm channel using an Odyssey® Imaging System. For single colour western blotting, membranes were immediately placed in blocking solution. For two-colour western blots, the membrane was incubated in 5 mL of REVERT™ Reversal solution after imaging the membrane. Membranes were incubated in REVERT™ Reversal solution until the stain was no longer visible by eye, after 5-10 mins. The membrane was rinsed briefly in water and immediately followed with blocking.

The membrane was blocked in either TBS-T with 5% (w/v) non-fat milk (NFM) for non-phosphorylated proteins or in Odyssey Blocking Buffer (TBS, Cat. No.: P/N 927-50100, LI-COR Biosciences) for the detection of phosphorylated proteins. The blots were incubated for 1 hr at RT, followed by overnight incubation with primary antibodies in TBS-T with 2% (w/v) NFM at 4^{o}C under gentle shaking. For the detection of phosphorylated proteins, NFM was omitted in antibody solutions. Membranes were washed 3 times for 10 mins with TBS-T and incubated with secondary antibody in TBS-T with 2% (w/v) NFM for 1 hr at RT. LI-COR secondary antibodies (Table 2.4) were detected using the LI-COR scanner at 700 nm.

Target Antibody	Supplier and Catalogue Number	Clonality	Optimal Dilution	Secondary Antibody
α-synuclein syn211	Fisher: AFMA112874	Mouse monoclonal	1:2000	Goat anti-mouse
Phosphorylated α-synuclein (S129)	Abcam: AB59264	Rabbit polyclonal	1:2000	Goat anti-rabbit
GPX4	Abcam: AB125066	Rabbit polyclonal	1:1000	Goat anti-rabbit
Tyrosine hydroxylase	Sigma: T1299	Mouse monoclonal	1:7500	Goat anti-mouse
IRDye® 680LT Goat anti-mouse IgG (H+L)	Licor: 925-68070	Goat polyclonal	1:15000	N/A
IRDye® 680RD Goat anti-rabbit IgG (H+L)	Licor: 925-68071	Goat polyclonal	1:15000	N/A

Table 2.2-2. *Antibody information for western blotting.* All antibodies were diluted in 1 x TBS.

2.6.5 Total protein quantification using REVERT Total Protein Stain

REVERT™ Total Stain analysis was used to monitor protein transfer across the entire blot and to normalise proteins levels of target proteins. In order to quantify target proteins in each lane, Total Protein Stain (TPS) levels (700 nm) were first quantified before analysing target proteins in either the 700 nm or 800 nm channels (see section 2.6.4 for two-colour detection after TPS). To quantify target proteins, the lane normalisation factor was calculated from each lane of the Total Protein Stain image, using the following calculation:

$$Lane\ normalisation\ factor = \frac{TPS}{TPS\ signal\ for\ the\ lane\ with\ the\ highest\ signal}$$

To calculate the normalised signal for target quantification, the normalised signal for each band was divided by the signal for each band by the Lane Normalisation Factor for the lane the band is in, using the following calculation:

$$Normalised\ signal = \frac{Target\ band\ signal}{Lane\ normalisation\ factor}$$

Normalised signals were used for quantitative comparisons (Fig. 2.3).

A

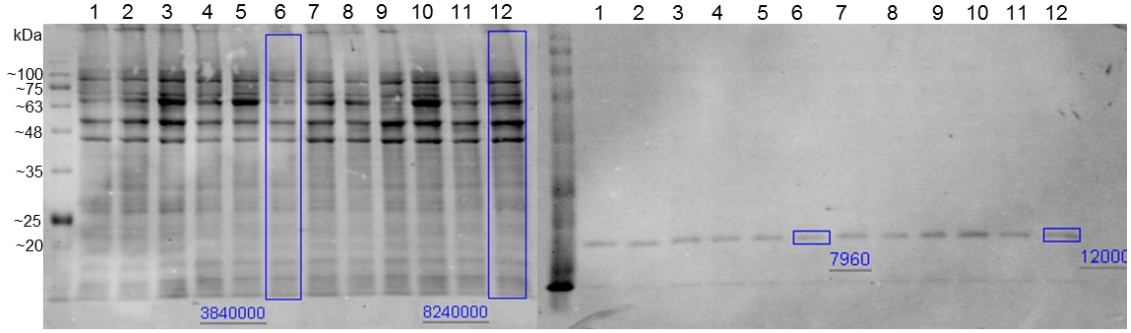

C

Lane Number	Signal (700 nm)	Highest Signal	Lane Normalisation Factor
6	3840000	8240000	0.466
12	8240000		1

D

Lane Number	Signal (800 nm)	Signal/Normalisation Factor @ 800 nm
6	7960	17081
12	12000	12000

Figure 2.3. *Example of REVERT™ Total Protein Stain Lane Normalisation.* **(A)** Visualisation of REVERT™ Total Protein Stain at 700 nm. Lanes highlighted to represent the highest signal (lane 12) on the blot and an example lane used for normalisation (lane 6). **(B)** Visualisation of GPX4-positive bands in the 800 nm channels. Lanes 6 and 12 shown as an example of normalisation. **(C)** Lane normalisation factor was calculated by dividing the signal at 700 nm by the highest signal (at 700 nm). In this example, lane 12 has the highest signal of 8240000, therefore the other lanes are divided by this value to give the lane normalisation factor. **(D)** Lane normalisation factor is used to calculate the relative signal intensity of the band of interest (GPX4, **B**). The signal at 800 nm in this example is divided by the lane normalisation factor to give the normalised signal.

2.7 Dot blotting

Nitrocellulose membranes (0.45 µm, GE Healthcare) were spotted with 1 µL of sample and allowed to air dry. Samples were blocked for 1 hr in 5% (w/v) NFM in TBS-T. Primary antibody was diluted in 1% (w/v) NFM in TBS-T and incubated for 1 hr at RT under gentle shaking. Three wash steps were performed with TBS-T before the addition of secondary antibodies. Secondary antibodies were diluted in 1% (w/v) NFM in TBS-T and incubated with membranes for 1 hr at RT under gentle shaking. Visualisation was performed using the LI-COR Odyssey and Odyssey Imaging software (LI-COR Biosciences, UK).

2.8 α-Syn ELISA

Human α-syn ELISA was performed using the Abcam Human Alpha-Synuclein SimpleStep ELISA® kit according to manufacturer's protocols (Cat. No. AB210973, Abcam). Briefly, protein samples were normalised using protein concentrations calculated from BSA assay and diluted either 1:5, 1:10 or 1:50 in 1x Cell Extraction Buffer PTR. A standard curve was prepared first by the addition of 1 mL of 1x Cell Extraction Buffer PTR to the human α-syn lyophilised recombinant protein provided

in the kit (stock standard, 5,000 pg/mL). 140.4 µL of 1x Cell Extraction Buffer PTR was added to tube number 1 and 130 µL was added tubes numbered 2-8. A serial dilution was prepared by transferring 249.6 µL from the stock standard to tube number 1, then 260 µL from tubes 1-7. Standard 8 was classed as no protein control (blank). 50 µL of sample or standards were added to wells with 50 µL Antibody Cocktail. The plate was sealed and incubated for 1 hr at RT on a plate shaker at 400 rpm. Each well was subsequently washed 3x 350 µL with 1x Wash Buffer PT. Following wash steps, 100 µL TMB substrate was added to each well and incubated for 10 mins in the dark on a plate shaker at 400 rpm. For an endpoint reading, 100 µL of Stop Solution was added to each well for 1 minute on a plate shaker. The plate was scanned at 450 nm using a CLARIOstar® plate reader. α-Syn concentrations of samples were calculated by using the equation of the α-syn standard curve and multiplying by the dilution factor used for each sample.

2.9 RNA Extraction and qPCR

2.9.1 RNA extraction from 2D cell cultures

Total RNA was extracted from 1 x 10^6 cells using either the ReliaPrep™ RNA Cell Miniprep System (Cat. No. Z6011, Promega, UK) or using TRIzol® reagent (Cat. No. 15596026, Invitrogen). Total RNAs were prepared using the ReliaPrep™ RNA Cell Miniprep System according to the manufacturer's protocols. Briefly, cell pellets were washed once with ice-cold, sterile 1x PBS and centrifuged at 300 x *g* for 5 mins to collect the cells. 250 µL BL + TG buffer (for 1 x 10^6 cells) was added to the cell pellet and mixed by vortexing and pipetting. 85 µL isopropanol (for 1 x 10^6 cells) was added to cells in BL + TG buffer and vortexed for 5 seconds. Lysates were transferred to a ReliaPrep™ Minicolumn and centrifuged at 13,000 x *g* for 30 seconds at RT. 500 µL RNA Wash Solution was added to the ReliaPrep™ Minicolumn with bound nucleic acids, and centrifuged at 13, 000 x *g* for 30 seconds. DNase I enzyme (24 µL Yellow Core Buffer, 3 µL 0.09 M $MnCl_2$ and 3 µL DNase I enzyme/sample) was incubated on the column membrane for 15 mins at RT. After incubation, 200 µL of Column Wash Solution was added to the column, followed by centrifugation at 13,000 x *g* for 15 seconds. 500 µL RNA Wash Solution was added and centrifuged at 13,000 x *g* for 30 seconds, followed by another wash step with 300 µL RNA Wash Solution and centrifuged for 2 mins at 13,000 x *g*. Isolated RNAs were eluted using nuclease-free water by adding 30 µL of nuclease-free water (for 1

x 10^6 cells) to membranes and centrifuged at 13,000 x *g* for 1 minute. RNA was subsequently used for cDNA synthesis or stored at -80^{o}C for future work.

For RNA extraction using TRIzol® reagent, cells were harvested and washed with ice-cold PBS before extraction. Cells were lysed with 1 mL of TRIzol® reagent at RT for 10 mins. 0.2 mL of chloroform was added per 1 mL of TRIzol® reagent, vortexed for 15 seconds and incubated at RT for 10 mins for phase separation of RNA (aqueous phase, colourless, top), DNA (interphase, white, middle) and proteins/lipids (organic phase, red/pink, bottom). The aqueous phase was transferred to a new tube and RNA precipitated with the addition of 0.5 mL isopropanol per 1 mL of TRIzol® reagent. Samples were transferred to -80^{o}C to precipitate RNA for at least an hr, or for greater yields, overnight. RNA was harvested by centrifugation at 12,000 x *g* for 15 mins at 4^{o}C. The resultant RNA pellet was washed with 75% ethanol and centrifuged at 7,500 x *g* for 10 mins at 4^{o}C. RNA pellets were air-dried on ice for 10-15 mins prior to solubilisation in nuclease-free water. Isolated RNA was used for subsequent cDNA synthesis or stored at -80^{o}C for future work.

2.9.2 RNA extraction from 3D cell cultures

2.9.2.1 Extraction using Corning® Cell Recovery Solution

Cells were recovered from the Matrigel following the dissolution of the matrix using Corning® Cell Recovery Solution (Corning, UK). The medium was removed from 3D cultures and washed with ice-cold PBS 3 times. Three hundred µL Matrigel gel culture was added to 3 mL of ice-cold Corning® Cell Recovery Solution in an ice-cold falcon tube and left on ice for 1 hr. The tube containing the Matrigel and Corning® Cell Recovery Solution was inverted and left on ice until dissolved before centrifugation at 1000 rpm at 4^{o}C for 5 mins. To completely release from the gel, cells were washed with ice-cold PBS before centrifugation 2 more times. Total RNAs were prepared using the ReliaPrep™ RNA Cell Miniprep System (Promega, UK) according to the manufacturer's protocols.

2.9.2.2 Extraction using TRIzol®

For extraction of RNA from 3D cultures using TRIzol® reagent, Matrigel™ cultures were incubated in 1 mL TRIzol® reagent for 10 mins to lyse cells. RNA isolation was subsequently carried out according to section 2.8.1.

2.9.3 RNA Yield and Quality

RNA concentration and quality were determined using the NanoDrop spectrophotometer and RNA integrity was determined using agarose gel electrophoresis. Good quality and intact RNA was determined to be samples with an A260/A280 ratio of 2.0-2.1 and A260/A230 ratio >2.0 and the presence of distinct 28s and 18s subunits following electrophoresis, with the absence of any genomic contamination or smearing.

2.9.4 cDNA synthesis

Complementary DNAs (cDNA) were synthesised by the nanoScript 2 Reverse Transcriptase kit (Cat. No. RT-NanoScript2, Primerdesign Ltd, UK). For the annealing step, 2 µg RNA template was incubated with oligo-dT, random nonamer primers and RNase/DNase free water (in 10 µL reaction volume) for 5 mins at 65^{o}C before immediately cooling on ice. For the extension step, a 10 µL mixture of nanoScript2 4x Buffer (5 µL), sNTP mix 10 mM (1 µL), RNase/DNase free water (3 µL) and nanoScript2 enzyme (1 µL) was added to each reaction from the annealing step on ice. Tubes were mixed briefly by vortexing and incubated at 25^{o}C for 5 mins then at 42^{o}C for 20 mins. The reaction was inactivated by incubation at 75^{o}C for 10 mins. cDNA samples were subsequently used for qPCR either straightaway or stored at -20^{o}C for short term storage or at -80^{o}C for long-term storage.

2.9.5 qPCR

Quantitative real-time polymerase chain reaction (qPCR) was undertaken using Precision®PLUS qPCR Master Mix formulated for Applied Biosystems StepOnePLUS or LifeTechnologies QuantStudio (Cat. Nos. PPLUS-LR and PPLUS-R, Primerdesign) and pre-validated primer sets purchased from Primerdesign (Cat. No. SY-HU for *TH, DAT, NES, MAP2, VMAT2 or TUBB3*) or Sigma-Aldrich (KiCqStart® SYBR® Green Primers, Cat. No. KSPQ12012 for *SLC7A11, SLC3A2, SLC7A5, VDAC 1, VDAC2 and VDAC3*). For the qPCR reaction, cDNA samples were diluted to 5 ng/mL in nuclease-free water and 5 µL of sample added to in duplicate to the wells of a Bright White qPCR plate (Cat. No. BW-FAST, Primerdesign). A master mix was prepared to contain 10 µL PrecisionPLUS qPCR Master Mix, 1 µL primer/probe and 4 µL RNase/DNase free water per sample and added to each well containing diluted cDNA. Plates were sealed and centrifuged to collect samples at the bottom of the wells. The amplification was performed in a final

volume of 20 µL under the following conditions: 2 min at 95ºC and then 50 cycles at 95ºC for 15 sec and 60ºC for 60 sec followed by a post PCR melt curve analysis. The sizes of PCR products were confirmed using agarose gel electrophoresis. Gene expression levels were normalised against reference genes for each sample and fold changes were calculated using the $2^{-\Delta\Delta Ct}$ method (Schmittgen and Livak, 2008) by setting the expression levels of each gene in undifferentiated SH-SY5Y/untreated cells as 1. Data collected from at least three independent biological replicates was calculated and plotted as mean log10-fold changes ±SEM.

2.9.5.1 GeNorm Analysis

Reference gene analysis was undertaken using the geNormPLUS kit (Primerdesign) and Qbase+ software to identify inherently stable reference genes for RT-PCR between different treatment groups following differentiation of SH-SY5Y with RA and BDNF. A reference gene mixture was made up with 1 µL primer, 10 µL Primerdesign 2x *PrecisionPLUS*™ master mix and 4 µL of RNase/DNase free water per well, according to the plate set up. Five µL of diluted cDNA samples were added to wells for a final well volume of 20 µL. The amplification was done in a final volume of 20 µL under the following conditions: 2 min at 95ºC and then 40 cycles at 95ºC for 10 sec and 60ºC for 60 sec followed by a post PCR melt curve analysis. Optimal reference genes were calculated using Qbase+ software (Biogazelle).

2.9.6 Agarose gel electrophoresis

PCR products and isolated RNA were separated on a 1% (w/v) agarose gel to check RNA quality and confirm the size of PCR products. 50x tris-acetate-EDTA (TAE) buffer (40 mM Tris, 20 mM acetate and 1 mM EDTA, pH 8.6) and diluted 1:50 for use in electrophoresis. A 1% (w/v) agarose gel UltraPure™ Agarose (Cat. No.: 16500500, ThermoFisher) in 1x tris-acetate-EDTA (TAE) buffer and heating in 30 sec bursts in a microwave until all agarose was dissolved. The solution was allowed to cool before the addition of 0.5 µg/mL ethidium bromide (Cat. No.: 15585011, ThermoFisher). Gels were poured into a Bio-Rad gel tray sealed with a Bio-Rad gel caster with the addition of a well-comb then allowed to set at RT. Agarose gels were placed in a Bio-Rad horizontal electrophoresis tank (Mini-Sub® Cell GT Cell) and submerged in 1x TAE buffer. DNA or RNA samples were mixed with 10x gel loading buffer (Cat. No.: A3481.0010, VWR, Leicestershire, UK) and loaded into wells (2 µL of loading buffer per 20 µL DNA/RNA). A 100 base pair (bp) to 2,000 bp ladder (Cat.

No.: 15628050, Invitrogen) was added alongside DNA/RNA samples to aid in size estimation. Samples were resolved at 100 volts for 1-1.5 hrs and viewed on a NuGenius/NuGenius+ gel imaging system.

2.10 Expression of WT recombinant α-synuclein and production of oligomers

2.10.1 Transformation of competent *E. coli*

BL21 (*DE3*) *E. coli* competent cells (Agilent Technologies, 200121) were thawed on ice and incubated with a pET 23a^{+} vector containing the human WT α-syn sequence or negative control (BL21 (*DE3*) competent cells with no plasmid added) for 30 mins at RT with periodic gentle agitation. Cells were exposed to heat shock at 42^{o}C for 45 seconds and returned to ice for 5 mins. Five hundred µL LB broth (1% (w/v) tryptone, 1% (w/v) sodium chloride and 0.5% (w/v) yeast extract) was added to each tube and incubated in a shaking incubator at 200 rpm, 37^{o}C for 1 hr to allow cells to express antibiotic resistance genes. One hundred µL of the reaction was spread onto LB agar plates containing the selectable marker ampicillin (100 mg/mL) and incubated overnight at 37^{o}C. Colonies were observed 24 h after transformation apart from plates inoculated with negative control cells (no plasmid added).

2.10.2 Expression and purification of recombinant protein

Single colonies were inoculated into starter cultures containing 100 mL LB media and 100 µL of 100 mg/mL ampicillin solution and incubated in a shaking incubator at 200 rpm, 37^{o}C overnight. Ten mL starter cultures were added to auto-induction medium (Formedium, UK) and incubated in a shaking incubator at 200 rpm, 37^{o}C for 24 hrs to induce expression of WT α-syn. Bacterial cells were harvested by centrifugation at 4^{o}C, 8,000 rpm. The resulting pellet was resuspended in lysis buffer (10 mM Tris-HCl, pH 8, 100 µg/mL lysozyme, 20 µg/mL DNase, 20 µg/mL RNase, 1 mM PMSF and 1x protease inhibitor mini-tablet EDTA free) and incubated for 30 mins before the addition of 1 mM EDTA and sonication of the cell pellet to enhance cell lysis. Following lysis, the cell lysate was centrifuged at 10,000 x g for 40 mins to remove cellular debris. The supernatant was acidified to pH 4.5 and centrifuged again at 10,000 x g for 40 mins to remove any aggregated protein. The pH of the resulting supernatant was adjusted to pH 8 before the crude lysate was subjected to further purification by anion exchange and size exclusion chromatography using the Äkta start and Äkta purifier systems (GE Healthcare).

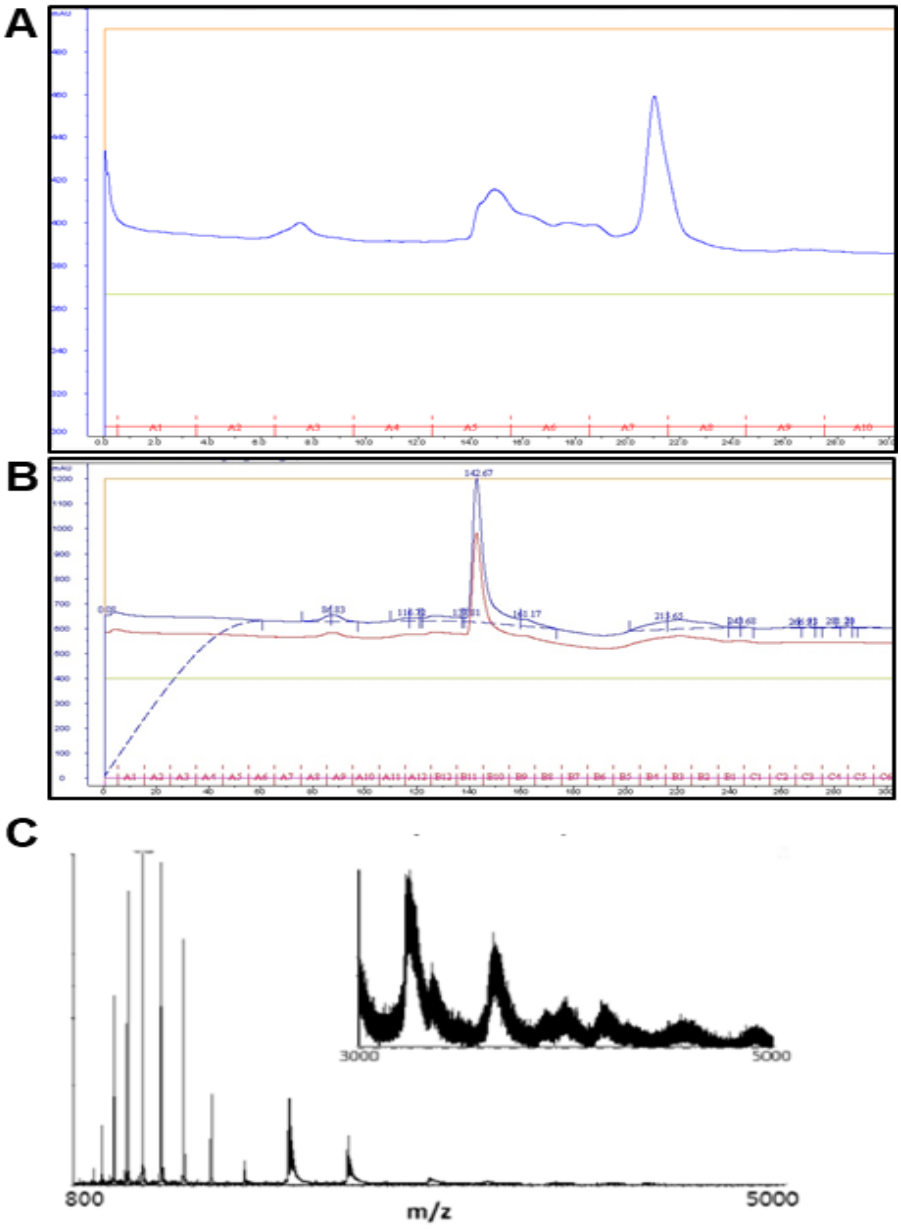

Figure 2.4. *Characterisation of α-syn oligomers by size exclusion chromatography and mass spectrometry analysis.* Elution profile of oligomeric α-syn **(A)** and monomeric α-syn **(B)** by size exclusion chromatography monitored at 214 nm. Absorption is measured in milli absorbance units (mAU). **(C)** ESI-IMS-MS analysis of seeding oligomers. Spectra of seeding oligomers shown (with expended region of 3000-5000 m/z inset) reveals presence of oligomeric species derived from the seeding oligomer preparation in section 2.10.3. Image credit Mason (2018).

For anion exchange, a 50 mL Q-Sepharose column (Q1126; Q-Sepharose Fast Flow, Sigma-Aldrich) was equilibrated with two column volumes of buffer A (25 mM Tris-HCl, pH 8) followed by loading of the column with crude lysate. Bound protein was eluted with a 0-100% linear gradient of buffer B (25 mM Tris-HCL, 1 M NaCl, pH 8) in 5 mL fractions. After elution, the protein was dialysed overnight at 4^{o}C with at least 6 changes of water prior to freeze-drying. The resultant lyophilised protein was subject to size exclusion chromatography. For size exclusion chromatography, a Hi-Load 26/200 Superdex 200 pg column (28989336; GE Healthcare) was equilibrated with three column volumes of buffer A. Lyophilised protein was dissolved in 3 mL buffer A before injection. Protein was eluted in 5 mL fractions before being subjected

to dialysis and freeze-drying. Lyophilised purified α-syn was stored at -20^{o}C. Protein concentration was measured using a UV/vis spectrophotometer (Jenway 6715) at absorbance 214 nm with an extinction coefficient of 5960 M^{-1} cm^{-1}.

2.10.3 Production of α-synuclein oligomers

Seeding oligomers were prepared as previously described by Danzer *et al.* (2009), omitting the addition of 10 µM $FeCl_2$. Briefly, lyophilised α-syn was dissolved in 50 mM sodium phosphate buffer (pH 7.0) containing 20% (v/v) ethanol to a final concentration of 7 µM. Following overnight incubation at 21^{o}C with continuous shaking, oligomers were concentrated 1:14 using ultracentrifugation (VivaSpin 500 columns, MWCO 30 kDa, GE Healthcare), allowing the separation of oligomeric species from monomeric protein. Each batch of oligomers was used immediately for experiments. Oligomers were determined to be present by size exclusion chromatography and mass spectrometry analysis (Fig. 2.4).

2.11 Detection of lipid peroxidation using BODIPY C11 581/591

2.11.1 Fluorescent microscopy

For 2D SH-SY5Y cell culture, cells were plated at a density of 1.875 x 10^5 cells/cm^2 in a 6-well plate containing 2 mL DMEM containing 10% (v/v) FBS and 1% (v/v) P/S. Cells were left to adhere and expand to 70% of the culture surface prior to treatment with test agents. For the detection of lipid peroxidation after iron (II) chloride treatment, cells were incubated with either: media only control, solvent control (highest amount of nitrilotriacetic acid trisodium salt (NTA) used), 200 µM or 1000 µM iron (II) chloride (with 1:2 ratio of iron (II) chloride to NTA) for 12, 24 or 72 hrs at 37^{o}C. 30 mins before the end of the treatment, 5 µM C11-BODIPY581/591 (Cat. No. D3861, ThermoFisher Scientific, UK) was added to the cultures. The medium was removed after 30 mins and cells washed three times with PBS before imaging. Oxidation of C11-BODIPY581/591 was indicated by the change of BODIPY fluorescence from red (non-oxidised) to green (oxidised). Fluorescent microscopy was undertaken using an IX51Inverted fluorescence microscope (Olympus). Quantification of red and green signals was performed using ImageJ software (US National Institutes of Health, Bethesda, MD, USA). Data was analysed by counting cells positive for lipid peroxidation (oxidised, green) and calculating the percentage

lipid peroxidation as a percentage of the total number of cells per field of view (non-oxidised, red) using the formula ((green/ (green+red)) x 100(%)).

2.11.2 Flow cytometry

Two dimensional SH-SY5Y were cultured until 70% confluent in T75 flasks before treatment with media, solvent (NTA only), 200 µM or 1000 µM iron (II) chloride (with 1:2 ratio of iron (II) chloride to NTA) for 24 hrs or 72 hrs. 24 hr treatment with 10 µM menadione was used as a positive control. Following treatment, cells were washed with warmed PBS and incubated in 2 µM C11-BODIPY581/591 in PBS for 30 mins at 37^{o}C. Cells were harvested, pelleted and resuspended in 5mL PBS and subjected to flow cytometric analysis. C11-BODIPY581/591 exhibits a shift in fluorescence emission from ~590 nm to ~510 nm as detected by flow cytometry. Dyes were excited using a 488 nm Ar laser and detected with the FL1 and FL4 detectors on a FACSCalibur flow cytometer (BD Biosciences, Berkshire, UK). Ten thousand cells were counted for each measurement. For every assay, unstained cells were used to set a gating strategy. Data was analysed using FlowJo® software (BD Bioscience) with the median fluorescent intensity used for subsequent data analysis, including the calculation of percentage lipid peroxidation ((green/ (green+red)) *100(%).

2.12 Glutathione quantification

Glutathione quantification was undertaken using the GSH/GSSG-Glo^{TM} Glutathione Assay according to the manufacturer's instructions (V6611, Promega). Briefly, 2 x 10^4 cells/well were cultured and treated in white-opaque walled 96-well plates. Test compounds (media-only, solvent control (NTA only), 200 µM iron (II) chloride and 1000 µM iron (II) chloride and 10 µM menadione as a positive control) were incubated for 24 hrs. Test compounds were removed from cells and replaced with 50 µL of Total Glutathione Lysis Reagent or Oxidised Glutathione Lysis Reagent as appropriate. 50 µL of Total Glutathione Lysis Reagent was also added to no-cell controls and wells containing a range of glutathione concentrations (0-16 µM) to produce a standard curve. The plate was then shaken at 5 mins at RT before the addition of 50 µL/well of Luciferin Generation Reagent and incubated for 30 mins at RT. One hundred µL of Luciferin Detection Reagent was added per well and incubated for 15 mins at RT. Luminescence was recorded using a CLARIOStar® plate reader. The concentration of total and oxidised glutathione in treated cells was determined using the equation of the standard curve.

2.13 CellROX™ Assay

Oxidative stress was measured using CellROX™ Green reagent following the manufacturer's guidelines (Cat. No's: C10444, ThermoFisher). SH-SY5Y cells were cultured on coverslips in 6-well plates and treated with oligomers or iron (II) chloride at 70% confluent for 2, 24 or 72 hrs. The CellROX™ Green reagent was added to treated cells at a final concentration of 5 µM and the cells incubated for 30 mins at 37ºC. Nuclei were counterstained using Hoechst 33342 (Cat. No. H3570, ThermoFisher) diluted 1:2,000 to each well. The medium was then removed, and cells washed with PBS, followed by fixing with 10% formalin before mounting and curing overnight at 4ºC in the dark prior to image capture using an Olympus BX60 bright field/fluorescent microscope. Corrected total cell fluorescence was calculated as described in section 2.3.1.

2.14 ICP-MS analysis of cultures

Cells (2D and 3D cultures) were harvested following treatment with media, solvent (NTA only), 200 µM or 1000 µM iron (II) chloride (with 1:2 ratio of iron (II) chloride to NTA) for 24 hrs. Cell lysates were prepared by removal of culture medium and cells washed twice with sterile PBS. Protein was extracted using lysis buffer (CellLytic ™, 1 mM PMSF and 1x protease inhibitor cocktail) at 4ºC under gentle shaking for 15 mins. Following lysis, cells were scraped and centrifuged at high speed for 10 mins to separate protein from cellular debris. The resulting supernatant containing protein was frozen at -80ºC until further use. A BCA assay was conducted to determine protein concentrations. Five hundred µg of each sample (3 biological repeats, 12 samples total) was freeze-dried. Samples were digested with nitric acid by incubating with 150 µL nitric acid at 90ºC on a hot block, followed by hydrogen peroxide incubation at 90ºC. Standards were prepared by diluting trace metals in dH_2O to final concentrations of 0, 0.5, 1, 5, 10, 50 and 100 nM iron. Iron concentrations of samples were calculated using the equation of the standard curve.

2.15 Statistical analysis

Statistical analysis was undertaken using StatsDirect version 3.0.126. Data were unpaired and determined to be non-parametric following the Shapiro–Wilk test of normality; therefore, a Kruskal–Wallis test was undertaken with post hoc analysis. Post hoc analysis was only undertaken if the initial significance test was at $P<0.05$.

Dwass-Steel-Chritchlow-Fligner was used for data points >6 and Conover-Inman post hoc analysis for <6 data points. *P*-values are denoted on the graphs.

Chapter 3 : Development of a 3D model of Parkinson's disease

3.1 Introduction

Aggregation of α-syn into intracellular LB-inclusions represents one of the major neuropathological hallmarks of PD. The mechanisms underlying LB formation and the influence of α-syn pathology on disease pathogenesis remain poorly understood, largely due to the lack of whole-animal or cell-based models that recapitulate the development of these inclusions. One of the significant barriers in PD research surrounds the difficulty in obtaining cultures of the A9 dopamine-producing neuronal population that are specifically affected in the disease (Arenas, Denham and Villaescusa, 2015). To address this animal and cell culture systems have been developed to model the complex pathogenesis of the disorder (Arenas, Denham and Villaescusa, 2015; Xicoy, Wieringa and Martens, 2017). The cost incurred, time constraints and ethical framework required for animal-based research are inhibitory for many laboratories making cell culture-based systems attractive (Barré-Sinoussi and Montagutelli, 2015). The recent development of 3D culture models and organoids represent feasible alternatives to animal models (Choi *et al.*, 2014; Hoarau-Véchot *et al.*, 2018). In the following sections, popular cellular models used in PD research will be highlighted and the limitations/advantages associated with each discussed.

3.1.1 Cell models used in Parkinson's disease research

3.1.1.1 SK-N-SH and SH-SY5Y cell line

An *in vitro* model popular for use in PD research is the SH-SY5Y neuroblastoma cell line, a subline of SK-N-SH (Xicoy, Wieringa and Martens, 2017). Due to the difficulty in obtaining and maintaining primary neurons, most PD research is performed using immortalised cell lines, with the most popular choice being the neuroblastoma SH-SY5Y cell line. The popularity of the cell line is attributed to both the dopaminergic characteristics and ease of culture (Forster *et al.*, 2016). The SK-N-SH cell line is originally derived from a bone marrow metastasis of a 4-year-old patient suffering from neuroblastoma and established *in vitro* in the 1970s (Biedler, Helson and Spengler, 1973). SK-N-SH comprised of two morphologically distinct cell

populations, a small neuritic cell and a large epithelioid cell (Biedler *et al.*, 1978; Deinum *et al.*, 2004). SH-SY5Y is a more commonly used neuroblast-like subclone of the SK-N-SH used in PD research. SK-N-SH was subcloned three times, first to the neuroblast-line SH-SY, then to SH-SY5 and finally SH-SY5Y (Kovalevich *et al.*, 2013). SH-SY5Y share morphological features of the parental SK-N-SH line including the presence of distinct phenotypes of neuroblast-like cells and epithelial-like cells, corresponding to 'N' and 'S' subtypes, respectively (Encinas *et al.*, 2000; Kovalevich *et al.*, 2013). SH-SY5Y also displays a catecholaminergic phenotype, with the machinery to synthesise both dopamine and noradrenaline (TH and dopamine β-hydroxylase, respectively) (Kovalevich *et al.*, 2013). Using whole-genome analysis of SH-SY5Y, most of the genes belonging to major PD pathways were intact in the SH-SY5Y, including those related to dopamine metabolism (Krishna *et al.*, 2014).

SH-SY5Y can be differentiated into a more neuronal phenotype using a variety of chemical agents, including RA, phorbol esters such as 12-*O*-tetradecanoyl-phorbol-13 acetate (TPA), cAMP, nerve growth factor, and BDNF, amongst others (Encinas *et al.*, 2000; Constantinescu *et al.*, 2007; Dwane, Durack and Kiely, 2013; Teppola *et al.*, 2016; Xicoy, Wieringa and Martens, 2017). A review of SH-SY5Y culture conditions by Xicoy *et al.* (2017) reveals only 17% of papers utilising the SH-SY5Y cell line in PD research report using a differentiation protocol. Among the papers that used differentiated cells, the differentiation treatments were: 10 µM RA with or without reduced serum media (~10% of studies overall), other concentrations of RA (~3% of studies), 10 µM RA and 80 nM TPA (~2% studies), 10 µM RA and 50 ng/mL BDNF (~1% studies) and other (~1% of studies) (Xicoy, Wieringa and Martens, 2017). Upon differentiation, cells express dopamine receptors (D2 and D3), DAT and VMAT2 (Kovalevich *et al.*, 2013).

Although more studies are utilising the differentiation of SH-SY5Y in PD research, the phenotypic outcome can give contradicting outcomes (Xicoy, Wieringa and Martens, 2017). Some studies report the development of a dopaminergic or cholinergic phenotype following differentiation (Hashemi *et al.*, 2003; Korecka *et al.*, 2013; Ito *et al.*, 2017). The original source of cells either from the American Type Culture Collection (ATCC) or European Collection of Authenticated Cell Cultures (ECACC) can also have a huge influence in the phenotype of SH-SY5Y and logically

this would affect the ability of cells to differentiate (Donato *et al.*, 2007; Nishida *et al.*, 2008; Xicoy, Wieringa and Martens, 2017). Due to the cancerous properties of the cell line, SH-SY5Y does not wholly represent the cell type post-mitotic nature of neurons affected in PD. The cancerous properties influence differentiation fate, viability, metabolic properties and genomic instability. However, genes associated with major PD pathways are expressed in SH-SY5Y (Krishna *et al.*, 2014). However, the importance of differentiation of SH-SY5Y is apparent given the increased susceptibility to neuronal toxins such as MPP^+ and 6-OHDA when compared to undifferentiated counterparts (Presgraves *et al.*, 2004). Increased expression of the MPP^+ transporter, DAT, in differentiated cells compared to undifferentiated explains the differences in susceptibility to neuronal toxins (Presgraves *et al.*, 2004; Schildknecht *et al.*, 2009). LUHMES cells following differentiation into a dopaminergic phenotype also show increased susceptibility to MPP^+ (Schildknecht *et al.*, 2009). The differences between mitotically active and post-mitotic cells should not be underestimated, given continually dividing cells can be influenced by agents that inhibit cell proliferation which MPP^+ is known to do (Soldner *et al.*, 1999). Treatment with α-syn oligomers has been shown to induce the formation of α-syn-positive intracellular inclusions with different morphologies in differentiated and undifferentiated cells, with differentiated cultures showing greater resemblance to *in vivo* morphologies and is the subject of this chapter (Taylor-Whiteley *et al.*, 2019).

3.1.1.2 Immortalised human embryonic mesencephalic cells (LUHMES and ReNcell)

LUHMES is a clone of the MESC2.10 (derived from eight-week-old human mesencephalic cells) and immortalised by use of a retroviral vector containing the tetracycline controlled *v-myc*-oncogene (Hoshimaru *et al.*, 1996; Lotharius *et al.*, 2002; Lotharius, 2005). In the absence of tetracycline, *v-myc* is constitutively expressed allowing cells to proliferate continuously in culture (Lee and Reddy, 1999). Addition of low, non-toxic, levels of tetracycline abolishes *v-myc* expression, allowing cells to exit the cell cycle and differentiate in a post-mitotic state (Hoshimaru *et al.*, 1996). LUHMES cells can undergo differentiation using tetracycline, cAMP and glial-derived neurotrophic factor (GDNF), resulting in the development of mature electrically active dopaminergic-like neurons that express TH, DAT, VMAT2, βIII-tubulin and increased levels of α-syn (Lotharius *et al.*, 2002; Schildknecht *et al.*,

2009; Scholz *et al.*, 2011; Smirnova *et al.*, 2016). In regards to PD, LUHMES have been used to investigate MPP^+/rotenone associated neurodegeneration (Schildknecht *et al.*, 2009; Pöltl *et al.*, 2012; Krug *et al.*, 2014; Smirnova *et al.*, 2016; Harris *et al.*, 2018), neuroprotection (e.g. upregulation of hypoxia-inducible factor (HIF) genes) (Johansen *et al.*, 2010), lysosomal dysfunction (Gan *et al.*, 2015), cell death mechanisms (e.g. apoptosis/ferroptosis) (Do Van *et al.*, 2016). With regards to α-syn aggregation in LUHMES, there isn't the wealth of data available as with the more commonly used cell line SH-SY5Y, due to the number of studies using LUHMES cells being limited. However, as the use of the cell line is becoming more popular, the number of studies will increase.

Although LUHMES represent a promising cellular model for modelling PD *in vitro*, the use of the cell line does have its negatives. For example, LUHMES need to be cultured on poly-L-lysine and fibronectin-coated culture surfaces but this support matrix is degraded by the growing/differentiating cultures. Monolayer cultures tend to detach from culture vessels as early as 72 hrs after differentiation (Smirnova *et al.*, 2016). This has been circumvented by culturing in 3D spheroid culture, allowing for prolonged survival of the differentiated cells and suitability of the 3D model for long-term neurotoxicity studies (Smirnova *et al.*, 2016; Harris *et al.*, 2018).

3.1.1.3 Non-neuronal cell lines

HEK-293 is a cell line originally derived from normal embryonic kidney cells from the kidney of an aborted human embryo (Graham *et al.*, 1977). Transfection of the cell line was achieved following exposure and incorporation of mechanically sheared adenovirus type 5 DNA into chromosome 19 of the host genome (Graham *et al.*, 1977; Louis, Evelegh and Graham, 1997; Thomas and Smart, 2005). HEK-293 is widely used in cell biology and biotechnology mainly due to the ease of growth in culture and as an excellent cell line to use in transfection experiments (Thomas and Smart, 2005). Although derived from kidney cells, HEK-293 display some properties associated with cells of a neuronal lineage, as demonstrated by the strong immunoreactivity to neurofilaments (NF-M, NF-L and a small amount of NF-H) and mRNAs normally expressed in early differentiating neurons (Shaw *et al.*, 2002; Thomas and Smart, 2005). Several other adenoviral transformed cells derived from human embryonic kidney cells also express a similar expression of intermediate filaments indicative of an early differentiating neuronal phenotype (Shaw *et al.*,

2002). Later analysis indicated the adenovirus transformed the small percentage of cells of neuronal lineage in the original HEK-293 culture, explaining the difficulty in establishing the original cell line (Shaw *et al.*, 2002). In PD research, the cell line is mainly used for stably expressing mutant or normal α-syn typically in conjunction with other proteins of interest e.g. DAT (Lehmensiek *et al.*, 2006; Shavali *et al.*, 2008; Luk *et al.*, 2009). Of interest, the addition of a fibrillar seed to α-syn overexpressing HEK-293 was shown to induce the formation of LB-like inclusions by actively recruiting endogenous α-syn (Luk *et al.*, 2009). Importantly, these LB-like aggregates underwent several modifications characteristic of LBs *in vivo* including phosphorylation and ubiquitination, demonstrating the potential role of fibrillar seeds in the pathogenesis of PD (Luk *et al.*, 2009).

3.1.1.4 PC12 and Neuro-2a

The rat-derived PC12 pheochromocytoma cell line exists as a mixture of neuroblastic cells and eosinophilic cells that are able to synthesize, release, take up and store catecholamines (Greene and Tischler, 1976). PC12 differentiate in response to serum-free media and nerve growth factor (NGF) (Greene, 1978). Upon differentiation, cells cease to be mitotically active, extend neuronal-like processes and are classed as sympathetic-neuron-like cells (Greene and Rein, 1977; Greene, 1978). PC12 cells are sensitive to several toxins that mimic PD and therefore are used as a cell model to study neurodegeneration and neuroprotection in relation to mitochondrial toxins 6-OHDA (Walkinshaw and Waters, 1994; Ryu *et al.*, 2002), MPP^+ (Ryu *et al.*, 2002; Chakraborty *et al.*, 2017), rotenone (Mirzaei *et al.*, 2006; Jing *et al.*, 2014) and paraquat (Yang and Sun, 1998). Iron and paraquat treatment in PC12 cells was shown to exacerbate lipid peroxidation and subsequent cell death (when compared to paraquat treatment alone), therefore indicating the importance of iron in PD (Yang and Sun, 1998). This is especially interesting as in recent years the iron-dependent cell death pathway, ferroptosis, has been linked to pathology in PD (Do Van *et al.*, 2016).

N2a is a mouse neural crest-derived cell line able to differentiate into either cholinergic or dopaminergic cells depending on culture conditions (Kojima *et al.*, 1994; Tremblay *et al.*, 2009). Differentiation of N2a with dibutyryl cAMP (dbcAMP) was shown to increase expression of TH and dopamine in contrast to other cultures additives of GDNF, RA, transforming growth factor and bone morphogenic protein 4

(Wu *et al.*, 1998; Tremblay *et al.*, 2009). Use of N2a in PA research is not particularly widespread but have been used to investigate neurotoxicity of MPP^+ due to the high affinity for MPP^+ uptake and vulnerability which exceeds other cell lines of PC12 and SH-SY5Y (Mazzio and Soliman, 2003; Deguil *et al.*, 2007; Soliman *et al.*, 2009).

3.1.1.5 Induced pluripotent stem cells

Embryonic stem cells (ESCs), derived from the inner cell mass of mammalian blastocysts, are able to differentiate into any cell type while maintaining the ability to grow indefinitely (Evans and Kaufman, 1981). Induced pluripotent stem cells (iPSCs) are pluripotent stem cells that can be generated from adult cells whilst maintaining the ability to differentiate into any tissue type (Takahashi and Yamanaka, 2006). The programming of mouse fibroblasts into iPSCs was achieved by exposing cells to four transcription factors Octamer binding transcription factor-4 (Oct4), Sex determining region Y (Sox2), Kruppel-like factor 4 (Klf4) and c-Myc (Takahashi and Yamanaka, 2006). iPSCs reprogrammed from adult human fibroblasts was subsequently reported using the same transcription factors (K. Takahashi *et al.*, 2007; Park *et al.*, 2008). Disease modelling can be achieved by harvesting skin fibroblasts or blood cells from patients and reprogrammed into the cell type to be investigated (i.e. A9-like dopaminergic neurons) or by introducing specific mutations into wild-type (WT) iPSCs (Caiazzo *et al.*, 2011; Devine *et al.*, 2011).

Culture of ESCs and iPSCs is time-consuming and associated with high cost, with the need for expensive reagents for reprogramming and labour costs during clonal selection and expansion (Beers *et al.*, 2015). During the expansion stage of iPSC samples (where colonies are selected, expanded and frozen), colonies may appear at different time points requiring researchers to juggle several samples at different stages of reprogramming. For this reason, researchers are limited to 2-4 reprogramming samples per person (Beers *et al.*, 2015). Beers *et al.* (2015) quote as much as $10,000 in reagents for a full-time researcher to generate a six sample iPSC project (3 controls and 3 patients) before characterisation and clonal selection. However, optimised methods of iPSC generation have recently reduced the cost associated with reprogramming (from ~$1,300/ sample to $150-200/sample) and have reduced the need for labour-intensive cell culture (from 2 samples/person to 20-40 samples/person) meaning iPSCs are becoming more accessible to smaller laboratories (Beers *et al.*, 2015).

3.1.1.6 Primary cell lines

Primary cells isolated from rat or murine tissue provides an alternative to the use of immortalised cell lines in scientific research. Cultures prepared from the midbrain of rats are not solely dopaminergic neuronal preparations, but rather a mixture of different kinds of neurons and glia (Falkenburger, Saridaki and Dinter, 2016). Approximately 5-10% of neurons cultured are dopaminergic, with only 1-2% positive for TH (Visanji *et al.*, 2008; Schüle, Pera and Langston, 2009; Falkenburger, Saridaki and Dinter, 2016). Dissociated rodent superior cervical sympathetic ganglia are the primary neuronal counterpart to the PC12 immortalised cell line and succumb to 6-OHDA and MPP^+ (Grau and Greene, 2012).

3.1.2 Three dimensional cell culture

Recent progress in 3D cell culture systems has facilitated the development of human cellular disease models to study the pathogenesis of disease in a more physiologically relevant context when compared to traditional 2D culture models. Much of our understanding of cell biology processes is based on studies of cells grown in 2D monolayer cultures on flat polystyrene or glass surfaces whereby cells are in contact with homogenous amounts of nutrients and growth factors (Breslin and O'Driscoll, 2013). However, cells *in vivo* exist in complex tissues with cells interacting with multiple extracellular matrix (ECM) components, other cell populations and various cell-secreted factors. The limitation in the interaction between other cells and or/ECM has an enormous impact both on cellular structure and cellular function, including survival, differentiation, proliferation and migration (Abbott, 2003). 3D cultures have been shown to more closely mimic cellular *in vivo* characteristics when compared to 2D counterparts, including the development of a more mature neuronal phenotype when cultured in 3D (Jo *et al.*, 2016; Marchini *et al.*, 2019).

There are several formats and materials suitable for use in 3D culture. Cells can be cultured in scaffold-based or scaffold-free systems (Vinci *et al.*, 2012). Scaffold-based cultures involve culturing cells either on synthetic/biologically-derived scaffolds (Breslin and O'Driscoll, 2013; Eglen and Klein, 2017). Synthetic scaffolds include the cultivation of cells grown on a hard material based support such as 3D-printed structures (made metals, ceramics or other polymers), polystyrene-based 3D culture materials (e.g. 3D Biotek Inserts™), sponge-like structures (e.g. foams) or fibres (Caicedo-Carvajal *et al.*, 2011; Accardo *et al.*, 2017; Xu *et al.*, 2018).

Biologically-derived scaffolds typically consist of hydrogel cultures which can be classified as ECM protein-based hydrogels (e.g. Matrigel™, laminin, and collagen), natural hydrogels (e.g. alginate beads and dextran) and synthetic hydrogels (e.g. polyethylene glycol, polyvinyl alcohol, polycaprolactone and polyhydroxyethyl methacrylate) (Lim F. and Sun A.M., 1980; Hughes, Postovit and Lajoie, 2010). Scaffold-free systems involve the formation of multi-cellular aggregates generally known as spheroids, whereby interactions between cells produce their own ECM components. Spheroid cultures can be produced by culturing cells on low adherence substrates, using hanging-drop methods and agitation-based approaches (continuous gyratory culture) (Smirnova *et al.*, 2016).

3.2 Aims and objectives

The purpose of this chapter was to develop a 3D cell culture model utilising differentiated SH-SY5Y and an extracellular matrix-based (Matrigel™-based) 3D culture system. The growth and maturation of a mesencephalic neuronal cell line in a Matrigel™-based 3D culture system demonstrated the development of key events in AD, including extracellular aggregation of amyloid-β (Aβ) and accumulation of hyperphosphorylated tau/aggregated tau as neurofibrillary tangles (Choi *et al.*, 2014). This culture system was shown to promote deposition of Aβ species; therefore, it was posited that a Matrigel™-based culture system would promote the aggregation of α-syn in SH-SY5Y.

The specific aims of this chapter were:

- To establish a differentiation protocol for SH-SY5Y, in 2D initially, that gives rise to a more neuronal phenotype for further development in 3D culture.
- To determine the dopaminergic phenotype of differentiated cells cultured in 2D prior to culture in 3D.
- To develop 3D cell culture methods utilising the differentiation protocol used in 2D cultures, including optimisation of cell densities, Matrigel™ concentrations and methods for downstream analysis of cultures.
- To determine the dopaminergic phenotype of the 3D-differentiated SH-SY5Y.

3.3 Results

3.3.1 Differentiation of SH-SY5Y with retinoic acid and aphidicolin results in the development of a ‘neuron-like’ phenotype contaminated with mitotically active non-differentiating ‘S-type’ cell population

Prior to developing the 3D model, cells were differentiated in 2D to determine a protocol that could yield post-mitotic neuron-like cells. Initially, cells differentiated in 2D were monitored for development of neuron-like characteristics by evaluation of cell morphology by phase-contrast microscopy. Undifferentiated SH-SY5Y cells display characteristic morphology of two distinct phenotypes: neuroblastic (‘N-type’); and substrate adherent (‘S-type’) (Fig. 3.1 and 3.4). In agreement with others (Korecka *et al.*, 2013; Forster *et al.*, 2016; Ito *et al.*, 2017), upon treatment with 10 µM RA, for 4 days the neuroblastic SH-SY5Y cells differentiated into a more neuron-like phenotype as judged by the development of extended neurites (Fig. 3.1) in both 1% and 10% FBS groups. Continued treatment with 10 µM RA at day 7, 10 and 14 lead to the death of the ‘neuron-like’ cells with extended neurites and the growth of the substrate-adherent, non-neuronal ‘S-type’ cells. As RA promotes exit from the cell cycle, ‘neuron-like’ cells become post-mitotic and do not go through cell division. The ‘S-type’ cells do not differentiate into neurons and are not affected by RA, therefore are able to continue cell division and can progressively overgrow the culture flask. For long term culture in 3D, the ‘S-type’ cell could potentially overgrow the culture and lose the neuronal population. To address the issue of the mitotically active ‘S’ type from overgrowing the neuronal population, the mitotic inhibitor aphidicolin was added to RA-differentiated cultures (Poluha *et al.*, 1996). Aphidicolin is a reversible inhibitor of nuclear DNA replication and blocks the cell cycle in S phase (Jensen, 1987). Addition of aphidicolin to pre-differentiated SH-SY5Y resulted in a lot of cell death and did not prevent the growth of the ‘S’ type cells, as they were still detectable at day 14 (Fig. 3.2). To conclude, differentiation of SH-SY5Y with 10 µM RA ± aphidicolin resulted in the extension of neurites of the 'N-type' population, with overgrowth of the non-neuronal 'S-type' population.

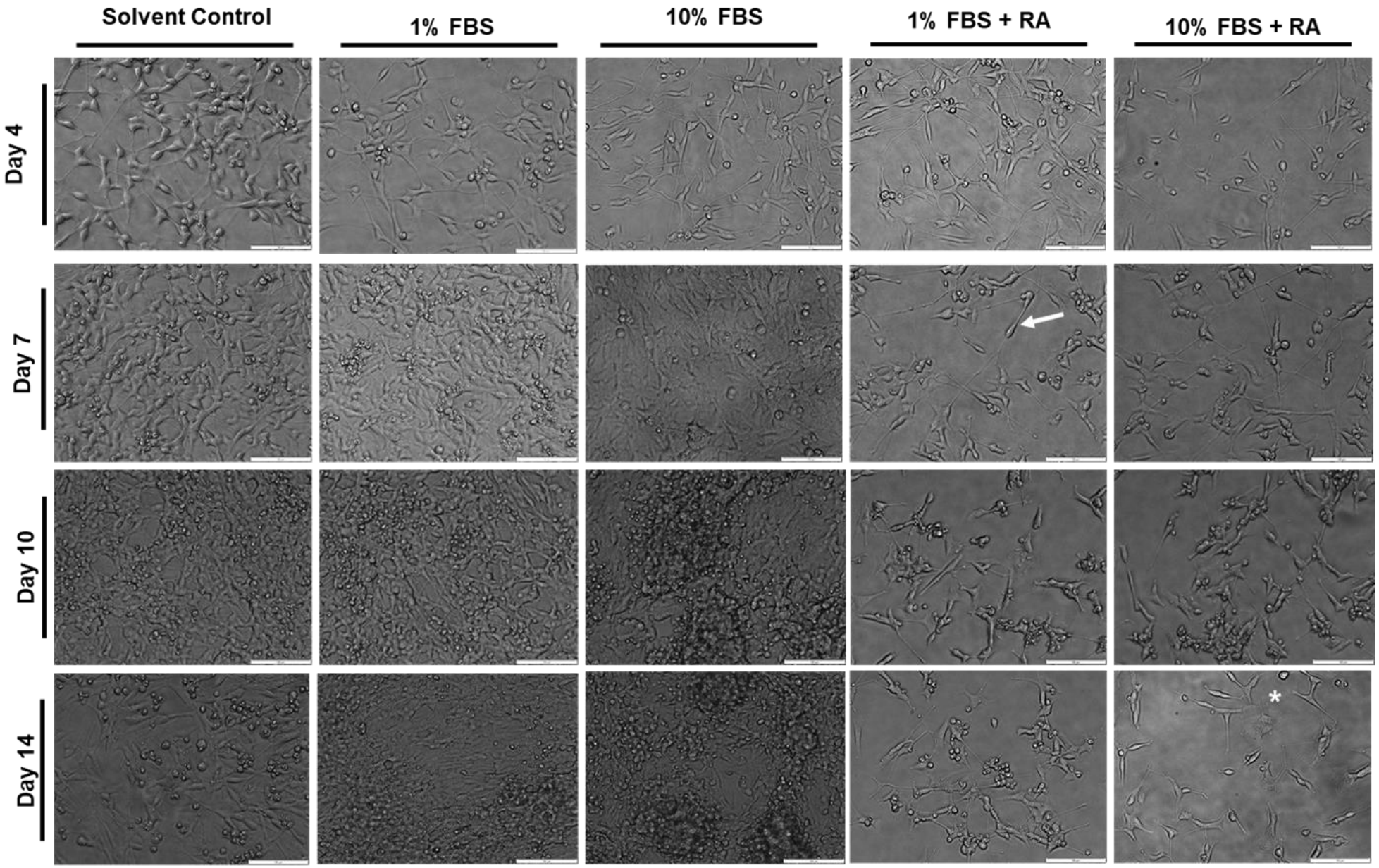
Solvent Control
1% FBS
10% FBS
1% FBS + RA
10% FBS + RA
Day 4
Day 7
Day 10
Day 14
*

Figure 3.1. *Effects of RA treatment in SH-SH5Y cells shown in phase-contrast micrographs growing in complete medium (DMEM with 10% FBS), reduced-serum media (DMEM with 1% FBS), and in medium containing 10 μM RA (DMEM with either 1% or 10% FBS) for 4, 7, 10 and 14 days.* Treatment with RA resulted in neurite outgrowth by day 7 in both RA groups (1% or 10% FBS added to DMEM) when compared to solvent control and 1%/10% FBS groups without FBS. White arrow highlights a 'N-type' cell with extended neurites. As culture time increased, 'N-type' cells with neurites are still detectable, however, 'S-type' non-neuronal cells progressively overgrow the culture. Scale bar represents 100 μm. *Abbreviations*: FBS, foetal bovine serum; RA, retinoic acid.

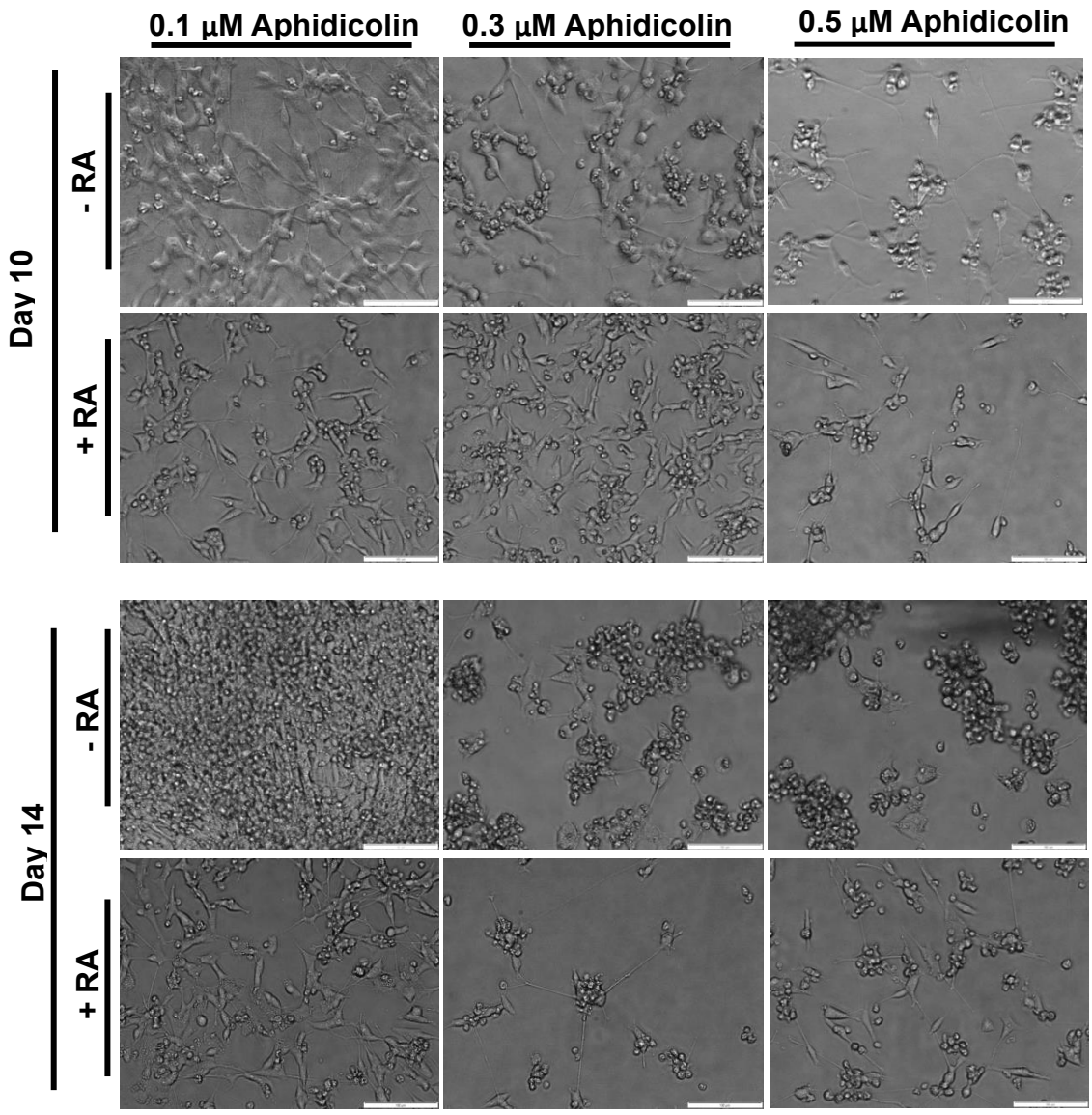

Figure 3.2. *Effects of RA and aphidicolin treatment in SH-SH5Y cells shown in phase-contrast micrographs growing in medium with or without 10 μM RA initially followed by sequential treatment of aphidicolin (either 0.1, 0.3, 0.5 μm) for 10 or 14 days.* Addition of the mitotic inhibitor aphidicolin to RA-differentiated SH-SY5Y resulted in extensive cell death in all groups examined as demonstrated by large clumps of cells detaching from the culture surface. Scale bar represents 100 μm. *Abbreviations*: RA, retinoic acid.

3.3.2 Differentiation of SH-SY5Y with retinoic acid and brain-derived neurotrophic factor yields 'neuron-like' phenotype and suppression of growth of mitotically active 'S-type' cells

In order to fully differentiate the SH-SY5Y cell line and remove the residual S-type cells, an alternative strategy was undertaken. Sequential treatment of RA

and brain-derived neurotrophic factor (BDNF) was investigated as a potential differentiation protocol for use in 3D cultures. Initial treatment with 10 μM RA induced the development of cells with extended neurites (Fig. 3.1). Subsequent addition of BDNF in serum-free media further promoted the development of a neuronal phenotype as determined by extensive neurite outgrowth, neurite extension and development of complex neurite networks in response to the neurotrophic factor (Fig. 3.3 and 3.4 A). The removal of serum prevented the growth of the mitotically active 'S-type' cells (Encinas et al., 2000). Pre-differentiation with 10 μM RA in 1% FBS (in contrast to 10% FBS) followed by sequential treatment with 50 ng/mL BDNF was not chosen for further experiments due to the death of all cells at day 12 (Fig. 3.3, left column). Quantification of neurite length in undifferentiated, RA and RA + BDNF-differentiated SH-SY5Y reveals an average neurite length and standard deviation of 51.22 ± 22.87 μm (undifferentiated), 64.91 ± 33.07 μm (RA) and 130.50 ± 77.91 μm (RA+BDNF). There was deemed to be a significant change in neurite length between all group (<P=0.0001; Fig. 3.4B).

Figure 3.3. *Effects of RA and BDNF treatment in SH-SH5Y cells shown in phase-contrast micrographs growing in medium with 10 μM RA initially followed by sequential treatment of 50 ng/mL BDNF for 7 or 12 days.* Addition of 50 ng/mL BDNF to cultures previously differentiated in culture medium with either 10% FBS, 1% FBS + 10 μM RA, or 10% FBS + 10 μM RA demonstrate the development of neurites in all groups at day 7. The 1% FBS + 10 μM RA group has extensive neurites when compared to 10% FBS alone and 10% FBS + 10 μM RA. However, at day 12, cells have detached from the culture vessel due to cell death in the 1% FBS + 10 μM RA group. Neuronal-like cells with long neurites and cell bodies are detected in both 10% FBS and 10% FBS + 10 μM RA, with extended neurites in the latter group. Scale bar represents 100 μm. *Abbreviations:* BDNF, brain-derived neurotrophic factor; FBS, foetal bovine serum; RA, retinoic acid.

1

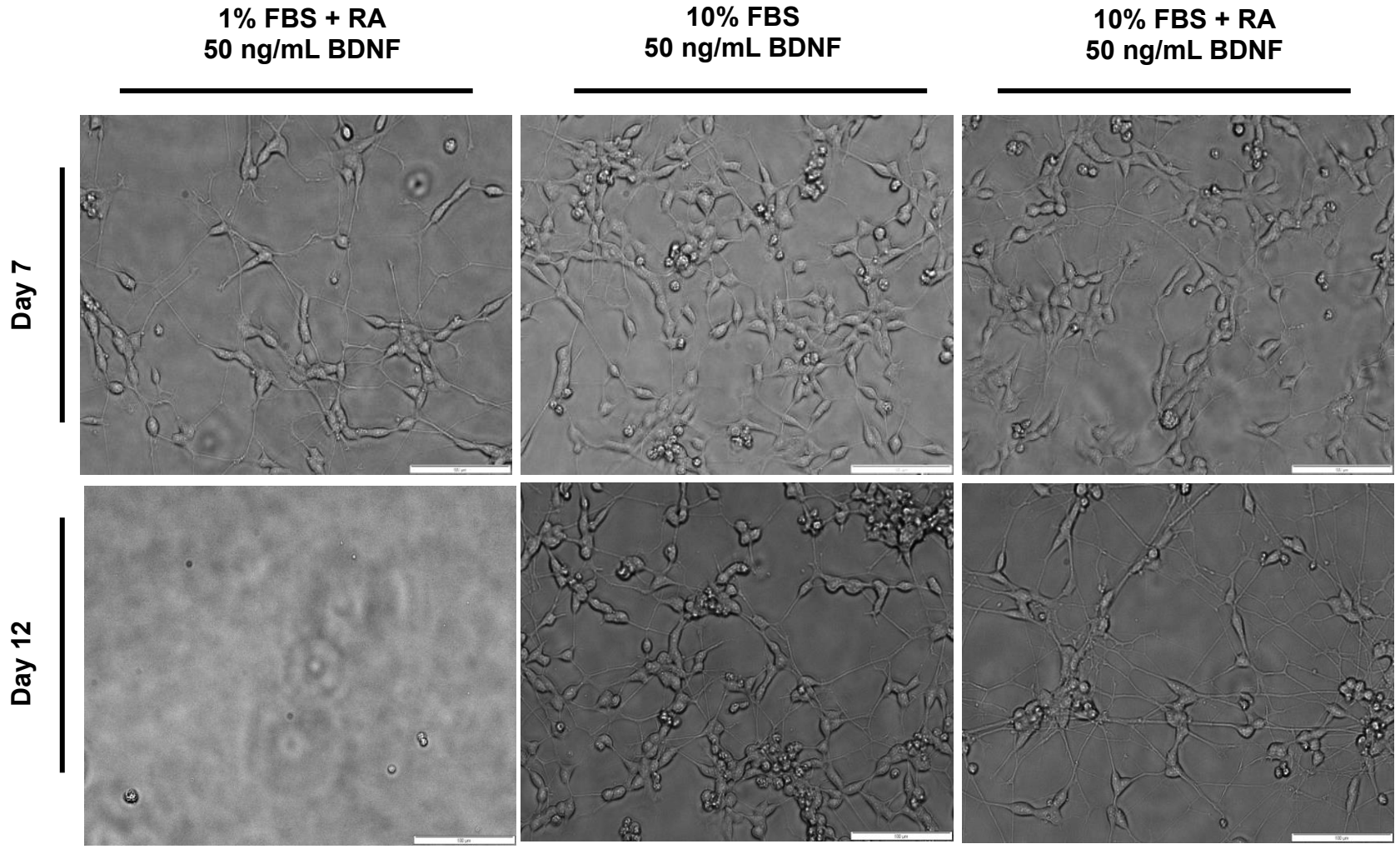
1% FBS + RA
50 ng/mL BDNF
10% FBS
50 ng/mL BDNF
10% FBS + RA
50 ng/mL BDNF
Day 7
Day 12

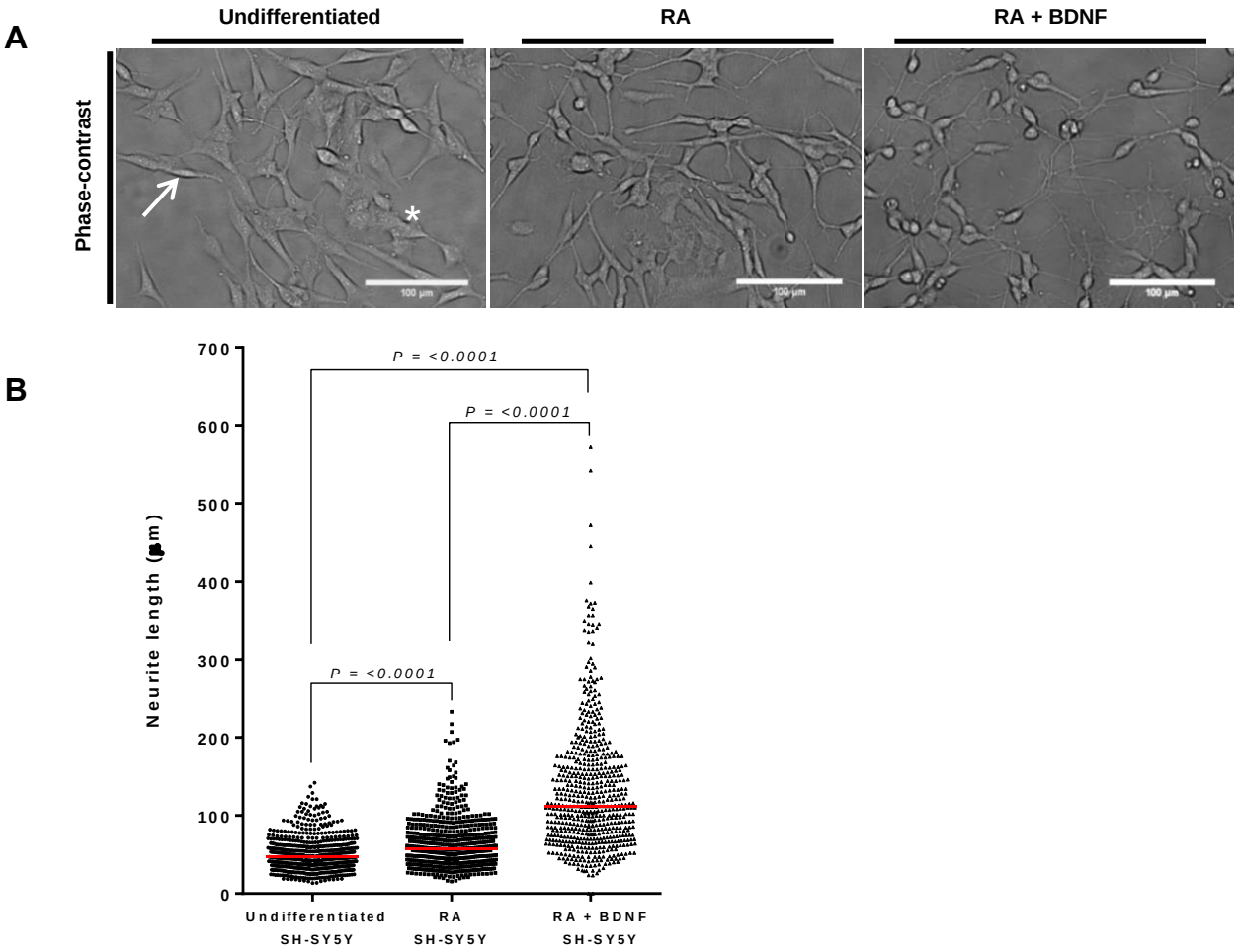

Figure 3.4. *Phase contrast analysis of SH-SY5Y differentiation with retinoic acid and brain-derived neurotrophic factor.* **(A)** Representative phase contrast images of SH-SY5Y differentiated with RA alone or sequential treatment with RA and BDNF. Neuroblastic ('N-type'; arrow) and substrate adherent ('S-type'; asterisk) cells are shown. Scale bar represents 100 µm. **(B)** Neurite length analysis of undifferentiated, RA only and sequential treatment with RA and BDNF SH-SY5Y. 200 neurites were measured per repeat treatment group, with three independent biological repeats. All data is presented with the mean shown as a straight line (in red). Statistical significance determined by Kruskal-Wallis test with post-hoc Dwass-Steel-Chritchlow-Fligner. Results of initial Kruskal-Wallis test *P= <0.0001*. *P*-values are displayed on the figure.

3.3.3 SH-SY5Y differentiated with sequential treatment of RA and BDNF in 2D culture express markers of dopaminergic neurons as evaluated by qPCR and immunocytochemistry

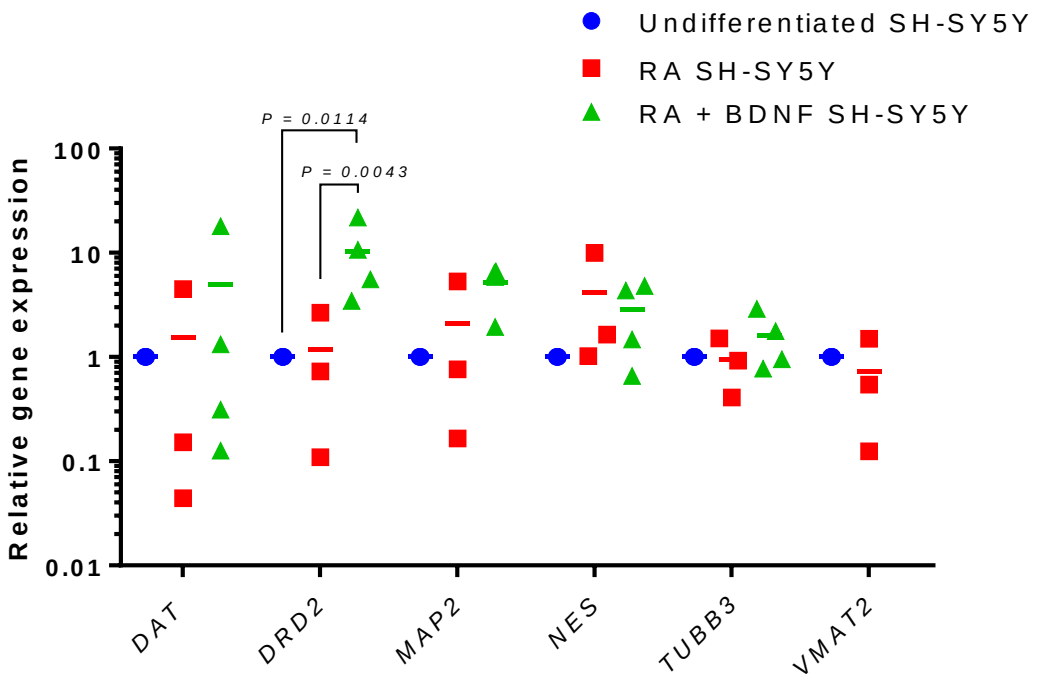

Figure 3.5. *qPCR analysis of dopaminergic and neuronal markers in undifferentiated, retinoic acid only and retinoic and brain derived neurotrophic factor SH-SY5Y.*Undifferentiated (blue), RA treatment group (red) and RA+BDNF treatment group (green). Relative gene expression normalised to reference genes (*ACTB* and *YWHAZ*) and undifferentiated SH-SY5Y. Neuronal (*TUBB3* and *MAP2*) and dopaminergic markers showed increased expression in the RA+BDNF (green). Data presented as all data points and mean (straight line) of at least three independent experiments. Statistical significance determined by Kruskal-Wallis test with post-hoc Conover-Inman. Results of initial Kruskal-Wallis test *P*= 0.0321. *P*-values are displayed on the figure. *Abbreviations:* DAT, dopamine transporter; DRD2, dopamine receptor 2; MAP2, microtubule-associated protein 2; NES, nestin; TUBB3, βIII-tubulin; VMAT2, vesicular monoamine transporter 2.

Key to the development of an effective cell culture model of PD is the expression of relevant neuronal markers. Evaluation of mRNA levels by quantitative real-time PCR (qPCR) after each differentiation protocol was used to determine the transcriptional levels of genes specifically associated with dopaminergic neurons (Fig. 3.5). Increased expression of neuronal markers βIII-tubulin (*TUBB3*) and microtubule-associated protein 2 (*MAP2*) upon differentiation with RA + BDNF confirmed the development of a more neuronal phenotype than was observed with RA or undifferentiated SH-SY5Y. Nestin (*NES*), an immature neuronal marker, was not significantly changed by differentiation with either RA alone of RA + BDNF treatment. A greater dopaminergic phenotype in RA + BDNF cultures was observed, indicated by elevated expression levels of dopamine transporter (*DAT*), dopamine receptor-2

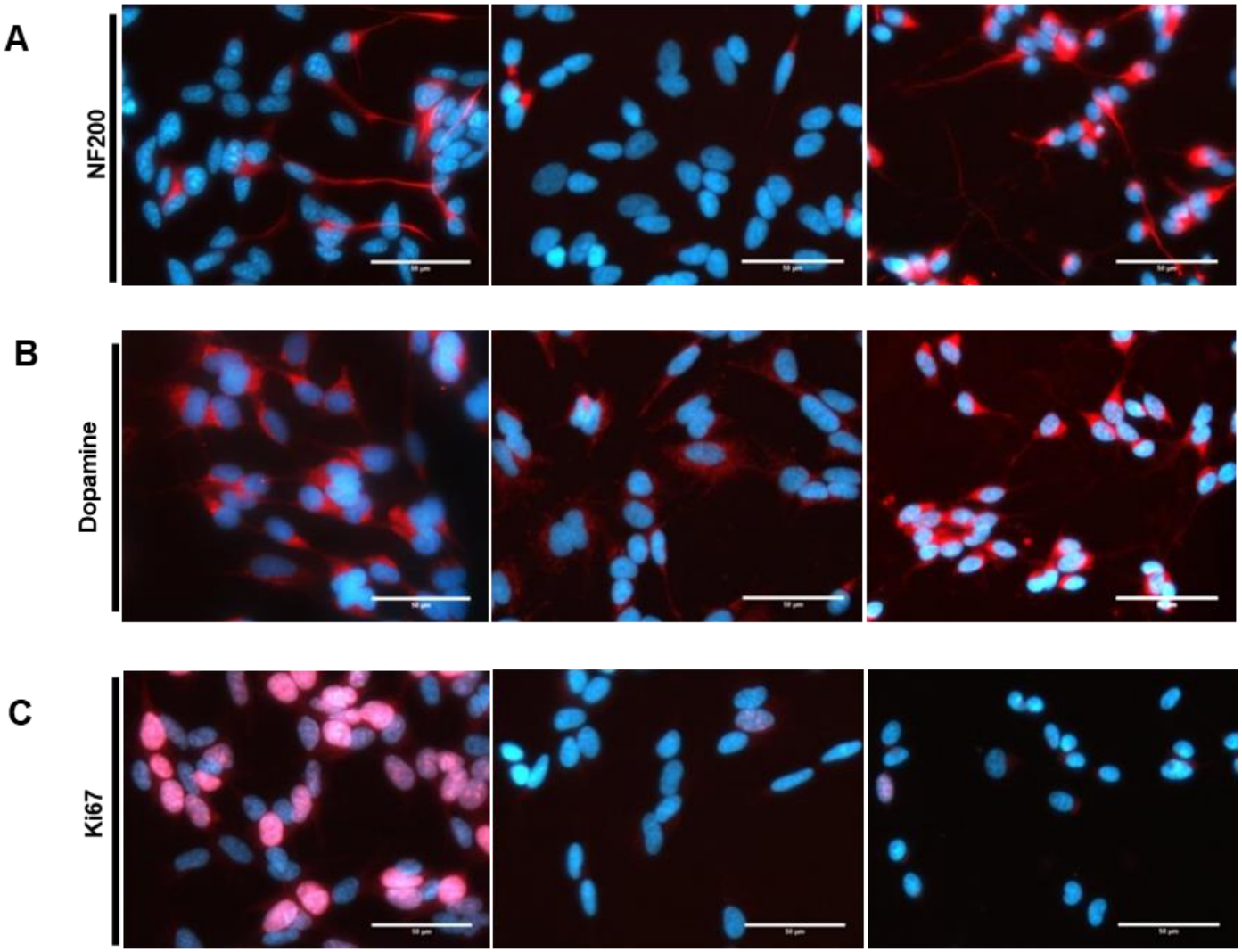

1

Figure 3.6. *Immunocytochemistry analysis of undifferentiated, retinoic acid only, and retinoic and brain derived neurotrophic factor SH-SY5Y.* **(A)** NF200. **(B)** Dopamine. **(C)** Ki67. *C*ultures stained for neurofilament 200 (NF200), dopamine and Ki67 (red). Nuclei were visualised using DAPI staining (blue).

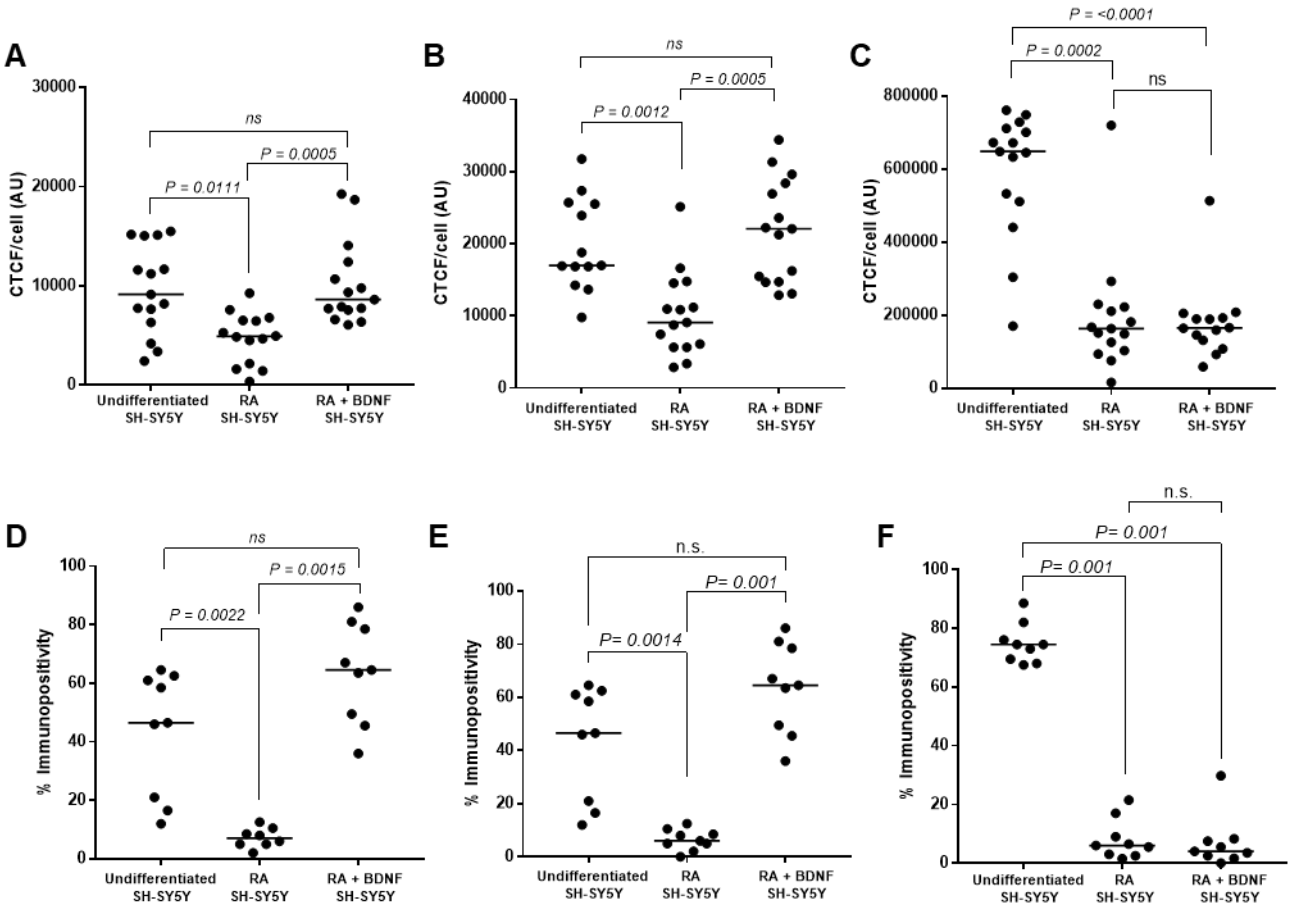

Figure 3.7. ***Corrected total cell fluorescence and percentage cells positive for staining analysis of undifferentiated, retinoic acid, and retinoic acid and brain-derived neurotrophic factor of immunocytochemistry images in Fig. 3.6.*** **(A-C)** Corrected total cell fluorescence image analysis of NF200 **(A)**, dopamine **(B)**, and Ki67 **(C)**. **(D-F)** Percentage of cells positive for immunostaining with NF200 **(D)**, dopamine **(E)**, and Ki67 **(F)**. **(A-F)** Individual data points presented with straight line (median). Statistical significance determined by Kruskal-Wallis test with post-hoc Dwass-Steel-Chritchlow-Fligner. Results of initial Kruskal-Wallis test *P= 0.0001* **(A)**, *P=<0.0001* **(B)**, *P= 0.0001* **(C)**, *P=0.0001* **(D)**, *P= <0.0001* **(E)** *P= 0.0002* **(F)**. P-values are displayed on the figure.

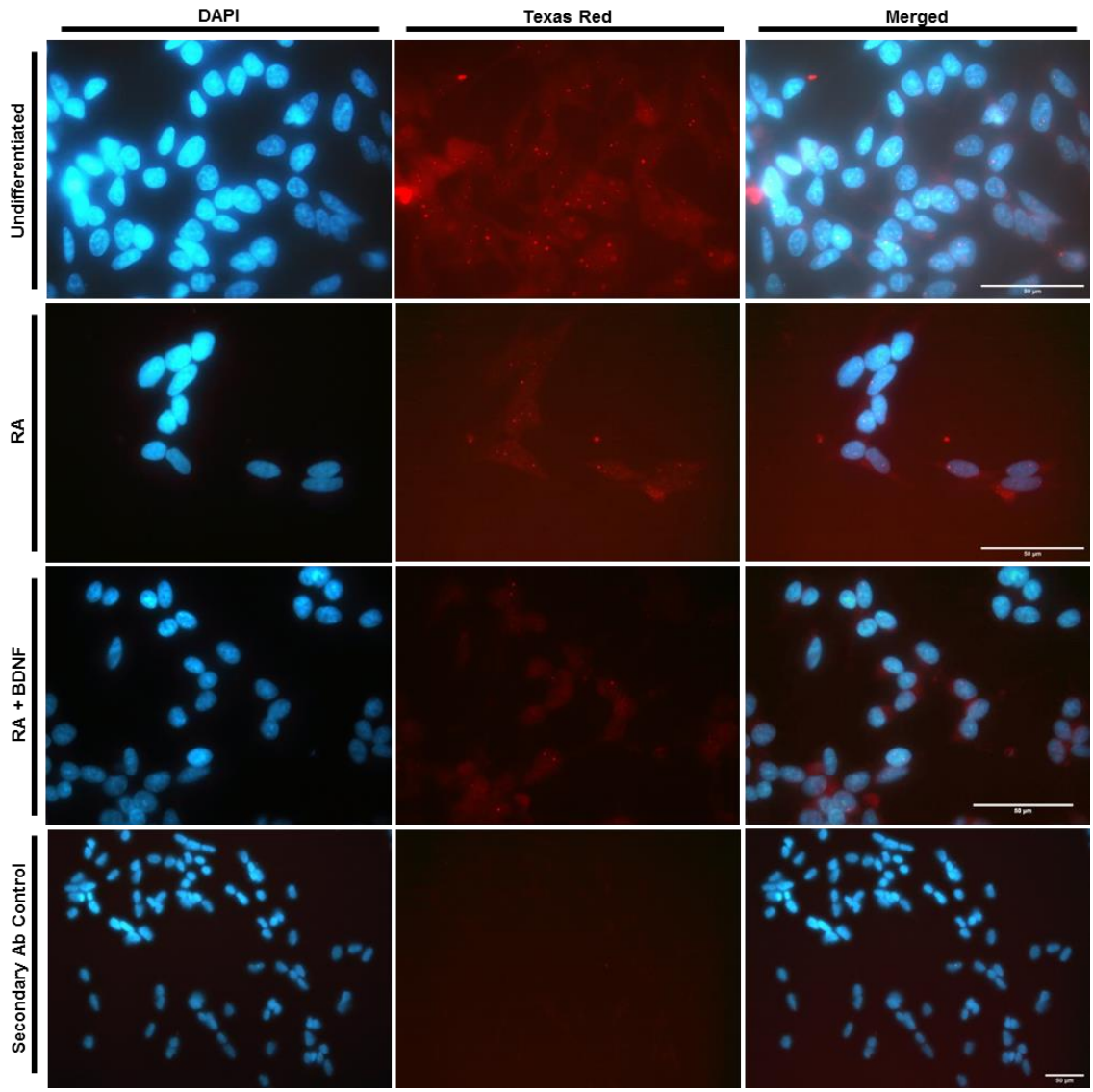

Figure 3.8. *Immunocytochemistry analysis of undifferentiated, retinoic acid only and retinoic and brain derived neurotrophic factor SH-SY5Y with tyrosine hydroxylase (TH) antibody.* Representative images of three independent biological repeats. Scale bars represent 50 µm.

(DRD2) and vesicular monoamine transported member-2 (VMAT2) when compared to the other two cell populations (Fig. 3.5).

Cells at all stages of differentiation were stained with antibodies for the neuronal marker neurofilament 200 (NF200), presence of dopamine, proliferation marker (Ki67) and tyrosine hydroxylase (TH) (Fig. 3.6 and 3.7). NF200 staining was reduced following differentiation with RA (7±3%) compared to undifferentiated SH-SY5Y (43±21%). NF200 immunopositivity was increased in RA + BDNF (64±17%) compared to undifferentiated and RA groups (Fig. 3.7 A, D).

Dopamine is the neurotransmitter produced by dopaminergic neurons of the *SNPc* and therefore an antibody for dopamine was used to determine the presence of the neurotransmitter in all stages of differentiation (Fig. 3.7 B, E).

The anti-dopamine antibody used here has previously been demonstrated to be specific for dopamine through cross-reactivity studies (Banks *et al.*, 2017). Dopamine immunoreactivity was significantly increased in RA + BDNF cultures [21,800±7126 corrected total cell fluorescence (CTCF)/cell] compared to undifferentiated cells (19,800±6371 CTCF/cell) or RA (10,216±5823 CTCF/cell) (Fig. 3.7 B).

Ki67 is a protein associated with cell proliferation and is present in the G_1, S and G_2 phases of cell cycling and mitosis but absent in the G_0 resting state. Undifferentiated cultures expressed this marker, typically associated with the nucleus (591,943±171,477 CTCF/cell). A significant reduction in expression seen in the RA (193,629±160,908 CTCF/cell) and RA + BDNF (180,465±105,445 CTCF/cell) cells indicate that they are terminally differentiated (Fig. 3.7 C, F).

Tyrosine hydroxylase (TH) is a key enzyme in the production and homeostasis of dopamine within catecholamine neuronal cell types (Daubner, Le and Wang, 2011) and is expressed in all three cell types (Fig. 3.8).

Overall, these observations are in line with previously published work on differentiated SH-SY5Y cell lines in which RA + BDNF was utilised and demonstrate that these conditions result in terminally differentiated cells expressing many of the key markers of a dopaminergic neuron (Agholme *et al.*, 2010; Ito *et al.*, 2017; Xicoy, Wieringa and Martens, 2017). Importantly, for use in 3D cultures, the addition of BDNF in serum-free media reduces the proliferation of the non-differentiating ‘S-type’ cell population preventing overgrowth within the cultures.

3.3.4 Cell number optimisation of 3D cultures

To achieve the tissue-like structural integrity of *in vivo* organs the cell number density is important to ensure cellular communication. In addition, the concentration of ECM used for 3D cultures can impact cellular health and differentiation of cultures. Therefore, a variety of cell densities and Matrigel™ concentrations were used to evaluate the optimal cell conditions for differentiation in 3D. Initially, in ‘thin-layer’ cultures (100 µL matrix volumes in 8 well chamber slides), incremental increases in cell densities from $5x10^5$ cells/mL to $1x10^7$ cells/mL were investigated by LIVE/DEAD staining to determine overall

culture health and distribution of cells throughout the cultures (Fig. 3.9 A). At low cell densities, cells clumped together and were not distributed evenly throughout the 3D matrix (Fig. 3.9 A).

LDH assay was also undertaken to assess the health of 3D cultures (Fig. 3.9 B). Increasing culture density from $7.5x10^6$ cells/mL to $2x10^7$ cells/mL with increments of $2.5x10^5$ cells/mL steadily decreased the viability of cells within the matrix (Fig. 3.9 B). The lower cell densities $1x10^6$ cells/mL to $7.5\ x10^6$ cells/mL were investigated further for the expression of neuronal and dopaminergic markers by qPCR.

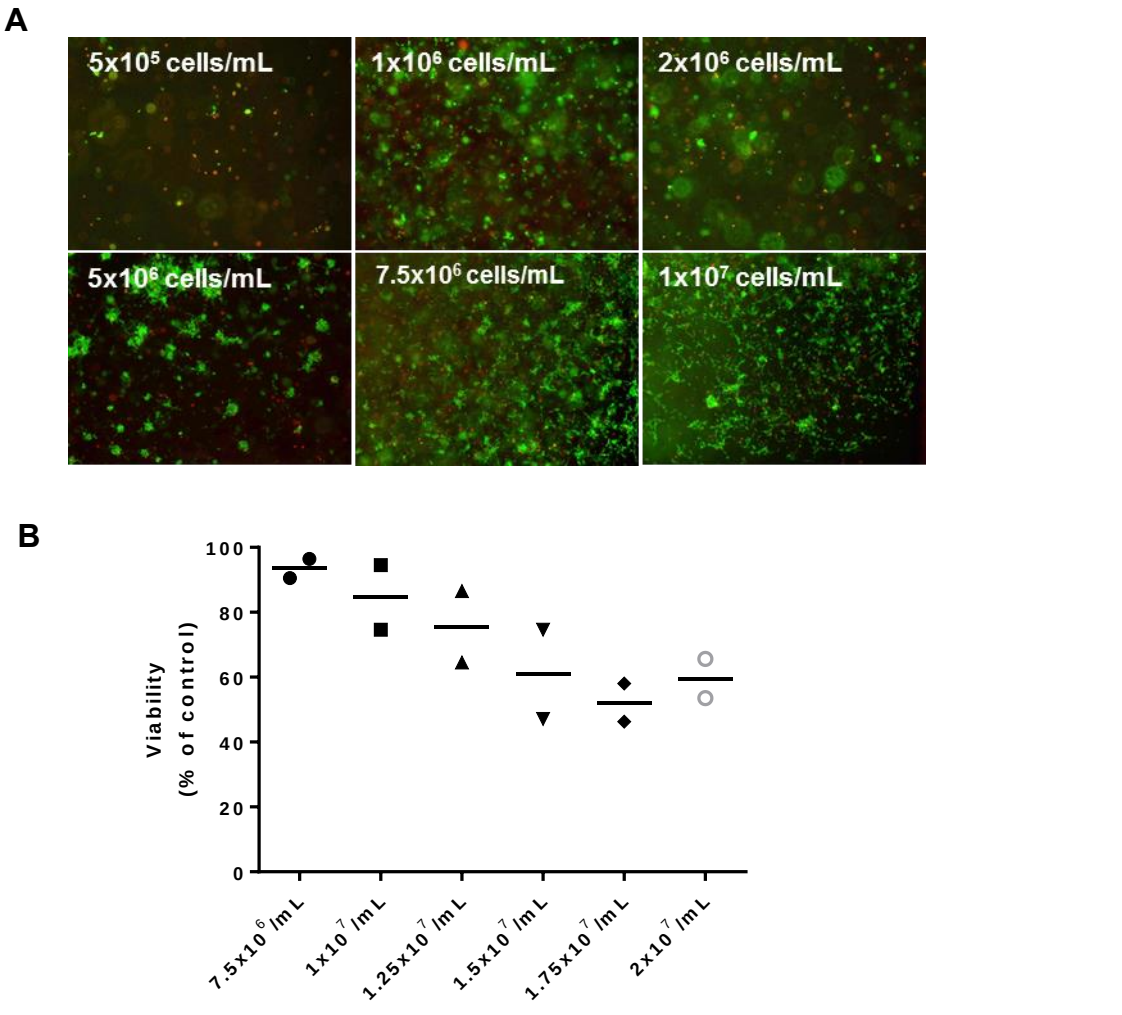

Figure 3.9. *Cell number optimisation of 3D cultures using LIVE/DEAD staining and lactate dehydrogenase (LDH) assay.* **(A)** LIVE (green)/DEAD (red) imaging analysis of RA+BDNF-differentiated cultures in 3D. Representative images of two independent biological repeats. **(B)** LDH assay of 3D cultures. Data presented as individual points and median (straight line) of two independent biological repeats.

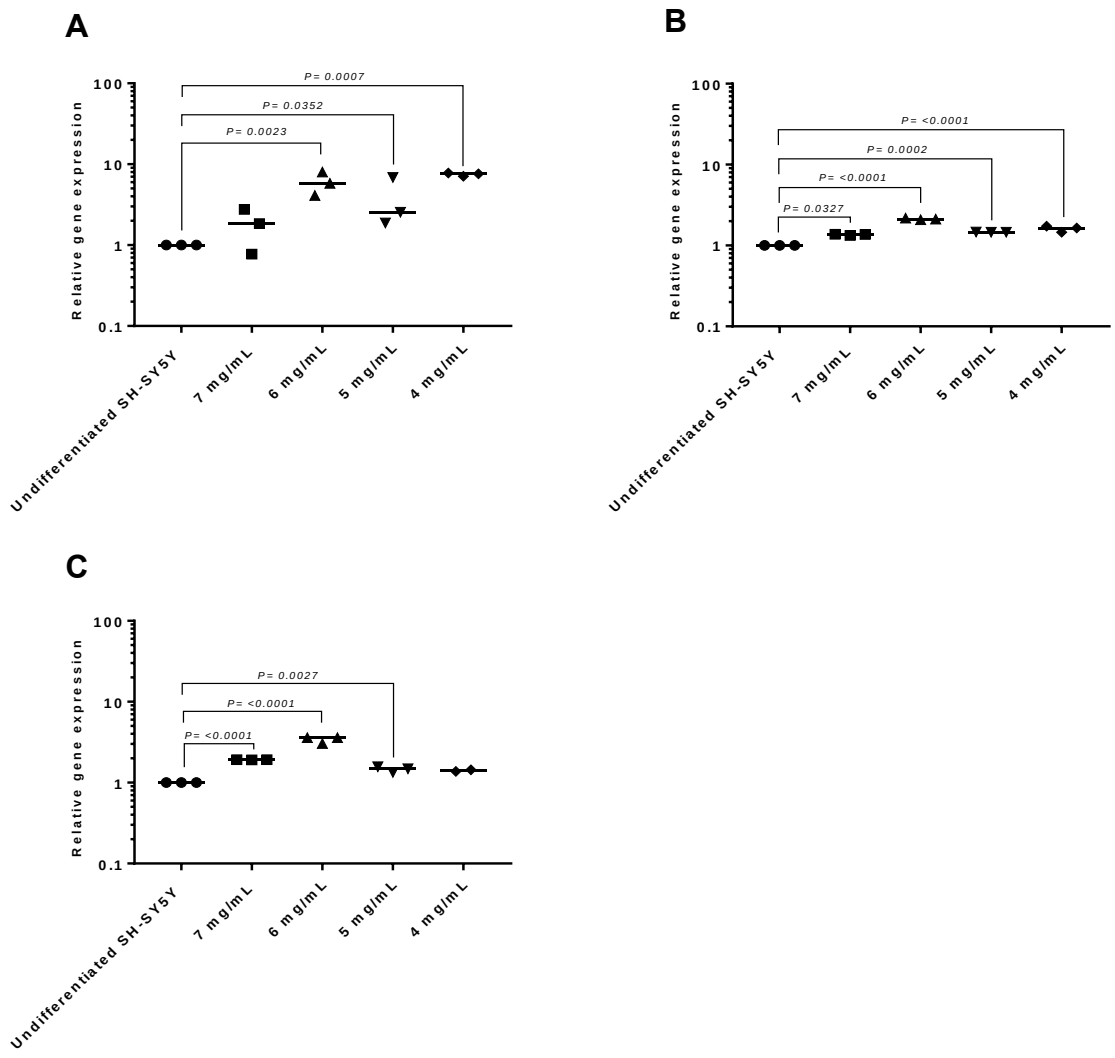

Figure 3.10. *Optimisation of Matrigel concentrations for 3D cultures as analysed by qPCR.* **(A)** Dopamine transporter (*DAT*). **(B)** β-III tubulin (*TUBB3*). **(C)** Microtubule-associated protein 2 (*MAP2*). Data points presented as individual points and median (straight line) of three independent biological repeats. Relative gene expression normalised to reference genes (*RPL13A* and *SDHA*) and undifferentiated SH-SY5Y. Statistical significance determined by Kruskal-Wallis test with post-hoc Conover-Inman. Results of initial Kruskal-Wallis test *P*= 0.0276 **(A)**, *P*=0.0113 **(B)**, *P*= 0.0164 **(C)**. *P*-values are displayed on the figure.

Matrigel™ as a 3D matrix can be diluted from a stock concentration to a variety of working concentrations. Previous studies (Choi *et al.*, 2014) that employed the use of this matrix did so by diluting the stock solution 1:1, 1:3 etc. However, because stocks of Matrigel™ can differ in protein concentration, working concentrations were employed using protein concentrations in mg/mL allowing for differences in protein concentrations in different batches. To determine which protein concentration to use in 3D cultures, qPCR was employed to determine gene expression of *DAT*, *TUBB3* and *MAP2* in Matrigel™ concentrations of 4, 5, 6 and 7 mg/mL (Fig. 3.10). Significant increases in *DAT*,

TUBB3 and *MAP2* were observed in concentrations of 4, 5 and 6 mg/mL. *TUBB3* and *MAP2* were significantly increased in the 7 mg/mL

Matrigel™ concentration. The 6 mg/mL protein concentration of Matrigel™ was used for future experiments due to the greatest increase in expression of all three genes investigated when compared to other the protein concentrations of 4, 5 and 7 mg/mL.

To further investigate optimal cell densities to use in future 3D experiments, LDH assay was undertaken to determine the cell viability of 3D cultures at various cell densities (Fig. 3.11 A). Following on from the dramatic reduction of cell viability in cultures with high cell numbers (Fig. 3.9 B), the cell viabilities of lower cell concentrations of $1x10^6$ to $1.25x10^7$ cells/mL were determined in 'thick-layer' cultures of 300 µL (in 24-well inserts) (Fig. 3.11 A). Incremental increases in densities from $1x10^6$ to $1.25x10^7$ cells/mL by $2.5x10^5$ cells/mL steadily decreased the viability of cells within the matrix (~17% decrease) as measured by LDH concentration (Fig. 3.11 A).

In 300 µL matrix volumes, expression of genes associated with dopaminergic and neuronal markers in 3D cultures was undertaken using qPCR (Fig. 3.11 B, C). Like in 2D-differentiated cultures, expression levels of *DAT*, *DRD2*, *MAP2*, *NES, TUBB3* and *VMAT2* were determined. Upon differentiation in the 3D matrix, gene expression of *DRD2, MAP2* and *VMAT2* was increased (compared to undifferentiated SH-SY5Y) in the $7.5x10^6$ cells/mL group (Fig. 3.11 B). A substantial increase in *VMAT2* expression within the same cells differentiated in 3D compared to 2D indicated the development of a more neuronal phenotype (Fig. 3.11 B). Gene expression data of cell densities $1x10^7$ cells/mL and $1.25x10^7$ cells/mL were not included due to the decrease in cell viability (Fig.3.11 A) and great variability in gene expression between biological repeats.

Comparing expression of *DAT*, *DRD2*, *MAP2*, *NES*, *TUBB3* and *VMAT2* in 3D-differentiated cultures with 2D-differentiated cultures reveals no significant difference in gene expression but reveals a much higher increase in *VMAT2* expression in 3D cultures (Fig. 3.11 C).

Based on these observations, a cell density of $7.5x10^6$ cells/mL was selected for further studies. At this cell density, the expression levels of *DAT*, *DRD2*,

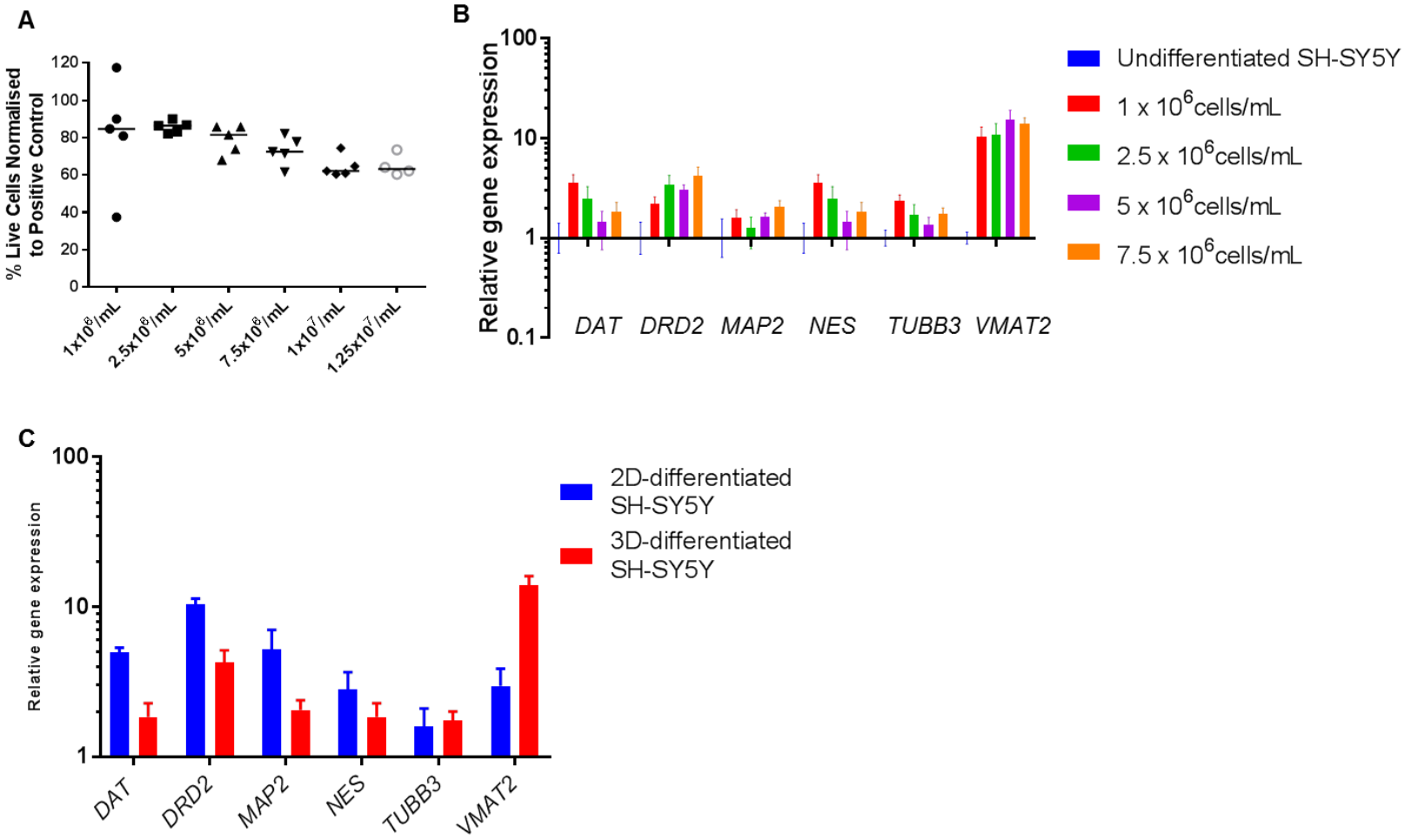

Figure 3.11. *Cell number optimisation of 3D cultures SH-SY5Y analysed by LDH assay and qPCR.* **(A)** Cell number optimisation of thick-layer 3D-differentiated SH-SY5Y using LDH cell viability assay. An incremental increase in cell density is associated with decreased cell viability (~17% decrease from 1 x 10^6 cells/mL to 1.25 x 10^6 cells/mL. LDH cell viability was normalised to cell-density-matched positive controls. All data points are presented with median (straight line) of at least four independent biological repeats. **(B)** mRNA levels of genes specifically associated with dopaminergic neurons were evaluated by qPCR. Relative gene expression normalised to reference genes (*ACTB* and *YWHAZ*) and undifferentiated SH-SY5Y. Data presented as mean ± SEM of at least three independent experiments. **(C)** Comparison of mRNA levels of genes specifically associated with dopaminergic neurons in 2D-differentiated and 3D-differentiated SH-SY5Y cultures as evaluated by qPCR. Relative gene expression normalised to reference genes (*ACTB* and *YWHAZ*) and undifferentiated SH-SY5Y. Data presented as mean ± SEM of at least three independent experiments.

MAP2, TUBB3 and VMAT2 were all increased in relation to undifferentiated SH-SY5Y, and expression of NES was decreased in comparison to other cell densities. Cells displayed a homogenous distribution within the matrix, in contrast to lower densities where clusters of cells were observed (Fig. 3.9 A). In addition, this was the highest cell density at which cell viability was unaffected. Hence, $7.5x10^6$ cells/mL was the optimal balance between cell viability and homogeneity within the matrix.

3.3.5 SH-SY5Y differentiation in 3D culture retains a dopaminergic phenotype

Using qPCR, 3D-differentiated cultures revealed the expression of both neuronal and dopaminergic markers. Immunohistochemistry was used to confirm the expression of proteins related to neurons (NF200 and βIII-tubulin), the mitotic status of cells (Ki67) and presence of the neurotransmitter dopamine. Prior to this, optimisation of staining techniques was investigated in order to carry out immunohistochemistry protocols. Initially, 3D-cultures of 300 µL matrix volumes (in 24-well inserts) were fixed and sectioned using paraffin-embedded sectioning and subsequent staining of cultures using Haematoxylin and Eosin (H + E) (Fig. 3.12 A). Visualisation of these cultures revealed shrinking of the 3D cultures that were difficult to section and subsequently stain. Cryostat sectioning was determined to provide a viable method of fixing, sectioning and staining of the 3D cultures (Fig. 3.12 B). In contrast to paraffin-embedded sectioning, cryostat sections were not subjected to shrinking and nuclei were easily identified following H + E staining (Fig. 3.12 A, B). Therefore, cryostat sectioning was used to prepare sections for further immunohistochemical staining.

βIII-tubulin staining was used to develop an immunofluorescence-based immunohistochemistry protocol and confirmed the expression of neuron-specific proteins (Fig. 3.13 A). Due to difficulty observing the fluorescence on the microscopes available at the time of the study, DAB staining was chosen over immunofluorescence staining. Staining with NF200 again confirmed the neuronal phenotype of cells differentiated in 3D cultures (Fig. 3.13 B). Anti-dopamine staining revealed the presence of the neurotransmitter within these cultures (Fig. 3.13 B). Ki67 staining was also undertaken to determine the mitotic state of cells in 3D cultures.

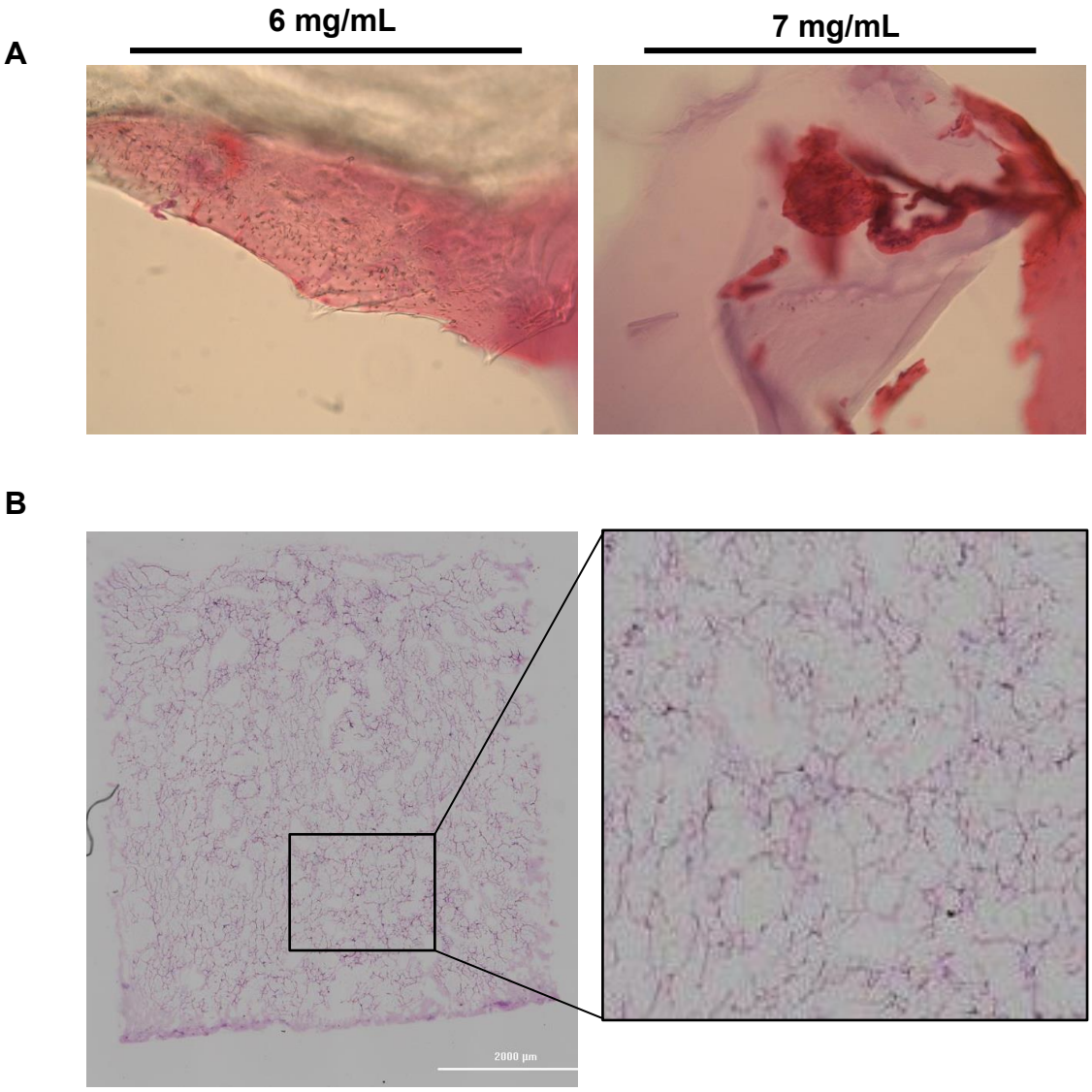

Figure 3.12. *Optimisation of staining techniques for 3D cultures*. Cultures stained using H + E staining where nuclei are stained purple and proteins in the cytoplasm are stained pink. **(A)** Paraffin-embedded sectioning of 3D cultures reveals shrinking of cultures. Cultures stained using H + E staining where nuclei are stained purple and proteins in the cytoplasm are stained pink. **(B)** Cryostat sectioning of 3D cultures allows for identification of cells in contrast to paraffin-embedded sectioning. Scale bar represents 2000 µm.

1

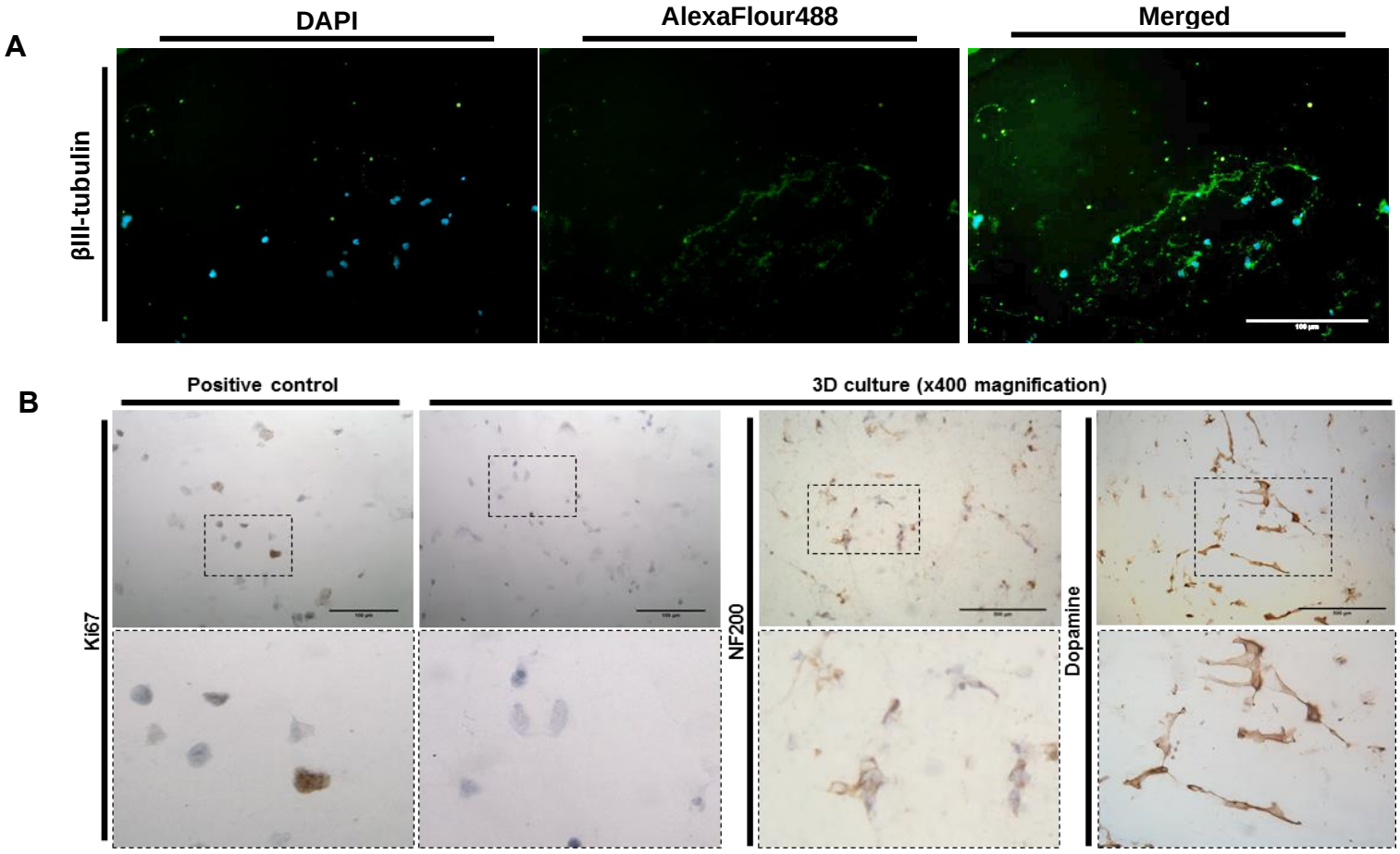

Figure 3.13. *Neuron-like cells cultured in 3D retain a dopaminergic phenotype.* **(A)** Immunofluorescence staining of β-III tubulin staining (AlexaFluor; green). Nuclei were visualised using DAPI (blue). Scale bar represents 100 µm. **(B)** 3D-differentiated SH-SY5Y cultures retain a post-mitotic neuronal dopaminergic phenotype in 3D as determined by the absence of Ki67 staining and positive staining for NF200 and dopamine. Haematoxylin was used as a counter stain for nuclei (purple). Positive control for Ki67 staining is undifferentiated SH-SY5Y cultured in 3D. Scale bar represents 100 µm.

Absence of Ki67staining in 3D-differentiated cultures demonstrated the post-mitotic phenotype of these neuron-like cells (Fig. 3.13 B). A positive control for Ki67 staining was included, undifferentiated SH-SY5Y cells were grown in the 3D matrix for 24 hrs before subjected to cryostat sectioning and staining. Undifferentiated SH-SY5Y was determined to be positive for Ki67 expression as shown by the nuclear associated brown DAB staining (Fig. 3.13 B). Isotype controls demonstrate no non-specific staining for Ki67, NF200 or dopamine. This body of work establishes a 3D cell culture model in which fully differentiated neuronal SH-SY5Y cells have been encapsulated within a Matrigel™ scaffold.

3.4 Discussion

The objective of this chapter was to develop a 3D cell culture model utilising the easily accessible SH-SY5Y neuroblastoma cell line, to be used to further model the aggregation of α-syn in a more physiologically-relevant cell culture model. SH-SY5Y have long since been used in PD research for several reasons, including the expression of genes associated with a dopaminergic phenotype (*DAT*, *DRD2, VMAT2* and *TH*), ease of culture and induction of differentiation into a more neuronal phenotype (Smidt and Burbach, 2007). Importantly for this study, α-syn has been shown to form aggregates in SH-SY5Y (Danzer *et al.*, 2007; Illes-Toth *et al.*, 2015). At present, there are relatively few cell culture models that model the development of LB-like α-syn aggregates that faithfully recapitulate *in vivo* phenotypes. Therefore, the primary aim of this work was to adapt a differentiated SH-SY5Y model to 3D, with the hypothesis that culturing in 3D would promote α-syn-cell interaction and enhance aggregate formation (Choi *et al.*, 2014).

Although relatively few papers have employed the use of this protocol (1-2%), differentiation of SH-SY5Y with the sequential treatment of RA and BDNF leads to the development of a homogenous neuronal population with the expression of neuronal markers and reduction of cell proliferation (Encinas *et al.*, 2000; Goldie, Barnett and Cairns, 2014; Xicoy, Wieringa and Martens, 2017). Pre-differentiation for at least 5 days with RA coincides with peak expression of the tropomyosin receptor kinase B (TRKB) required for biological responsiveness of BDNF (Kaplan *et al.*, 1993; Encinas *et al.*, 2000; Nishida *et al.*, 2008). BDNF stimulates the phosphorylation of TRKB and subsequent activation of PI3K/AKT

and Ras/MAPK pathways, resulting in the promotion of cell survival and neurite outgrowth (Kaplan *et al.*, 1993; Encinas *et al.*, 1999, 2000). Removal of serum in media when culturing with BDNF results in the ablation of 'S' type cell growth due to the lack of expression of neuron-specific markers and failure to induce TRKB (Encinas *et al.*, 2000).

Controversy remains as to whether RA or RA + BDNF promotes SH-SY5Y cell differentiation and the development of a terminal dopaminergic phenotype (Lopes *et al.*, 2010; Korecka *et al.*, 2013; Xicoy, Wieringa and Martens, 2017). Induction of neurite growth, expression of dopaminergic markers and exit from the cell cycle was explored in RA + BDNF differentiation cultures prior to culture in 3D. In addition, the above was also explored in RA-only differentiated SH-SY5Y, as this represents the most commonly used differentiation protocol for use in PD research (Xicoy, Wieringa and Martens, 2017). In agreement with previous publications, RA and RA + BDNF promoted the differentiation of SH-SY5Y as demonstrated by the formation of extended neurites. RA + BDNF demonstrated the most marked extension of neurites that form complex networks (Encinas *et al.*, 2000; Mastroeni *et al.*, 2009). NF200 (neurofilament heavy polypeptide, neurofilament H), exclusively localised in neurons, is a key constituent of the neuronal cytoskeleton with an important function in mature axons (Yuan Aidong, Rao Mala V. , Veeranna, 2017). Presence of NF200 was observed in both undifferentiated and RA + BDNF SH-SY5Y, with little staining detectable in RA SH-SY5Y. The reduction in NF200 staining in RA compared to undifferentiated SH-SY5Y could be related to the continued presence of the 'S' type non-neuronal cell type within the RA population (Constantinescu *et al.*, 2007). All cultures stained positive for dopamine and TH, demonstrating the ability for cells to synthesis DA, critical for a dopaminergic phenotype. DA uptake and release have previously been shown in RA + BDNF cultures (Mastroeni *et al.*, 2009). Ki67, a protein associated with cell proliferation was used to determine the post-mitotic status of each stage of differentiation (Gerdes *et al.*, 1983; Bullwinkel *et al.*, 2006). Reduction of Ki67 staining was observed in RA and RA + BDNF, indicating the removal of cells from the cell cycle. Using other methods, such as BrdU/EdU and propidium iodide staining and flow cytometry analysis also indicate withdrawal from the cell cycle (Encinas *et al.*, 2000; Ito *et al.*, 2017). However, not all studies confirm the

inhibition of cell growth following differentiation (Teppola *et al.*, 2016). In the previous study, cell growth was monitored by counting cell nuclei in contrast to the assessment of the stage of the cell cycle (either by staining with BrdU/EdU/PI or presence of proteins associated with the cell cycle e.g. Ki67), meaning cell number could be affected by the death of cells that have not responded to differentiation, or if treatment has stabilised cell populations (Encinas *et al.*, 2000).

All SH-SY5Y cultures expressed markers of a dopaminergic phenotype as determined by qPCR, including *DRD2, DAT* and *VMAT2*, independent of differentiation (Cheung *et al.*, 2009; Mastroeni *et al.*, 2009; Korecka *et al.*, 2013). In conjunction, dopamine and TH immunostaining indicates a dopaminergic phenotype. When compared to undifferentiated and RA SH-SY5Y, RA + BDNF treated cultures show increased expression of *DAT, DRD2* and *VMAT2*. This may again be due to the presence of 'S' type cells in the undifferentiated and RA populations. Expression of neuronal proteins *MAP2* and *TUBB3* were also upregulated following treatment with RA + BDNF, indicating the development of a neuronal phenotype following differentiation. Expression of the neural stem/progenitor cell marker *NES* was increased (although not significantly) in both RA and RA + BDNF cultures, compared to undifferentiated cultures. Following differentiation, this would be expected to be downregulated as *NES* is replaced by tissue-specific intermediate filament proteins, e.g. neurofilaments (Lendahl, Zimmerman and McKay, 1990; Hendrickson *et al.*, 2011). *NES* plays an important role in the remodelling of the cell's cytoskeleton by assisting in the assembly and disassembly of intermediate filament proteins (Hendrickson *et al.*, 2011). *NES* expression may be related to the development of axons in differentiating cells, therefore increased expression is indicative of neuronal development and remodelling of the cytoskeleton during differentiation. Similarly, *NES* expression was still observed to form cytoskeletal structures in fully post-mitotic LUHMES (Scholz *et al.*, 2011). Other reasons could be that SH-SY5Y have a limited maturation capacity under the culture conditions presented here, or the downregulation of *NES* could require a longer differentiation time.

It is important to note that the differentiation of cells in 2D was difficult due to cells detaching from the culture vessel before the end of differentiation with

BDNF. Culturing in 3D circumvented this issue by preventing cells washing away, therefore allowing for more robust handling methods and analysis. Adaptation of the culturing and differentiation method for SH-SY5Y to 3D was achieved by culturing RA pre-differentiated SH-SY5Y in a 3D matrix for further differentiation in serum-free media with the addition of BDNF. Matrigel™, a basement protein preparation, was chosen as a 3D support due to the previous observation that culturing cells within this matrix allowed for enhanced Aβ deposition in a model of AD (Choi *et al.*, 2014). Moreover, encapsulation of cells can be achieved through moderate thermal changes and provides a brain-like environment rich in laminin, entactin, collagen and heparan sulphate proteoglycans (Hughes, Postovit and Lajoie, 2010; Choi *et al.*, 2014; Kim *et al.*, 2016).

Following encapsulation in 3D and further differentiation, cells were demonstrated to retain a dopaminergic phenotype as indicated by expression of *DAT, DRD2* and *VMAT2* and immunostaining with dopamine. Immunostaining of 3D cultures with Ki67, dopamine and NF200 showed a similar phenotype to 2D-differentiated cells. Optimisation of various techniques such as qPCR and immunostaining of the 3D model demonstrated the adaptability of the culture system to general laboratory techniques widely used by scientists. One particular advantage of the 3D-differentiated SH-SY5Y model is the ability to expand and bulk up cell numbers relatively cheaply and easily (no expensive culture additives) prior to culture in 3D. A point to note is that as Matrigel™ is a biological product, batch-to-batch variation is an important factor that could lead to a disparity between experiments (Hughes, Postovit and Lajoie, 2010). These differences include protein and growth factor concentration between batches, therefore, using the same the batch and reduced growth-factor Matrigel™ is a viable option and was used in this study.

In conclusion, culturing differentiated SH-SY5Y in both 2D and 3D formats produced cells displaying features of neurons relevant to PD. These features include the development of extended neurites (mature neurons) and expression of key proteins associated with dopaminergic neurons (*DAT, DRD2, VMAT2),* in addition to positive immunostaining for dopamine. Culture of SH-SY5Y cells was easily adapted to 3D culture conditions, providing an easily accessible culture model that has the potential to be used in diverse areas of PD research.

Chapter 4 : Characterisation of the effect of α-synuclein seeding oligomers on 2D and 3D SH-SY5Y cultures

4.1 Introduction

The mechanisms underlying LB formation and the influence of α-syn pathology on disease pathogenesis remain poorly understood, largely due to the lack of whole-animal or cell-based models that recapitulate the development of these inclusions. Relatively few studies have observed the development of LB pathology without overexpressing high levels of human versions of α-syn (Volpicelli-Daley *et al.*, 2011; Falkenburger, Saridaki and Dinter, 2016). In addition, a predominant number of studies rely on the introduction of a familial mutation into α-syn (e.g. A53T) to increase aggregation propensity (Uversky, Li and Fink, 2001; Koprich, Kalia and Brotchie, 2017). α-Syn in *Drosophila* mirrors the formation of LB-like structures and neuronal loss, but this has unfortunately not been replicated in higher-order organisms or human-cell-based models (Feany and Bender, 2000). Interestingly, rodent models of PD that overexpress human α-syn by mutations in the SNCA gene (e.g. the M83 strain, overexpressing mutant human A53T α-syn) do develop inclusions but the anatomical distribution is widely variable among animals and often coincides with areas of substantial neuroinflammation (Lee *et al.*, 2002; Dawson, Ko and Dawson, 2011; Sacino *et al.*, 2014; Fares *et al.*, 2016). Impaired human α-syn fibrillisation can occur in rodent models due to an interaction with endogenously expressed murine α-syn (Fares *et al.*, 2016). Such interactions highlight a fundamental experimental caveat when investigating LB formation in murine models or rodent-derived primary neuronal cultures (Fares *et al.,* 2016). Species differences between rodent models (including primary rodent cell culture systems) make it difficult to model and extrapolate findings to human subjects (Ioannidis, 2012; Goldie, Barnett and Cairns, 2014; Pound and Bracken, 2014).

In previous human-cell-based models, limitations have also arisen from the use of traditional 2D monolayer cultures. Intracellular α-syn aggregates are often observed as multiple cytoplasmic punctate inclusions rather than recapitulating the typical large singular inclusions associated with human pathology (Desplats *et al.*, 2009;

Danzer *et al.*, 2009). Formation of LB-like pathology in human cell culture models has only been achieved through overexpression of α-syn, either driven from viral promoters or in cell lines not associated with the disease, such as those from human embryonic kidney lines (HEK-293) (Luk *et al.*, 2009; Volpicelli-Daley *et al.*, 2011; Sacino *et al.*, 2013). Such viral promotors do not allow the study of transcriptional and translational modulations brought about during the disease pathogenesis. To address these issues, *in vitro* 3D culture systems are increasingly being utilised for a multitude of disease models, with the aim of more closely mimicking an *in vivo* environment with tissue-like cell density and cell-to-cell as well as cell-to-extracellular-matrix contacts (Griffith and Swartz, 2006; Tang-Schomer *et al.*, 2014; Kim *et al.*, 2016; Smirnova *et al.*, 2016). Taken together, the current limitations of both *in vitr*o and *in vivo* models demonstrate a greater need to develop a human-relevant culture system to model LB pathology.

4.2 Aims and Objectives

The purpose of this chapter was to investigate the neurotoxicity of α-syn seeding oligomers using 3D SH-SY5Y cell culture as a model of PD and identify whether exogenously added forms of α-syn in the 3D model recapitulate traditional 2D systems. Numerous *in vitro* preparations of α-syn oligomers and fibrils have been reported with two main gain-of-function mechanisms of neurotoxicity in 2D cell culture: Ca^{2+} influx and prion-like seeding (Danzer *et al.*, 2007). A specific population of α-syn oligomer, identifiable by mass spectrometry, have been shown to induce intracellular aggregation in a 2D culture system (Illes-Toth *et al.*, 2015). Using these compact, high order ring-like oligomers, the neurotoxicity and seeding effects were to be investigated in both 2D and 3D SH-SY5Y cultures.

The specific aims of this chapter were:

- To determine neurotoxicity of seeding oligomers in SH-SY5Y cell populations.
- To determine whether seeding oligomers induced the intracellular aggregation of α-syn in SH-SY5Y cell populations.
- To identify whether seeding oligomers induced the intracellular aggregation of α-syn in a 3D culture that recapitulates LB formation.

4.3 Results

4.3.1 Production of recombinant α-syn

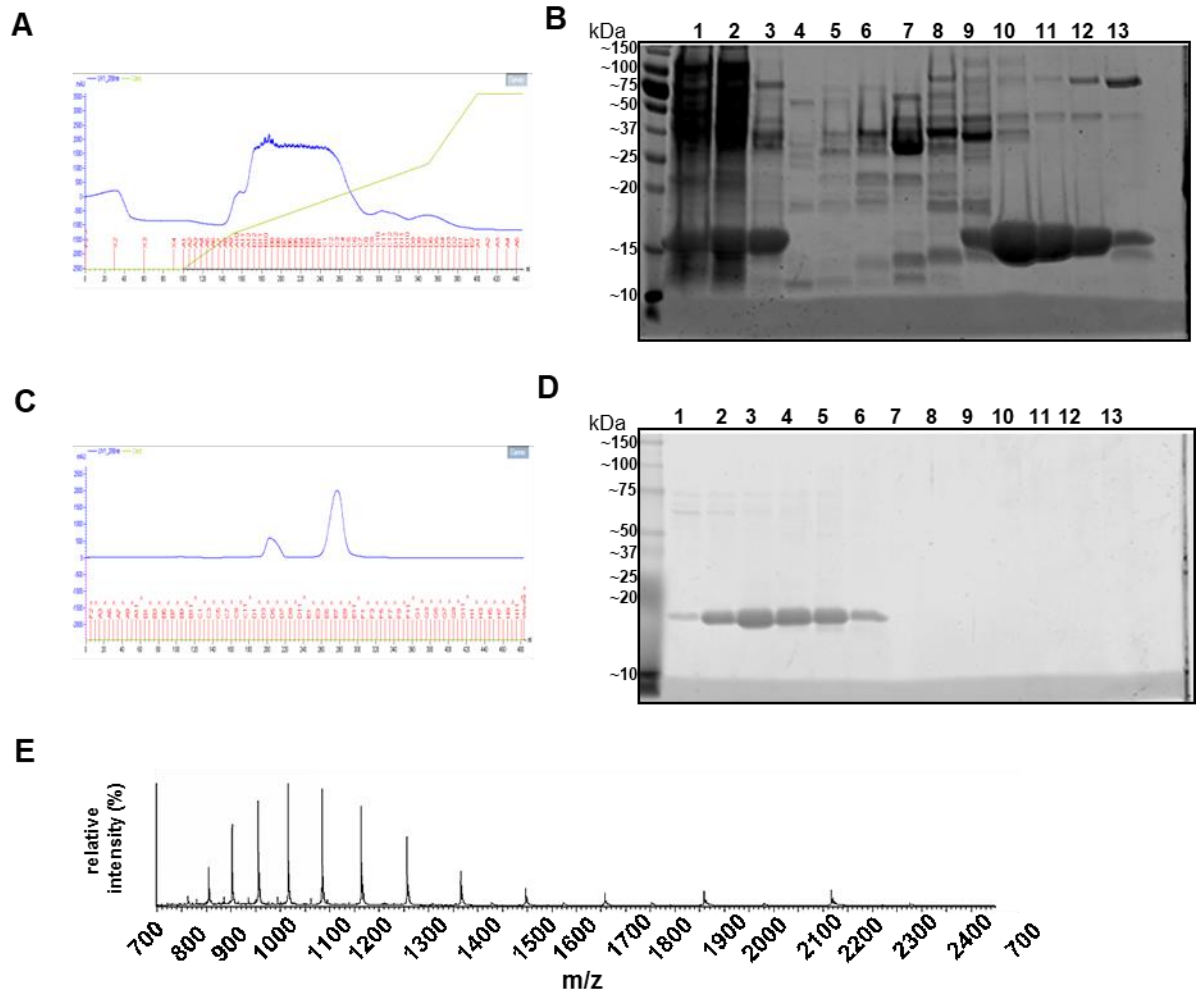

Figure 4.1. *Typical column chromatography UV chromatograms and SDS-PAGE analysis of recombinant α-syn during purification.* **(A)** Crude lysate prepared from E. coli overexpressing α-syn was subjected to anion exchange chromatography through a 50 mL Q-Sepharose anion exchange column. A sodium chloride gradient eluted the bound proteins from the column and fractions were subjected to SDS-PAGE electrophoresis. **(B)** SDS-PAGE gel of fractions eluted from anion exchange column. Lanes 1-3 show samples from the crude purification process prior to anion exchange. Lanes 9-13 show fractions with high levels of α-syn, corresponding to MW of ~15 kDa. **(C)** Following selection of fractions containing α-syn from anion exchange, samples were lyophilised before being subjected to size exclusion chromatography using a HiLoad® 26/600 Superdex™ 200 size exclusion column. **(D)** SDS-PAGE gel of fractions eluted from size exclusion column. Lanes 1-7 show the presence of α-syn in these fractions. **(E)** Mass spectrometric analysis of recombinant α-syn shows intact protein of the expected mass.

Certain species of α-syn have the ability to be internalised from the extracellular environment and induce the aggregation of endogenous α-syn (Danzer *et al.*, 2007; Luk *et al.*, 2009; Aulic *et al.*, 2014). This mechanism of seeding and subsequent propagation has the potential to explain the spread of α-syn species throughout the PD brain. To investigate whether the oligomers produced here were capable of seeding the intracellular aggregation of α-syn, undifferentiated and differentiated SH-SY5Y in 2D and 3D cultures were exposed to exogenous α-syn oligomeric species,

monomeric and solvent controls. Recombinant α-syn was produced in *E. coli* and seeding oligomers were produced by incubation overnight in 50 mM sodium phosphate buffer, with 20% ethanol at pH 7, followed by ultracentrifugation (Fig. 4.1).

4.3.2 Application of α-syn oligomers are not associated with toxicity in 2D SH-SY5Y cultures

Seeding oligomers are capable of inducing the intracellular aggregation of α-syn without necessarily being neurotoxic to cell preparations, in contrast to treatment with pore-forming oligomers (Danzer *et al.*, 2007; Illes-Toth *et al.*, 2015). Prior to investigating the intracellular aggregation of α-syn in all SH-SY5Y differentiation protocols, cell viability was investigated using the resazurin reduction assay (Fig. 4.2). Treatment with 10% v/v solvent, 10% v/v monomer and 10% v/v oligomer for 24 hrs did not induce any significant changes in cell viability in undifferentiated or RA-differentiated SH-SY5Y (Fig. 4.2 A, B). In contrast, the same treatments to RA + BDNF-differentiated cultures induced large amounts of cell death (Fig. 4.2 C).

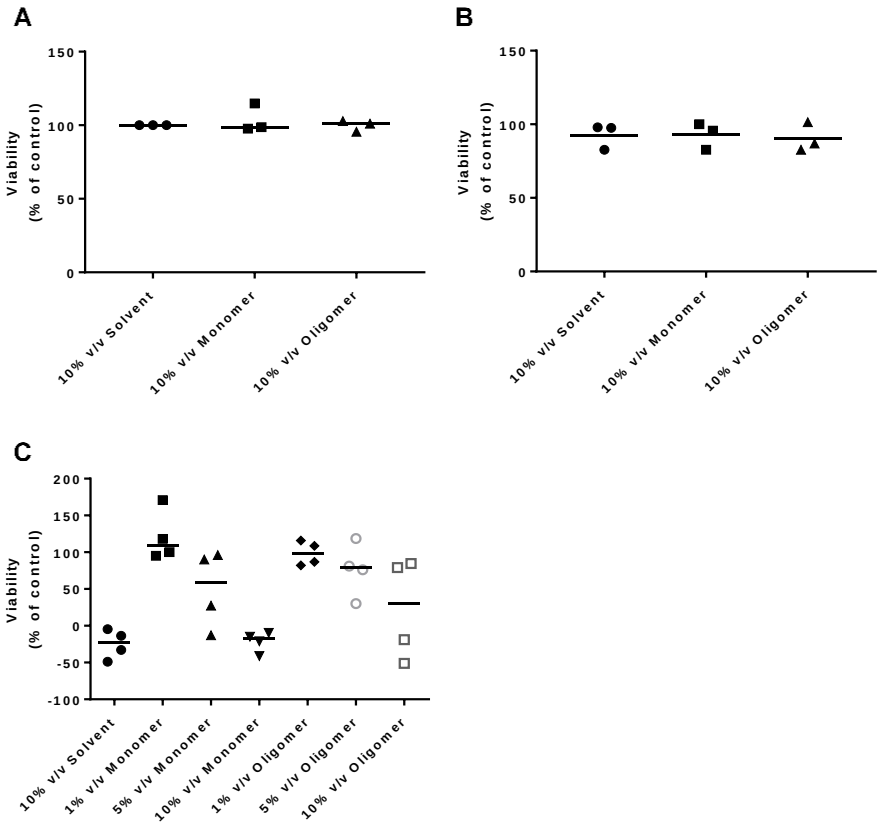

Figure 4.2. *Resazurin cell viability assays of 2D undifferentiated and differentiated SH-SY5Y following 24 hr treatment with solvent, monomeric and oligomeric preparations.* **(A)** Undifferentiated SH-SY5Y. **(B)** RA-differentiated SH-SY5Y. **(C)** RA + BDNF-differentiated SH-SY5Y. **(A-C)** Data presented as median with all data points shown of either 3 or 4 independent biological repeats. No significant differences determined between data sets.

4.3.3 Intracellular aggregation properties of ‘seeding’ oligomers

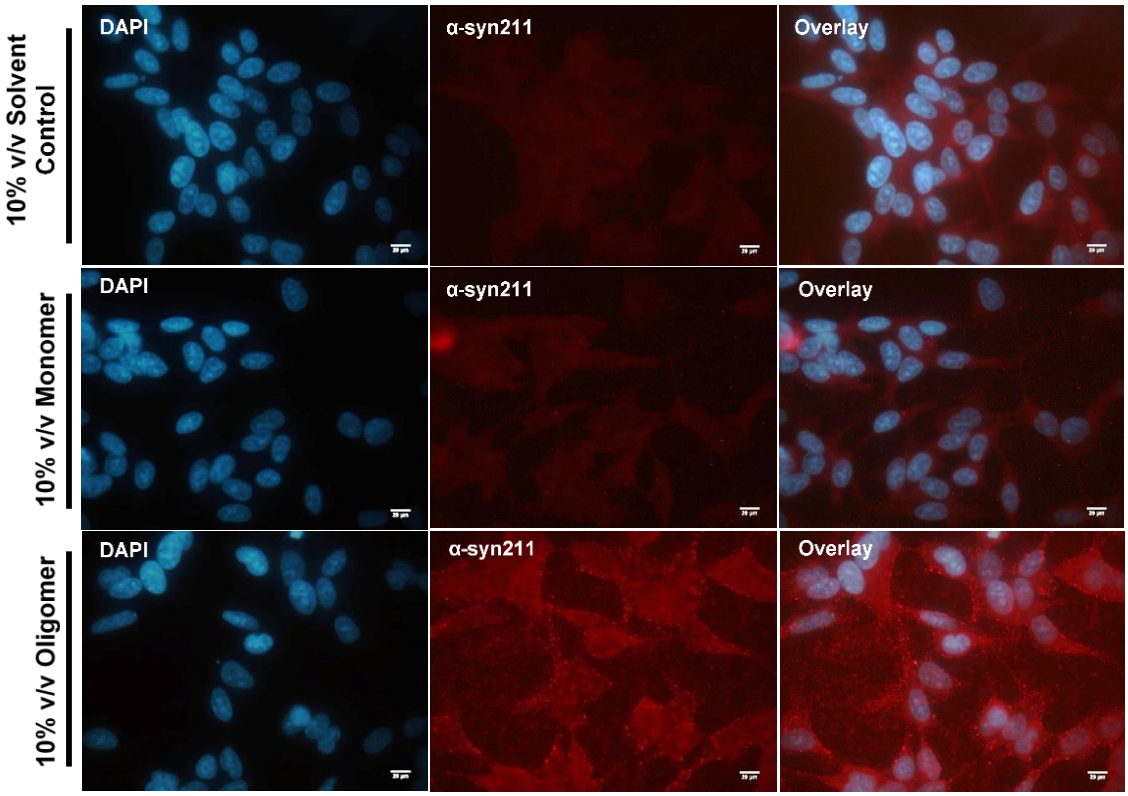

Figure 4.3. *Exogenous addition of oligomers induces intracellular aggregation of α-syn in 2D undifferentiated SH-SY5Y cultures.* Double immunostaining with α-syn (Texas Red, red) and nuclei (DAPI, blue) reveals the presence of multiple, small inclusions throughout the cytoplasm in 10% v/v oligomer-treated cultures when compared to diffuse staining in 10% v/v solvent control (sodium phosphate buffer + 20% ethanol) and 10% v/v monomer control. Scale bar represents 20 µm.

Application of seeding oligomers to 2D undifferentiated SH-SY5Y cell populations was demonstrated to be non-toxic (Fig. 4.2), therefore the intracellular aggregation of α-syn was investigated (Fig. 4.3, 4.4). Treatment with seeding oligomers to undifferentiated SH-SY5Y resulted in a reduction in the homogenous cytoplasmic staining of α-syn and development intracellular α-syn-immunopositive aggregates, consistent with Danzer *et al.* 2007 (Fig. 4.3). This is in contrast to both solvent and monomeric treatments that did not induce the development of intracellular inclusions (Fig. 4.3). Western blotting analysis revealed an increase in intracellular levels of α-syn following treatment with oligomers and monomer when compared to media only and solvent controls (Fig. 4.4).

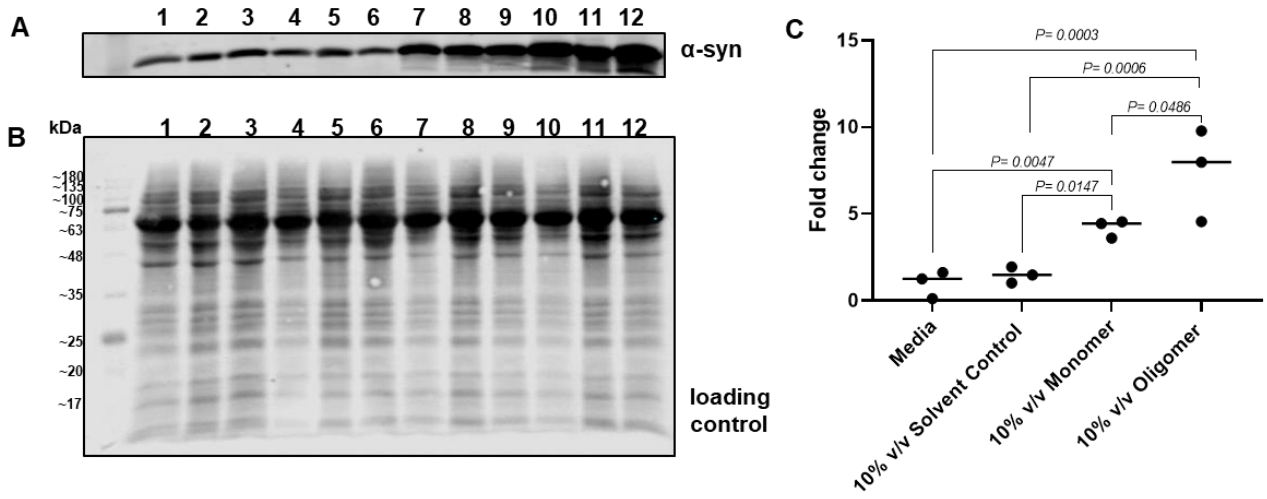

Figure 4.4. *Western blot analysis of α-syn levels in 2D undifferentiated SH-SY5Y treated with oligomers and controls.* **(A)** α-syn blot. **(B)** Loading control. **(A, B)** All biological repeats were run on the same blot. Lanes 1-3 represent media samples, lanes 4-6 represent 10% v/v solvent, lanes 7-9 represent 10% v/v monomer and lanes 10-12 represent 10% v/v oligomer treatments. **(C)** Fold change of α-syn levels. Data presented as median with all data points present. Statistical analysis was undertaken using Kruskal-Wallis with post-hoc Conover-Inman with all P values presented on the graph. Results of initial statistical test *P= 0.0237.*

Within the PD brain, LB pathology is only observed in a discrete cell population within *ex vivo* material (Braak *et al.,* 2003). As demonstrated above, all cells of undifferentiated SH-SY5Y treated with oligomeric α-syn developed inclusions (Danzer *et al.*, 2009; Illes-Toth *et al.*, 2015). Here, it was investigated whether the extent of cellular differentiation resulted in alterations in the intracellular aggregation propensity of the cell line. Following the addition of oligomeric α-syn to undifferentiated SH-SY5Y cells, the presence of multiple punctate α-syn-positive cytoplasmic inclusions with an average inclusion size of 0.28 μm^2 was confirmed in our model (Fig. 4.5 A, B). The addition of the same oligomer treatment on RA-differentiated cultures also produced several small cytoplasmic inclusions within each cell, but the average inclusion size was significantly (*P<0.0001*) larger (0.82 μm^2) than in the undifferentiated SH-SY5Y cells (Fig. 4.5 A, B). In both undifferentiated and RA-differentiated SH-SY5Y cells, all surviving cells developed the punctate inclusions (Fig. 4.5 C). In contrast, the addition of the same soluble oligomeric α-syn preparation to RA+BDNF-differentiated culture media demonstrated the development of a single perinuclear inclusion, consistent with a large LB-like aggregate (Fig. 4.5 A, asterisks and arrows, bottom panel), with an average inclusion size of 8.95 μm^2. Cellular inclusions could be detected 24 h after treatment, but only 31% of the cell population developed these structures (Fig. 4.5 C). To our

knowledge, this is the first observation of single large inclusions within a genetically unmodified cell culture model.

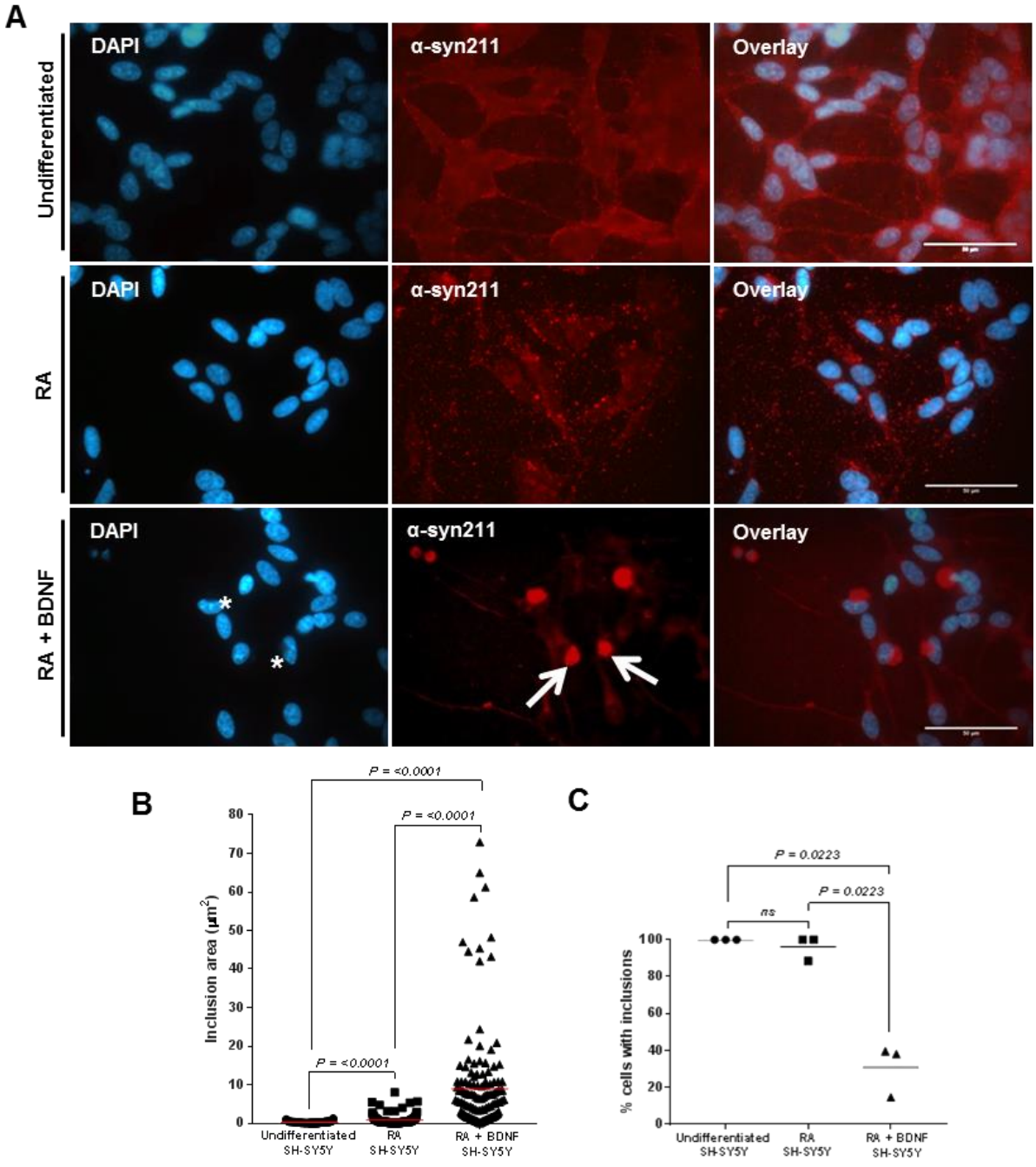

Figure 4.5. *Exogenous addition of α-syn oligomers induces the intracellular aggregation of α-syn in 2D SH-SY5Y cultures.* **(A)** Double immunostaining of undifferentiated and differentiated SH-SY5Y cells reveals intracellular aggregation of α-syn following 24 h incubation with seeding oligomers. α-syn inclusions in undifferentiated cells display several distinct, punctate accumulations dispersed throughout the cytoplasm, consistent with aggregates. In contrast, the RA+BDNF cell lines show a single prominent accumulation (red; arrows) and obscure the nucleus (asterisks). Scale bars: 50 µm. **(B)** Quantification of inclusion area (reflected as μm^2) shows inclusions that are present in differentiated cells to be much larger than those in undifferentiated cells (measurements obtained from three independent experiments; n=50). All data points are present, with mean shown as a straight line (red). **(C)** The percentage of cells containing inclusions was determined by counting 100 cells per repeat. Cells were deemed to contain inclusions if aggregation matched that in reference images when compared to controls. Data points are presented from three independent biological repeats. **(B, C)** Differences between treatments were tested for significance using Kruskal–Wallis test with post-hoc Dwass-Steel-Chritchlow-Fligner for >6 data points and Conover-Inman for <6 data points. P-values are displayed in the figures.

4.3.4 Application of exogenous oligomers induce the development of α-syn-immunopositive inclusions reminiscent of *in vivo* Lewy body pathology in 3D-differentiated SH-SY5Y

Using the 3D model described in Chapter 3, oligomeric α-syn was added to RA + BDNF-differentiated 3D cultures to determine whether the intracellular inclusions developed in these cells following the addition of the oligomeric seed. Cell viability was investigated in both thin-layer and thick-layer 3D cultures following 24 hr treatment with 10% v/v solvent, 10% v/v monomer and 10% v/v oligomer using LDH assay (Fig. 4.6). Addition of oligomeric preparations to cells differentiated in either thin-layer or thick-layer cultures did not induce cell death (Fig. 4.6). This is in contrast to the same preparations when added to 2D RA + BDNF-differentiated SH-SY5Y whereby treatment of oligomers caused significant cell death (Fig. 4.7). As such cells grown in 3D appear resilient to oligomer-induced cell death.

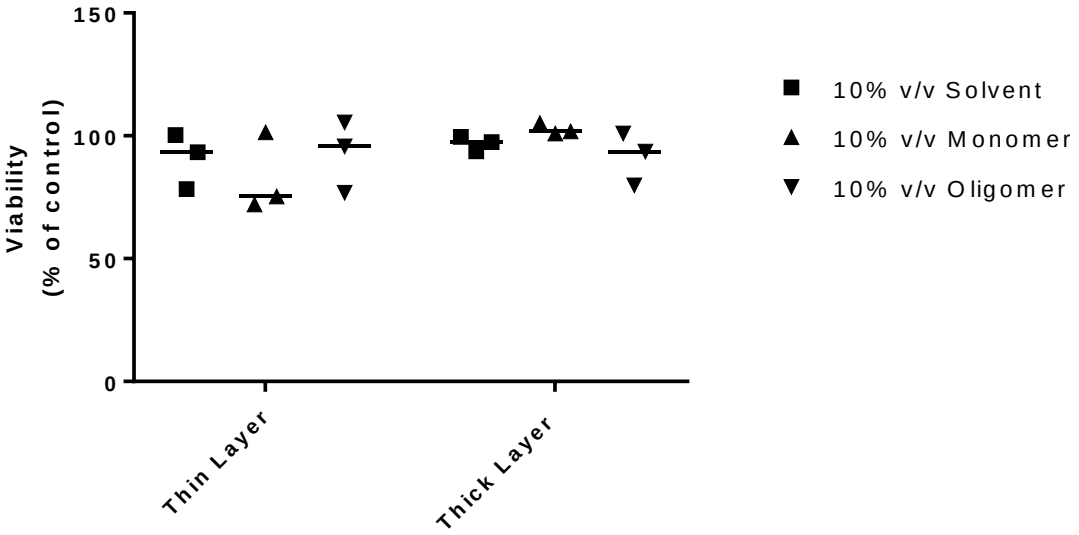

Figure 4.6. *Lactate dehydrogenase assay of 3D thin layer and 3D thick layer cultures following 24 hr treatment with solvent, monomeric and oligomeric preparations*. Data presented as median with all data points shown. No statistical differences between groups.

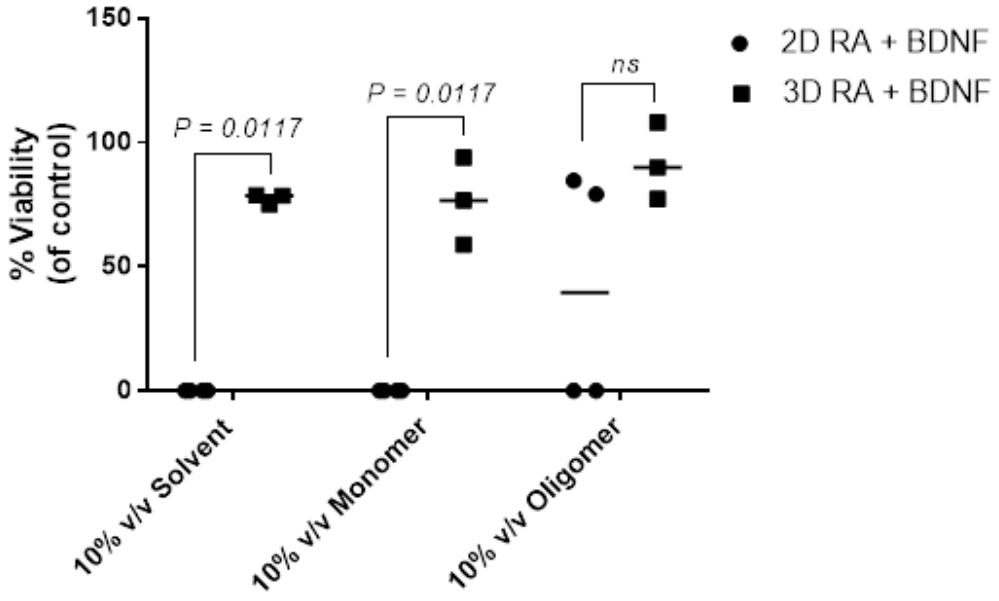

Figure 4.7. *Resazurin assay of 2D-differentiated and 3D-differentiated SH-SY5Y cultures following treatment with solvent, monomeric and oligomeric preparations.* Data presented as median with all data points shown. Differences between treatments were tested for significance using Kruskal–Wallis test with post-hoc Conover-Inman.

In vivo LBs are phenotypically more complex than the punctate aggregates of α-syn seen in 2D cell culture models. To determine the morphological changes in intracellular aggregates in 3D culture, fully differentiated cells within the matrix were treated with preformed α-syn oligomers. Similar to our observations in 2D cultures (Fig. 4.3 and 4.5); inclusions in our 3D cell culture model were detectable 24 h after α-syn oligomer treatment (Fig. 4.8, 4.9 and 4.10). Immunostaining of these nuclear-associated inclusions in our 3D model confirmed that they were α-syn positive (Fig. 4.9) and equivalent size to those seen *in vivo* (Fig. 4.10). Fig. 4.9 shows the percentage of α-syn immunopositivity in 3D cultures treated for 24 h with media, 10% v/v solvent or α-syn in 10% v/v monomeric or 10% v/v oligomeric preparations. The data demonstrate that oligomer-treated cells develop significantly more inclusions than control cells (media, solvent and monomeric preparations). The percentage of cells containing observable inclusions also significantly increased relative to controls (Fig. 4.10). Immunostaining for ubiquitin in the oligomer-treated 3D cell cultures demonstrated diffuse nuclear-associated staining that co-localised with the LB-like aggregates (Fig. 4.10 B). Co-staining using both anti-α-syn and anti-ubiquitin antibodies demonstrates co-localisation of both proteins within the same inclusion (Fig. 4.10 C).

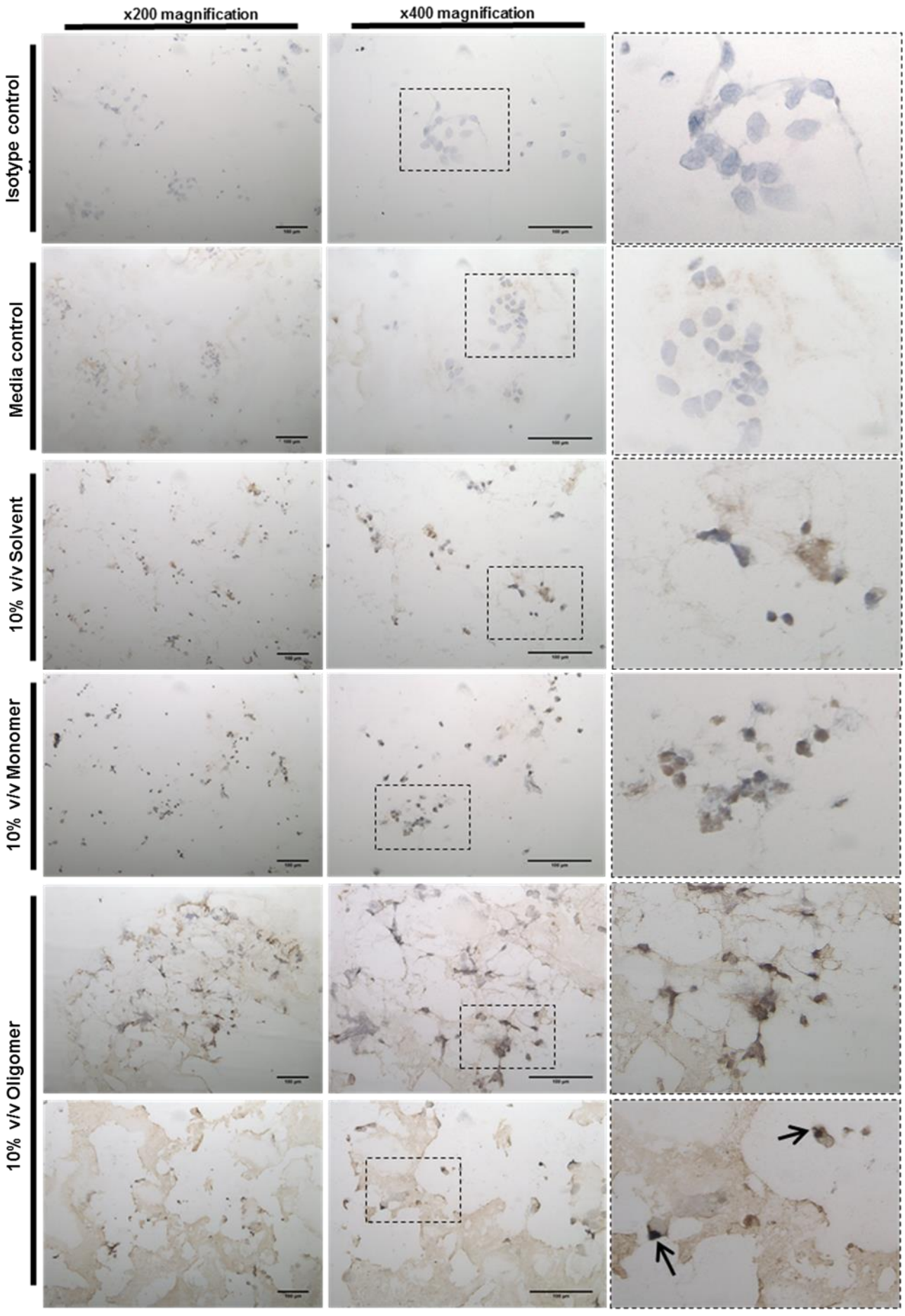
x200 magnification
x400 magnification
Isotype control
Media control
10% v/v Solvent
10% v/v Monomer
10% v/v Oligomer

Figure 4.8. *Exogenous α-syn oligomers seed the development of intracellular inclusions in 3D SH-SY5Y cultures.* Representative images of α-syn staining with syn211 monoclonal antibody (brown) with nuclei visualised using DAPI staining (blue/purple). α-Syn oligomer treatment to cells leads to strong immunoreactivity for α-syn compared to isotype controls, media only, or treatment with solvent or α-syn monomer. Arrows indicate the location of the intracellular inclusions. Scale bars: 100 μm.

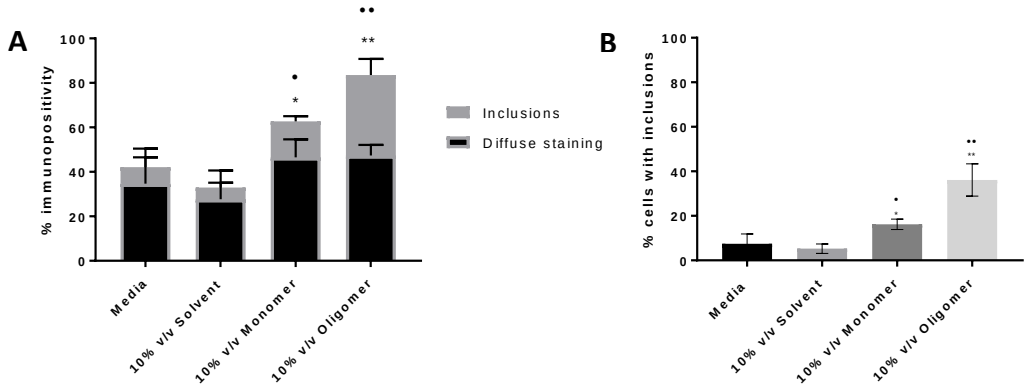

Figure 4.9. *Cell counts of 3D cultures following treatment with media, solvent, monomeric and oligomeric preparations.* **(A**) Percentage of α-syn immunopositivity in 3D cultures treated for 24 h with media, solvent or α-syn in monomeric or oligomeric preparations. Cells were deemed to contain inclusions if aggregation matched that in reference images when compared to controls. Data presented as mean ± SEM. of three independent experiments. **(B)** Monomeric and oligomeric α-syn treatments resulted in an increase in the percentage of cells with inclusions. Statistical significance in the oligomer-treated cultures related to the increase in large inclusions compared with media and solvent controls. Data presented as mean± SEM. of three independent experiments. (*, compared to media; •, compared to solvent). Evaluation of immunohistochemical staining was performed by counting 200 cells per slide, with ten slides counted per repeat (2000 cells counted in each treatment group for three independent experiments). **(A, B)** Statistical differences were determined using the Kruskal–Wallis test with post hoc Conover-Inman (*/•P≤0.05, **/••P≤0.01).

These inclusions are highly reminiscent of LBs *in vivo* (Shults, 2006), and completely absent in the isotype controls and untreated cultures (Fig. 4.10). Immunohistochemical detection of phosphorylated α-syn at S129 using a selective antibody was not able to show evidence of phosphorylation following 24 h treatment. This would indicate that the aggregates have either formed without the requirement for phosphorylation or that the S129 epitope is protected within these aggregates (Walker *et al*., 2013). To unmask antigenic sites within the 3D cultures antigen retrieval methods were used but did not show evidence of phosphorylation at S129. The antigen retrieval methods used included heat-mediated and enzymatic retrieval (described in Chapter 2 Section 2.4.4.1). The lack of observable phosphorylation within the inclusions would suggest that this post-translational modification may not be required for aggregate formation within this model or occurs within a timeframe exceeding that was investigated here. If so, then the LB-like inclusions observed here could represent an early aggregated morphology. Sequential extraction of aggregated species from cultures in 3D using TBS-soluble and TBS-insoluble/2% SDS-soluble fractions revealed increased α-syn concentrations in oligomer-treated

cultures in both fractions when measured by α-syn ELISA (Fig. 4.11). Overall, the 3D differentiated SH-SY5Y culture model presented here can produce LB-like aggregates when treated with preformed oligomeric material that recapitulates characteristic *in vivo* LB.

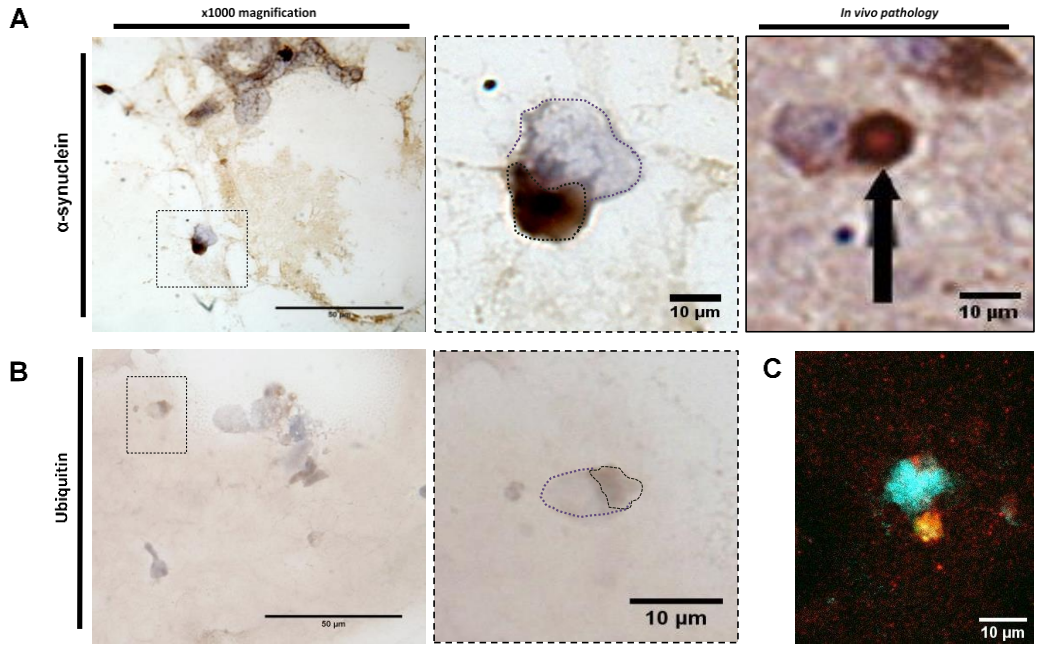

Figure 4.10. *α-Syn-seeded inclusions in 3D are indicative of in vivo Lewy body inclusions.* α-syn oligomer treatments to 3D-differentiated cultures develop α-syn positive inclusions that demonstrate the same morphology as *in vivo* Lewy bodies (LBs; **A**) and are positive for the marker ubiquitin **(B)**. Dotted line in purple highlights cell nuclei, whereas brown dotted line highlights stained area. **(C)** Immunofluorescence shows co-localisation of α-syn (red) and ubiquitin (green) staining. Nuclei were visualised using DAPI staining (blue). Scale bars: 50 µm (left) and 10 µm (right). *In vivo* pathology image displayed with permission from Springer Nature. This image is not published under the terms of the CC-BY license of this article. For permission to reuse, please see (Chesselet and Richter, 2012).

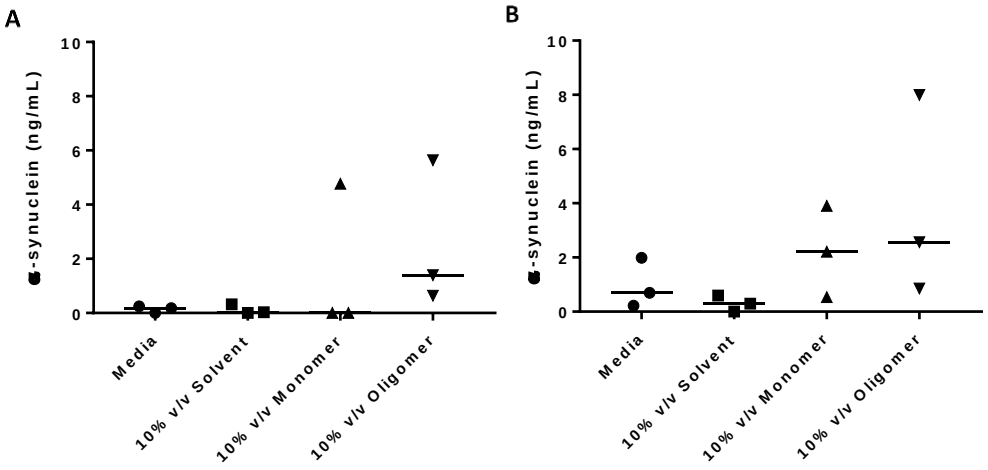

Figure 4.11. *α-Syn ELISA analysis of TBS-soluble and TBS-insoluble fractions from media, solvent, monomeric and oligomeric-treated 3D cultures.* **(A)** TBS-soluble fraction. **(B)** TBS-insoluble fractions. Data presented as median and all data points shown. No statistical differences between groups.

4.4 Discussion

Previously, the Sheffield Hallam University group (Illes-Toth *et al.*, 2015) and others (Danzer *et al.*, 2007; Danzer *et al.*, 2009) have reported the induction of punctate intracellular aggregates in 2D undifferentiated cells when specific preparations of oligomeric α-syn are added to the cell culture media. Findings presented here describe a human 3D cell culture model that recapitulates LB-like formation. Inclusions are initiated by oligomeric α-syn preparations when introduced to terminally differentiated post-mitotic, neuron-like SH-SY5Y cells within a 3D matrix. Importantly, although the LB-like structures present here do not show evidence of phosphorylation, they are positive for α-syn and ubiquitin, closely resembling the morphology of inclusions found within the human pathology (Goedert *et al.*, 2013).

Certain forms of α-syn located in the extracellular environment have recently been shown to be internalised by neurons through several receptor-mediated mechanisms and induce self-aggregation of endogenous α-syn (Bieri, Gitler and Brahic, 2018). Seeding oligomers, originally described by Danzer *et al.* (2007), were used in this study to determine the seeding effect upon the 3D-differentiated SH-SY5Y cell populations. The seeding oligomers were described as globular and protofibrillar structures between 4 and 10 nm in size capable of inducing the intracellular aggregation of α-syn as determined by immunocytochemistry. Co-localisation of endogenous α-syn with the exogenously added Alexa-Fluor-labelled oligomers provides evidence for recruitment of cellular forms of α-syn into inclusions, a key characteristic of seeding and propagation (Danzer *et al.*, 2007; Grozdanov and Danzer, 2018). This prion-like propagation has been proposed to explain the spread of the disease through the neuronal network and justify the post-mortem observations of α-syn aggregates in a PD patient that had undergone midbrain embryonic neuronal transplants (Heiko Braak, Del Tredici, *et al.*, 2003; Jeffrey H Kordower *et al.*, 2008; Chu and Kordower, 2010).

The results of this study demonstrate the addition of seeding oligomers to SH-SY5Y cultures are capable of inducing the same intracellular aggregation as previously described (Danzer *et al.*, 2007; Illes-Toth *et al.*, 2015). Homogenous, cytoplasmic staining of α-syn is apparent in the 10% v/v solvent and 10% v/v monomeric controls when added to SH-SY5Y in all stages of differentiation (undifferentiated, RA-

differentiated, RA + BDNF-differentiated) (Fig. 4.3, 4.5 and Appendix Fig. 1 and 2). Upon treatment with the oligomeric seed, the development of aggregates is observed as punctate spots throughout the cell cytoplasm of all cells in both undifferentiated and RA-differentiated SH-SY5Y (Fig. 4.5). In contrast, treatment of oligomer preparations to RA + BDNF-differentiated SH-SY5Y in 2D resulted in the development of large, singular α-syn positive inclusions in a small subset of cells (~31%) (Fig. 4.5). Addition of solvent and monomeric controls to RA + BDNF-differentiated SH-SY5Y in 2D did not result in the development of intracellular inclusions, but homogenous staining of cytoplasmic α-syn is evident (Appendix Fig. 2.). These inclusions were reminiscent of LB-pathology given the size of inclusions, positive staining for α-syn and perinuclear location. One caveat of using the 2D RA + BDNF-differentiated cells was that cells easily detached from the culture surface following media changes after differentiation, similar to that which has been observed previously with LUHMES cell culture (Smirnova *et al.*, 2016). This could account for the variation in inclusion size in these cultures (Fig. 4.5 C) and toxicity of 10% v/v solvent, 10% v/v monomer and 10% v/v oligomer treatment (Fig. 4.2 C).

Given that use of SH-SY5Y in PD research is generally undertaken using the undifferentiated cultures in 2D (83% of papers), the morphology of inclusions in these cells do not represent what is observed *in vivo* (Goldie, Barnett and Cairns, 2014). Several small inclusions are apparent throughout the cell cytoplasm in both undifferentiated and RA-differentiated SH-SY5Y in contrast to the large, singular inclusion observed *in vivo*. One potential reason for the difference in morphology observed in undifferentiated SH-SY5Y is due to the fact that this is a continually dividing cell line, with a doubling time of ~27 hrs, and could potentially divide the protein load into daughter cells akin to yeast replication (Tuite and Cox, 2003; Kovalevich *et al.*, 2013). Aulic *et al.* (2014) demonstrated the addition of short amyloid fibrils were capable of spreading pathology in subsequent cellular passages once inoculated at P0 and was detected at P6 (Aulic *et al.*, 2014). However, the same inclusion morphology was observed in RA-differentiated SH-SY5Y cells which were previously demonstrated to have exited the cell cycle (Chapter 3) as indicated by the absence of Ki67 staining. Another explanation could be that oligomers are taken up by cells and processed by the cell to be degraded and exported to the extracellular space. Therefore, the morphology of inclusion formation would correlate

to the subcellular location of the ubiquitin-proteasome in cells (Bennett *et al.*, 1999; Zhao, 2003). Cells with morphology as in undifferentiated and RA-differentiated SH-SY5Y, with a nucleus surrounded by abundant amounts of cytoplasm in the absence of developed axons, would stain for the 26 S proteasome throughout the cytoplasm, in accordance with the pattern of aggregate formation (Zhao, 2003). This is supported by a time-course experiment whereby aggregate formation was induced by the addition of oligomeric seed (same oligomer preparation as used in this study) over 16 hrs. At 30 hrs, the presence of cellular inclusions was reduced but increased extracellular background staining was observed, suggesting the cell has attempted to decrease cellular protein load (Mason, 2018). Interestingly, in RA-differentiated cultures where cells are not actively undergoing mitosis, there is increased extracellular α-syn staining, suggesting increased clearance (Fig. 4.5 A). In contrast to the abundant cytoplasmic staining of α-syn aggregates in undifferentiated and RA-differentiated SH-SY5Y, singular, large nuclear-associated inclusions were observed in RA + BDNF-differentiated 2D cultures where cellular morphology consists of the nucleus surrounded by scant cytoplasm and long, thin axons (Fig. 4.5). Staining with a proteasome antibody would demonstrate whether α-syn inclusion formation correlates to the cellular localisation of the proteasome.

Addition of oligomers to 3D-differentiated cultures demonstrated the development of LB-like aggregates reminiscent of *in vivo* pathologies such as staining for α-syn and ubiquitin, size of inclusions and perinuclear location (Fig. 4.9 and 4.11). Importantly, these inclusions were apparent in a cell line with no genetic manipulation and in a more physiologically-relevant culture system where cells are in contact with the ECM and other cells in 3D. Inclusions were not observed in isotype, media, solvent and monomeric controls (Fig. 4.9). A major component of LBs is the presence of α-syn phosphorylated at S129 at <90% in synucleinopathies compared to normal conditions of >4% implicates this post-translational modification as important in the pathogenesis of PD (Fujiwara *et al.*, 2002; Anderson *et al.*, 2006). Staining with a phosphorylation-specific antibody (S129) revealed the absence of phosphorylated α-syn within these inclusions due to either the antibody not binding due to epitope masking, phosphorylation not being required for inclusion formation or phosphorylation occurring in a time-frame outside what was used in this study (24 hrs) (Walker *et al.*, 2013). Indeed, a previous study by Luk *et al.* (2009)

demonstrated phosphorylation was not required for the development of LB-like aggregates in a cell culture model stably expressing α-syn (Luk *et al.*, 2009). Phosphorylation of α-syn at S129 is associated with clearance, toxicity and stability of α-syn in addition to being associated with cellular stress (Machiya *et al.*, 2010; Oueslati, 2016). Phosphorylation at S129 is selectively targeted for degradation by the proteasome and extensively aggregated forms are unable to be degraded by the proteasome and accumulate as LBs (Machiya *et al.*, 2010; Arawaka *et al.*, 2017). This could mean that phosphorylated α-syn that has already been degraded and processed by the cell to the extracellular space (by ubiquitin-proteasome and autophagy-lysosomal pathways) and therefore not detectable in inclusions (Chau *et al.*, 2009; Machiya *et al.*, 2010; Lashuel, Overk, A. Oueslati, *et al.*, 2013). Interestingly, previous work in our group has demonstrated the ability of seeding oligomers to induce the release of phosphorylated α-syn species to cell culture media (Mason, 2018). The late-stage disease could then be associated with accumulation of p-α-syn, therefore, the lack of phosphorylated presented here would represent an early aggregated model of PD (Beach *et al.*, 2009; Walker *et al.*, 2013).

Following internalisation, the ability of α-syn to trigger oligomerisation of endogenous α-syn potentially occurs through the induction of oxidative or other stress responses (Deas *et al.*, 2016; Di Maio *et al.*, 2016). Although the precise series of events surrounding the development of these inclusions remains to be established, a model system such as the one described here opens the opportunity to investigate these mechanisms within a controlled environment, without the need to genetically modify or overexpress α-syn. In multifactorial disorders such as PD, dissecting the complex pathological processes into simpler molecular events may allow us to better interpret disease progression. Using the 3D cell culture model described here may allow us to identify therapeutic interventions and the pathways leading to LB development before translating them to more complex models of the brain (e.g. transgenic mouse models) in which confounders such as neuroinflammation and innate immunity could mask the pathways required to be studied.

Chapter 5 : The role of ferroptosis to the aggregation and propagation of α-synuclein in *in vitro* models

5.1 Introduction

Medical management of PD has largely focussed on replacement of the dopamine deficit caused by loss of dopaminergic neurons in the disease, through the administration of the dopamine precursor L-DOPA (Birkmayer and Hornykiewicz, 1961; Cotzias, Papavasiliou and Gellene, 1969; Korczyn *et al.*, 1999). Levodopa remains the gold standard therapy for PD patients and as such almost all patients are prescribed this particular treatment. L-DOPA (levodopa) therapies are generally administered in conjunction with other drugs to help the bioavailability of L-DOPA and reduce some side effects associated with L-DOPA. 3,4-dihydroxyphenylaline (DOPA) decarboxylase inhibitors, catechol-o-transferase (COMT) inhibitors and monoamine oxidase (MAO) inhibitors (Riederer and Laux, 2011; Nyholm, Klangemo and Johansson, 2012). For example, carbidopa, a DOPA decarboxylase inhibitor, is administered to patients alongside levodopa to prevent the breakdown of levodopa in the periphery, thereby increasing concentration of levodopa reaching the brain. By increasing the amount of levodopa reaching the brain, carbidopa allows for a lower dose of levodopa, which reduces the side effects of nausea and vomiting if levodopa was administered alone (Muddapu *et al.*, 2020). Administration of levodopa/carbidopa shifts the peripheral pathway of levodopa to a secondary pathway involving COMT, subsequently reducing the bioavailability of levodopa (Nevrly *et al.*, 2010). Therefore, triple therapy with added COMT inhibitors in the levodopa/carbidopa preparations inhibits this method of metabolism to increase the bioavailability and half-life of levodopa (Hinz, Stein and Uncini, 2011; Muddapu *et al.*, 2020). Importantly, the use of levodopa only provides symptomatic relief in the management of PD and does not treat the underlying pathology. Moreover, long-term levodopa therapy loses its efficacy and is associated with a range of adverse side effects (Hinz, Stein and Uncini, 2011). Symptoms of late-stage disease respond poorly to levodopa therapy due to degeneration in other brain regions. Loss of neurons from these regions ensure deficits in the non-dopaminergic transmission of involving acetylcholine, glutamate, norepinephrine, and serotonin neurotransmitters.

Degeneration of cholinergic neurons, and subsequent depletion of acetylcholine, can cause dementia, gait abnormalities, and falls (Perez-lloret and Barrantes, 2016).

As a consequence of no disease-modifying therapies available to either slow down the progression of the disease or prevent neuronal cell death in the *SNPc* in patients of PD, there is an urgent need identify new molecular targets to be able to slow the progression of the disease and subsequent neurodegeneration (Smith *et al.*, 2012). The various mechanisms of neuronal degeneration in PD are associated with multiple cell death pathways; however, it is currently not known how these contribute to disease. A newly discovered cell death pathway, ferroptosis, has recently been implicated in the pathogenesis of PD (Dixon *et al.*, 2012; Do Van *et al.*, 2016). Ferroptosis is characterised by the accumulation of iron-dependent ROS, depletion of cellular GSH/GPX4 and lipid peroxidation, leading to cell death (Dixon *et al.*, 2012). These features of ferroptosis are all pathogenic changes associated with PD. Chelation of iron and administration of ferroptosis inhibitors have shown to be promising therapeutic options in the treatment of PD (Devos *et al.*, 2012, 2014). Deferiprone, an oral iron chelator, has shown promise in a recent phase III trial of early-stage PD patients whereby therapy was associated with reduced motor symptoms and slowing the progression of motor deficits (Devos *et al.*, 2014). Replication of this result in a larger-scale clinical trial could lead to the first disease-modifying therapy for PD. Although promising, only one paper has been published to date directly relating ferroptosis to cell death in PD and it is currently unknown if α-syn is linked to ferroptotic cell death (Do Van *et al.*, 2016). In this section, cell death pathways of apoptosis, autophagy and ferroptosis involved in PD are discussed.

5.1.1 Cell death mechanisms

Programmed cell death (PCD) plays a fundamental role in the development and tissue homeostasis in biological systems (Fuchs and Steller, 2011). Developing tissues rely on a balance between cellular proliferation and PCD to prevent the development of hyper-proliferative diseases through the regulation of cell numbers (Arya and White, 2015). Approximately half of the neurons generated in the central nervous system (CNS) are eventually eliminated by PCD to maintain appropriate cell numbers (Yamaguchi and Miura, 2015). An abundance of cells in tissue development allows for selection of the 'fittest' cells to optimise organ function. Cells that are deemed 'unfit' for tissue function are eliminated by PCD, preventing the

survival of cells that have developed differentiation defects (Baehrecke, 2002; Hanahan and Weinberg, 2011; Arya and White, 2015). The 'neurotrophic factor hypothesis' describes one method of regulating cell numbers of the peripheral nervous system (PNS) in which the overproduction of neurons is regulated by the competition for survival-promoting neurotrophic factors (Oppenheim *et al.*, 1991; Yuen *et al.*, 1996). PCD also serves as a 'quality control' mechanism to eliminate potentially dangerous cells in response to cellular defects such as DNA damage, response to viral infection and cell fate defects (Suzanne and Steller, 2013; Upton and Chan, 2014; Nagata and Tanaka, 2017). Abnormal regulation PCD processes are associated with human disease, including the development of cancer, developmental disorders and neurodegeneration (Hanahan and Weinberg, 2011).

Exposure of cells to an instantaneous, catastrophic form of cellular stress (physical, chemical or mechanical) results in accidental cell death (ACD), a form of cell death not defined by a molecular mechanism of action in contrast to the forms of PCD discussed below (Galluzzi *et al.*, 2015). PCD exhibits a molecular 'fingerprint' specifically initiated by the cell as a consequence of intracellular/extracellular stress (Vandenabeele *et al.*, 2010; Galluzzi *et al.*, 2015, 2018). As cell death progresses macroscopic morphological alterations and the mechanisms by which cells are disposed of, have been classified into three major mechanisms: type I cell death or apoptosis, type II cell death or autophagy and type III cell death or necrosis (Galluzzi *et al.*, 2015, 2018). The discovery of more specific cell death mechanisms has challenged the mechanism of cell death in various disease states, including in neurodegeneration (Table 5.1) (Agostini, Tucci, & Melino, 2011). Pharmacological intervention has the potential to modify these cell death modalities therefore it is crucial to understand the mechanisms of cell death and survival in PD.

Cell death type	Morphological features	Biochemical features	Key proteins	Inducers and inhibitors	References
Apoptosis (intrinsic and extrinsic)	• packaging of apoptotic bodies •shrinking and blebbing of cell membrane	Activation of caspases	p53, BAX, BAK, BCL-2, initiator caspases- 2, 8, 9, 10 and effector caspases- 3, 6, 7	**Inducers:** Staurosporine, apicidin, apoptosis activator 2, cisplatin, cyclophosphamide, rifaximin **Inhibitors:** Z-VAD, QVD-OPh	(Jorgensen and Miao, 2016; Ito *et al.*, 2017)
Autophagy	•in chaperone mediated autophagy, selective degradation of cytosolic proteins •in microautophagy, double membrane structures to sequester cell material for degradation	Substrate degradation	Hsp70 (Hsc70), LAMP-2A, Hsc73, ATG7, ATG5, Beclin-1	**Inducers:** MG-132, SAHA, trichostatin-A, Z-VAD-FMK **Inhibitors:** metformin, perifosine, rapamycin, everolimus, resveratrol	(Todde, Veenhuis and Klei, 2009)
Necrosis	•increased cell volume •swelling of organelles •plasma membrane permeabilisation •cellular collapse and subsequent release of cellular contents, triggering inflammatory response	Activation of specific death receptors including FAS and TNFR1 Caspase inactivation	TNFR1, RIPK1/RIPK3, MLKL oligomers	**Inducers:** TNFα, FASL, TRAIL **Inhibitors:** Nec-1, necrosulfonamide, ponatinib, pazopanib, sorafenib, hydroxyanisole, diphenyleneiodonium, caspase-8, necrostatin-1, GSK'872, necrosulfonamide	(Xie *et al.*, 2016; Ito *et al.*, 2017; Cho, 2018)
Ferroptosis	•intact cell membrane, no blebbing •mitochondrial alterations including dense, small mitochondria with vestigial cristae •normal size nucleus, no chromatin condensation	Accumulation of toxic lipid peroxides as a result of ROS generated from iron metabolism GSH depletion and inhibition of system xc (cystine/glutamate antiporter)	VDAC 2/3, SLC7A11, GPX4, ACSL4, LO	**Inducer:** Erastin, RSL3, sorafenib, sulfasalazine, DP17, buthionine sulfoximine (BSO), acetaminophen, artesunate, lanperisone, iron, ROS **Inhibitors:** Trolox, cycloheximide, ebselen, deferoxamine, ferrostatin-1, liproxstatin-1, vitamin E, n-acetylcysteine (NAC)	Yang and Stockwell, 2008; Dixon *et al.*, 2012, 2014; Do Van *et al.*, 2016; Xie *et al.*, 2016; Doll *et al.*, 2017)
Oxytosis	•morphologically similar to ferroptosis	GSH depletion, ROS production, lipoxygenase	GPX4, LO, apoptosis-inducing	**Inducers:** iron, aminoadipate, homocysteate, quisqualate, BSO, ROS	(Tan, Schubert and Maher, 2001; Liu

	•mitochondria appear swollen and degraded	(LO) activation and lethal calcium influx	factor (AIF)	**Inhibitors:** NAC, deferoxamine, quercetin, vitamin E, vitamin C, ibdebenone, α-tocopherol	and Schubert, 2009; Lewerenz *et al.*, 2018)
Pyroptosis	•pore formation in the plasma membrane by gasdermin D (GSDMD) oligomerisation •water and ions rush into cells causing cell swelling and lysis •release of cellular contents •chromatin condensation but intact nuclei •DNA damage (lower intensity to that of apoptosis)	Initiated by inflammatory caspases Proteolytic maturation of inflammatory cytokines interleukin-1β (IL-1β) and IL-18 following caspase 1 activation	Caspases – 1, 3, 4, 5, 11, GSDMD	**Inducers:** gram-negative bacteria, lipopolysaccharide, influenza A virus **Inhibitors:** ablation of caspase 1, 11, 4 or 5, caspase 1 inhibitor z -YVAD-fmk	(Cookson and Brennan, 2001; Fink and Cookson, 2006; Bergsbaken, Fink and Cookson, 2009; Jorgensen and Miao, 2016; Sborgi *et al.*, 2016)
Parthanatos	•large scale DNA fragmentation and chromatin condensation	Hyperactivation of poly (ADP-ribose) polymerase 1 (PARP1) NAD+ and ATP depletion resulting in bioenergetic and redox collapse Accumulation of poly (ADP-ribose) polymers at mitochondria leading to MOMP	AIF, PARP1, macrophage inhibitory factor, hexokinase 1	**Inducers:** N-methyl-N'-nitro-N-nitrosoguanidine, UV light, ionizing radiation, reactive nitrogen species **Inhibitors:** PARP inhibitors; isoquinolinones, quinazolinones, quinazoline diones, phthalazinones and phenanthridinones,	(Yu *et al.*, 2002; Curtin and Szabo, 2013; Galluzzi *et al.*, 2018)

Table 5-1.1. *Morphological and biochemical features of distinct mechanisms of cell death.* Listed are some examples of inducers and inhibitors specific to a mechanism of cell death but it is not an exhaustive list.

5.1.2 Cell death mechanisms in Parkinson's disease

5.1.2.1 Apoptosis

Apoptosis is a form of PCD characterised by a cascade of executioner caspases that ultimately leads to cell death through one of two pathways - intrinsic or extrinsic pathway (Table 5.1 and Fig. 5.1). Intrinsic apoptosis is initiated by several environmental perturbations including growth factor withdrawal, DNA damage, endoplasmic reticulum (ER) stress, ROS, mitotic defects, amongst others (Nuñez *et al.*, 1990; Czabotar *et al.*, 2014; Shim *et al.*, 2014; Pihán, Carreras-Sureda and Hetz, 2017; Galluzzi *et al.*, 2018). Extrinsic apoptosis is defined as a modality initiated by perturbations of the extracellular environment, driven by the two types of membrane receptors: death receptors and dependence receptors (Wang and El-Deiry, 2003; Flusberg and Sorger, 2015; Galluzzi *et al.*, 2018). Both result in the activation of executioner caspase proteins that irreversibly lead to cell death (Fig. 5.1) (Flusberg and Sorger, 2015). These executioner caspases are responsible for the morphological and biochemical features of apoptosis including: cell shrinkage, chromosome condensation, DNA fragmentation, formation of apoptotic bodies and phosphatidylserine exposure (Xu *et al.*, 2002; Galluzzi *et al.*, 2018).

Apoptosis has been linked to PD in both humans and cell models. Several post-mortem studies have identified apoptotic neurons in the *SNPc* of PD patients, either by detection of apoptosis by terminal deoxynucleotidyl transferase dUTP nick-end labelling (TUNEL) staining, morphological characterisation of neurons and immunostaining for caspase proteins (Mochizuki *et al.*, 1996; Tatton and Kish, 1997; Tatton, 2000). Nigrostriatal dopaminergic neurons of late-onset PD patients expressed increased immunostaining for caspases 3, 8, 9 in addition to elevated activities of caspase 3 in the *SNPc* (Hartmann *et al.*, 2001; Viswanath *et al.*, 2001; Nazli *et al.*, 2016). Models of PD using the toxins 1-methyl-4- phenyl-1,2,3,6-tetrahydropyridine (MPTP), rotenone and 6-hydroxydopamine (6-OHDA) lead to the activation of caspase 8 in both the *SNPc* of animal models and cultured cells (Hartmann *et al.*, 2001; Vila *et al.*, 2001; Viswanath *et al.*, 2001; Recasens *et al.*, 2014). MPTP-induced neurodegeneration in murine models can be rescued with the application of caspase inhibitors (Q-VD-OPH), highlighting the role of apoptosis in these models (Yang *et al.*, 2004).

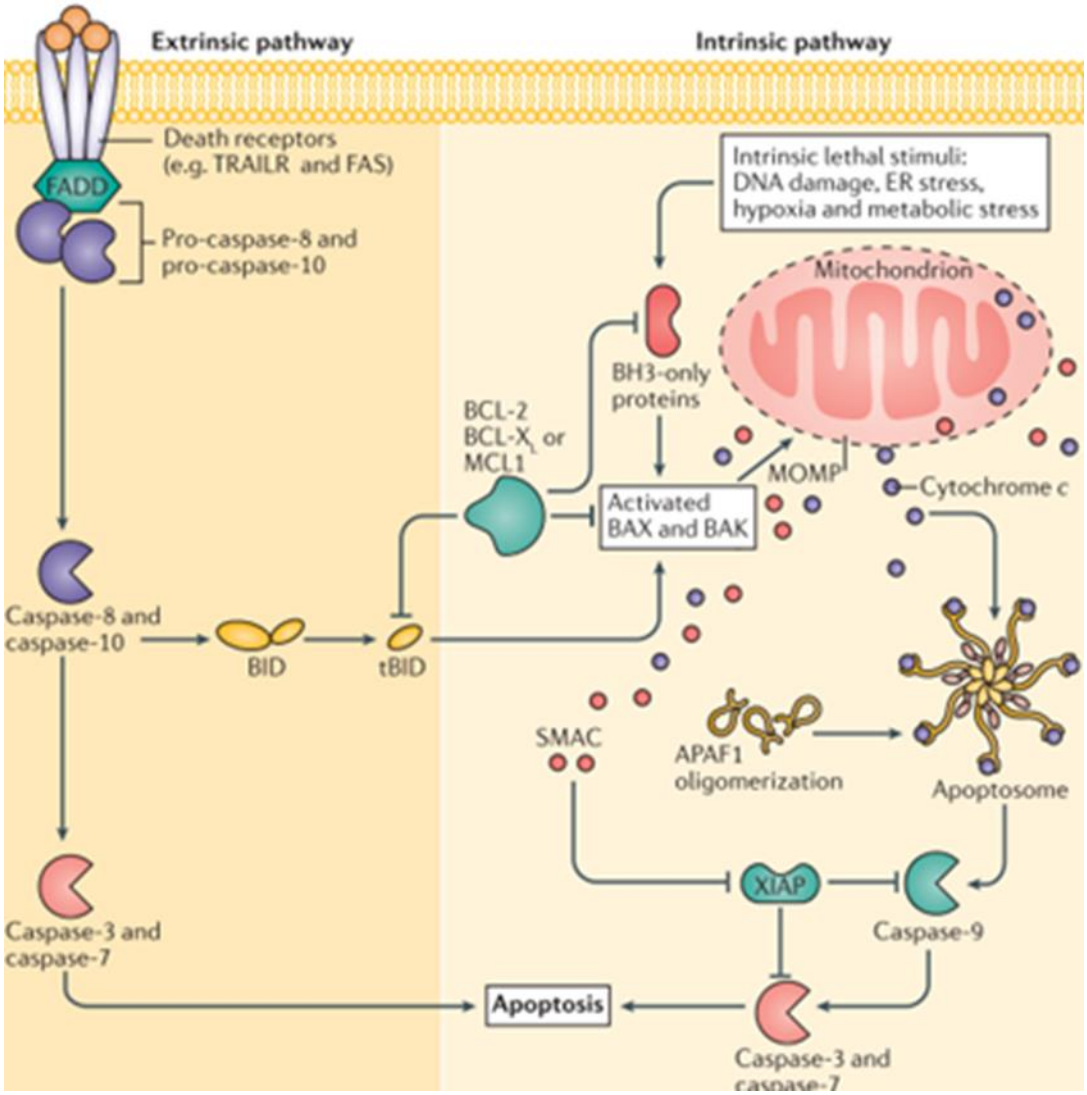

Figure 5.1. *Intrinsic and extrinsic apoptotic signalling pathways.* Extrinsic pathway: ligand binding to death receptors activates CASP8 and CASP10. Active CASP8 and CASP10 then cleave executioner caspases, CASP3 and CASP7, leading to cell death. Intrinsic pathway: mitochondrial outer membrane permeabilisation (MOMP) initiated by the BCL2 apoptosis regulator family (Galluzzi, Kepp and Kroemer, 2016). In response to cellular stresses, members of the BCL2 family including BCL2 associated X (BAX) and/or BCL2 antagonist/ killer 1 (BAK1), together with BCL2 family apoptosis regulator (BOK) mediate MOMP. BAX and BAK are activated by pro-apoptotic BH3 proteins (Gavathiotis *et al.*, 2010; Czabotar *et al.*, 2013; Zhang *et al.*, 2016). Once activated, BAX and BAK can form rings or oligomers that perforate the outer mitochondrial membrane (OMM) (Kuwana *et al.*, 2002; Schafer *et al.*, 2009; Grosse *et al.*, 2016). MOMP releases apoptotic factors that normally reside within the mitochondria into the cytosol, including cytochrome c somatic (CYCS) and secondary mitochondrial activator of caspases (SMAC). CYCS binds to apoptotic peptidase activating factor-1 (APAF1) and pro-caspase 9 (CASP9) to form the apoptosome complex, activating CASP9 (Hu et al., 2014). Activated CASP9 catalyses the activation of executioner caspases (CASP3 and CASP7) and in turn, results in cell degradation in both intrinsic and extrinsic apoptosis. Reprinted by permission from Springer Nature: License Number 4658840206496, Springer Nature, Nature Reviews Cancer, A fate worse than death: apoptosis as an oncogenic process, Gabriel Ichim and Stephen W. G. Tait, Jul 1, 2016 (Ichim and Tait, 2016).

Overexpression of WT α-syn or expression of mutant α-syn (e.g. A53T) in cultured cell lines and animal models leads to the activation of apoptosis, which can be rescued by caspase inhibitors or knockdown of caspase-12 (Saha *et al.*, 2000; Stefanova *et al.*, 2001; Tanaka *et al.*, 2001; Martin, 2006). The association of α-syn

with apoptosis has been linked to; interaction of α-syn with pro-apoptotic BCL2 family members (e.g. BCL2-associated death promoter; BAD) (Saha *et al.*, 2000), oxidative stress (Stefanova *et al.*, 2001) and mitochondrial DNA damage (Stefanova *et al.*, 2001; Tanaka *et al.*, 2001; Martin, 2006). A 53-83-kD complex of α-syn has been shown to bind anti-apoptotic 14-3-3 protein (Xu *et al.*, 2002). 14-3-3 proteins are a family of highly conserved eukaryotic regulatory molecules important for the regulation of biological processes such as cell death (Masters and Fu, 2001). Sequestration of 14-3-3 by α-syn prevents the inactivation of pro-apoptotic factors (e.g. BCL2 family members, BAD) leading to a pro-apoptotic environment whereby neurons are increasingly vulnerable to apoptosis by elevated levels of α-syn (Xu *et al.*, 2002). This observation was specific to expression of WT α-syn in human foetal DA neurons in contrast to non-DA human cortical neurons where expression of α-syn protected cells and increased neuron survival (Xu *et al.*, 2002). Accumulation of α-syn rendered endogenous levels of DA toxic, demonstrating a selective vulnerability in DA-producing neurons (Xu *et al.*, 2002). In *Saccharomyces cerevisiae*, WT, A53T and A30P α-syn were all shown to trigger apoptosis, with ROS thought to be the primary trigger of apoptosis in this system (Flower *et al.*, 2005).

5.1.2.2 Autophagy

Autophagy “self-digesting” is a form of PCD that relies on the components of autophagic machinery that promote proteolytic degradation of cytosolic components of the lysosome initiated through multiple signalling events (Table 5.1, Fig. 5.2) (Glick, Barth and Macleod, 2010). The self-destructive process of autophagy can be initiated in response to nutrient deficiency, organelle damage (e.g. through ROS), hypoxia, drug treatment and ER stress (Chen, Kang and Fu, 2018).

The central pathogenic events important to understanding PD pathogenesis (e.g. ROS production, oxidative stress, mitochondrial dysfunction, aggregation of proteins) are linked to autophagy. The pentapeptide recognition sequence of α-syn is consistent with the CMA recognition sequence ($_{95}$VKKDQ$_{99}$), highlighting CMA as the main route for degradation of α-syn (Dice, 1990; Cuervo *et al.*, 2004). Mutant forms of α-syn (e.g. A30P and A53T) and multimeric species of the protein (e.g. oligomers) prevent the degradation of α-syn by the CMA pathway leading to toxic aggregation in the cell (Webb *et al.*, 2003; Cuervo *et al.*, 2004; Martinez-vicente *et al.*, 2008). In addition, overexpression of α-syn inhibits macroautophagy by prevention of

autophagosome formation via inhibition of RAB1A and subsequent mislocalisation of the transmembrane protein ATG9 required in an early step of macroautophagy (Winslow *et al.*, 2010; Winslow and Rubinsztein, 2011).

Mitochondrial dysfunction is intrinsically linked to PD. Several genes associated with familial PD including the genes *PARK2 (*PARKIN*), PARK6 (*PINK1*), PARK7 (*DJ-1*)* and *PARK8* (LRRK2*)* are associated with the impairment of mitophagy (autophagic degradation of mitochondria) (Bonifati *et al.*, 2003; Hague *et al.*, 2003; Maria, Patrick and Muqit, 2004; Berg *et al.*, 2005; Pchelina, Emel'ianov and Usenko, 2014; Ryan *et al.*, 2015). PINK-1 and PARKIN are important in mitochondrial homeostasis whereby WT PINK-1 recruits PARKIN to damaged mitochondria during mitophagy, leading to degradation of damaged mitochondria through the trafficking of defective mitochondria to the lysosome-rich perinuclear area (Clark *et al.*, 2006; Heeman *et al.*, 2009; Vives-bauza *et al.*, 2009). Loss of PINK-1 or PARKIN results in an altered mitophagy process, resulting in the persistence of damaged ROS-producing mitochondria (Pickrell and Youle, 2015). DJ-1, a transcriptional regulator, is a neuroprotective factor involved as a redox sensor/reductase that influences mitophagy (Wilson *et al.*, 2004). Mutant forms of DJ-1 are associated with a decrease in consumption of H_2O_2 by brain mitochondria, resulting in cell death through increased ROS production (Lopert and Patel, 2014). Mutant DJ-1 interacts with α-syn to cause the formation of α-syn aggregates, which further inhibits cellular autophagy (e.g. CMA) (Xilouri *et al.*, 2009; Zondler *et al.*, 2014). Mutant LRRK2 is associated with a wide range of negative cellular effects on mitochondria including regulating mitochondrial dynamics, mitochondrial uncoupling (leading to increased basal oxygen consumption and reduced ATP level) (Li, Tan and Yu, 2014). LRRK2 mutants impair the autophagy/lysosomal pathway resulting in a defective CMA complex, impairing autophagy which subsequently leads to the inhibition of α-syn degradation and aggregate formation (Orenstein *et al.*, 2013).

5.1.2.3 Ferroptosis

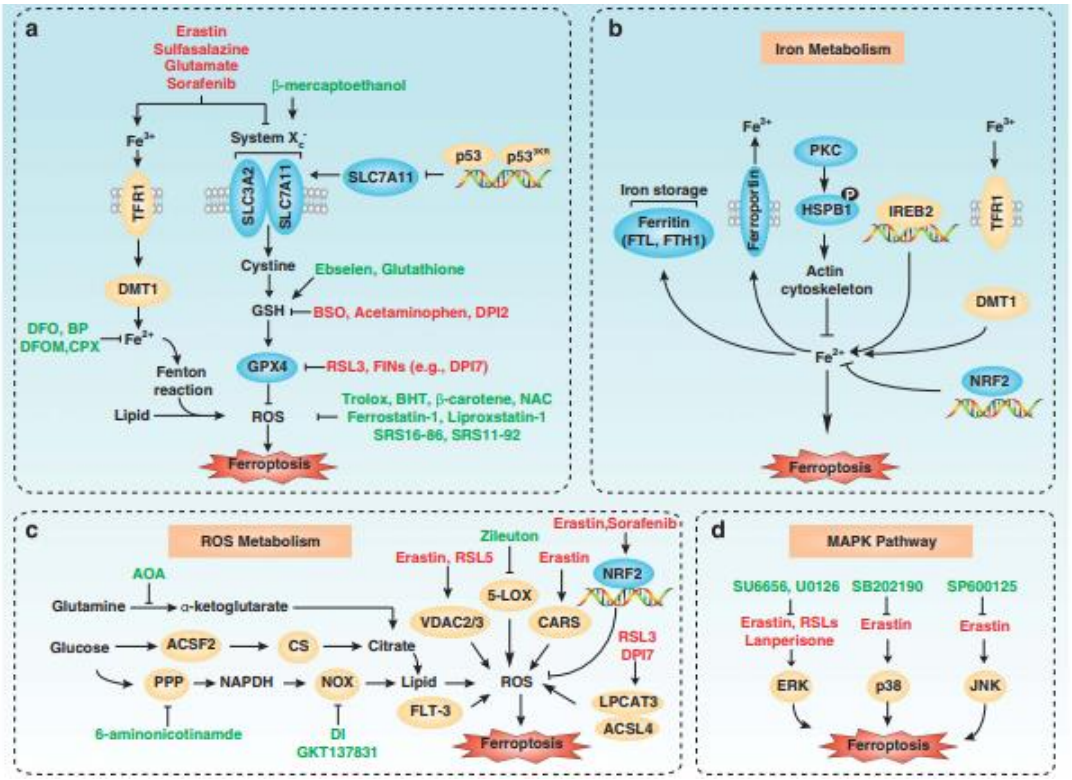

Figure 5.2. *Signalling pathways in ferroptosis.* The inability to detoxify iron-associated ROS by GPX4 and GSH is central to cell death in ferroptosis (Friedmann Angeli *et al.*, 2014; Yang *et al.*, 2014). ROS generated from iron interacts with the bisallylic methylene of a polyunsaturated fatty acid (PUFA; such as arachidonic and adrenic acid) in the lipid bilayer creating a lipid peroxyl radical LOO·, which interacts with another bisallylic methylene to generate LOOH (Repetto, Ferrarotti and Boveris, 2010; Kagan *et al.*, 2017). Propagation of LOOH can occur by way of interaction with new substrates thus creating new radicals, damaging multiple residues within lipid bilayers. To prevent this cycle of LOO· production, antioxidants are able to donate an electron to the radicals, resulting in termination of this process (Gaschler and Stockwell, 2017). Lipid peroxidation results in wide ranging alterations of the lipid bilayer, impacting membrane fluidity, lipid-lipid and lipid-protein interactions, membrane integrity, ion and nutrient transport, membrane-initiated signalling pathways leading to cell death (Catalá and Díaz, 2016; Gaschler and Stockwell, 2017). Reprinted by permission from Springer Nature: License Number 4658830436428, .Springer Nature, Cell Death and Differentiation, Ferroptosis: process and function, Y Xie, W Hou, X Song, Y Yu, J Huang *et al.* Jan 22, 2016 (Xie *et al.*, 2016).

Ferroptosis, a recently discovered form of non-apoptotic form of cell death, is exclusively dependent on intracellular iron in contrast to other metals (Table 5.1, Fig. 5.3) (Dixon *et al.*, 2012; Yang *et al.*, 2014). The key characteristics of ferroptosis involve the iron-dependent accumulation of ROS, reduction in cellular glutathione (GSH) levels, loss of glutathione peroxidase 4 (GPX4) activity and lipid peroxidation (phosphatidylethanolamines containing arachidonic and adrenic acid) that eventually leads to cellular death through loss of membrane functionality (Fig. 5.3) (Friedmann Angeli *et al.*, 2014; D'Herde and Krysko, 2017; Doll *et al.*, 2017; Ito *et al.*, 2017; Kagan *et al.*, 2017). Morphologically, ferroptotic cells display rounding up of cells, mitochondrial abnormalities and normal nuclei in contrast to cells undergoing apoptosis/necrosis/autophagy (Xie *et al.*, 2016). Dysregulation of ferroptosis has been implicated in multiple pathological processes including neurodegenerative

diseases, cancer, acute renal failure, hepatic and heart ischaemia/reperfusion injury, T cell immunity and drug-induced hepatotoxicity (Friedmann Angeli *et al.*, 2014; Linkermann *et al.*, 2014; Yang *et al.*, 2014; Lőrincz *et al.*, 2015; Matsushita *et al.*, 2015; Martin-Sanchez *et al.*, 2017).

GSH is an important antioxidant synthesised in cells from the amino acids L-cystine, L-glutamic acid and glycine (Cardoso *et al.*, 2017). GSH is required as a substrate for the lipid repair function of GPX4, a class of selenium-containing enzymes expressed principally in the brain, testes and spermatozoa (Cardoso *et al.*, 2017). The primary function of GPX4, along with other GPX enzymes is as an antioxidant to protect against oxidative stress. Existing as a membrane-anchored glycoprotein, GPX4 is required for a vital lipid repair function by mediating the reduction of lipid hydroperoxides (LOOH) (Thomas *et al.*, 1990; Wang *et al.*, 2013; Pitts *et al.*, 2014). Ferroptosis inducers, such as ras-selective lethal small molecule-3 (RSL3) and erastin, induce cell death by increasing the amount of lethal lipid ROS generated through inactivation of GPX4 and inhibition of the system x_c^- cystine/glutamate antiporter, respectively (Yagoda *et al.*, 2007; Dixon *et al.*, 2012; Yang *et al.*, 2014). Erastin contributes to ferroptosis by preventing the uptake of cystine through inhibition of the system x_c^- cystine/glutamate antiporter (Dixon *et al.*, 2012). Cystine starvation results in the depletion of GSH and fundamentally the loss of GPX4 activity (Dolma *et al.*, 2003; Gao *et al.*, 2015; Feng and Stockwell, 2018; Gaschler *et al.*, 2018). Depletion of GSH itself by inhibition of the glutamate-cystine ligase complex with *L*-buthionine sulfoximine can also lead to the same iron- and ROS-dependent phenotype (Friedmann Angeli *et al.*, 2014). Addition of iron chelators (e.g. deferoxamine, deferiprone) to reduce iron overload protects against ferroptosis-induced cell death (Yang and Stockwell, 2008; Dixon *et al.*, 2012). Compounds that prevent lipid peroxidation are also able to inhibit ferroptosis (e.g. Vitamin E, ferrostatin-1, liproxstatin-1) (Do Van *et al.*, 2016; Ito *et al.*, 2017; Feng and Stockwell, 2018).

The role of iron in neurons of the *SNPc* has been previously discussed in Chapter 1 section 1.2.4. This section will instead focus on the link of ferroptosis to PD. Iron accumulation in the *SNPc,* genetic disorders resulting in brain iron accumulation (e.g. haemochromatosis) and neuroprotection by chelation of iron provide evidence for the role of iron in PD pathogenesis (Sofic *et al.*, 1988; Gorell *et al.*, 1995; Costello

et al., 2004; Weinreb *et al.*, 2013; Devos *et al.*, 2014). As a consequence of oxidative stress, decreased GSH levels and increased levels of lipid peroxidation are common features in the *SNPc* of PD patients (Dexter *et al.*, 1989; Jenner *et al.*, 1992; Sian *et al.*, 1994).

α-Syn, the major protein component of LBs has been linked to the pathogenesis of PD and is intrinsically linked to iron. α-Syn has an iron response element within the 5'-untranslated region (UTR) of mRNA that regulates the translation of the protein, resulting in increased protein translation in cases of iron overload (Friedlich, Tanzi and Rogers, 2007). In addition, α-syn has a strong binding affinity for both ferric and ferrous iron which is associated with aggregate formation *in vitro* and cell culture systems (Ostrerova-Golts *et al.*, 2000; Li, Uversky and Fink, 2001; Golts *et al.*, 2002; Peng *et al.*, 2010; Xiao *et al.*, 2018). Additionally, the presence of dopamine in the *SNPc* enhances the pro-aggregative effect of iron on α-syn, due to ROS present in cells catalysing the oxidation of iron to the ferric form and promoting α-syn aggregation (Hashimoto *et al.*, 1999; Ostrerova-Golts *et al.*, 2000). α-Syn has also been demonstrated to modulate iron homeostasis through the interaction of α-syn with TfR in the trafficking of iron (Bourdenx *et al.*, 2015). The discovery of an iron-dependent mechanism of cell death suggests a potential to pharmacologically modulate the progression of the disorder (Chen *et al.,* 2015).

5.2 Aims and objectives

Ferroptosis has recently been linked to cell death pathways in PD; however, it is not clear how α-syn aggregation is involved in ferroptosis. The overriding hypothesis is that disruption of α-syn functional interactions with the plasma membrane (including iron importation and dopamine vesiculation) induces a harmful ROS environment that leads to cell death by ferroptosis. The ROS environment favours structural changes of α-syn, including oligomerisation, subsequently leading to propagation of pathogenic species in a prion-like mechanism.

The specific aims of this chapter were:

- To determine whether treatment with iron (Fe^{2+}) and/or oligomeric α-syn activate the ferroptosis pathway, resulting in lipid peroxidation in 2D and 3D SH-SY5Y models (described in Chapters 3 and 4).
- To determine the influence of ferroptosis on the formation of α-syn aggregates using both Fe^{2+} and ferroptosis inducers (e.g. erastin and RSL3).
- To determine the expression levels of the ferroptosis-associated GPX protein, GPX4, alongside levels of cellular ROS following treatment with Fe^{2+} and/or oligomeric α-syn.

5.3 Results

5.3.1 Iron (III) chloride is internalised by SH-SY5Y in 2D and 3D cultures and is toxic to cells at high concentrations

To determine whether iron (II) chloride contributes to ferroptosis and aggregation of α-syn in SH-SY5Y cell models, the concentration of iron (II) chloride to use for future experiments was determined. SH-SY5Y were grown in monolayer undifferentiated cultures or differentiated in 3D cultures prior to treatment with iron. ICP-MS analysis was undertaken to determine iron uptake in SH-SY5Y cultures (Fig. 5.4) and the resazurin cell viability assay was undertaken to determine the toxicity of iron (II) chloride (Fig. 5.5).

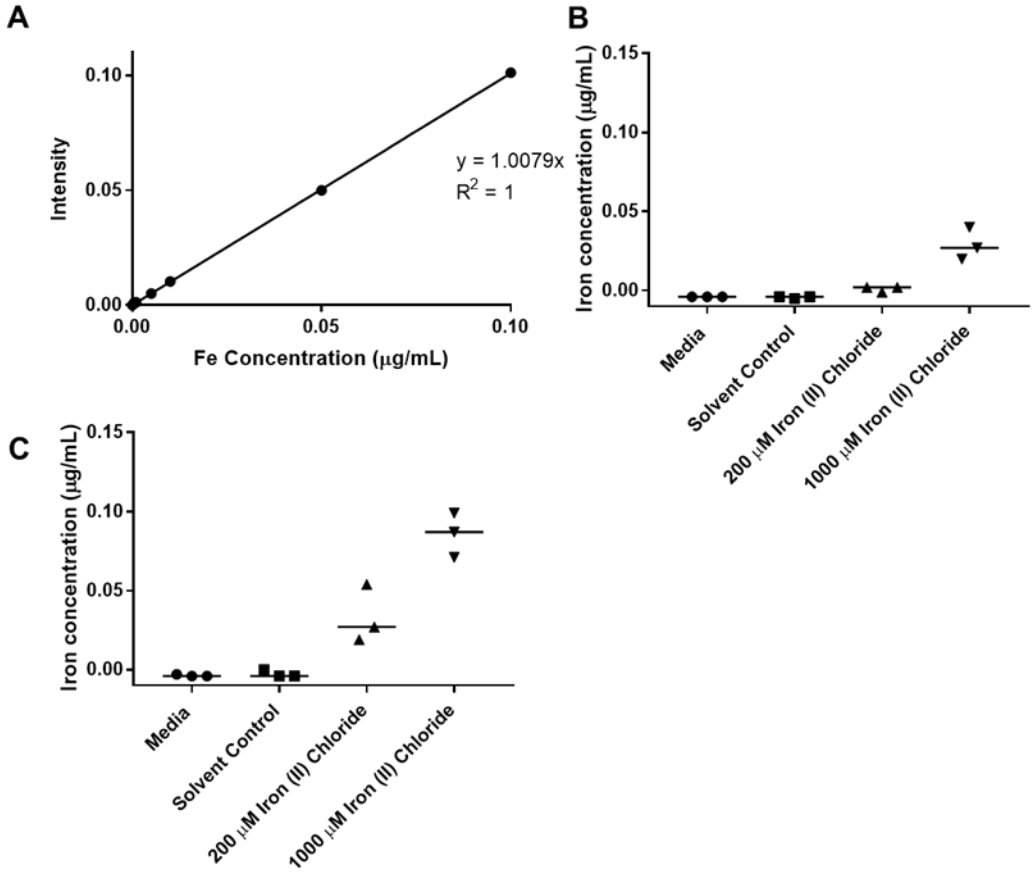

Figure 5.3. *ICP-MS analysis of iron content of 2D and 3D SH-SY5Y following 24 hr treatment with iron (II) chloride.* **(A)** Iron calibration curve. **(B)** 2D-undifferentiated SH-SY5Y. **(C)** 3D-differentiated SH-SY5Y. **(B, C)** Protein levels were normalised to 500 µg protein prior to ICP-MS analysis. Data presented as individual data points and median (straight line) of three independent biological repeats. No statistical significance was observed between groups.

ICP-MS analysis revealed iron content of 2D, and 3D cultures increased in a dose-dependent manner following treatment with iron (II) chloride and appropriate controls (Fig. 5.4). In 2D cultures, intracellular iron concentrations rose to 0.03 µg/mL ± 0.01

in the 1000 µM iron (II) chloride treatment group. In 3D cultures, intracellular iron concentrations were increased in comparison to 2D cultures at 0.09 µg/mL ± 0.01 in the 1000 µM iron (II) chloride treatment group.

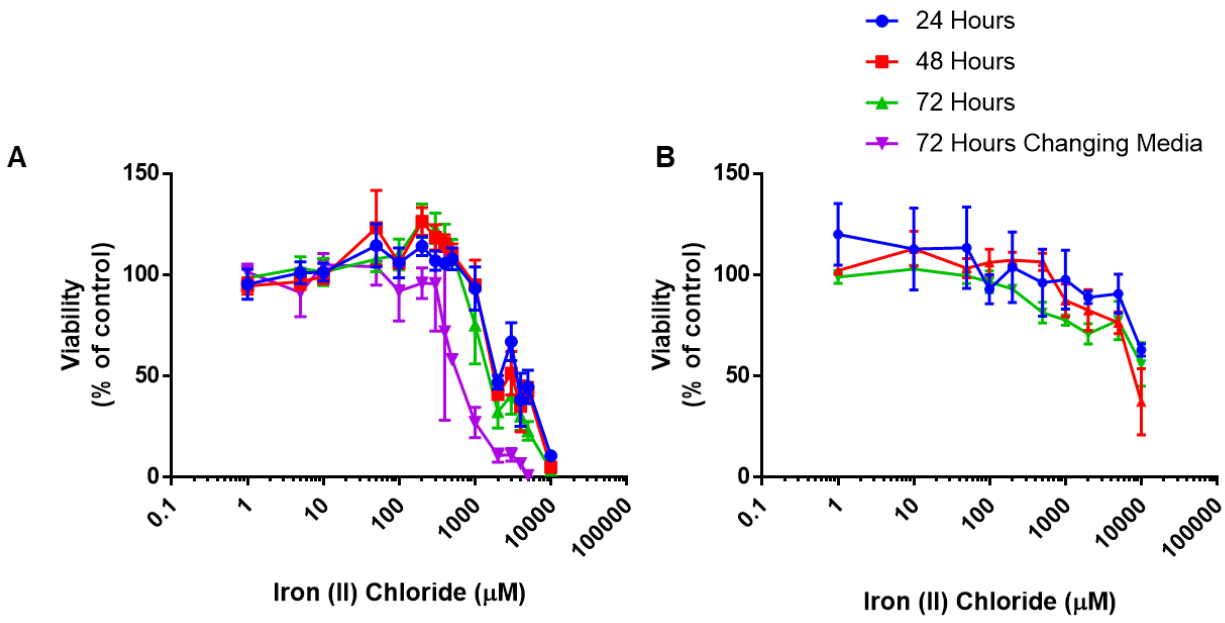

Figure 5.4. *Resazurin reduction cell viability assays of 2D and 3D SH-SY5Y at 24, 48 or 72 hrs following treatment with iron (II) chloride.* **(A)** 2D-undifferentiated SH-SY5Y. **(B)** 3D-differentiated SH-SY5Y. Data presented as mean and +/- SEM of at least three independent biological repeats. No statistical significance was observed between groups.

Measurement of cell viability using the resazurin assay revealed exposure to iron (II) chloride caused a concentration-dependent reduction in the viability of both 2D and 3D SH-SY5Y (Fig. 5.5). In 2D cultures (Fig. 5.5 A), viability decreased substantially at >1000 µM, with 10,000 µM iron (II) chloride leading to 100% death of the cell populations (0% viability). Due to the high levels of iron needed to induce cell death in both cell populations (Fig. 5.5) and the possibility that the iron was potentially precipitating out of solution at these high concentrations, a 'continual stress treatment' was included (described in Chapter 2 Fig. 2.1). In this treatment, fresh iron (II) chloride (+ NTA) was added to cell populations every 24 hrs for 72 hrs. In the "continual stress" group a lower concentration of 5000 µM iron (II) chloride was sufficient to induce 100% cell death (0% viability) (Fig. 5.5 A). 3D SH-SY5Y were more resistant to cell death induced by iron (II) chloride (Fig. 5.5 B), with viabilities following treatment of 10000 µM iron (II) chloride at 24, 48 and 72 hrs at 62% ± 16, 56% ± 15 and 37% ± 23, respectively. Concentrations of 200 µM and 1000 µM iron (II) chloride were chosen for use in future experiments. Cell survival was also

confirmed by visual inspection in addition to the resazurin assay, whereby cells with 0% viability were rounded and detaching from the culture vessel (*data not shown*). It is important to note that the normal cellular concentration of iron in neurons of the *SNPc* is 0.54 ± 0.2 mM (Reinert *et al.*, 2019).

5.3.2 Iron induced increased expression of α-synuclein

Iron has been shown to accelerate the formation of α-syn aggregates in previous cell culture and *in vitro* systems (Ostrerova-Golts *et al.*, 2000; Golts *et al.*, 2002; Wan *et al.*, 2017). To determine whether iron (II) chloride treatment induced the formation of α-syn aggregates in this culture system, 2D and 3D cultures were treated with iron (II) chloride and appropriate controls for 24 or 72 hrs and investigated using immunocytochemistry, confocal imaging and western blotting (Fig. 5.6, 5.7 and 5.8). Using immunocytochemistry and confocal analysis, aggregate volume was slightly increased (not statistically significant) in 1000 µM iron (II) chloride treatment group at 0.96 μm^3 ± 0.05 in comparison to media control at 0.73 μm^3 ± 0.21, solvent control at 0.93 μm^3 ± 0.24 and 200 µM iron (II) chloride at 0.86 μm^3 ± 0.04 (Fig. 5.6 A and 5.6 A). Aggregate volume was substantially decreased at 72 hrs and 72 hrs ("continual stress) in comparison to the aggregate volume at 24 hrs when comparing groups e.g. media at 24 hrs compared to media at 72 hrs (Fig. 5.7).

Aggregate volume at 72 hrs was again slightly increased in the 1000 µM iron (II) chloride group at 0.14 μm^3 ± 0.04 in comparison to media control 0.08 μm^3 ± 0.02, solvent control at 0.11 μm^3 ± 0.01 and 200 µM iron (II) chloride at 0.1 μm^3 ± 0.03 (Fig. 5.6 B and 5.7 B). In contrast, aggregate volume was highest in the media control in the 72 hrs ("continual stress") treatment group at 0.13 μm^3 ± 0.50 in comparison to solvent control at 0.11 μm^3 ± 0.32, 200 µM iron (II) chloride at 0.10 μm^3 ± 0.03 and 1000 µM iron (II) chloride at 0.11 μm^3 ± 0.01 (Fig. 5.6 C and 5.7 C).

Western blot analysis of α-syn protein levels from 2D iron (II) chloride treated cultures revealed similar levels of α-syn in all groups (media, solvent, 200 µM iron (II) chloride and 1000 µM iron (II) chloride) at 24 and 72 hrs (Fig. 5.7 A, B and 5.8 A and B). Increased levels of both α-syn and phosphorylated α-syn (p-α-syn) were observed in the 72 hr ("continual stress") group in both iron (II) chloride treatment groups when compared to media and solvent controls (Fig. 5.7 C and 5.8 C). The fold change of α-syn increased significantly from 1 ± 0.2879 in media control to 1.596

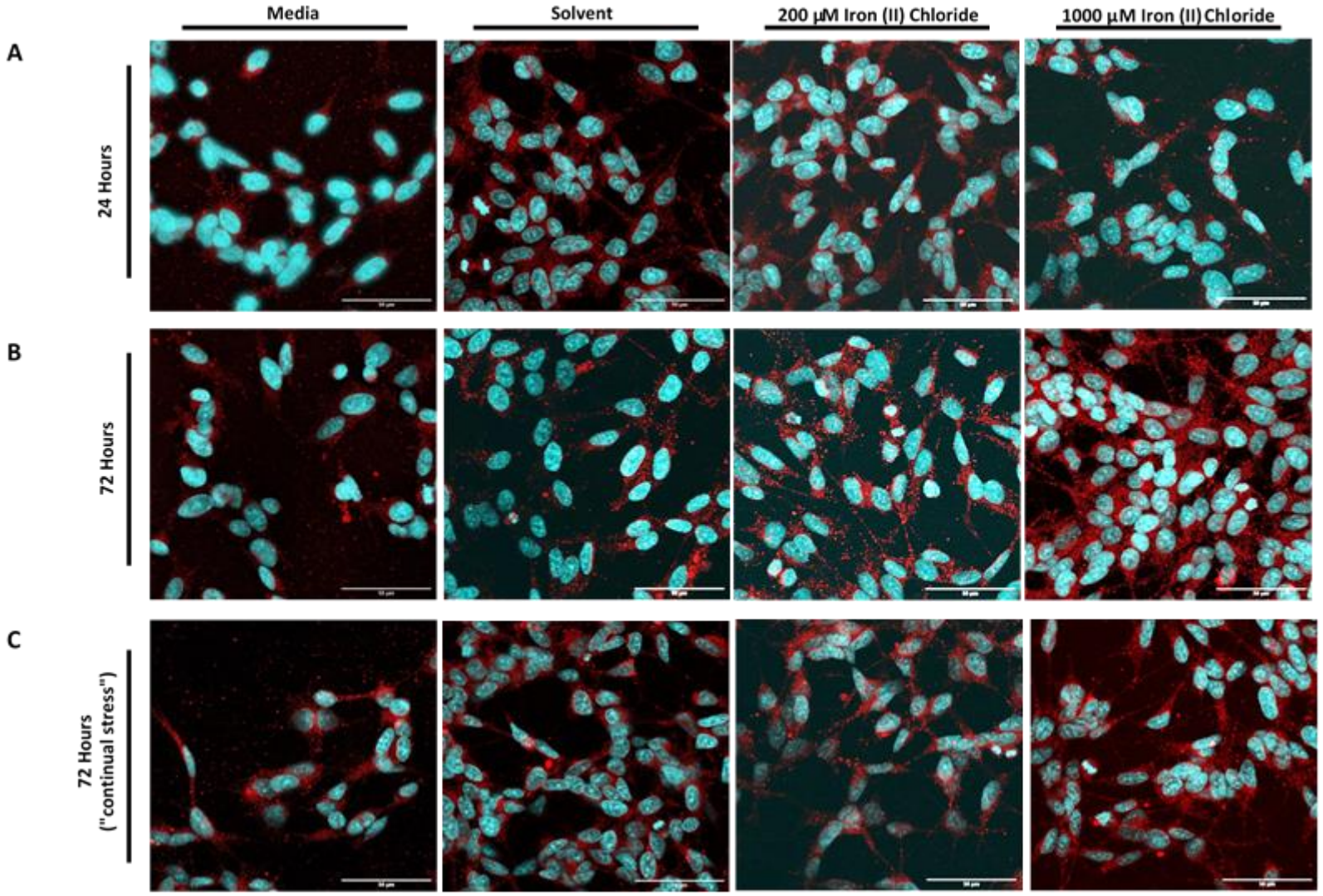

Figure 5.5. *Aggregation of α-syn in 2D cultures following treatment with iron (II) chloride.* Double immunostaining of α-syn (*red*) and nuclei (*blue*) following treatment at 24 hrs **(A)**, 72 hrs **(B)** and 72 hrs ("continual stress") **(C)**. Images presented are representative of three independent biological repeats. Scale bar represents 50 µm.

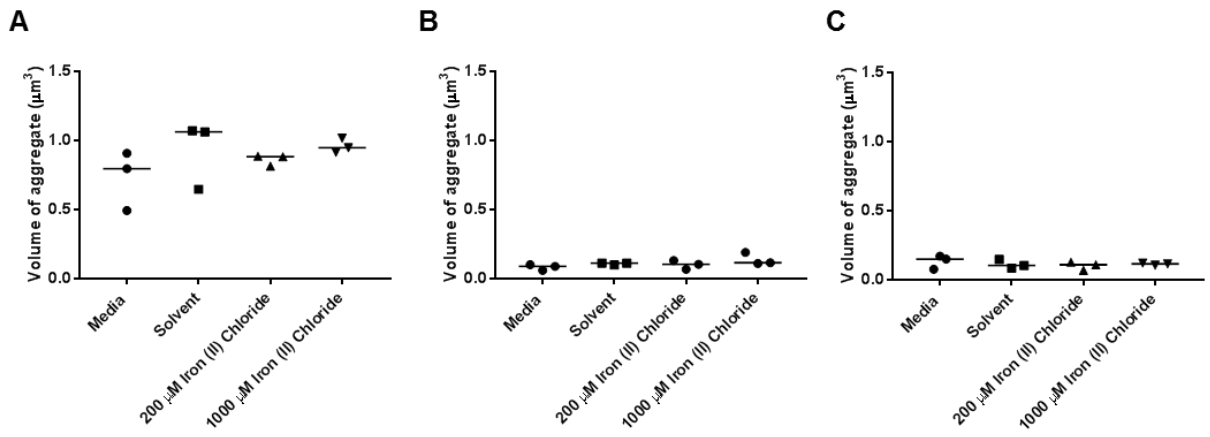

Figure 5.6. *Volume (µm^3) of α-syn-positive aggregates in 2D cultures following treatment with iron (II) chloride.* **(A)** 24 hrs. **(B)** 72 hrs. **(C)** 72 hrs ("continual stress"). Data presented as individual data points and median (straight line) of three independent biological repeats. No statistical significance was observed between groups.

± 0.4197 and 1.528 ± 0.1869 in the 200 and 1000 µM iron (II) chloride treatment groups, respectively (Fig. 5.7 C). The same trend was observed when detecting p-α-syn at S129, with levels increased in the 200 and 1000 µM iron (II) chloride treatment groups at 2.15 ± 0.38 and 2.32 ± 0.74, respectively, compared to media control at 1 ± 0.74 (Fig. 5.8 C).

To determine whether α-syn expression was increased in 3D cultures, cells were treated with iron (II) chloride for 24 or 72 hrs and stained with an anti-α-syn antibody. Increased staining was principally observed in the 1000 µM iron (II) chloride following 72 hr treatment, however, no obvious aggregates were observed in any of the treatment groups (Fig. 5.9 A). At 24 hrs, % cells positive for α-syn staining increased from 42% in the media control group to 58%, 77% and 56 % in the solvent, 200 and 1000 µM iron (II) chloride groups, respectively (Fig. 5.9 B). At 72 hrs, % cells positive for α-syn staining increased from 67% in the media control group to 70%, 82% and 85% in the solvent, 200 and 1000 µM iron (II) chloride, respectively (Fig. 5.9 C).

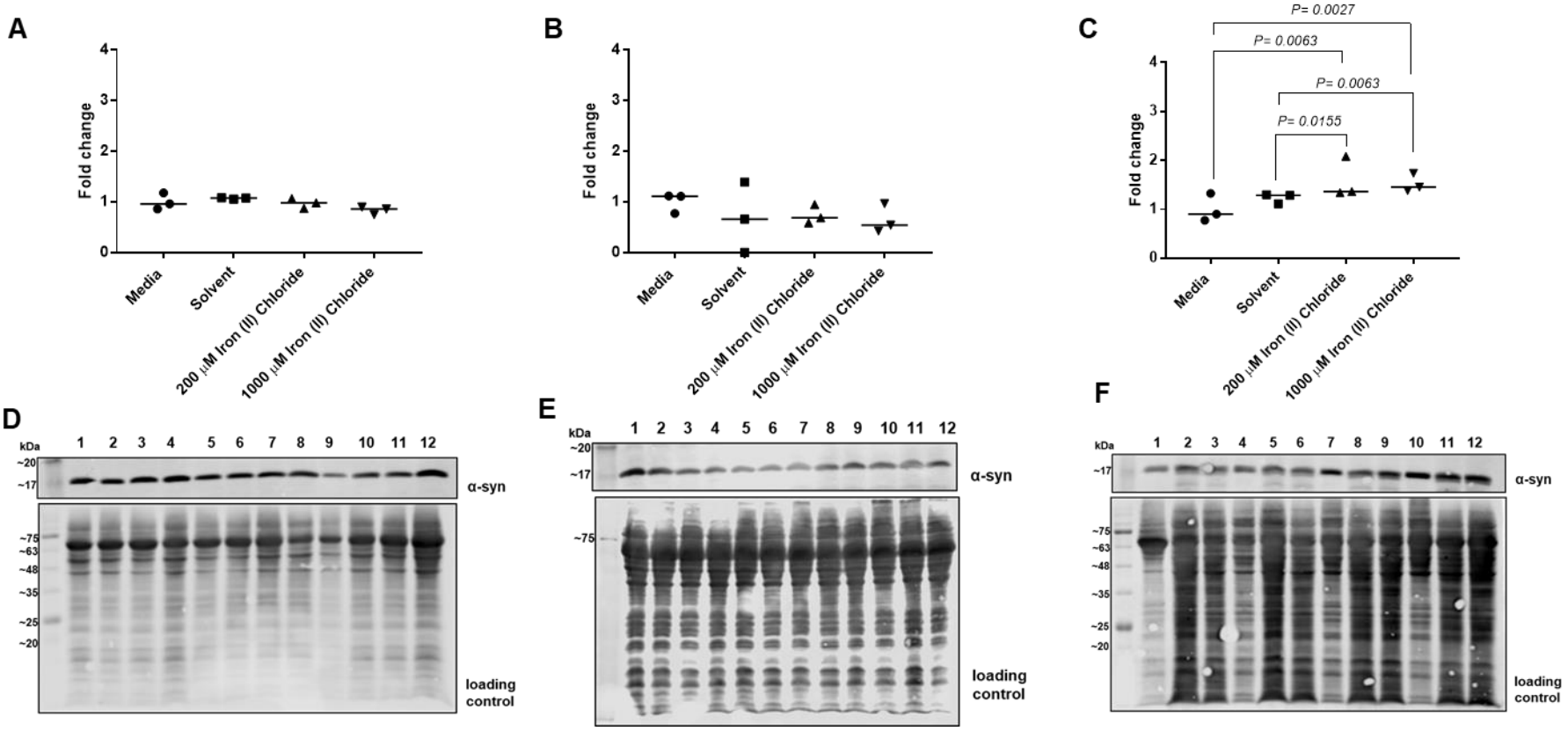

Figure 5.7. *Fold change of α-syn in 2D cultures following treatment with iron (II) chloride compared to media control as analysed by western blotting.* **(A, B, C)** Western blotting undertaken using the α-syn211 antibody and the representative blots **(D, E, F). (A, D)** 24 hr treatment. **(B, E)** 72 hr treatment. **(C, F)** 72 hrs ("continual stress") treatment. Data presented as individual data points and median (straight line) of three independent biological repeats. **(C)** Statistical significance determined by Kruskal-Wallis test with post-hoc Conover-Inman. **(A, B)** No statistical significance between groups. **(C)** Result of initial Kruskal-Wallis test *P= 0.0361*.

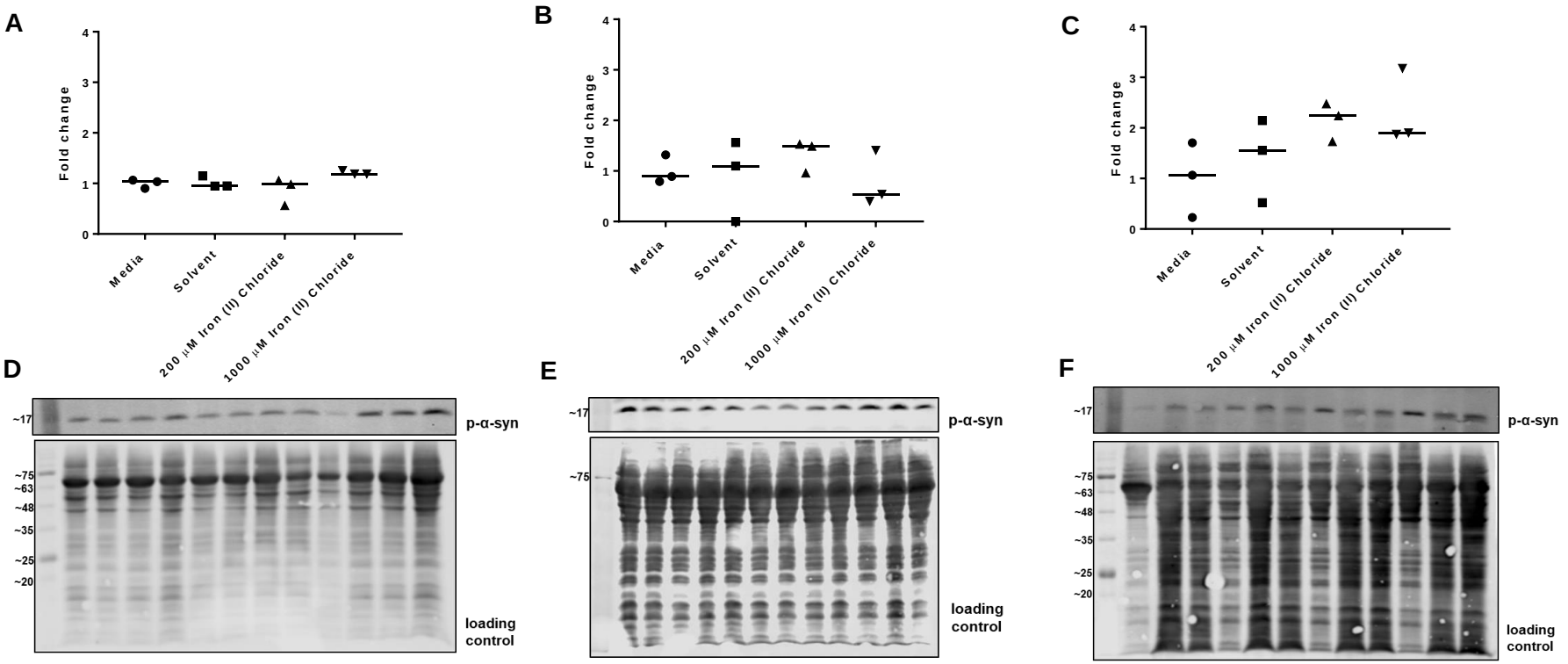

Figure 5.8. *Fold change of phosphorylated-α-syn in 2D cultures following treatment with iron (II) chloride compared to media control as analysed by western blotting.* **(A, B, C)** Densitometry analysis of western blots undertaken using an antibody recognising the phosphorylation of α-syn at S129 and the representative blots **(D, E, F). (A, D)** 24 hr treatment. **(B, E)** 72 hr treatment. **(C, F)** 72 hrs ("continual stress") treatment. Data presented as individual data points and median (straight line) of three independent biological repeats. No statistical significance between groups.

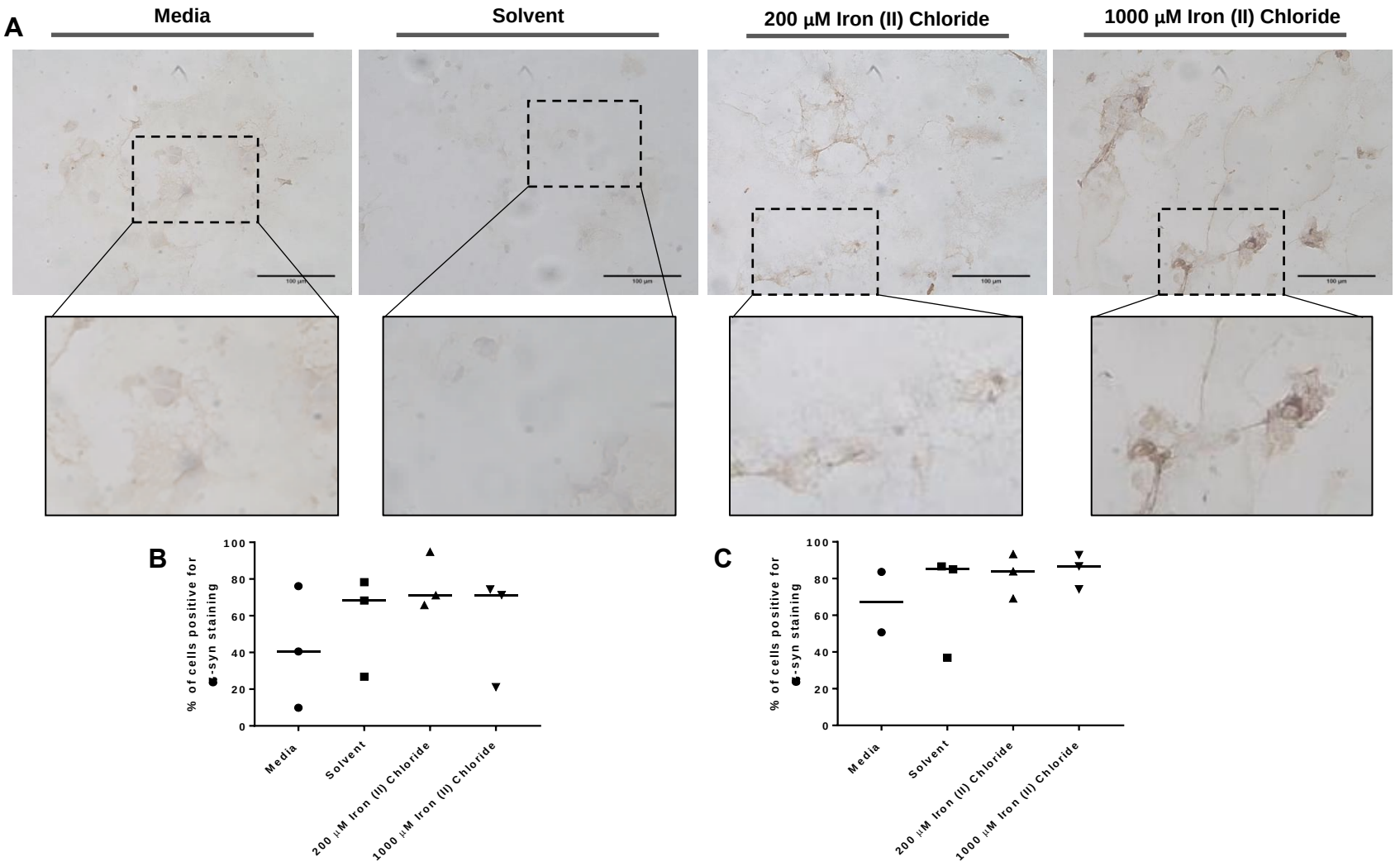

Figure 5.9. *α-Syn staining of 3D cultures following treatment with iron (II) chloride.* **(A)** Representative images of α-syn staining in 3D cultures following treatment with either media only, solvent control, 200 µM iron (II) chloride or 1000 µM iron (II) chloride for 72 hrs. Scale bar represents 100 µm. **(B)** % α-syn immunopositivity at 24 hrs. **(C)** % α-syn immunopositivity at 72 hrs. **(B, C)** Data presented as individual data points and median (straight line) of three independent biological repeats (except for C, media only control only has two data points). No statistical significance was determined between groups.

5.3.3 Ferroptosis is not an effective pathway for inducing SH-SY5Y cell death

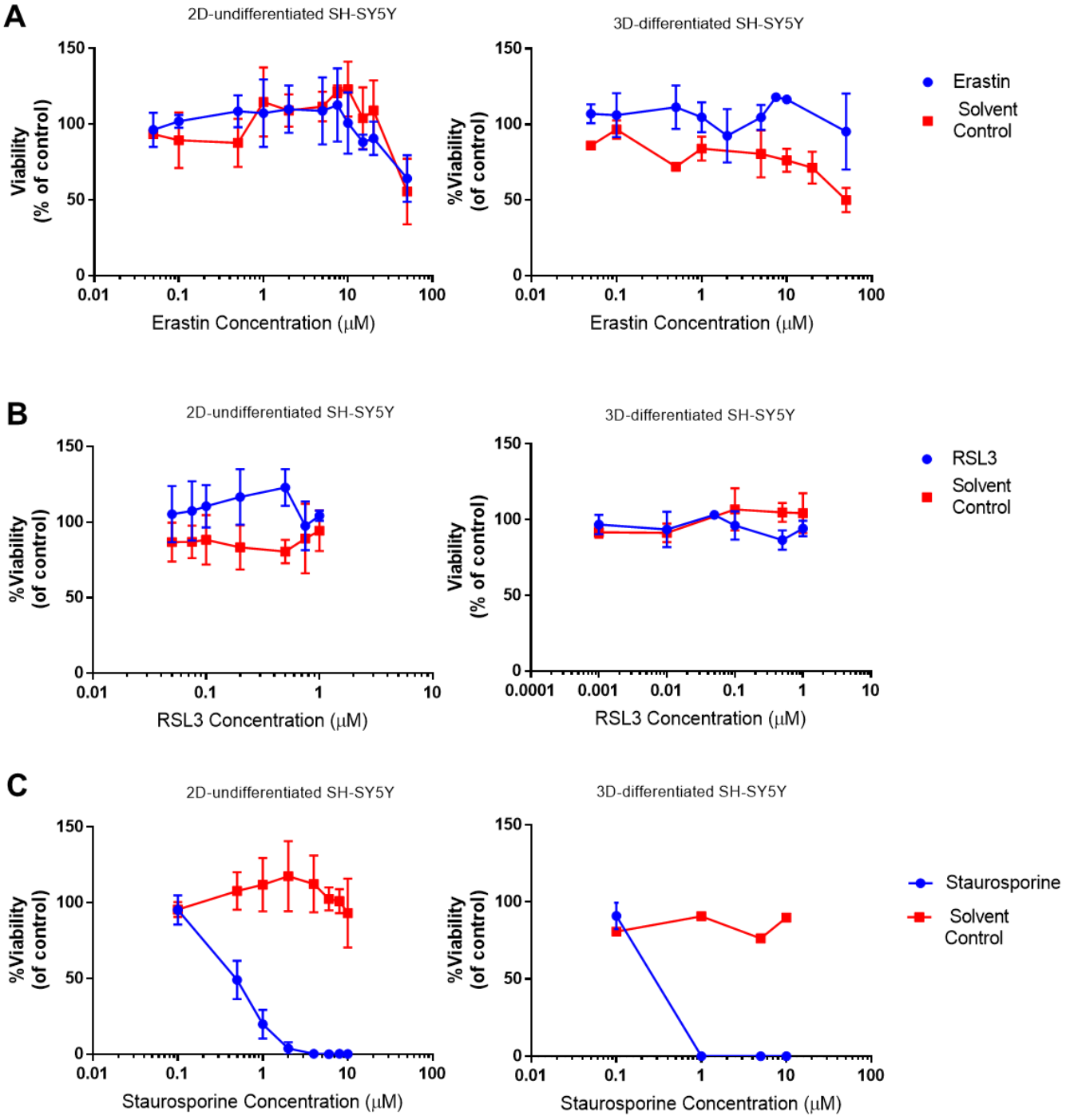

Figure 5.10. *Resazurin cell viability assays of 2D and 3D SH-SY5Y following 24 hr treatment with erastin, RLS3 and staurosporine.* **(A)** Erastin. **(B)** RSL3. **(C)** Staurosporine. **(A, B, C)** Appropriate solvent controls were also incubated for 24 hrs. Data presented as mean and +/- SEM of at least three independent biological repeats.

Ferroptosis, a form of non-apoptotic cell death, has been linked to the pathogenesis of PD through the involvement of iron deposition, ROS generation, lipid peroxidation and eventual cell death (Do Van *et al.*, 2016). However, it is not known whether the iron-induced aggregation of α-syn is related to this mechanism of necroptosis,

5.3.4 Iron induces oxidative stress in SH-SY5Y

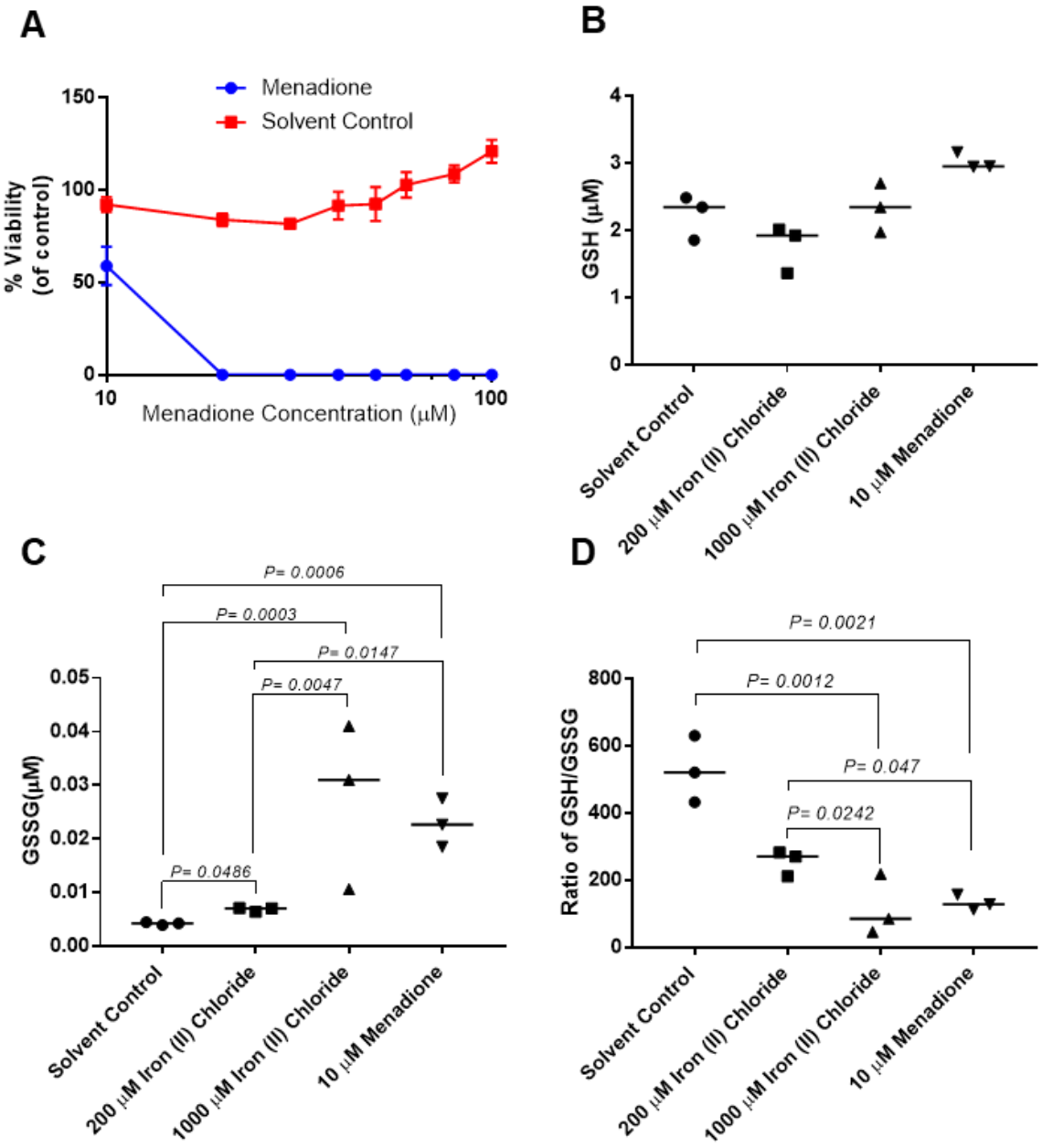

Figure 5.11. *Glutathione assay of SH-SY5Y cells treated for 24 hrs with iron (II) chloride.* **(A)** Resazurin cell viability assay of menadione (positive control for ROS generation) and solvent control (ethanol). Data presented as mean and +/- SEM of three independent biological repeats. **(B)** GSH concentration per well. **(C)** GSSG concentration per well. **(D)** Ratio of GSH/GSSG. **(B, C, D)** Data presented as individual data points and median (straight line) of three independent biological repeats. Statistical significance was determined using Kruskal-Wallis with post-hoc Conover-Inman. Result of initial statistical test (Kruskal-Wallis) for **(B)** *P= 0.0513* (not statistically significant) **(C)** *P= 0.0237* **(D)** *P= 0.0329*.

therefore the relationship of α-syn aggregation to ferroptosis was investigated. First, the ferroptosis inducers erastin and RSL3 were investigated for the ability to induce cell death in SH-SY5Y cultures. Change in cell viability was investigated in both 2D and 3D cultures using the resazurin reduction assay (Fig. 5.10 A, B). Treatment with erastin or RSL3 revealed no significant changes in cell viability in 2D or 3D cultures

when compared to solvent controls. Increasing concentration of erastin to 50 μM did not alter cell viability when compared to solvent controls (data not shown). In contrast, SH-SY5Y were highly sensitive to an inducer of apoptosis, staurosporine, resulting in 100% cell death (0% cell viability) at 2 μM (2D) and 1 μM (3D) (Fig. 5.10 C).Reduction of reduced GSH and increase in oxidised GSH (GSSG) concentrations in cells is indicative of cellular oxidative stress and a cardinal feature of ferroptosis. To determine whether GSH levels were altered during iron (II) chloride treatment, cellular levels of both reduced and oxidised GSH was determined using the using the GSH/GSSG-Glo™ Glutathione Assay kit (Promega) (Fig. 5.11). Menadione was used as a positive control for inducing oxidative stress in cultures (Fig. 5.11 A). The concentration of reduced GSH increased slightly (not significant) following treatment with 10 μM menadione (positive control) but remained unchanged in both 200 and 1000 μM iron (II) chloride groups when compared to solvent only control (Fig. 5.11 B). In contrast, treatment with 200, 1000 μM iron (II) chloride and 10 μM menadione increased the levels of GSSG significantly when compared to solvent-only control, indicating cellular defence against oxidative stress induced by iron (II) chloride and menadione (Fig. 5.11 C). A reduced GSH:GSSG ratio is also used to demonstrate the cellular response to oxidative stress and was shown to be significantly decreased after 1000 μM iron (II) chloride and 10 μM menadione when compared to solvent only control and 200 μM iron (II) chloride (Fig. 5.11 D).

Generation of cellular ROS following iron treatment was investigated using the CellROX® green oxidative stress reagent. CellROX® green is a DNA dye that upon oxidation is mainly localised in the nucleus and mitochondria. In the absence of ROS, CellROX® green is non-/very weakly fluorescent and is distributed throughout the cytoplasm. Cellular ROS is detected following 72 hr treatment with both 200 and 1000 μM iron (II) chloride and 10 μM menadione (positive control) as evidenced by the association of CellROX® green with the cell nucleus (Fig. 5.12). In contrast, weak staining was observed throughout the cytoplasm of SH-SY5Y in both media and solvent controls (Fig. 5.12). At 72 hrs ("continual stress"), there was a complete absence of nuclear-associated CellROX® green staining in all groups (Fig. 5.13). ICP-MS measurement of iron concentration in cell cultures revealed a decrease in iron concentration in the 72 hr ("continuous stress") group when compared to 72 hrs

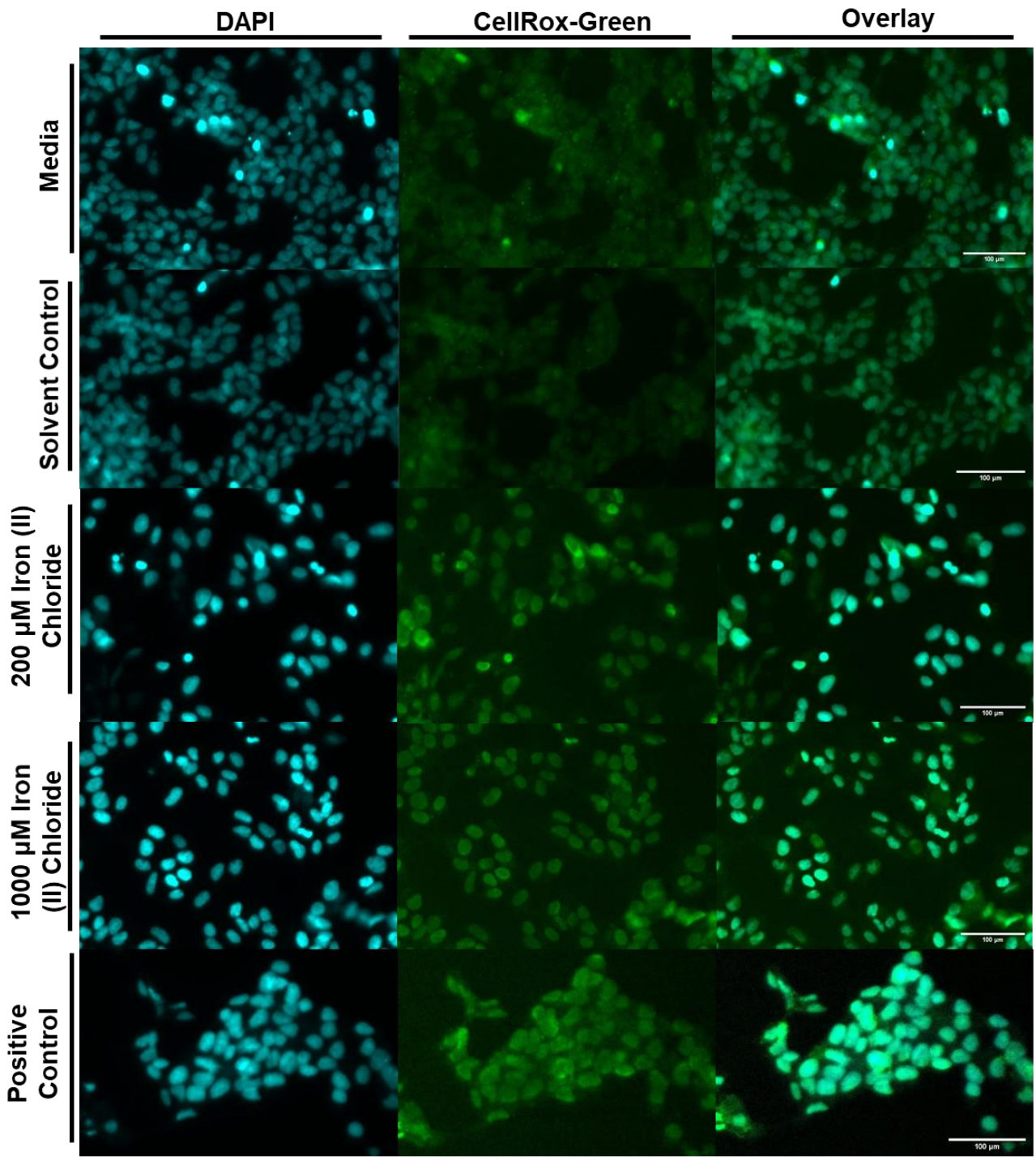

Figure 5.12. *CellRox Green assay of iron (II) chloride treated 2D cultures at 72 hrs following treatment.* Images presented are representative of three independent biological repeats. 2D SH-SY5Y cultures were incubated with media, NTA-only solvent control, 200 µM iron (II) chloride, 1000 µM iron (II) chloride, and positive control (10 µM menadione) for 72 hours. After incubation, 5 µM CellRox Green reagent was added to cells detect intracellular ROS. In media and solvent control, the ROS-specific signal was low and diffusely distributed throughout the cytoplasm. In 200 µM, 1000 µM iron (II) chloride , and positive control samples focal nuclear staining was observed consistent with ROS-mediated oxidation of the CellRox Green reagent and subsequent binding of the oxidised reagent to DNA. Scale bar represents 100 µm.

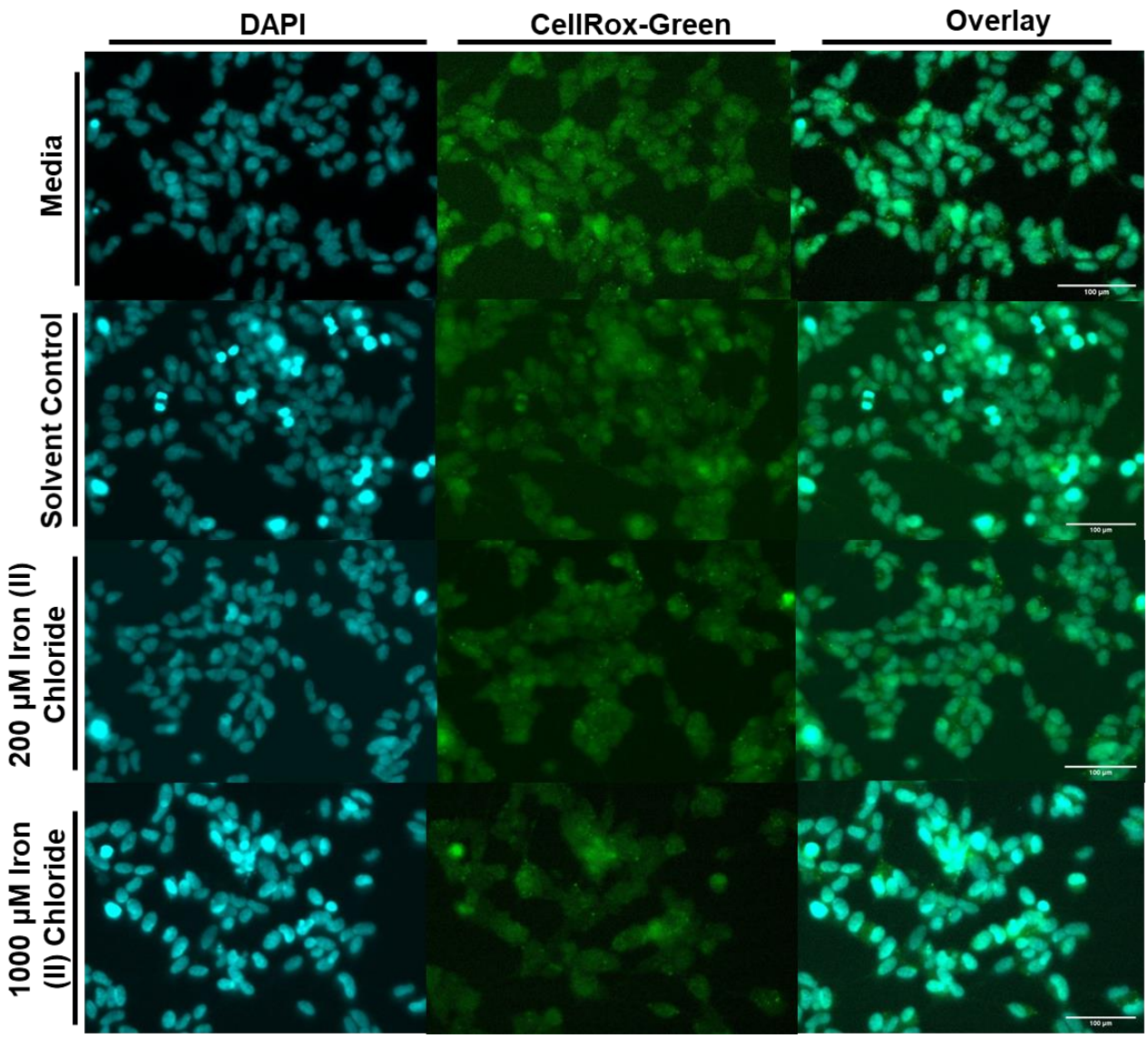

Figure 5.13. *CellRox Green assay of iron (II) chloride treated 2D cultures at 72 hrs ("continual stress") following treatment.* Figure 5.12. Images presented are representative of three independent biological repeats. 2D SH-SY5Y cultures were incubated with media, NTA-only solvent control, 200 µM iron (II) chloride, 1000 µM iron (II) chloride, and positive control (10 µM menadione) for 72 hours. After incubation, 5 µM CellRox Green reagent was added to cells detect intracellular ROS. In all groups, the ROS-specific signal was low and diffusely distributed throughout the cytoplasm. In 200 µM, 1000 µM iron (II) chloride , and positive control samples focal nuclear staining was observed consistent with ROS-mediated oxidation of the CellRox Green reagent and subsequent binding of the oxidised reagent to DNA. Scale bar represents 100 µm.

(Fig. 5.14), correlating to the cellular ROS level observed by CellROX® green staining.

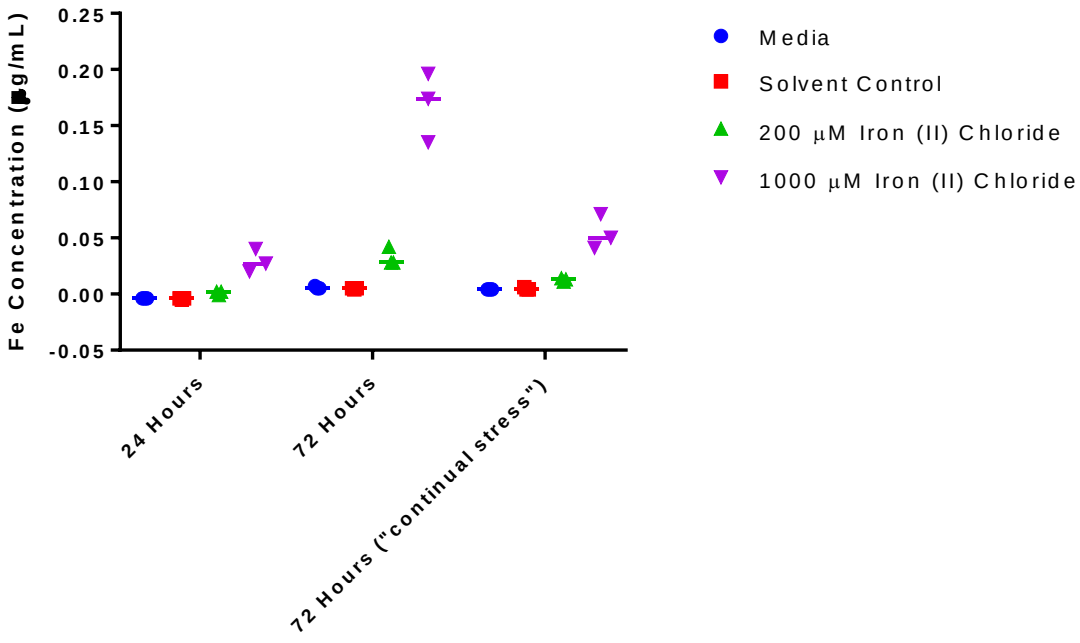

Figure 5.14. *ICP-MS analysis of iron levels in 2D SH-SY5Y following treatment with iron (II) chloride for either 24 or 72 hrs.* Data presented as individual data points and median (straight line) of three independent biological repeats. No statistical significance was determined between groups.

5.3.5 Iron-induced oxidative stress shares features of ferroptosis in SH-SY5Y including ablation of GPX4 expression and presence of lipid peroxidation

Although SH-SY5Y cells were not sensitive to treatment with ferroptosis inducers, ROS production and ferroptotic markers (lipid peroxidation, GSH levels and GPX4 levels) were investigated in cultures following iron (II) chloride treatment. The resulting lipid peroxidation following iron (II) chloride treatment was investigated using the BODIPY™ 581/591 C11 lipid peroxidation dye. Lipid peroxidation was shown to affect cells in the 1000 µM iron (II) chloride treatment group following 12 hr treatment as shown by the reduction in non-oxidised lipid (red staining) and increase in oxidised lipids (green) (Fig. 5.15). It is clear to see that only a small percentage of cells are affected, with approximately 3/4 cells (~1% of cells) per field of view showing oxidised lipids (green) (Fig. 5.15).

Investigation of lipid peroxidation at later time points of 24 and 72 hrs following treatment with 1000 µM iron (II) chloride demonstrated slightly more cells positive for lipid peroxidation (Fig. 5.16). Interestingly, cells positive for lipid peroxidation do not show the typical complete reduction in staining for non-oxidised (red) to oxidised (green) lipids, but rather show co-localisation of both (Fig. 5.15). Flow cytometry analysis was undertaken to quantify the levels of

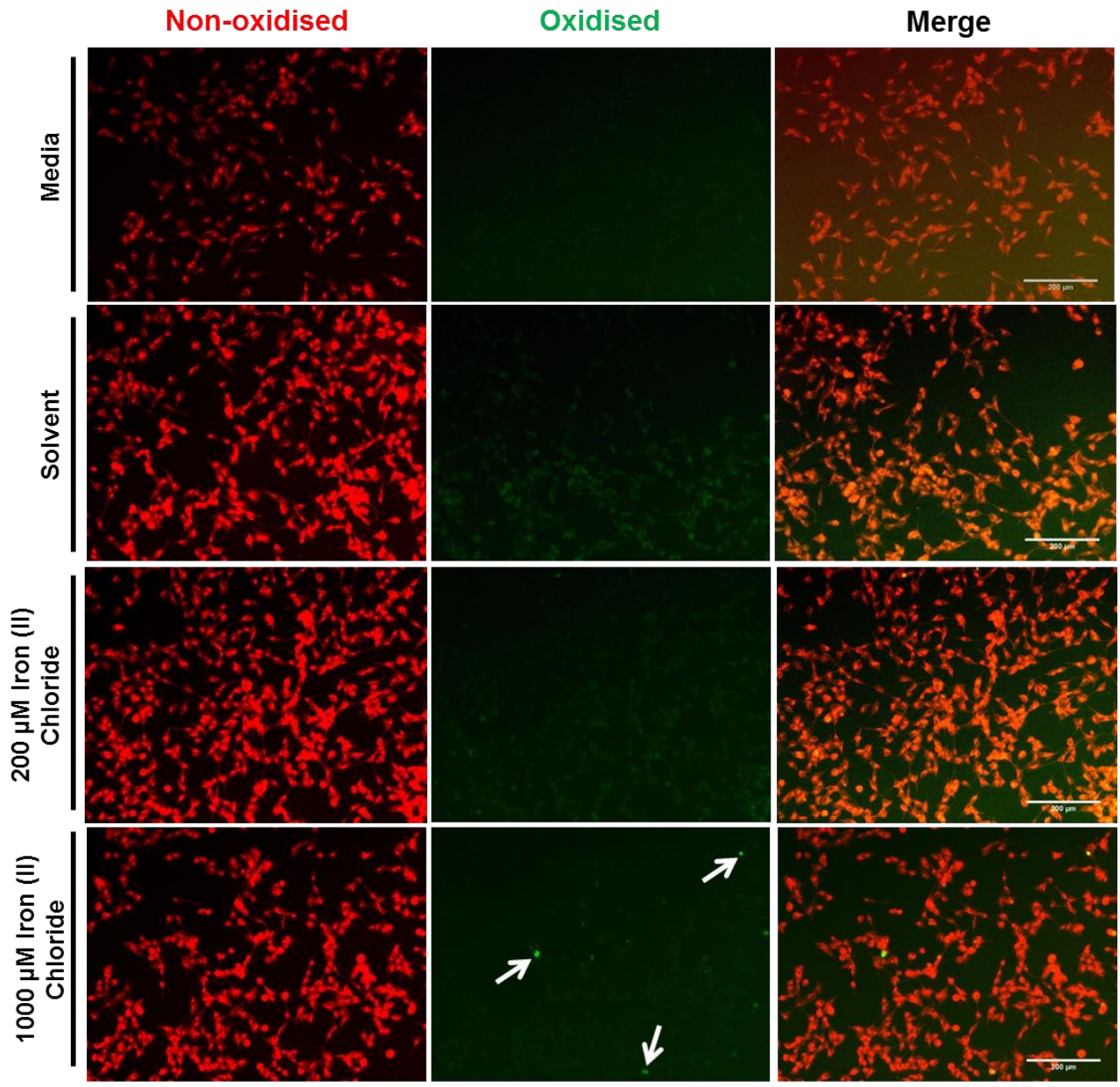

Figure 5.15. *Lipid peroxidation following 12-hr treatment with iron (II) chloride.* Representative images of SH-SY5Y treated with media only, solvent control, 200 µM iron (II) chloride or 1000 µM iron (II) chloride. Cells positive for lipid peroxidation are identified by reduction in red staining (loss of non-oxidised lipids) and increase in green staining (gain of oxidised lipids; *white arrows*). Scale bar represents 200 µm. Images shown are representative of three biological repeats.

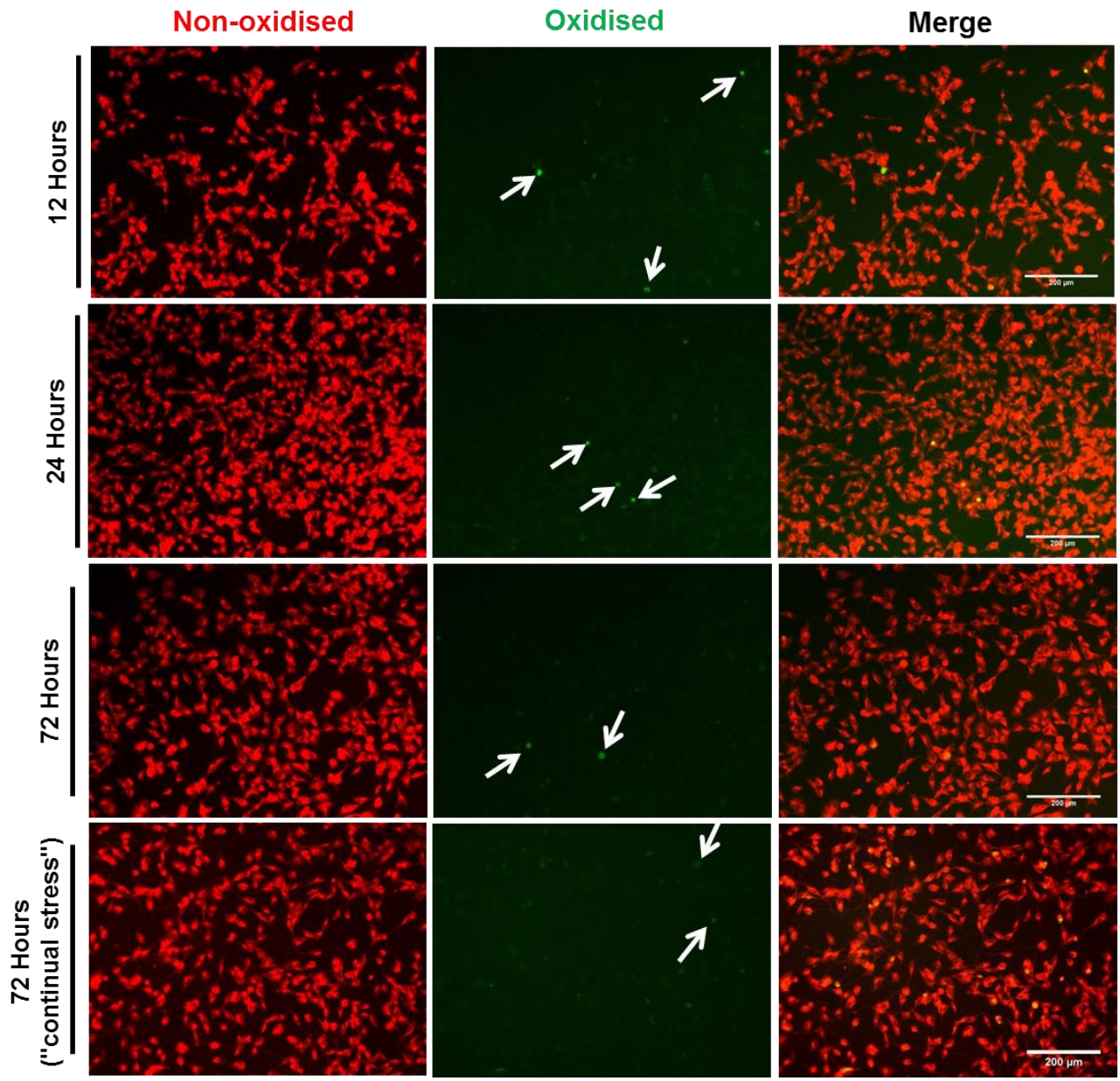

Figure 5.16. *Lipid peroxidation of SH-SY5Y following treatment with 1000 µM iron (II) chloride at 12, 24, 72 and 72 hrs ("continual stress").* Cells positive for lipid peroxidation are identified by reduction in red staining (loss of non-oxidised lipids) and increase in green staining (gain of oxidised lipids; *white arrows*). Scale bar represents 200 µm. Images shown are representative of three biological repeats.

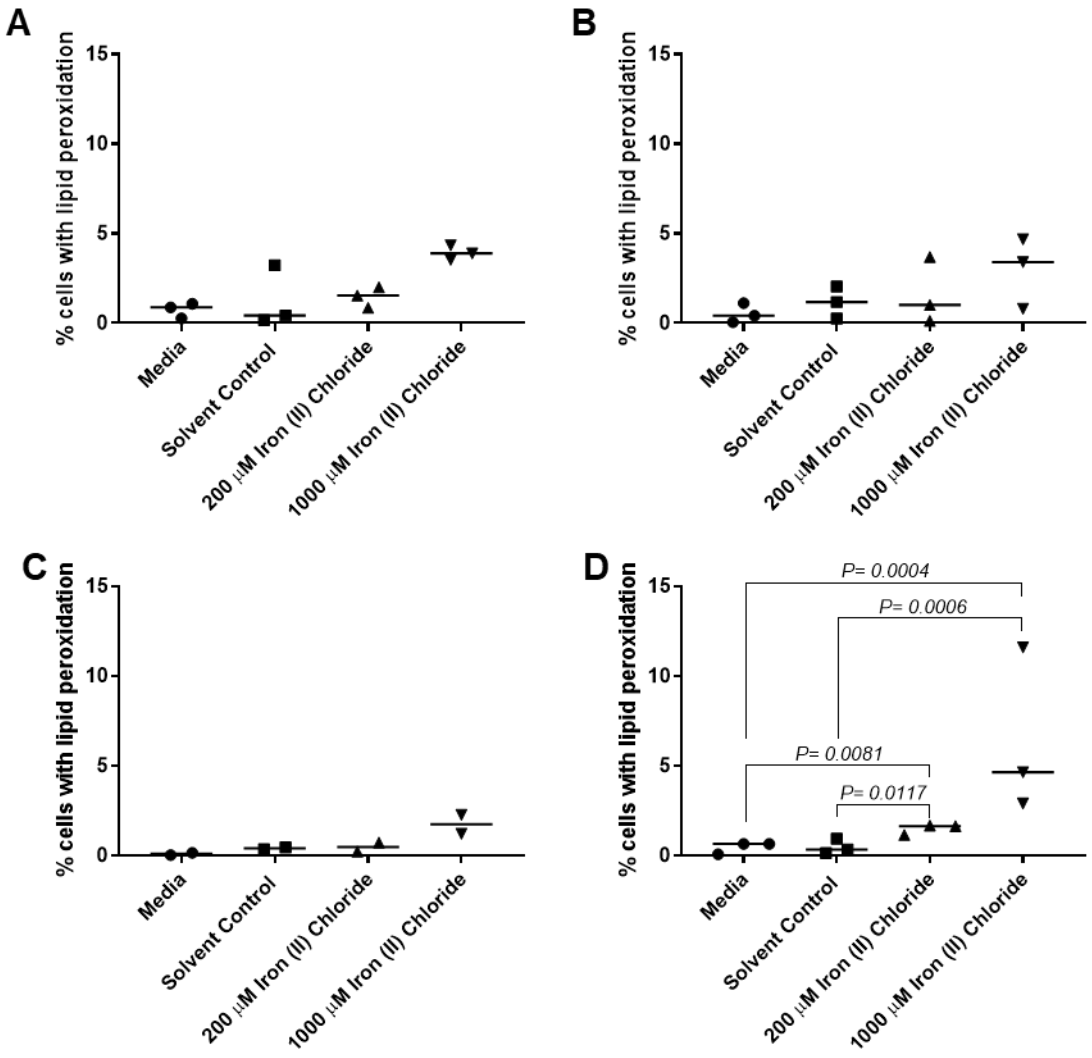

Figure 5.17. *Cell counts of lipid peroxidation in SH-SY5Y following treatment with media, NTA-only solvent control, 200 μM, and 1000 μM iron (II) chloride at 12, 24, 72 and 72 hrs ("continual stress").* **(A)** 12 hours. **(B)** 24 hours. **(C)** 72 hours. **(D)** 72 hours ("continual stress"). Cells positive for lipid peroxidation are identified by reduction in red staining (loss of non-oxidised lipids) and increase in green staining (gain of oxidised lipids; *white arrows*). No statistical differences between groups in A-C. **(D)** Result of initial Kruskal-Wallis test *P= 0.0249.* **(A-D)** Data presented as all data points of independent biological repeats.

lipid peroxidation within treatment groups (Fig. 5.18). At all time points measured, lipid peroxidation increased in both 200 and 1000 μM iron (II) chloride groups when compared to media and solvent only controls (Fig. 5.16, 5.17). Statistical significance was observed only in the 72 hr ("continual stress") group in cell counts (Fig. 5.17 D), but only observed in the 72 hour group when analysed by flow cytometry (Fig. 18).

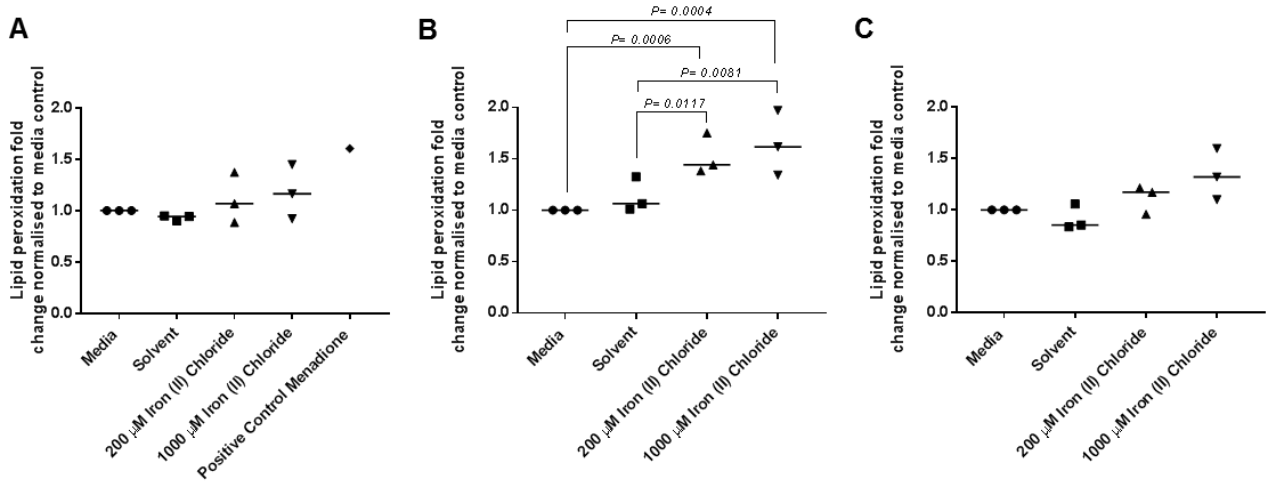

Figure 5.18. *Flow cytometry analysis of lipid peroxidation in iron-treated 2D cultures.* **(A)** 24 hrs. **(B)** 72 hrs. **(C)** 72 hrs ("continual stress"). Data presented as individual data points and median (straight line). Statistical significance was determined using Kruskal-Wallis with post-hoc Conover-Inman. Result of initial statistical test (Kruskal-Wallis) for **(B)** *P= 0.4264* (not statistically significant) **(C)** *P= 0.0234* **(D)** *P= 0.0906* (not statistically significant).

GPX4, an antioxidant defence enzyme active in repairing oxidative damage in lipids, is a key inhibitor of ferroptosis. Ablation of GPX4 activity by either pharmacological methods (erastin or RSL3) or knock-out leads to lipid peroxidation and cellular death (Yang *et al.*, 2014; L. Chen *et al.*, 2015). GPX4 levels in 2D cultures following treatment with iron (II) chloride were determined using western blotting (Fig. 5.19). At all-time points assayed, GPX4 expression was drastically reduced in the 1000 μM iron (II) chloride group when compared to media and solvent-only controls. In this group, GPX4 expression was completely abolished at 24 hrs (Fig. 5.19 A) and only slightly increased at 72 hrs (0.13 ± 0.06; Fig. 5.19 B) and 72 hrs (“continual stress”) (0.34 ± 0.05; Fig. 5.19 C).

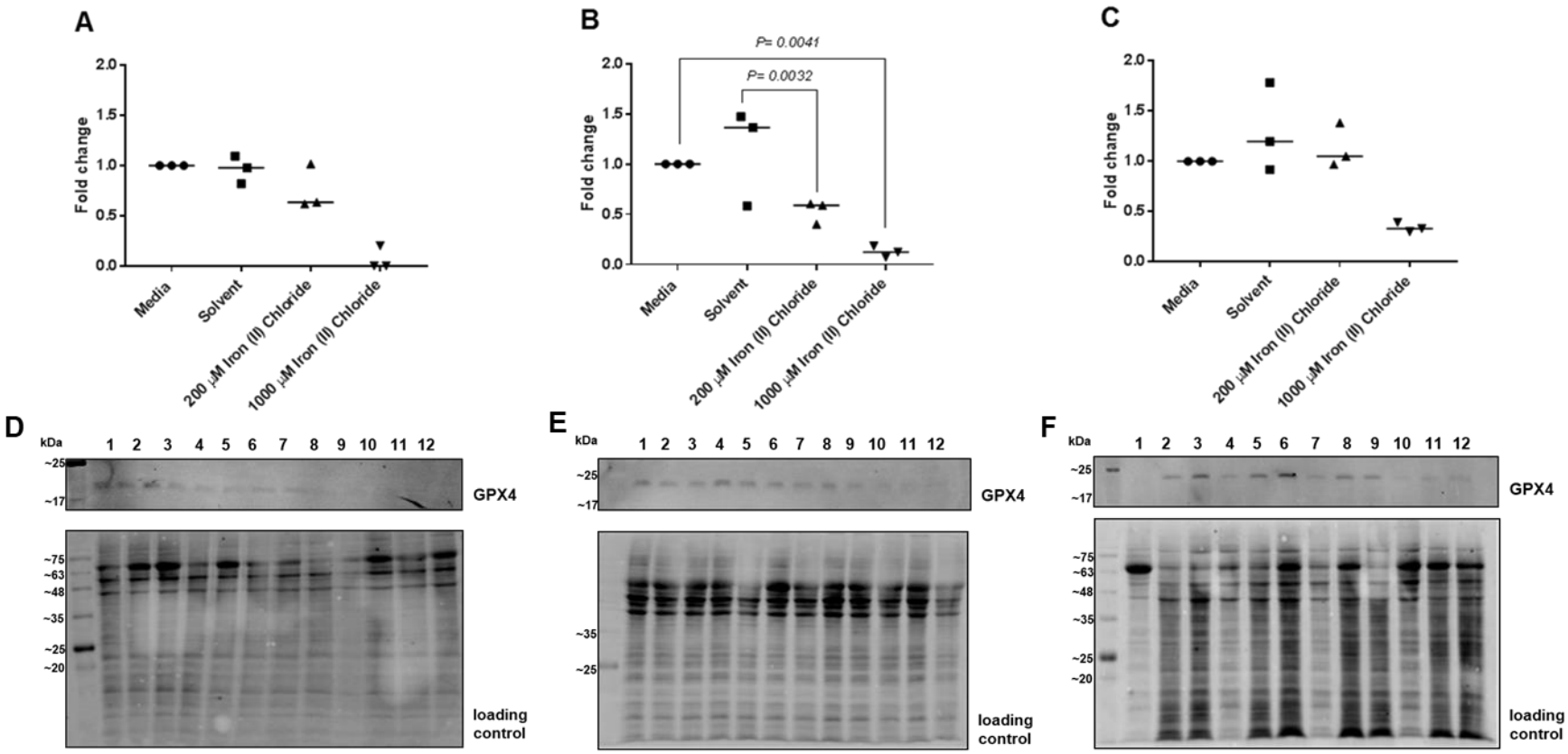

Figure 5.19. *Fold change of GPX4 in 2D cultures following treatment with iron (II) chloride compared to media control as analysed by western blotting.* Densitometry analysis of GPX4 levels **(A-C)** and western blots **(D-F)**. Lanes 1-3 media, lanes 4-6 solvent control, lanes 7-9 200 μM iron (II) chloride, and 1000 μM iron (II) chloride. **(A, D)** 24 hrs. **(B, E)** 72 hrs. **(C, F)** 72 hrs ("continual stress"). Data presented as individual data points and median (straight line) of three independent biological repeats. Statistical significance determined by Kruskal-Wallis test with post-hoc Conover-Inman. Results of initial Kruskal-Wallis test **(A)** *P= 0.0713* (not statistically significant) **(B)** *P= 0.041* **(C)** *P= 0.0827* (not statistically significant

5.3.6 Treatment of iron-treated cells with the ferroptosis inhibitor liproxstatin-1 is associated with reduction in phosphorylated α-syn

Ferroptosis inhibitors, liproxstatin-1 and ferrostatin-1, have previously been shown to prevent lipid peroxidation as free radical-trapping antioxidants (Zilka *et al.*, 2017). Treatment with 100 nM liproxstatin-1 in addition to iron (II) chloride in the 72 hr ("continual stress") group revealed the reduction in p-α-syn levels (Fig. 5.20) in contrast to omission of liproxstatin-1 (Fig. 5.8). A significant decrease in p-α-syn was observed in both the 200 and 1000 μM iron (II) chloride groups (*P= 0.0117*) (Fig. 5.20).

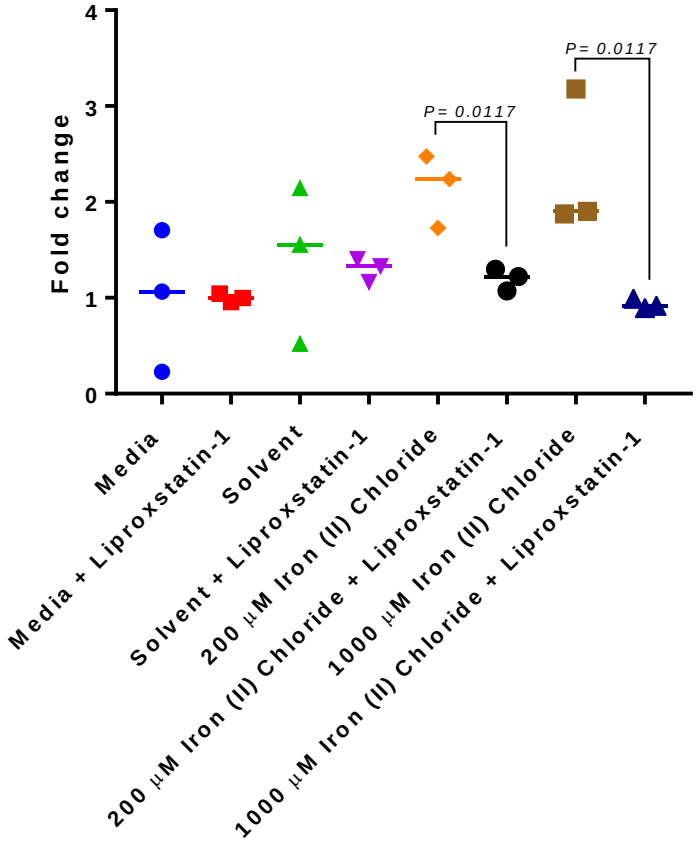

Figure 5.20. *Comparison of phosphorylated α-syn levels at 72 ("continual stress") following treatment with iron (II) chloride and iron (II) chloride + 100 nM liproxstatin-1 as analysed by western blotting.* Data presented as individual data points and median (straight line) of three independent biological repeats. Accompanying western blots shown in Appendix Figures 3 and 5.

5.3.7 SH-SY5Y express low/negligible levels of key proteins implicated in ferroptosis

Expression of mitochondrial voltage-dependent anion channels (VDACs 1, 2, 3), system L (SLC7A5/SLC3A2) and system x_c^- proteins (SLC7A11/SLC3A2) have been

implicated in the susceptibility of cells to ferroptosis and factors in PD neurodegeneration (Yagoda *et al.*, 2007; Dixon *et al.*, 2012; Do Van *et al.*, 2016). As SH-SY5Y was resistant to ferroptosis inducers, the expression of these proteins was determined using qPCR. The LUHMES has previously been shown to be sensitive to ferroptosis (Do Van *et al.*, 2016) and was used to determine differences in expression of VDACs and SLCs compared to SH-SY5Y. Expression levels of all proteins were increased in the ferroptosis-sensitive LUHMES cell line in comparison to both 2D and 3D SH-SY5Y cultures (Fig. 5.21). Expression of VDAC 1 and VDAC 3 was significantly increased in differentiated LUHMES (VDAC 1: 6.56 +/- 5.68; VDAC 3: 6.04 +/- 4.45) in contrast to 2D undifferentiated SH-SY5Y (VDAC 1: 0.17 +/- 0.05;

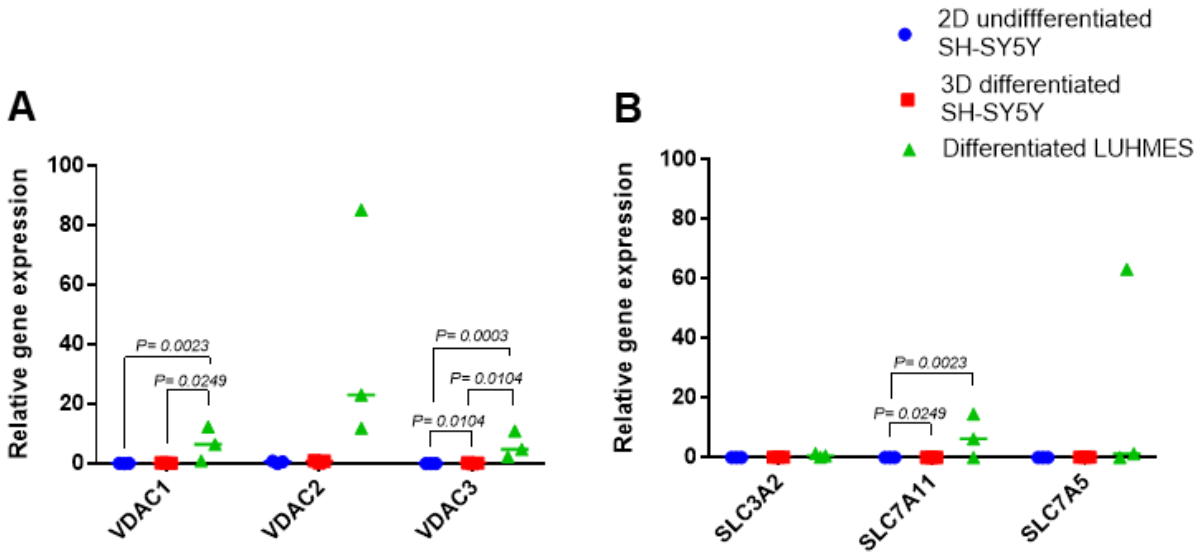

Figure 5.21. *VDAC and SLC expression in 2D undifferentiated SH-SY5Y, 3D differentiated SH-SY5Y and differentiated LUHMES as determined by qPCR.* Data presented as individual data points and median (straight line) of three independent biological repeats. qPCR data presented as relative gene expression normalised to β-actin. **(A)** VDAC 1, 2 and 3 expression levels. **(B)** SLC3A2, SLC7A11 and SLC7A5 expression levels. Statistical significance determined by Kruskal-Wallis test with post-hoc Conover-Inman. Results of initial Kruskal-Wallis test **(A)** VDAC1 *P= 0.039*, VDAC2 *P= 0.0509* (not statistically significant) and VDAC3 *P= 0.0273.* **(B)** SLC3A2 *P= 0.0509* (not statistically significant), SLC7A11 *P= 0.039* and SLC7A5 *P=0.3012* (not statistically significant).

VDAC 3: 0.0008 +/- 0.001) and 3D undifferentiated SH-SY5Y (VDAC 1: 0.12 +/- 0.09; VDAC 3: 0.16 +/- 0.13) (Fig. 5.21 A). Expression of VDAC 2 was 55-80 times higher in LUHMES compared to SH-SY5Y (Fig. 5.21 A). SLC expression was also increased in LUHMES, with significantly higher expression of SLC7A11 (6.99 +/- 7.31) compared to 2D undifferentiated SH-SY5Y (0.00009 +/- 0.00008; Fig. 5.21 B).

5.3.8 LUHMES are sensitive to iron and erastin-induced cell death

Given the increased expression of VDACs and SLCs in the LUHMES cell line, sensitivity of LUHMES to iron and erastin was investigated by resazurin reduction assay (Fig. 5.22). Differentiated LUHMES showed greater susceptibility to iron-induced cell death at 24 hrs compared to SH-SY5Y cultures (Fig. 5.22 A). LUHMES were also sensitive to the ferroptosis inducer erastin (Fig. 5.22 B) in contrast to SH-SY5Y (Fig. 5.10).

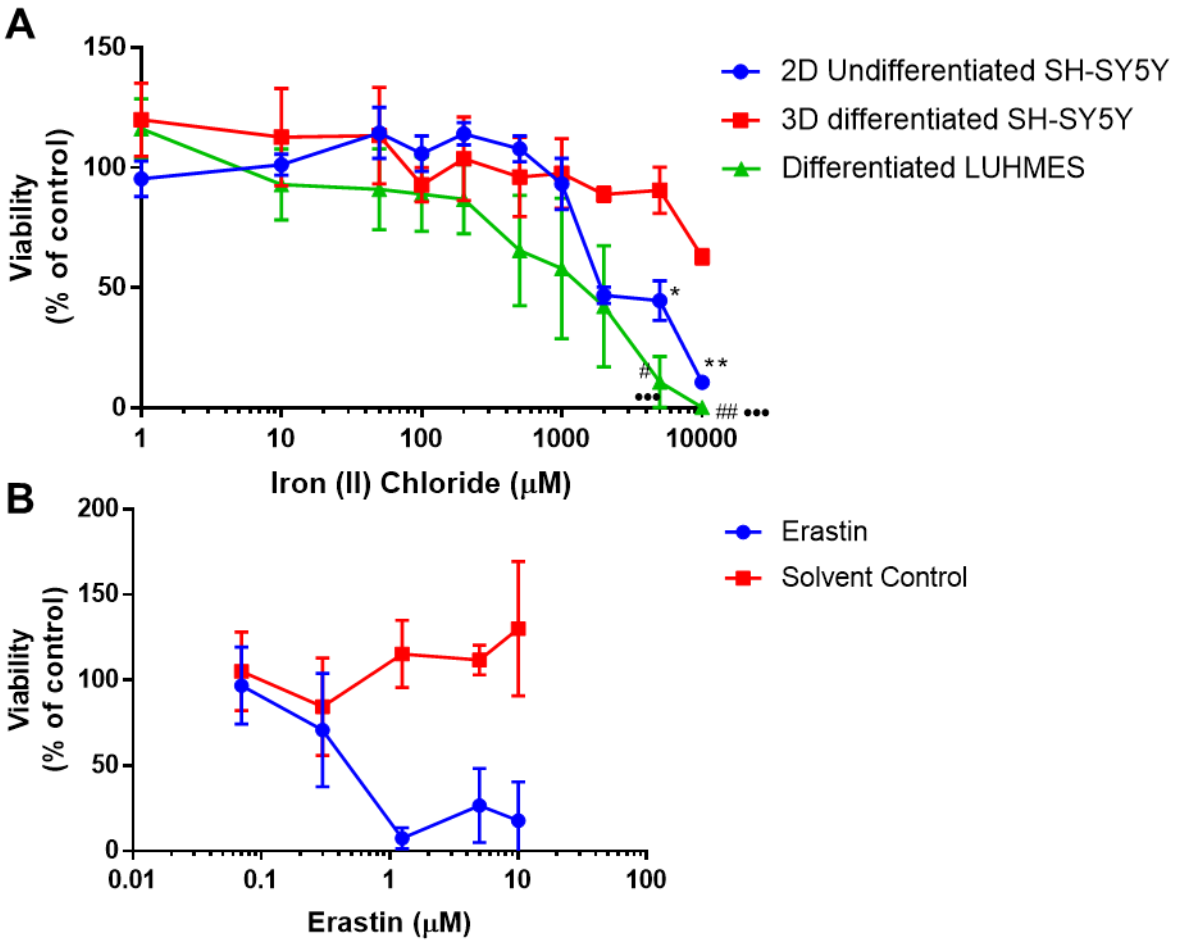

Figure 5.22. *Resazurin cell viability assays of LUHMES following 24 hr treatment with iron (II) chloride and erastin.* **(A)** Iron (II) chloride. **(B)** Erastin. Appropriate solvent controls were also incubated for 24 hrs. Data presented as mean and +/- SEM of at least three independent biological repeats. * *P* = ≤0.05, ** *P*= *≤0.01,* *** *P*= ≤0.001. *= 2D vs. 3D SH-SY5Y, #= 2D SH-SY5Y vs. LUHMES and •= 3D SH-SY5Y vs. LUHMES.

5.3.9 Addition of oligomeric species to SH-SY5Y did not induce lipid peroxidation

Oligomeric species of α-syn were shown to form Lewy body-like aggregates in 3D SH-SY5Y cultures (Chapter 4; Taylor-Whiteley *et al.*, 2019). Lipid peroxidation has previously been linked to the addition of α-syn species, therefore oligomeric species of α-syn were investigated in relation to the ability to induce features of ferroptosis (Angelova *et al.*, 2015). By staining unoxidised (red)/oxidised (green) lipids using the lipid peroxidation sensor BODIPY C11 581/591, no increase in oxidised lipids was observed following treatment with oligomeric species (Fig. 5.23 A). Quantification of lipid peroxidation signals using flow cytometry again revealed no increase in oxidised lipid signal (Fig. 5.23 B, C). In contrast to iron (II) chloride treatment (Fig. 5.19), addition of oligomeric α-syn species did not reduce levels of the ferroptosis-associated GPX protein, GPX4 (Fig. 24).

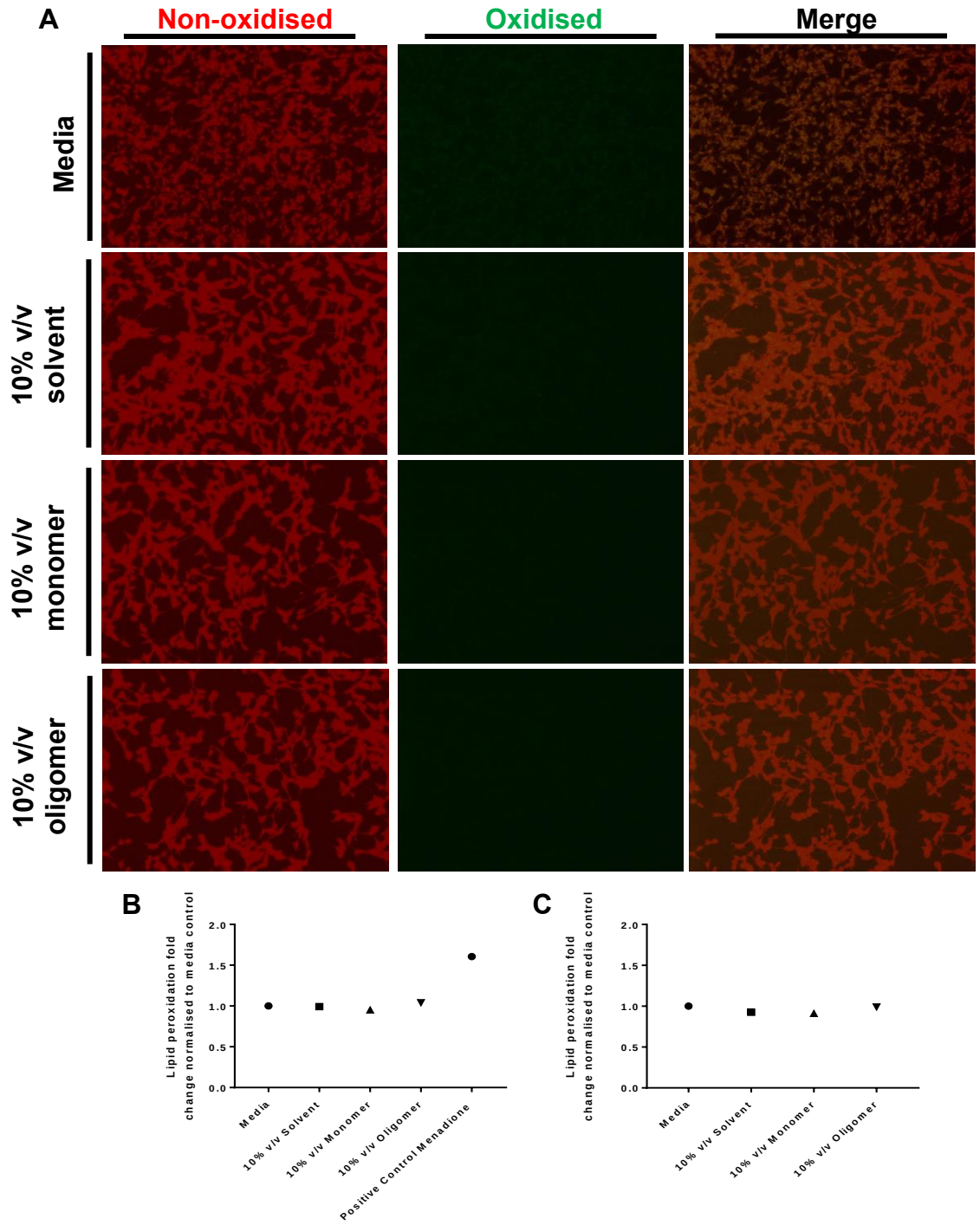

Figure 5.23. *Lipid peroxidation in 2D cultures following treatment with seeding oligomers.* **(A)** Representative images of SH-SY5Y treated with media only, solvent control, 10% v/v monomer and 10% v/v oligomer after 24 hr treatment. Cells positive for lipid peroxidation are identified by reduction in red staining (loss of non-oxidised lipids) and increase in green staining (gain of oxidised lipids; *white arrows*). Scale bar represents 200 µm. Images shown are representative of three biological repeats. **(B, C)** Flow cytometry analysis of lipid peroxidation reveals no change in lipid peroxidation following treatment of seeding oligomers at either 24 hrs **(B)** or 72 hrs **(C)**. Data presented as individual data points of one independent biological repeat.

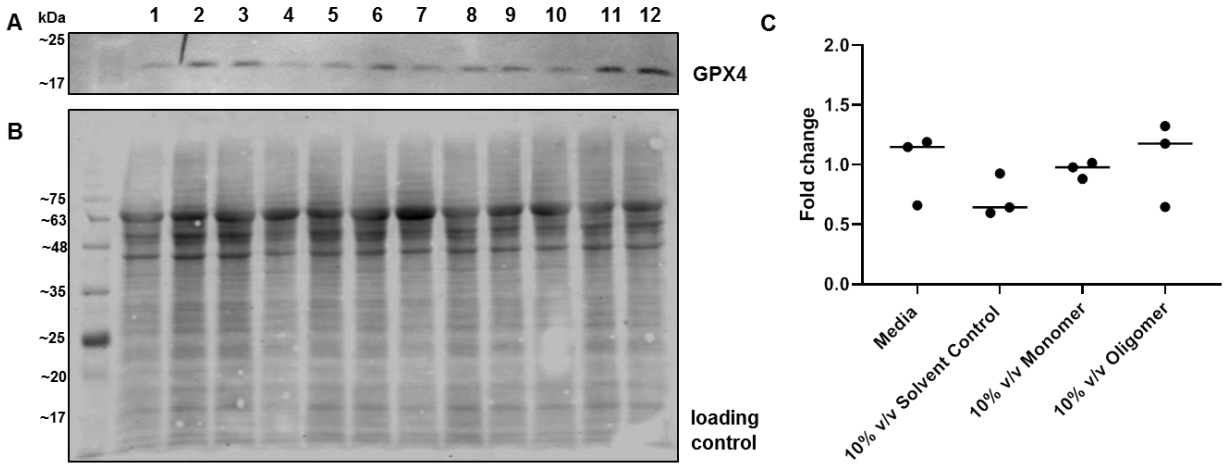

Figure 5.24. *Fold change of GPX4 in 2D cultures following treatment with seeding oligomers compared to media control as analysed by western blotting.* **(A)** GPX4 blot. **(B)** Loading control. **(A, B)** All biological repeats were run on the same blot. Lanes 1-3 represent media sample, lanes 4-6 represent 10% v/v solvent, lanes 7-9 represent 10% v/v monomer and lanes 10-12 represent 10% v/v oligomer treatments **(C)** Fold change of GPX4 levels. Data presented as individual data points and median (straight line) of three independent biological repeats. Results of initial Kruskal-Wallis test *P= 0.2479* (not statistically significant).

5.4 Discussion

Ferroptosis, a newly discovered cell death pathway, involving the iron-dependent generation of ROS, depletion of GPX4, lipid peroxidation and subsequent cell death has recently been implicated in the pathogenesis of PD (Dixon *et al.*, 2012; Do Van *et al.*, 2016). Post-mortem features of PD have long since implicated cellular ROS, altered GSH levels and lipid peroxidation in the pathogenesis of the condition (Dexter *et al.*, 1987, 1989; Jenner *et al.*, 1992; Sian *et al.*, 1994). The discovery of the ferroptosis pathway links both the potential susceptibility of the dopaminergic cells of the *SNPc*, iron accumulation with age and a mechanism of cell death with the potential for pharmacological manipulation. However, in familial and sporadic PD, the presence of a highly aggregated insoluble form of α-syn as the major protein component in Lewy bodies has implicated the protein in the pathogenesis of the disorder (Spillantini *et al.*, 1997; Anderson *et al.*, 2006). The newly discovered link of PD to ferroptosis and the relevance of α-syn to the disease have raised the possibility that α-syn is involved in this pathway and could potentially interact to exacerbate toxicity. To date, there are no studies that have explored whether α-syn is involved in ferroptotic cell death. Utilising the 3D SH-SY5Y model presented in chapters 3 and 4 of this thesis, the aggregation of α-syn in iron overload and the link to ferroptosis was investigated.

Iron has previously been demonstrated to induce the aggregation of α-syn both *in vivo* and *in vitro* (Uversky, Li and Fink, 2001; Duan *et al.*, 2008). The discovery of an iron-responsive element (IRE) in the 5' untranslated region suggests a role in iron regulation (Friedlich, Tanzi and Rogers, 2007). In agreement with previous studies, iron treatment was associated with the reduction of cell viability in a dose-dependent manner (Fig. 5.5) and α-syn aggregation (Fig. 5.6) (W. J. Li *et al.*, 2010; He *et al.*, 2011; Wan *et al.*, 2017). To the best of our knowledge, this is the first study to investigate iron-induced α-syn aggregation in a 3D model (Fig. 5.9). Unlike the large LB-like structures observed after oligomer treatment in 3D (Chapter 4 Fig. 4.8, 4.9 and 4.10; Taylor-Whiteley *et al.*, 2019), increased diffuse α-syn staining was observed. Therefore, iron treatment alone is not able to induce LB formation.

α-Syn undergoes many PTMs (e.g. phosphorylation, ubiquitination, acetylation etc.), the PTM commonly associated with PD and associated synucleinopathies is phosphorylation at serine 129 within the c-terminal region of the protein (Fujiwara *et*

al., 2002; Anderson *et al.*, 2006; Fauvet *et al.*, 2012; Muntané, Ferrer and Martinez-Vicente, 2012). Phosphorylation of α-syn at serine 129 is thought to play a central role in the pathogenesis of PD due to the observation that ~90% of α-syn in aggregates is phosphorylated at S129 in contrast to ~4% of total α-syn that is phosphorylated at this position in normal brain (Fujiwara *et al.*, 2002; Muntané, Ferrer and Martinez-Vicente, 2012). Levels of p-α-syn in blood plasma and skin biopsies are significantly higher in patients with PD when compared to healthy age-matched controls (Allsop *et al.*, 2013; Doppler *et al.*, 2014). Taken together, these observations implicate p-α-syn as an important PTM related to PD and synucleinopathies. Using western blotting, α-syn levels were increased following treatment with iron (II) chloride (Fig. 5.8). Levels of α-syn and p-α-syn at S129 were only increased in the 72 hr ("continual stress") group following treatment with 200 and 1000 µM iron (II) chloride (Fig. 5.8 C, F), consistent with previous results (Wang et al., 2019). Interestingly, the addition of the ferroptosis inhibitor liproxstatin-1 to iron-treated cultures was associated with reduced levels of p-α-syn in the 72 hrs (“continual stress”) group (Fig. 5.19). Removal of cellular ROS using an oxidative stress scavenger, N-acetylcysteine (NAC), was shown to result in the reduction of p-α-syn by downregulation of kinases (polo-like kinase 2/casein kinase 2) responsible for specific phosphorylation of α-syn at S129 (R. Wang *et al.*, 2019). Liproxstatin-1 is an antioxidant preventing the propagation of toxic lipid peroxides in the cell (Zilka *et al.*, 2017). The results presented here suggest that the increase of p- α-syn following iron overload could be associated with oxidative stress, consistent with the reduction of p-α-syn following liproxstatin-1 treatment.

Although Fe^{2+} is the predominant form within the cell, Fe^{3+} has the greater affinity for α-syn; however, phosphorylation of α-syn (ser129 and tyrosine 125) has been associated with increased binding affinity for Fe^{2+} (Binolfi *et al.*, 2006b; Lu *et al.*, 2011). The significantly shorter half-life of p-α-syn ($t_{1/2}$ = 54.9 ± 6.4 min) compared to non-phosphorylated ($t_{1/2}$ > 240 min) and specific degradation of p-α-syn (S129) by the proteasome or autophagic pathway indicates a cellular role of p-α-syn in clearance (Cuervo *et al.*, 2004; Machiya *et al.*, 2010). Taken together, the iron-binding capacity of p-α-syn and the shorter half-life of p-α-syn indicate a potential role in an iron-induced oxidative stress response, potentially mediating clearance of toxic species (M. Takahashi *et al.*, 2007; R. Wang *et al.*, 2019). The work presented

here demonstrates under iron-induced oxidative stress, p-α-syn levels increase (if only in the 72 hr “continual stress” group). Interestingly, the increase in p-α-syn levels (Fig. 5.8) is in conjunction with much lower intracellular iron levels when compared to the 72 hr treatment group (Fig. 5.18). Where intracellular iron concentration was higher at 72 hrs (Fig. 5.18), this co-ordinated with much lower levels of p-α-syn, suggesting p-α-syn may have a role in the efflux of iron from the cell, protecting the cell from iron-mediated cellular ROS. This is supported by the observation that intracellular ROS was detected at 72 hrs (Fig. 5.14) as determined by the nuclear-associated CellROX™ green signal, in contrast to 72 hrs (“continual stress”) group whereby CellROX™ signals were unchanged between controls and treatments (Fig. 5.15). An experiment to measure amounts of α-syn, especially p-α-syn, in cell culture media would indicate whether p-α-syn is indeed effluxed from the cell under these conditions.

In the *SNPc*, the oxidative environment would require efficient protein degradation pathways to prevent the accumulation of oxidation-damaged proteins, however in aging both the proteasome and autophagic pathway undergo decline, resulting in reduced efficiency and function with advancing age (Rubinsztein, Mariño and Kroemer, 2011; Jana, 2012). This is supported by the observation of a reduction in proteasome activity observed in post-mortem *SNPc* of PD patients compared to age-matched controls (McNaught *et al.*, 2003). Importantly, familial mutations that affect the protein Parkin, a protein involved in targeting proteins to the proteasome, leads to an early-onset form of the disease (Arkinson and Walden, 2018). Mutant forms of α-syn have an inhibitory effect on the 20S proteasome, leading to reduced degradation of soluble species and increased formation of aggregates (Tanaka *et al.*, 2001; Emmanouilidou *et al.*, 2010). Aggregated forms of α-syn need to be unfolded before clearance, therefore aggregated forms of α-syn require clearance through other pathways, such as autophagy (Alvarez-Erviti *et al.*, 2011). The increase in iron concentration in the *SNPc* as a consequence of aging is well known and interestingly, iron deposition has also been shown to lead to autophagic function (Wan et al., 2017).

Taken together, the increased levels of both α-syn and p-α-syn due to oxidative stress could, in an aging brain where proteasomal and autophagic pathways are inhibited, result in the accumulation of α-syn species that in turn aggregate into LB

structures. Within this study, no proteasomal/autophagic inhibition treatment was added to the cells and this may be the reason for the lack of α-syn aggregates forming (Fig. 5.9), especially when we consider the short amount time the experiments were conducted over (72 hrs). In a highly ROS-rich environment such as the *SNPc,* the impaired ability to clear toxic species from neurons will, in turn, exacerbate the formation of ROS, resulting in cellular defects. In contrast to the oligomer-induced aggregate formation that was observed in as little as 24 hrs (Chapter 4), the lack of iron-induced aggregates in 3D suggests different mechanisms of aggregate formation.

SH-SY5Y were highly sensitive to apoptosis induced by staurosporine (Fig. 5.8C) (Belmokhtar, Hillion and Ségal-Bendirdjian, 2001; Robert *et al.*, 2012). The RAS-selective lethal (RSL) compounds, erastin and RSL3, initiate cell death by activating ferroptosis through inhibition of either system x_c^- (erastin) or GPX4 (RSL3) leading to depletion of GSH (Dixon *et al.*, 2012). In this study, the ferroptosis-inducers erastin and RSL3 had little effect on cell viability in these cultures (Fig. 5.8). This is in contrast to previous studies whereby erastin induced cell death in SH-SY5Y at >5 μM (Geng *et al.*, 2018; Zille *et al.*, 2019). The knockdown of the iron export protein, ferroportin, was shown to exacerbate erastin-induced cell death through the disruption of iron efflux from the cell and subsequent increase in lipid ROS (Geng *et al.*, 2018). However, even when erastin concentration was increased to 50 μM erastin (*data not shown*) there was no change in cell viabilities between treated and solvent control in WT SH-SY5Y used in this study. The targets for erastin (VDACs 1, 2, 3 and SLC7A5) were shown to be expressed at negligible levels in SH-SY5Y cultures when compared to expression in a ferroptosis-sensitive cell line (LUHMES). Resistance to erastin treatment is due to the absence of erastin targets in our SH-SY5Y model (Fig. 5.19) (Yagoda *et al.*, 2007; Dixon *et al.*, 2012). The differences in expression of VDAC isoforms may be one of the reasons *SNPc* neurons undergo degeneration in PD (Sun *et al.*, 2012; Triplett *et al.*, 2015; Do Van *et al.*, 2016). SLC7A11 repression leads to sensitivity to ferroptosis through the reduction in cystine uptake, however, SH-SY5Y again expressed negligible levels of SLC7A11 but did not show sensitivity to ferroptosis, suggesting ferroptosis is not an effective pathway to induce cell death in this cell line (Jiang *et al.*, 2015). In contrast, the LUHMES cell line expresses all VDAC isoforms in addition to SLC3A2, SLC7A11

and SLC7A5, the cell line is more susceptible to iron-induced cell death and is sensitive to ferroptosis in concordance with previous studies (Fig. 5.20) (Do Van *et al.*, 2016).

Although SH-SY5Y did not show sensitivity to ferroptosis inducers, features of ferroptosis include iron-dependent ROS generation, depletion of GSH, inactivation of GPX4 and lipid peroxidation were investigated following treatment with iron (II) chloride in SH-SY5Y cultures. Measurement of lipid peroxidation demonstrated the increase in oxidised (green) lipids following treatment with 1000 μM iron (II) chloride at all time points measured (Fig. 5.9, 5.10 and 5.11). Flow cytometry analysis of lipid peroxidation reveals increased lipid peroxidation at 72 hrs (Fig. 5.11) where total α-syn and p-α-syn levels were lower (Fig. 5.6) when compared to 72 hr ("continual stress") (Fig. 5.6 and 5.11). In the latter, elevated levels of α-syn and p-α-syn were associated with reduced levels of lipid peroxidation, suggesting a protective role of α-syn by prevention of lipid peroxidation in the context of iron-dependent cellular ROS.

GSH assay revealed the increase in GSSG, but there was no reduction in GSH levels (Fig. 5.12). GPX4, a major regulator of ferroptosis is essential for maintaining the redox capacity of the cell (Yang *et al.*, 2014). GPX4 levels as determined by western blotting were shown to be decreased in both iron (II) chloride treatment groups. In the 1000 μM iron (II) chloride group there was a complete absence in GPX4 expression at 24 hrs, with only marginal increases at 72 hrs and 72 hrs ("continual stress") (Fig. 5.13). Levels of intracellular ROS as measured by the CellROX™ green fluorescent dye revealed ROS in 200 and 1000 μM iron (II) chloride groups in addition to the positive control (10 μM menadione). Cell death by iron-induced ROS in SH-SY5Y shared some features of ferroptosis, but the low expression of key proteins thought to play a role in ferroptosis (such as VDAC isoforms) and lack of sensitivity to ferroptosis inducers erastin and RSL3 suggest cell death mechanisms in SH-SY5Y are distinct from ferroptosis (Ito *et al.*, 2017).

Chapter 6 : General Discussion

6.1 General Discussion

PD is the fastest growing neurological disorder in the world, with the incidence of disease predicted to double worldwide by 2040 (Dorsey and Bloem, 2018; Marras *et al.*, 2018; Parkinson's UK, 2018). Currently, there are no disease-modifying therapies available to alter disease progression; instead available therapies treat clinical symptoms rather than the cause of disease. The lack of such disease-modifying therapies is due in part to the incomplete knowledge of the molecular mechanisms involved in disease onset and progression. α-Syn has been linked to PD through both genetic and pathological evidence. Oligomeric species of α-syn have been implicated as the toxic species involved in both the spread of pathology and in mechanisms of cellular dysfunction, leading to cell death (Bengoa-Vergniory *et al.*, 2017).

The overall aim of this thesis was to develop a 3D cell culture model of PD utilising the human neuroblastoma SH-SY5Y cell line to investigate the propagation and intracellular aggregation induced by α-syn oligomers. In addition, the aggregation propensity of α-syn in relation to the cell death pathway, ferroptosis, was investigated. Chapter 3 presents data on the development of the 3D cell culture model. Specifically, the phenotype of SH-SY5Y cultured in 3D was characterised. Chapter 4 investigated the intracellular aggregation of α-syn within the 3D model. This section focussed on characterising the morphology of inclusions within 2D and 3D cultures. Data presented highlighted the morphology of inclusions in 3D cultures akin to *in vivo* LBs. Chapter 5 set out to investigate the impact of ferroptosis on the aggregation and propagation of α-syn in the 3D model. A summary of key findings from this body of work is provided below.

6.1.1 Human neuroblastoma cells cultured 3D express a dopaminergic, post-mitotic phenotype and develop intracellular inclusions reminiscent of LB-like inclusions

In this study, the development of a 3D cell culture model of PD was described and demonstrated the development of LB-like intracellular inclusions upon the addition of oligomeric α-syn to culture media. The mechanism of LB formation remains poorly understood, mainly due to the lack of whole-animal or cell-based models that

recapitulate the development of these inclusions. Much of the literature investigating α-syn aggregation has been performed in 2D in a variety of cell lines, including animal-derived cell lines. Normally, *in vivo*, cells in the physiological environment have constant interaction with other cells and ECM, which is important to regulate a variety of cellular characteristics. These characteristics, including cell shape and cell differentiation, are inhibited in 2D environments due to the lack of cell-to-cell and cell-to-ECM communication (Baker and Chen, 2012; Caddeo, Boffito and Sartori, 2017). Three-dimensional cell cultures address these challenges and allow for interaction of cells to the ECM and each other to further mimic the *in vivo* environment. Increasingly, 3D cell culture methods are being developed to provide a more biologically-relevant culture system (Eglen and Klein, 2017). In Chapter 3, the development of a 3D cell culture model of PD was described. Utilising a human-relevant SH-SY5Y neuroblastoma cell line, cells were differentiated initially in 2D to confirm an appropriate differentiation protocol for use within the 3D Matrigel™-based environment. Differentiation of SH-SY5Y with RA and sequential treatment of BDNF yielded a homogenous population of dopaminergic (expression of *DAT, DRD2, VMAT2*), post-mitotic (lack of expression of Ki67) neuron-like (expression of *TUBB3* and *MAP2*) cells. Upon encapsulation in the 3D matrix, cells retained a dopaminergic, post-mitotic neuron-like phenotype. The cell culture method described in this thesis is robust and easy to handle in standard laboratory settings.

Characterising the effect of prefibrillar oligomers is important to understanding the aberrant aggregation of α-syn and its role in the propagation of misfolded α-syn species (Killinger and Kordower, 2019). Seeding oligomers of α-syn are known to induce intracellular aggregation of endogenously expressed protein in a seeded-nucleation mechanism, and this mechanism is likened to a prion-like propagation of misfolded protein (Danzer *et al.*, 2007; Volpicelli-Daley *et al.*, 2011; Shrivastava *et al.*, 2020). Using the 3D model developed in Chapter 3, the intracellular aggregation of α-syn was investigated upon addition of oligomeric species to differentiated neuron-like cultures. Data presented in Chapter 4 demonstrated that addition of exogenous α-syn species to undifferentiated and RA-differentiated 2D cultures developed inclusion morphology previously seen in cell models, whereby inclusions were punctate and numerous throughout the cytoplasm (Danzer *et al.*, 2007; Illes-Toth *et al.*, 2015). This is in contrast to the large, singular LB observed in *in vivo*

pathology. However, the addition of preformed oligomers to RA + BDNF-differentiated cultures in 2D highlighted the development of singular, large α-syn-positive cellular inclusions, reminiscent of *in vivo* pathology. One caveat of this culture method (in 2D) was that cells easily detached from the culture vessel. Importantly, the differentiation of cells in the 3D environment prevented the detachment of cells from culture vessels. The morphology of inclusions formed following treatment with exogenous α-syn oligomers to 3D cultures highlighted the development of LB-like aggregates (Taylor-Whiteley *et al.*, 2019). These inclusions were highly reminiscent of *in vivo* LBs with similar morphologies and positive for markers α-syn and ubiquitin. Unfortunately, p-α-syn species were not detected in these inclusions. This could be because p-α-syn species were not detectable given the antibody used in this study or that aggregates formed without the need for phosphorylation (Volpicelli-Daley *et al.*, 2011). Another explanation could be that p-α-syn aggregates were undetectable given the short time frame of the experiment (24 hrs) and that phosphorylation could be a late-stage modification of α-syn aggregates (Walker *et al.*, 2013). Importantly, these inclusions formed without the need for genetic manipulation of the cell line. Given that α-syn structure and function is highly dependent on the complex equilibrium between monomer and multimeric structures *in vivo*, overexpression of α-syn alters this equilibrium and promotes aggregation through molecular crowding (Bartels, Choi and Selkoe, 2011; Davies, Moualla and Brown, 2011; Burré, Sharma and Südhof, 2014; Sian and Peter, 2020). Therefore, this model highlights the development of LB-like pathology without the need for overexpression of α-syn or other genetic manipulation.

Domert *et al.* (2016) described a similar 3D cell culture method for utilising SH-SY5Y cultured in an ECM-based matrix and investigated the uptake of α-syn monomers, oligomers, and fibrils in this culture system. In agreement with findings in this study, α-syn species were taken up by cells and developed intracellular aggregates over 24 hours with minimal (or completely absent) cellular toxicity as investigated by the XTT assay. In contrast, the aforementioned study investigated the transfer of these species between donor and acceptor cells and did not exclusively demonstrate the formation of large LB-like cellular aggregates, as shown here (Domert *et al.*, 2016). Interestingly, the oligomers were produced by incubation of the reactive aldehyde of 4-HNE with α-syn (Domert *et al.*, 2016). 4-HNE is a reactive aldehyde produced

when oxygen radicals produced during oxidative stress oxidise polyunsaturated fatty acids in cellular membranes (Xiang *et al.*, 2013; Barrera *et al.*, 2018). Because oxidative stress is integral to the pathogenesis of PD, this method for producing oligomers may provide a more relevant biological structure, in contrast to formation of oligomers by other methods (e.g. incubation with high concentrations of monomeric α-syn). Previously, work in other groups required the use of agents such as lipofectamine to introduce α-syn species to the intracellular environment, however, there are studies (including this) that do not require the use of these agents (P. Desplats *et al.*, 2009; Nonaka *et al.*, 2010). This may be due to differences in oligomer preparations between studies. For example, seeding oligomers (type B and C) are readily taken up by cells and induce intracellular aggregation, whereas other oligomer preparations promote membrane interaction, calcium influx and cell death (Danzer *et al.*, 2007; Grozdanov and Danzer, 2018). This model is adaptable for use in many laboratories and is amenable for use in diverse areas of PD research, including in development for high-throughput screening.

6.1.2 Aggregation of α-syn is not associated with a ferroptotic pathway in SH-SY5Y

Recently, ferroptosis, a cell death pathway intrinsically linked to iron metabolism, ROS production, and lipid peroxidation has been linked to neurodegeneration in PD (Do Van *et al.*, 2016; Guiney *et al.*, 2017). Several key features of ferroptosis can be linked to the molecular mechanisms of PD, with literature reports frequently describing depletion of the intracellular antioxidant glutathione, accumulation of lipid peroxidation products, decreased levels of GPX4, and neuroprotection from iron chelators or lipophilic antioxidants (Cardoso *et al.*, 2017; Galluzzi *et al.*, 2018). The dysregulation of iron can be observed by the use of MRI imaging of patients and analysis of post-mortem tissue, showing an increase in iron levels in the brain that are associated with aging and in neurodegenerative disease (Dexter *et al.*, 1987; Kwan *et al.*, 2012; Acosta-cabronero *et al.*, 2016). Additionally, α-syn has been pathologically linked to iron import and dysregulated iron homeostasis (Davies, Moualla and Brown, 2011; McDowall *et al.*, 2017). Targeting iron has shown some success in early phase clinical trials of iron chelators (e.g. deferiprone). Early indications are a slowing of the progression of motor deficits and reducing motor symptoms in early PD patients and represent the first successful disease-modifying

therapy for PD, but requires replication in a larger phase III trials (Devos *et al.*, 2014). However, at the time of writing, no study has investigated the role of α-syn concerning ferroptotic cell death (Guiney *et al.*, 2017).

Data presented in Chapter 5 investigated the influence of ferroptosis on the intracellular aggregation of α-syn in both 2D and 3D SH-SY5Y cell culture models. Importantly, in these models, intracellular α-syn aggregation was shown to form LB-like aggregates (Chapter 4). In this study, evidence was provided that aggregation of α-syn is not associated with ferroptotic cell death in the SH-SY5Y cell line. Many studies have used iron (II) chloride to increase the intracellular load of iron in a time- and dose-dependent manner to determine cellular effects of iron (ranging from 5 μM to 1000 μM) (Guan *et al.*, 2017; Wan *et al.*, 2017; Dige and Okoi, 2019). In agreement with these studies, iron (II) chloride (200μM and 1000 μM) increased cellular total iron content in SH-SY5Y and was therefore used to investigate the influence of iron, aggregation of α-syn, and induction of ferroptosis. Results presented here demonstrate increased expression of α-syn following treatment with iron (II) chloride as analysed by ICP-MS analysis, western blotting, and immunocytochemistry. Treatment with ferroptotic inducers did not result in cellular death of SH-SY5Y either in 2D or 3D cultures. However, treatment with an apoptosis inducer, staurosporine, resulted in extensive cell death, highlighting the sensitivity of the cell line to this mechanism of cell death (Dächert *et al.*, 2016; Sato *et al.*, 2018). Resistance to ferroptosis inducers by SH-SY5Y was attributed to low expression of key proteins associated with ferroptotic cell death including the proteins VDAC1, VDAC2, VDAC3, SLC3A5, SLC7A5 and SLC7A11 (Do Van *et al.*, 2016). Taken together, this data suggests that SH-SY5Y are not sensitive to ferroptosis, and therefore, not an appropriate cellular model for the study of ferroptosis. In contrast, this body of work highlights the preferred use of LUHMES cells when investigating ferroptosis, due to higher expression of the aforementioned proteins and sensitivity to ferroptosis inducers (Do Van *et al.*, 2016).

Although the SH-SY5Y cell line was not sensitive to cell death induced by the ferroptosis inducers erastin or RSL3, iron (II) chloride treatment was associated with several features of the ferroptotic pathway. These features include ablation of GPX4 expression, decreased GSH: GSSG ratio, increased ROS, and increase in lipid peroxidation (Imai *et al.*, 2017; Galluzzi *et al.*, 2018; Zille *et al.*, 2019). Importantly,

cell death mechanisms do not always operate in singular, discreet pathways, instead, several pathways may converge to induce cell death. Apoptosis can occur in conjunction with necroptosis and/or autophagy and autophagy can occur in association with necroptosis (Chen, Kang and Fu, 2018). For example, once activated, the apoptotic initiator caspase, caspase-8, can trigger downstream apoptosis signalling but can also inhibit necroptosis through the inactivation of RIPK1 and RIPK3 (Wang *et al.*, 2009; Linkermann *et al.*, 2014). Specifically, induction of cellular ROS can trigger ROS-dependent apoptosis and also ROS-dependent autophagy (Redza-dutordoir and Averill-bates, 2016; Cordani *et al.*, 2019). This is important given that ferroptosis is another form of cell death associated with ROS accumulation in cellular models, and has similar molecular mechanisms of another mechanism of cell death, oxytosis (Ito *et al.*, 2017; Lewerenz *et al.*, 2018). Delineating key differences between these pathways may help to identify treatments for several diseases, including in PD (Magtanong and Dixon, 2020).

Under normal conditions, <4% of the total α-syn is phosphorylated at p129, but there is a dramatic accumulation of p-α-syn in brains of patients with PD (Chen and Feany, 2005; Muntané, Ferrer and Martinez-Vicente, 2012). Therefore, p-α-syn has been implicated as a key player in the pathogenesis of PD. Additionally, although p-α-syn is not required for aggregate formation, it is associated with efflux of α-syn from the cell due to presence of p-α-syn in CSF and blood plasma (Foulds *et al.*, 2011; Killinger and Kordower, 2019). In this study, increased levels of p-α-syn were increased as a result of 'continual stress' treatment with iron (II) chloride and this was ablated by the addition of the ferroptosis inhibitor lip-1. Lip-1 is a potent ferroptosis inhibitor able to prevent lipid peroxidation via a ROS scavenging function (Zilka *et al.*, 2017). It could be hypothesised that Lip-1 reduced expression of α-syn through the modification of α-syn oligomerisation. 4-HNE, a product of lipid peroxidation, is capable of inducing oligomerisation of α-syn through the covalent modification of histidine and lysine residues to produce a structure capable of inducing seeding in an SH-SY5Y cell model (Formation and Park, 2013). Therefore, it could be that Lip-1 reduced the formation of lipid peroxidation products (e.g. 4-HNE), consequently reducing the formation of oligomeric species of α-syn of which are phosphorylated (Canerina-amaro *et al.*, 2019). Recent data suggests Lip-1 can also induce upregulation of GPX4 which would reduce ROS accumulation, subsequent lipid

peroxidation, and formation of lipid peroxidation-modified α-syn aggregates (Wu *et al.*, 2019). In the study by Singh *et al.* (2012), curcumin, a ROS scavenging molecule, was shown to bind to oligomeric species and reduce their toxicity through modification of their morphology and hydrophobic surface exposure. Therefore, if iron-induced ROS induced the formation of oligomeric α-syn which is subsequently phosphorylated, a mechanism in which Lip-1 binds to α-syn to prevent oligomerisation would reduce accumulation of pre-fibrillar oligomers capable of either toxic cellular effects or cell-to-cell spreading (Singh *et al.*, 2013). At present, there is no data available to determine whether Lip-1 binds to α-syn to interfere with protein aggregation. Therefore, Lip-1 highlights an attractive pharmaceutical compound in the treatment of PD, potentially to reduce lipid peroxidation (and induction of lipid peroxidation-associated cell death, e.g. ferroptosis in ferroptosis-sensitive cells), and reduction in the spread of pathology (by reducing the formation of ROS-induced oligomeric species).

Another important consideration must be given to the normal cellular function of α-syn as a cellular ferrireductase (Davies, Moualla and Brown, 2011; McDowall *et al.*, 2017). Structurally, as a ferrireductase, α-syn is a tetrameric structure that reduces Fe^{3+} to Fe^{2+}, to provide an important source of bioavailable iron required for cellular functions (e.g. as a cofactor for TH, mitochondrial functions) (Wei Wang *et al.*, 2011; Mcdowall *et al.*, 2017). Wang *et al.* (2011) demonstrated the α-syn tetrameric structure to be dependent on subunit concentration and environmental factors, with an equilibrium existing between unfolded monomer, compact oligomer, and amyloid-forming species. Therefore, overexpression of α-syn (or modification of the protein by point-mutations, posttranslational modifications, the formation of ROS-induced adducts) can result in a shift in the equilibrium from tetramer to oligomeric species. This shift in equilibrium would drastically reduce the function of α-syn as a ferrireductase, and it has been shown that the ferrireductase function of α-syn is altered in PD (McDowall *et al.*, 2017). The effect on the cell would be catastrophic. A loss of Fe^{2+}-dependent activities through the aggregation of α-syn and loss of ferrireductase activity would result in bioenergetic deficiencies and cell death. Increased activity of α-syn as a tetramer would induce excess Fe^{2+}, increased oxidative stress via Fenton's reaction, and result in cell death (Davies, Moualla and Brown, 2011). Therefore, the cell must efficiently maintain cellular levels of α-syn to

maintain functionality and cellular survival. In a situation whereby a cell has defective protein clearance mechanisms (e.g. decline in lysosomal-autophagy/proteasomal mechanisms), reduced chaperone activities (e.g. HSC70/HSP90), and increased oxidative environment as seen in aging cells, all create an environment preferential to the aggregation of α-syn (Burmann *et al.*, 2020).

6.3 Concluding Remarks

Together, data presented in this thesis have contributed novel findings and furthered knowledge in the field of α-syn research. Results have described a novel 3D human-relevant neuronal cell culture model and demonstrated that upon the addition of seeding oligomers develop LB-like α-syn inclusions reminiscent of *in vivo* pathology. Importantly, this model system does not require the overexpression of α-syn as in previous culture models. Additionally, the relationship between ferroptosis and α-syn aggregation was explored. The novel data presented in this thesis highlight the resistance of the SH-SY5Y cell line to ferroptosis yet demonstrate the potential implications of iron exposure, α-syn aggregation, and ferroptosis in the pathogenesis of PD. Furthermore, the work presented in this PhD project has raised new avenues for future study, which have the potential to extend knowledge of the role α-syn in PD and highlight potential therapeutic options (e.g. liproxstatin-1).

Chapter 7 : Appendix

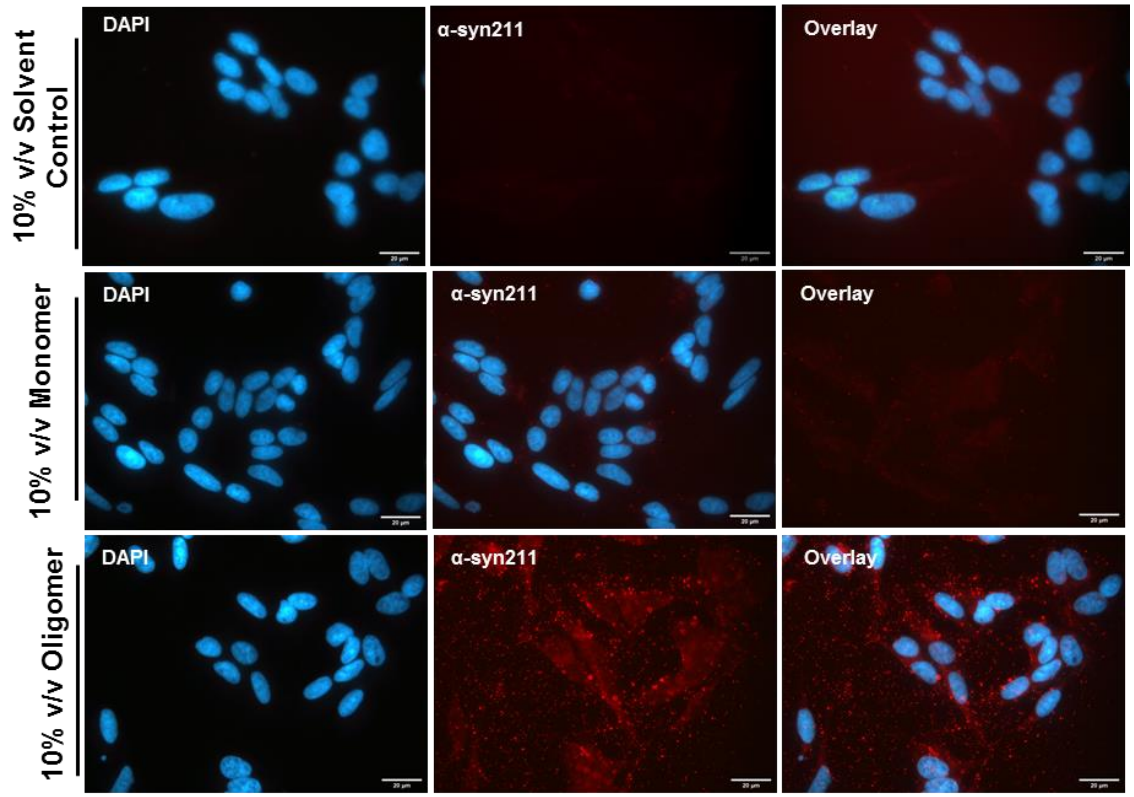

Appendix Figure 1. *Exogenous addition of α-syn oligomers induces the intracellular aggregation of α-syn in 2D RA-differentiated SH-SY5Y cultures.* Double immunostaining with α-syn (Texas Red, red) and nuclei (DAPI, blue) reveals the presence of multiple, small inclusions throughout the cytoplasm in 10% v/v oligomer-treated cultures when compared to diffuse staining in 10% v/v solvent control (sodium phosphate buffer + 20% ethanol) and 10% v/v monomer control. Scale bar represents 20 µm. Figure related to Chapter 4, Figure 4.5.

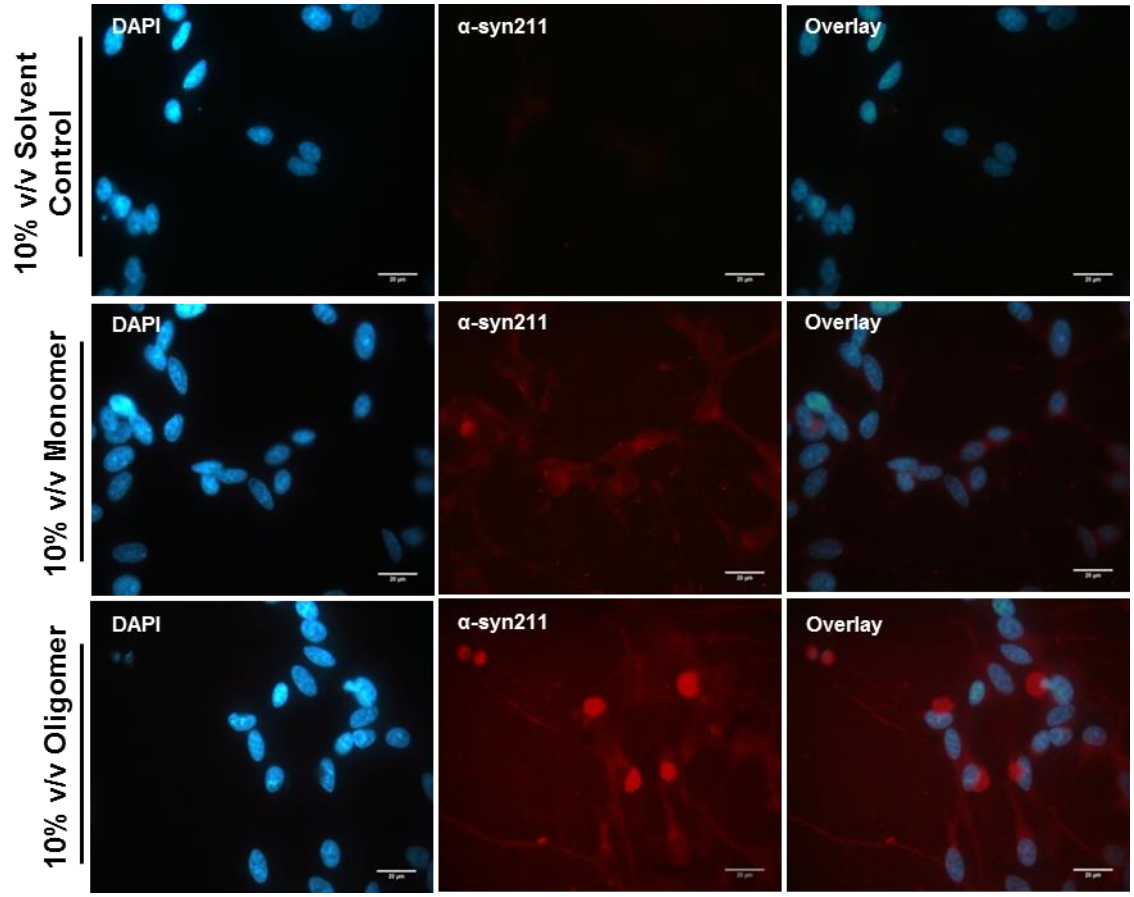

Appendix Figure 2. *Exogenous addition of α-syn oligomers induces the intracellular aggregation of α-syn in 2D RA + BDNF-differentiated SH-SY5Y cultures.* Double immunostaining with α-syn (Texas Red, red) and nuclei (DAPI, blue) reveals the presence of singular, large inclusions in 10% v/v oligomer-treated cultures when compared to diffuse staining in 10% v/v solvent control (sodium phosphate buffer + 20% ethanol) and 10% v/v monomer control. Scale bar represents 20 µm. Figure related to Chapter 4, Figure 4.5.

Chapter 8 : Bibliography

Abbott, A. (2003) 'Biology's new dimension', *Nature*, 424(August), pp. 870–872.

Abbott, A. (2016) 'The red-hot debate about transmissible Alzheimer's', *Nature*, 531(7594), pp. 294–297. doi: 10.1038/531294a.

Abounit, S. *et al.* (2016) 'Tunneling nanotubes spread fibrillar α-synuclein by intercellular trafficking of lysosomes', *The EMBO Journal*, 35(19), pp. 2120–2138. doi: 10.15252/embj.201593411.

Accardo, A. *et al.* (2017) 'Multiphoton Direct Laser Writing and 3D Imaging of Polymeric Freestanding Architectures for Cell Colonization', *Small*, 13(27), pp. 1–11. doi: 10.1002/smll.201700621.

Acosta-cabronero, X. J. *et al.* (2016) 'In Vivo MRI Mapping of Brain Iron Deposition across the Adult Lifespan', *The Journal of Neuroscience*, 36(2), pp. 364–374. doi: 10.1523/JNEUROSCI.1907-15.2016.

Agarraberes, F. A. and Dice, J. F. (2001) 'A molecular chaperone complex at the lysosomal membrane is required for protein translocation', *Journal lof Cell Science*, 114(13), pp. 2491–2499.

Agholme, L. *et al.* (2010) 'An In Vitro Model for Neuroscience : Differentiation of SH-SY5Y Cells into Cells with Morphological and Biochemical Characteristics of Mature Neurons', *Journal of Alzheimer's Disease*, 4(20), pp. 1069–1082.

Aguzzi, A. and Lakkaraju, A. K. K. (2016) 'Cell Biology of Prions and Prionoids: A Status Report', *Trends in Cell Biology*. Elsevier Ltd, 26(1), pp. 40–51. doi: 10.1016/j.tcb.2015.08.007.

Ahlskog, J. E. (2007) 'Beating a dead horse: Dopamine and Parkinson's disease', *Neurology*, 69(17).

Alais, S. *et al.* (2008) 'Mouse neuroblastoma cells release prion infectivity associated with exosomal vesicles', *Biology of the Cell*, 100(10), pp. 603–618. doi: 10.1042/BC20080025.

Alessi, D. R. and Sammler, E. (2018) 'LRRK2 kinase in Parkinson's disease', *Science*, 360(6384), pp. 36–37. doi: 10.1126/science.aar5683.

Allsop, D. *et al.* (2013) 'A longitudinal study on α-synuclein in blood plasma as a biomarker for Parkinson's disease', *Scientific Reports*, 3(1), pp. 1–6. doi: 10.1038/srep02540.

Alper, T. *et al.* (1967) 'Does the agent of scrapie replicate without nucleic acid?', *Nature*, 214, pp. 764–766.

Alvarez-Erviti, L. *et al.* (2011) 'Lysosomal dysfunction increases exosome-mediated alpha-synuclein release and transmission', *Neurobiology of Disease*. Elsevier Inc., 42(3), pp. 360–367. doi: 10.1016/j.nbd.2011.01.029.

Anderson, J. P. *et al.* (2006) 'Phosphorylation of Ser-129 Is the Dominant Pathological Modification of α-Synuclein in Familial and Sporadic Lewy Body Disease', *Journal of Biological Chemistry*, 281(40), pp. 29739–29752. doi: 10.1074/jbc.m600933200.

Andisheh, A. and Marie, S. A. (2013) 'Mechanisms of islet amyloidosis toxicity in type 2 diabetes', *FEBS Letters*, 587(8), pp. 1119–1127. doi: 10.1016/j.febslet.2013.01.017.

Andreeva, A. *et al.* (2019) 'Apparent deglycase activity of DJ-1 results from the conversion of free methylglyoxal present in fast equilibrium with hemithioacetals and hemiaminals', *The Journal of Biological Chemistry*, (3). doi: 10.1074/jbc.RA119.011237.

Andres-mateos, E. *et al.* (2007) 'DJ-1 gene deletion reveals that DJ-1 is an atypical peroxiredoxin-like peroxidase', *Proceedings of the National Academy of Sciences of the United States of America*, 104(37), pp. 14807–14812.

Angelova, P. R. *et al.* (2015) 'Lipid peroxidation is essential for a-synuclein induced cell death', *Journal of Neurochemistry*, 133, pp. 582–589. doi: 10.1111/jnc.13024.

Angelova, P. R. *et al.* (2016) ' Ca 2+ is a key factor in α-synuclein-induced neurotoxicity ', *Journal of Cell Science*, 129(9), pp. 1792–1801. doi: 10.1242/jcs.180737.

Appel-Cresswell, S. *et al.* (2013) 'Alpha-Synuclein p.H50Q , a Novel Pathogenic Mutation for Parkinson ' s Disease', *Movement Disorders*, 28(6), pp. 811–813. doi: 10.1002/mds.25421.

Araki, K. *et al.* (2016) 'A small-angle X-ray scattering study of alpha-synuclein from human red blood cells', *Science Reports*. Nature Publishing Group, 6(30473), pp. 1–8. doi: 10.1038/srep30473.

Arawaka, S. *et al.* (1998) 'Lewy body in neurodegeneration with brain iron accumulation type 1 is immunoreactive for alpha-synuclein.', *Neurology*, 51(3), pp. 887–889.

Arawaka, S. (2006) 'The Role of G-Protein-Coupled Receptor Kinase 5 in Pathogenesis of Sporadic Parkinson's Disease', *Journal of Neuroscience*, 26(36), pp. 9227–9238. doi: 10.1523/jneurosci.0341-06.2006.

Arawaka, S. *et al.* (2017) 'Mechanisms underlying extensive Ser129-phosphorylation in α-synuclein aggregates', *Acta neuropathologica communications*. Acta Neuropathologica Communications, 5(1), p. 48. doi: 10.1186/s40478-017-0452-6.

Arenas, E., Denham, M. and Villaescusa, J. C. (2015) 'How to make a midbrain dopaminergic neuron', *Development*, 142, pp. 1918–1936. doi: 10.1242/dev.097394.

Arkinson, C. and Walden, H. (2018) 'Parkin function in Parkinson's disease', *Science*, 360(6386).

Arnesen, T. *et al.* (2009) 'Proteomics analyses reveal the evolutionary conservation and divergence of N-terminal acetyltransferases from yeast and humans', *Proceedings of the National Academy of Sciences*, 106(20), pp. 8157–8162. doi: 10.1073/pnas.0901931106.

Arotcarena, M.-L., Teil, M. and Dehay, B. (2019) 'Autophagy in Synucleinopathy : The Overwhelmed and Defective Machinery', *Cells*, 8(565), pp. 1–24.

Arya, R. and White, K. (2015) 'Cell death in development: Signaling pathways and core mechanisms', *Seminars in Cell and Developmental Biology*. Elsevier Ltd, 39, pp. 12–19. doi: 10.1016/j.semcdb.2015.02.001.

Ascherio, A. *et al.* (2001) 'Prospective study of caffeine consumption and risk of Parkinson's disease in men and women.', *Annals of Neurology*, 50(10), pp. 56–63.

Atias, M. *et al.* (2019) 'Synapsins regulate α-synuclein functions', *Proceedings of the National Academy of Sciences*, 116(23), pp. 11116–11118. doi: 10.1073/pnas.1903054116.

Aulic, S. *et al.* (2014) 'Defined alpha-synuclein prion-like molecular assemblies spreading in cell culture', *BMC Neuroscience*, 15(69), pp. 1–12.

Ayton, S. *et al.* (2017) 'Cerebral quantitative susceptibility mapping predicts amyloid- b - related cognitive decline', *Brain*, 140, pp. 2112–2119. doi: 10.1093/awx167.

Baehrecke, E. H. (2002) 'How death shapes life during development', *Nature Reviews Molecular Cell Biology*, 3(10), pp. 779–787. doi: 10.1038/nrm931.

Bailey, R. M. *et al.* (2013) 'LRRK2 phosphorylates novel tau epitopes and promotes

tauopathy', *Acta Neuropathologica*, 126, pp. 809–827. doi: 10.1007/s00401-013-1188-4.

Baker, B. M. and Chen, C. S. (2012) 'Deconstructing the third dimension – how 3D culture microenvironments alter cellular cues', *Journal of Cell Science*, 125(13), pp. 3015–3024. doi: 10.1242/jcs.079509.

Baksi, S., Tripathi, A. K. and Singh, N. (2016) 'Alpha-synuclein modulates retinal iron homeostasis by facilitating the uptake of transferrin-bound iron : Implications for visual manifestations of Parkinson's disease', *Free Radical Biology and Medicine*. Elsevier, 97, pp. 292–306. doi: 10.1016/j.freeradbiomed.2016.06.025.

Baldereschi, M. *et al.* (2000) 'Parkinson's disease and parkinsonism in a longitudinal study Two-fold higher incidence in men', *Neurology*, 55(9).

Bandyopadhyay, U. *et al.* (2008) 'The Chaperone-Mediated Autophagy Receptor Organizes in Dynamic Protein Complexes at the Lysosomal Membrane □ †', *Molecular and Cellular Biology*, 28(18), pp. 5747–5763. doi: 10.1128/MCB.02070-07.

Banks, D. A. *et al.* (2017) 'MK-STYX Alters the Morphology of Primary Neurons , and Outgrowths in MK-STYX Overexpressing PC-12 Cells Develop a Neuronal Phenotype', *Frontiers in Molecular Biosciences*, 4(November), pp. 1–17. doi: 10.3389/fmolb.2017.00076.

Barbour, R. *et al.* (2008) 'Red Blood Cells Are the Major Source of Alpha-Synuclein in Blood', *Neurodegenerative Diseases*, 5, pp. 55–59. doi: 10.1159/000112832.

Barré-Sinoussi, F. and Montagutelli, X. (2015) 'Animal models are essential to biological research: issues and perspectives', *Future Science OA*, 1(4), pp. 4–6. doi: 10.4155/fso.15.63.

Barrera, G. *et al.* (2018) 'Lipid Peroxidation-Derived Aldehydes, 4-Hydroxynonenal and Malondialdehyde in Aging-Related Disorders', *Antioxidants*, 7(8), p. 102. doi: 10.3390/antiox7080102.

Bartels, T. *et al.* (2010) 'The N-terminus of the intrinsically disordered protein α-synuclein triggers membrane binding and helix folding', *Biophysical Journal*. Biophysical Society, 99(7), pp. 2116–2124. doi: 10.1016/j.bpj.2010.06.035.

Bartels, T. *et al.* (2014) 'N-alpha-acetylation of α-synuclein increases its helical folding propensity, GM1 binding specificity and resistance to aggregation', *PLoS ONE*, 9(7), pp. 1–10. doi: 10.1371/journal.pone.0103727.

Bartels, T., Choi, J. G. and Selkoe, D. J. (2011) 'a-Synuclein occurs physiologically as a helically folded tetramer that resists aggregation', *Nature*. Nature Publishing Group, 477(7362), pp. 107–111. doi: 10.1038/nature10324.

Basler, K. *et al.* (1986) 'Scrapie and cellular PrP isoforms are encoded by the same chromosomal gene', *Cell*, 46(3), pp. 417–428.

Basso, M. and Bonetto, V. (2016) 'Extracellular vesicles and a novel form of communication in the brain', *Frontiers in Neuroscience*, 10(MAR), pp. 1–13. doi: 10.3389/fnins.2016.00127.

Batelli, S. A. T. P. A. D. I. I. T. D. O. A.-S. W. T. A. *et al.* (2011) 'Macroautophagy and the proteasome are differently involved in the degradation of alpha-synuclein wild-type and mutated A30P in an in vitro inducible model', *Neuroscience*. Elsevier Inc., 195, pp. 128–137. doi: 10.1016/j.neuroscience.2011.08.030.

Beach, T. G. *et al.* (2009) 'Unified Staging System for Lewy Body Disorders: Correlation with Nigrostriatal Degeneration, Cognitive Impairment and Motor Dysfunction', *Acta*, 117(6), pp. 613–634. doi: 10.1371/journal.pone.0178059.

Beers, J. *et al.* (2015) 'A cost-effective and efficient reprogramming platform for large-scale

production of integration-free human induced pluripotent stem cells in chemically defined culture', *Scientific Reports*. Nature Publishing Group, 5(January), pp. 1–9. doi: 10.1038/srep11319.

Belmokhtar, C. A., Hillion, J. and Ségal-Bendirdjian, E. (2001) 'Staurosporine induces apoptosis through both caspase-dependent and caspase-independent mechanisms', *Oncogene*, 20(26), pp. 3354–3362. doi: 10.1038/sj.onc.1204436.

Bengoa-Vergniory, N. *et al.* (2017) 'Alpha-synuclein oligomers : a new hope', *Acta Neuropathologica*. Springer Berlin Heidelberg, 134(6), pp. 819–838. doi: 10.1007/s00401-017-1755-1.

Bennett, M. C. *et al.* (1999) 'Degradation of α -Synuclein by Proteasome', *The Journal of Biological Chemistry*, 274(14), pp. 33855–33859.

Bentea, E. *et al.* (2015) 'Nigral proteasome inhibition in mice leads to motor and non-motor deficits and increased expression of Ser129 phosphorylated α -synuclein', *Frontiers in Behavioural Neuroscience*, 9(March), pp. 1–18. doi: 10.3389/fnbeh.2015.00068.

Berg, D. *et al.* (2005) 'Type and frequency of mutations in the LRRK2 gene in familial and sporadic Parkinson's disease*', *Brain*, 128(12), pp. 3000–3011. doi: 10.1093/brain/awh666.

Bergsbaken, T., Fink, S. L. and Cookson, B. T. (2009) 'Pyroptosis: host cell death and inflammation', *Nature Reviews Microbiology*, 7(February), pp. 99–110. doi: 10.1038/nrmicro2070.

Berman, B. D. *et al.* (2016) 'Levodopa modulates small-world architecture of functional brain networks in Parkinson's disease', *Movement Disorders*, 31(11), pp. 1676–1684. doi: 10.1002/mds.26713.

Bharathi, Indi, S. S. and Rao, K. S. J. (2007) 'Copper- and iron-induced differential fibril formation in α-synuclein: TEM study', *Neuroscience Letters*, 424(2), pp. 78–82. doi: 10.1016/j.neulet.2007.06.052.

Biedler *et al.* (1978) 'Multiple Neurotransmitter Synthesis by Human Neuroblastoma Cell Lines and Clones', *Cancer Research*, 38(November), pp. 3751–3757.

Biedler, J. L., Helson, L. and Spengler, B. a (1973) 'Morphology and Growth , Tumorigenicity , and Cytogenetics of Human Neuroblastoma Cells in Continuous Culture Morphology and Growth , Tumorigenicity , and Cytogenetics of Human Neuroblastoma Cells in Continuous Culture1', *Cancer Research*, 33(NOVEMBER), pp. 2643–2652. doi: 10.1007/PL00000826.

Biere, A. L. *et al.* (2000) 'Parkinson's disease-associated a-synuclein is more fibrillogenic than b- and y-synuclein and cannot cross-seed its homologs', *Journal of Biological Chemistry*, 275(44), pp. 34574–34579. doi: 10.1074/jbc.M005514200.

Bieri, G., Gitler, A. D. and Brahic, M. (2018) 'Internalization, axonal transport and release of fibrillar forms of alpha-synuclein', *Neurobiology of Disease*. The Authors, 109, pp. 219–225. doi: 10.1016/j.nbd.2017.03.007.

Bieschke, J. *et al.* (2004) 'Autocatalytic self-propagation of misfolded prion protein.', *Proceedings of the National Academy of Sciences of the United States of America*, 101(33), pp. 12207–12211. doi: 10.1073/pnas.0404650101.

Biesecker, S. G. *et al.* (2018) 'The functional amyloid curli protects escherichia coli against complement-mediated bactericidal activity', *Biomolecules*, 8(1). doi: 10.3390/biom8010005.

Binolfi, A. *et al.* (2006a) 'Interaction of α-Synuclein with Divalent Metal Ions Reveals Key Differences: A Link between Structure, Binding Specificity and Fibrillation Enhancement', *Journal of the American Chemical Society*, 128(3), pp. 2045–2047. doi: 10.1021/JA0618649.

Binolfi, A. *et al.* (2006b) 'Interaction of α-Synuclein with Divalent Metal Ions Reveals Key Differences: A Link between Structure, Binding Specificity and Fibrillation Enhancement', *Journal of the American Chemical Society*, 128(3), pp. 2045–2047. doi: 10.1021/JA0618649.

Binolfi, A. *et al.* (2012) 'Bioinorganic chemistry of copper coordination to alpha-synuclein: relevance to Parkinson's disease', *Coordination Chemistry Reviews*, 256(1920), pp. 2188–2201.

Binolfi, A., Theillet, F.-X. and Selenko, P. (2012) 'Bacterial in-cell NMR of human a-synclein: a disordered monomer by nature?', *Biochemical Society Transactions*, 40(5), pp. 950–954.

Birkmayer, W. and Hornykiewicz, O. (1961) 'The L-3,4-dioxyphenylalanine (DOPA)-effect in Parkinson-akinesia', *Weiner klinische Wochenschrift*, 10(73), pp. 787–788.

Björkblom, B. *et al.* (2013) 'The Parkinson ' s disease protein DJ- 1 binds metals and protects against metal induced cytotoxicity', *The Journal of Biological Chemistry*, pp. 1–23. doi: 10.1074/jbc.M113.482091.

Bliederhaeuser, C. *et al.* (2016) 'Age-dependent defects of alpha-synuclein oligomer uptake in microglia and monocytes', *Acta Neuropathologica*. Springer Berlin Heidelberg, 131(3), pp. 379–391. doi: 10.1007/s00401-015-1504-2.

Bolam, J. P. and Pissadaki, E. K. (2012) 'Living on the edge with too many mouths to feed: Why dopamine neurons die', *Movement Disorders*, 27(12), pp. 1478–1483. doi: 10.1002/mds.25135.

Bolton, D. C., Meyer, R. K. and Prusiner, S. B. (1985) 'Scrapie PrP 27-30 is a sialoglycoprotein.', *Journal of virology*, 53(2), pp. 596–606.

Bonifati, V. *et al.* (2003) 'Mutations in the DJ-1 Gene Associated with Autosomal Recessive Early-Onset Parkinsonism', *Science Reports*, 299(January), pp. 256–260.

Bourdenx, M. *et al.* (2015) 'Lack of additive role of ageing in nigrostriatal neurodegeneration triggered by α-synuclein overexpression', *Acta neuropathologica communications*. Acta Neuropathologica Communications, 3, p. 46. doi: 10.1186/s40478-015-0222-2.

Bousset, L. *et al.* (2013) 'Structural and functional characterization of two alpha-synuclein strains', *Nature Communications*, 4. doi: 10.1038/ncomms3575.

Braak, H. *et al.* (2003) 'Idiopathic Parkinson's disease: Possible routes by which vulnerable neuronal types may be subject to neuroinvasion by an unknown pathogen', *Journal of Neural Transmission*, 110(5), pp. 517–536. doi: 10.1007/s00702-002-0808-2.

Braak, Heiko, Del Tredici, K., *et al.* (2003) 'Staging of brain pathology related to sporadic Parkinson's disease', *Neurobiology of Aging*, 24, pp. 197–211.

Braak, Heiko, Tredici, K. Del, *et al.* (2003) 'Staging of Brain Pathology Related to Sporadic Parkinson ' s Disease', *Neurobiology of Aging*, 4580(March 2003), pp. 197–211. doi: 10.1016/S0197-4580(02)00065-9.

Breslin, S. and O'Driscoll, L. (2013) 'Three-dimensional cell culture: The missing link in drug discovery', *Drug Discovery Today*. Elsevier Ltd, 18(5–6), pp. 240–249. doi: 10.1016/j.drudis.2012.10.003.

Bronk, P. *et al.* (2012) 'CSPa knockout causes neurodegeneration by impairing SNAP-25 function', *The EMBO Journal*, 31(4), pp. 829–841. doi: 10.1038/emboj.2011.467.

Brown, J. W. P. *et al.* (2018) 'Kinetic barriers to α-synuclein protofilament formation and conversion into mature fibrils', *Chemical Communications*. Royal Society of Chemistry, 54(56), pp. 7854–7857. doi: 10.1039/c8cc03002b.

Bu, B. *et al.* (2017) 'N-Terminal Acetylation Preserves α-Synuclein from Oligomerization by Blocking Intermolecular Hydrogen Bonds', *ACS Chemical Neuroscience*, 8(10), pp. 2145–2151. doi: 10.1021/acschemneuro.7b00250.

Bueler, H. *et al.* (1992) 'Normal development and behaviour of mice lacking the neuronal cell-surface PrP protein', *Nature*, 356, pp. 577–582.

Buell, A. K. *et al.* (2014) 'Solution conditions determine the relative importance of nucleation and growth processes in -synuclein aggregation', *Proceedings of the National Academy of Sciences*, 111(21), pp. 7671–7676. doi: 10.1073/pnas.1315346111.

Bullwinkel, J. *et al.* (2006) 'Ki-67 protein is associated with ribosomal RNA transcription in quiescent and proliferating cells', *Journal of Cellular Physiology*, 206(3), pp. 624–635. doi: 10.1002/jcp.20494.

Burke, R. E., Dauer, W. T. and Vonsattel, J. P. G. (2008) 'A critical evaluation of the Braak staging scheme for Parkinson's disease', *Annals of Neurology*, 64(5), pp. 485–491. doi: 10.1002/ana.21541.

Burmann, B. M. *et al.* (2020) 'Regulation of α-synuclein by chaperones in mammalian cells', *Nature*. Springer US, 577(July 2017). doi: 10.1038/s41586-019-1808-9.

Burré, J. *et al.* (2011) 'a-syn promotes SNARE-complex assembly in vivo and in Vitro', *Science*, 1663(2010), pp. 1663–1668. doi: 10.1126/science.1195227.

Burré, J. *et al.* (2013) 'Properties of native brain α-synuclein', *Nature*, 498(7453), pp. 107–110. doi: 10.1038/nature12125.

Burré, J., Sharma, M. and Südhof, T. C. (2014) 'α-Synuclein assembles into higher-order multimers upon membrane binding to promote SNARE complex formation', *Proceedings of the National Academy of Sciences*, 111(40), pp. E4274–E4283. doi: 10.1073/pnas.1416598111.

Bussell, R. and Eliezer, D. (2003) 'A structural and functional role for 11-mer repeats in α-synuclein and other exchangeable lipid binding proteins', *Journal of Molecular Biology*, 329(4), pp. 763–778. doi: 10.1016/S0022-2836(03)00520-5.

Butler, B. *et al.* (2015) 'Dopamine transporter activity is modulated by α-synuclein', *Journal of Biological Chemistry*, 290(49), pp. 29542–29554. doi: 10.1074/jbc.M115.691592.

Cabin, D. E. *et al.* (2002) 'Synaptic Vesicle Depletion Correlates with Attenuated Synaptic a-Synuclein', *The Journal of neuroscience*, 22(20), pp. 8797–8807.

Caddeo, S., Boffito, M. and Sartori, S. (2017) 'Tissue Engineering Approaches in the Design of Healthy and Pathological In Vitro Tissue Models', *Frontiers in Bioengineering and Biotechnology*, 5(July), pp. 1–22. doi: 10.3389/fbioe.2017.00040.

Caiazzo, M. *et al.* (2011) 'Direct generation of functional dopaminergic neurons from mouse and human fibroblasts.', *Nature*. Nature Publishing Group, 476(7359), pp. 224–7. doi: 10.1038/nature10284.

Caicedo-Carvajal, C. E. *et al.* (2011) 'Cancer tissue engineering: A novel 3D polystyrene scaffold for in vitro isolation and amplification of lymphoma cancer cells from heterogeneous Cell mixtures', *Journal of Tissue Engineering*, 2(1), pp. 1–10. doi: 10.4061/2011/362326.

Callis, J. (2014) 'The Ubiquitination Machinery of the Ubiquitin System', *The Arabidopsis Book*, 12, p. e0174. doi: 10.1199/tab.0174.

Canerina-amaro, A. *et al.* (2019) 'Differential Aggregation and Phosphorylation of Alpha Synuclein in Membrane Compartments Associated With Parkinson Disease', *Frontiers in Neuroscience*, 13(April), pp. 1–21. doi: 10.3389/fnins.2019.00382.

Cappai, R. *et al.* (2005) 'Dopamine promotes alpha-synuclein aggregation into SDS-resistant soluble oligomers via a distinct folding pathway.', *The FASEB Journal*, 19(10).

Cardoso, B. R. *et al.* (2017) 'Glutathione peroxidase 4: A new player in neurodegeneration?', *Molecular Psychiatry*, 22(3), pp. 328–335. doi: 10.1038/mp.2016.196.

Cartelli, D. *et al.* (2016) 'α-Synuclein is a Novel Microtubule Dynamase', *Scientific Reports*. Nature Publishing Group, 6(August), pp. 1–13. doi: 10.1038/srep33289.

Castilla, J. *et al.* (2008) 'Cell-free propagation of prion strains', *EMBO Journal*, 27(19), pp. 2557–2566. doi: 10.1038/emboj.2008.181.

Catalá, A. and Díaz, M. (2016) 'Editorial : Impact of Lipid Peroxidation on the Physiology and Pathophysiology of Cell Membranes', *Frontiers in Physiology*, 7(September), pp. 1–3. doi: 10.3389/fphys.2016.00423.

Cersosimo, M. G. (2015) 'Invasive procedures in Parkinson's disease: Let's be aware we are dealing with prion-like proteins', *Journal of the Neurological Sciences*. Elsevier B.V., 351(1–2), pp. 200–201. doi: 10.1016/j.jns.2015.02.033.

Chakraborty, S. *et al.* (2017) 'Inhibitory effects of curcumin and cyclocurcumin in 1-methyl-4-phenylpyridinium (MPP+) induced neurotoxicity in differentiated PC12 cells', *Scientific Reports*. Springer US, 7(1), pp. 1–9. doi: 10.1038/s41598-017-17268-3.

Chandra, S. *et al.* (2004) 'Double-knockout mice for alpha- and beta-synucleins: Effect on synaptic functions', *Proceedings of the National Academy of Sciences of the United States of America*, 101(41), pp. 14966–71.

Chartier-Harlin, M.-C. *et al.* (2004) 'alpha-synuclein locus duplication as a cause of familial Parkinson's disease', *Lancet*, 07, pp. 1167–1169.

Chau, K. Y. *et al.* (2009) 'Relationship between alpha synuclein phosphorylation, proteasomal inhibition and cell death: Relevance to Parkinson's disease pathogenesis', *Journal of Neurochemistry*, 110(3), pp. 1005–1013. doi: 10.1111/j.1471-4159.2009.06191.x.

Chaudhuri, K. R. and Schapira, A. H. (2009) 'Non-motor symptoms of Parkinson's disease: dopaminergic pathophysiology and treatment', *The Lancet Neurology*. Elsevier Ltd, 8(5), pp. 464–474. doi: 10.1016/S1474-4422(09)70068-7.

Chen, J. *et al.* (2013) 'Iron Accumulates in Huntington's Disease Neurons: Protection by Deferoxamine', *PLoS ONE*, 8(10), pp. 1–12. doi: 10.1371/journal.pone.0077023.

Chen, L. *et al.* (2015) 'Ablation of the Ferroptosis Inhibitor Glutathione Peroxidase 4 in Neurons Results in Rapid Motor Neuron Degeneration and Paralysis', *The Journal of Biological Chemistry*, 290(47), pp. 28097–28106. doi: 10.1074/jbc.M115.680090.

Chen, L. and Feany, M. B. (2005) 'α-synuclein phosphorylation controls neurotoxicity and inclusion formation in a Drosophila model of Parkinson disease', *Nature Neuroscience*, 8(5), pp. 657–663. doi: 10.1038/nn1443.

Chen, M. *et al.* (2015) 'Tea polyphenols alleviate motor impairments, dopaminergic neuronal injury, and cerebral α-synuclein aggregation in MPTP-intoxicated parkinsonian monkeys', *Neuroscience*, 286, pp. 383–392. doi: 10.1016/j.neuroscience.2014.12.003.

Chen, Q., Kang, J. and Fu, C. (2018) 'The independence of and associations among apoptosis, autophagy, and necrosis', *Signal Transduction and Targeted Therapy*. Springer US, 3(1), p. 18. doi: 10.1038/s41392-018-0018-5.

Chesselet, M.-F. and Richter, F. (2011) 'Modelling of Parkinson's disease in mice', *The Lancet Neurology*. Elsevier Ltd, 10(12), pp. 1108–1118. doi: 10.1016/S1474-4422(11)70227-7.

Chesselet, M. and Richter, F. (2012) ‘A Progressive Mouse Model of Parkinson ’ s Disease : The Thy1-aSyn (“ Line 61 ”) Mice’, *Neurotherapeutics*, 9, pp. 297–314. doi: 10.1007/s13311-012-0104-2.

Cheung, Y. T. *et al.* (2009) ‘Effects of all-trans-retinoic acid on human SH-SY5Y neuroblastoma as in vitro model in neurotoxicity research’, *NeuroToxicology*, 30(1), pp. 127–135. doi: 10.1016/j.neuro.2008.11.001.

Cho, Y. S. (2018) ‘The role of necroptosis in the treatment of diseases’, *BMB Reports*, 51(March), pp. 219–224.

Choi, B.-K. *et al.* (2013) ‘Large -synuclein oligomers inhibit neuronal SNARE-mediated vesicle docking’, *Proceedings of the National Academy of Sciences*, 110(10), pp. 4087–4092. doi: 10.1073/pnas.1218424110.

Choi, B. K. *et al.* (2015) ‘β-Amyloid and α-synuclein cooperate to block snare-dependent vesicle fusion’, *Biochemistry*, 54(9), pp. 1831–1840. doi: 10.1021/acs.biochem.5b00087.

Choi, S. H. *et al.* (2014) ‘A three-dimensional human neural cell culture model of Alzheimer’s disease’, *Nature*. Nature Publishing Group, 515(7526), pp. 274–278. doi: 10.1038/nature13800.

Choi, S. H. *et al.* (2016) ‘3D culture models of Alzheimer’s disease: a road map to a “cure-in-a-dish”’, *Molecular Neurodegeneration*. Molecular Neurodegeneration, 11(1), p. 75. doi: 10.1186/s13024-016-0139-7.

Chu, Y. and Kordower, J. H. (2010) ‘Lewy body pathology in fetal grafts’, *Annals of the New York Academy of Sciences*, 1184, pp. 55–67. doi: 10.1111/j.1749-6632.2009.05229.x.

Cieri, D., Brini, M. and Calì, T. (2017) ‘Emerging (and converging) pathways in Parkinson’s disease: keeping mitochondrial wellness’, *Biochemical and Biophysical Research Communications*. Elsevier Ltd, 483(4), pp. 1020–1030. doi: 10.1016/j.bbrc.2016.08.153.

Clark, I. E. *et al.* (2006) ‘Drosophila pink1 is required for mitochondrial function and interacts genetically with parkin’, *Nature Letters*, 441(June), pp. 1162–1166. doi: 10.1038/nature04779.

Clayton, D. F. and George, J. M. (1999) ‘Synucleins in synaptic plasticity and neurodegenerative disorders’, *Journal of Neuroscience Research*, 58, pp. 120–129.

Coleman, B. M. *et al.* (2012) ‘Prion-infected cells regulate the release of exosomes with distinct ultrastructural features’, *The FASEB Journal*, 26(10).

Collinge, J. (2001) ‘Prion diseases of Humans and Animals : Their Causes and Molecular Basis’, *Annual Reviews*, 24(McGowan 1922), pp. 519–50. doi: 10.1146/annurev.neuro.24.1.519.

Collins, G. A. and Goldberg, A. L. (2017) ‘The Logic of the 26S Proteasome’, *Cell*. Elsevier Inc., 169(5), pp. 792–806. doi: 10.1016/j.cell.2017.04.023.

Constantinescu, R. *et al.* (2007) ‘Neuronal differentiation and long-term culture of the human neuroblastoma line SH-SY5Y’, *Journal of Neural Transmission*, 72, pp. 17–28.

Conway, K. A. *et al.* (2006) ‘Accelerated Oligomerization by Parkinson’s Disease Linked α-Synuclein Mutants’, *Annals of the New York Academy of Sciences*, 920(1), pp. 42–45. doi: 10.1111/j.1749-6632.2000.tb06903.x.

Conway, K. A., Harper, J. D. and Lansbury, P. T. (1998) ‘Accelerated in vitro fibril formation by a mutant α-synuclein linked to early-onset Parkinson disease’, *Nature Medicine*, 4(11), pp. 1318–1320. doi: 10.1038/3311.

Cookson, B. T. and Brennan, M. A. (2001) 'Pro-inflammatory programmed cell death', *Trends in Microbiology*, 9(3), pp. 113–114.

Cookson, M. R. (2012) 'Parkinsonism Due to Mutations in PINK1, parkin, and DJ-1 and oxidative stress and mitochondrial pathways', *Cold Spring Harbor Perspectives in Medicine*, pp. 1–11. doi: 10.1101/cshperspect.a009415.

Corbille, A.-G., Neunlist, M. and Derkinderen, P. (2016) 'Cross-linking for the analysis of alpha-synuclein in the enteric nervous system', *Journal of Neurochemistry*, 139, pp. 839–847. doi: 10.1111/jnc.13845.

Cordani, M. *et al.* (2019) 'Interplay between ROS and Autophagy in Cancer and Aging : From Molecular Mechanisms to Novel Therapeutic Approaches', *Oxidative Medicine and Cellular Longevity*, 2019, pp. 3–5. doi: 10.1155/2019/8794612.

Costello, D. J. *et al.* (2004) 'Concurrent hereditary haemochromatosis and idiopathic Parkinson's disease: A case report series', *Journal of Neurology, Neurosurgery and Psychiatry*, 75(4), pp. 631–633. doi: 10.1136/jnnp.2003.027441.

Cotzias, G. C., Papavasiliou, P. S. and Gellene, R. (1969) 'Modification of Parkinsonism-Chronic Treatment with L-Dopa', *New England Journal of Medicine*, 280, pp. 337–345.

Cremades, N. *et al.* (2012) 'Direct Observation of the Interconversion of Normal and Toxic Forms of a -Synuclein', *Cell*. Elsevier Inc., 149(5), pp. 1048–1059. doi: 10.1016/j.cell.2012.03.037.

Cuervo, A. M. *et al.* (2004) 'Impaired Degradation of Mutant a-Synuclein by Chaperone-Mediated Autophagy', *Science*, 305(5688), pp. 1292–1295.

Cuervo, A. M. and Dice, J. F. (1996) 'A Receptor for the Selective Uptake and Degradation of Proteins by Lysosomes', *Science*, 273(5274), pp. 501–503.

Curtin, N. J. and Szabo, C. (2013) 'Molecular Aspects of Medicine Therapeutic applications of PARP inhibitors : Anticancer therapy and beyond', *Molecular Aspects of Medicine*. Elsevier Ltd, 34(6), pp. 1217–1256. doi: 10.1016/j.mam.2013.01.006.

Czabotar, P. E. *et al.* (2013) 'Bax crystal structures reveal how BH3 domains activate Bax and nucleate its oligomerization to induce apoptosis', *Cell*. Elsevier Inc., 152(3), pp. 519–531. doi: 10.1016/j.cell.2012.12.031.

Czabotar, P. E. *et al.* (2014) 'Control of apoptosis by the BCL-2 protein family: Implications for physiology and therapy', *Nature Reviews Molecular Cell Biology*. Nature Publishing Group, 15(1), pp. 49–63. doi: 10.1038/nrm3722.

D'Herde, K. and Krysko, D. V. (2017) 'Ferroptosis: Oxidized PEs trigger death', *Nature Chemical Biology*. Nature Publishing Group, 13(1), pp. 4–5. doi: 10.1038/nchembio.2261.

Dächert, J. *et al.* (2016) 'RSL3 and Erastin differentially regulate redox signaling to promote Smac mimetic-induced cell death.', *Oncotarget*, 7(39), pp. 1–14. doi: 10.18632/oncotarget.11687.

Dagher, A. and Zeighami, Y. (2018) 'Testing the Protein Propagation Hypothesis of Parkinson Disease', *Journal of Experimental Neuroscience*, 12, pp. 0–3. doi: 10.1177/1179069518786715.

Danzer, K. M. *et al.* (2007) 'Different Species of -Synuclein Oligomers Induce Calcium Influx and Seeding', *Journal of Neuroscience*, 27(34), pp. 9220–9232. doi: 10.1523/JNEUROSCI.2617-07.2007.

Danzer, Karin M *et al.* (2009) 'Seeding induced by alpha-synuclein oligomers provides evidence for spreading of alpha-synuclein', *Journal of Neurochemistry*, 111, pp. 192–203.

doi: 10.1111/j.1471-4159.2009.06324.x.

Danzer, K. M. *et al.* (2009) 'Seeding induced by α-synuclein oligomers provides evidence for spreading of α-synuclein pathology', *Journal of Neurochemistry*, 111(1).

Danzer, K. M. *et al.* (2012) 'Exosomal cell-to-cell transmission of alpha synuclein oligomers', *Molecular Neurodegeneration*. Molecular Neurodegeneration, 7(1), p. 1. doi: 10.1186/1750-1326-7-42.

Daubner, S. C., Le, T. and Wang, S. (2011) 'Tyrosine hydroxylase and regulation of dopamine synthesis.', *Archives of biochemistry and biophysics*. NIH Public Access, 508(1), pp. 1–12. doi: 10.1016/j.abb.2010.12.017.

Davidson, W. S. *et al.* (1998) 'Stabilization of alpha-synuclein secondary structure upon binding to synthetic membranes.', *The Journal of biological chemistry*, 273(16), pp. 9443–9. doi: 10.1074/jbc.273.16.9443.

Davies, P., Moualla, D. and Brown, D. R. (2011) 'Alpha-Synuclein Is a Cellular Ferrireductase', *PLoS ONE*, 6(1). doi: 10.1371/journal.pone.0015814.

Dawson, T. M., Ko, H. S. and Dawson, V. L. (2011) 'Genetic Animal Models of Parkinson's Disease', *Neuron*, 66(5), pp. 646–661. doi: 10.1016/j.neuron.2010.04.034.Genetic.

Deas, E. *et al.* (2016) 'Alpha-Synuclein Oligomers Interact with Metal Ions to Induce Oxidative Stress and Neuronal Death in Parkinson's Disease', *Antioxidants & Redox Signaling*, 24(7), pp. 376–391. doi: 10.1089/ars.2015.6343.

Deguil, J. *et al.* (2007) 'Neuroprotective effects of pituitary adenylate cyclase-activating polypeptide (PACAP) in MPP+-induced alteration of translational control in Neuro-2a neuroblastoma cells', *Journal of Neuroscience Research*, 85, pp. 2017–2025. doi: 10.1002/jnr.

Deinum, J. *et al.* (2004) 'DBH gene variants that cause low plasma dopamine beta hydroxylase with or without a severe orthostatic syndrome.', *Journal of medical genetics*, 41(4), pp. 1–5. doi: 10.1136/jmg.2003.009282.

Deleault, N. R. *et al.* (2012) 'Isolation of phosphatidylethanolamine as a solitary cofactor for prion formation in the absence of nucleic acids', *Proceedings of the National Academy of Sciences*, 109(22), pp. 8546–8551. doi: 10.1073/pnas.1204498109.

Delenclos, M. *et al.* (2017) 'Investigation of endocytic pathways for the internalization of exosome-associated oligomeric alpha-synuclein', *Frontiers in Neuroscience*, 11(MAR), pp. 1–10. doi: 10.3389/fnins.2017.00172.

Deng, H.-X. *et al.* (2016) 'Identification of TMEM230 mutations in familial Parkinson's disease', *Nature Genetics*. Nature Publishing Group, 48(7), pp. 733–739. doi: 10.1038/ng.3589.

Deriziotis, P. *et al.* (2011) 'Misfolded PrP impairs the UPS by interaction with the 20S proteasome and inhibition of substrate entry', *EMBO Journal*, 30(15), pp. 3065–3077. doi: 10.1038/emboj.2011.224.

Desplats, P. *et al.* (2009) 'Inclusion formation and neuronal cell death through neuron-to-neuron transmission of a-syn', *Proceedings of the National Academy of Sciences*, 106(32), pp. 13213–13218. doi: 10.1073/pnas.0906365106.

Desplats, Paula *et al.* (2009) 'Inclusion formation and neuronal cell death through neuron-to-neuron transmission of alpha-synuclein', *Proceedings of the National Academy of Sciences of the United States of America*, 106(31), pp. 13010–13015. doi: 10.1073/pnas.0909073106.

Dettmer, U. *et al.* (2013) 'In vivo cross-linking reveals principally oligomeric forms of α-

synuclein and β-synuclein in neurons and non-neural cells', *Journal of Biological Chemistry*, 288(9), pp. 6371–6385. doi: 10.1074/jbc.M112.403311.

Dettmer, U. *et al.* (2015) 'Parkinson-causing a-synuclein missense mutations shift native tetramers to monomers as a mechanism for disease initiation', *Nature Communications*. Nature Publishing Group. doi: 10.1038/ncomms8314.

Devi, L. *et al.* (2008) 'Mitochondrial import and accumulation of α-synuclein impair complex I in human dopaminergic neuronal cultures and Parkinson disease brain', *Journal of Biological Chemistry*, 283(14), pp. 9089–9100. doi: 10.1074/jbc.M710012200.

Devine, M. J. *et al.* (2011) 'Parkinson's disease induced pluripotent stem cells with triplication of the α-synuclein locus', *Nature Communications*. Nature Publishing Group, 2(1), pp. 410–440. doi: 10.1038/ncomms1453.

Devos, D. *et al.* (2012) 'Disease Modifying Strategy Based upon Iron Chelation in Parkinson's Disease: A Translational Study (P02.240)', *Neurology*, 78.

Devos, D. *et al.* (2014) 'Targeting Chelatable Iron as a Therapeutic Modality in Parkinson's Disease', *Antioxidants & Redox Signaling*, 21(2), pp. 195–210. doi: 10.1089/ars.2013.5593.

Devoto, V. M. P. *et al.* (2017) 'αsynuclein control of mitochondrial homeostasis in human-derived neurons is disrupted by mutations associated with Parkinson's disease', *Scientific Reports*, 7(1), pp. 1–13. doi: 10.1038/s41598-017-05334-9.

Dexter, D. T. *et al.* (1987) 'Increased nigral iron content in postmortem parkinsonian brain', *The Lancet*, 330(8569).

Dexter, D. T. *et al.* (1989) 'Basal Lipid Peroxidation in Substantia Nigra is Increased in Parkinson's Disease', *Journal of Neurochemistry*, 52(2), pp. 381–389.

Dice, J. F. (1990) 'Peptide sequences that target cytosolic proteins for lysosomal proteolysis', *Trends in Biochemical Sciences*, 15(8), pp. 305–309.

Dickson, D. W. *et al.* (1999) 'Multiple system atrophy: A sporadic synucleinopathy', *Brain Pathology*, 9(4), pp. 721–732. doi: 10.1111/j.1750-3639.1999.tb00553.x.

Dige, M. A. and Okoi, E. P. (2019) 'Evaluating the Effect of Iron (II) Chloride Induced Oxidative Stress in SH-SY5Y Cells and Its Role in Upregulation of α-Synuclein Expression', *International Journal of Biochemistry Research & Review*, 28(3), pp. 1–10. doi: 10.9734/IJBCRR/2019/v28i330148.

Dixon, S. J. *et al.* (2012) 'Ferroptosis: An iron-dependent form of nonapoptotic cell death', *Cell*. Elsevier Inc., 149(5), pp. 1060–1072. doi: 10.1016/j.cell.2012.03.042.

Do, J. *et al.* (2019) 'Glucocerebrosidase and its relevance to Parkinson disease', *Molecular Neurodegeneration*. Molecular Neurodegeneration, 14(36), pp. 1–16.

Doll, S. *et al.* (2017) 'ACSL4 dictates ferroptosis sensitivity by shaping cellular lipid composition', *Nature Chemical Biology*, 13(1), pp. 91–98. doi: 10.1038/nchembio.2239.

Dolma, S. *et al.* (2003) 'Identification of genotype-selective antitumor agents using synthetic lethal chemical screening in engineered human tumor cells', *Cancer Cell*, 3(3), pp. 285–296.

Domert, J. *et al.* (2016) 'Aggregated Alpha-Synuclein Transfer Efficiently between Cultured Human Neuron- Like Cells and Localize to Lysosomes', *PLoS One*. doi: 10.1371/journal.pone.0168700.

Donato, R. *et al.* (2007) 'Differential development of neuronal physiological responsiveness in two human neural stem cell lines', *BMC Neuroscience*, 8, pp. 1–11. doi: 10.1186/1471-2202-8-36.

Doppler, K. *et al.* (2014) 'Cutaneous neuropathy in Parkinson's disease: A window into brain pathology', *Acta Neuropathologica*, 128(1), pp. 99–109. doi: 10.1007/s00401-014-1284-0.

Dorsey, E. R. and Bloem, B. R. (2018) 'The Parkinson Pandemic- A Call to Action', *JAMA NeurologyA*, 75(1), pp. 9–10.

Double, K. L. *et al.* (2003) 'Iron-binding characteristics of neuromelanin of the human substantia nigra', *Biochemical Pharmacology*, 66(3), pp. 489–494. doi: 10.1016/S0006-2952(03)00293-4.

Dryanovski, D. I. *et al.* (2013) 'Calcium Entry and -Synuclein Inclusions Elevate Dendritic Mitochondrial Oxidant Stress in Dopaminergic Neurons', *Journal of Neuroscience*, 33(24), pp. 10154–10164. doi: 10.1523/JNEUROSCI.5311-12.2013.

Duan, W. *et al.* (2008) 'Single Particle Characterization of Iron-induced Pore-forming α-Synuclein Oligomers', *Journal of Biological Chemistry*, 283(16), pp. 10992–11003. doi: 10.1074/jbc.m709634200.

Dudek, J. (2017) 'Role of Cardiolipin in Mitochondrial Signaling Pathways', *Frontiers in Cell and Developmental Biology*, 5(September), pp. 1–17. doi: 10.3389/fcell.2017.00090.

Dwane, S., Durack, E. and Kiely, P. A. (2013) 'Optimising parameters for the differentiation of SH-SY5Y cells to study cell adhesion and cell migration', *BMC Research Notes*. BMC Research Notes, 6(1), p. 1. doi: 10.1186/1756-0500-6-366.

Ebrahimi-fakhari, D. *et al.* (2011) 'Distinct Roles In Vivo for the Ubiquitin – Proteasome System and the Autophagy – Lysosomal Pathway in the Degradation of ⎵ -Synuclein', *The Journal of Neuroscience*, 31(41), pp. 14508–14520. doi: 10.1523/JNEUROSCI.1560-11.2011.

Eglen, R. M. and Klein, J. L. (2017) 'Three-Dimensional Cell Culture: A Rapidly Emerging Approach to Cellular Science and Drug Discovery', *SLAS Discovery*, 22(5), pp. 453–455. doi: 10.1177/2472555217702448.

El-Agnaf, Omar M.A. *et al.* (1998) 'Aggregates from mutant and wild-type α-synuclein proteins and NAC peptide induce apoptotic cell death in human neuroblastoma cells by formation of β-sheet and amyloid-like filaments', *FEBS Letters*, 440(1–2), pp. 71–75. doi: 10.1016/S0014-5793(98)01418-5.

El-Agnaf, O. M. A. *et al.* (1998) 'Effects of the mutations Ala30 to Pro and Ala53 to Thr on the physical and morphological properties of α-synuclein protein implicated in Parkinson's disease', *FEBS Letters*, 440(1–2).

Elhadi, S. A. *et al.* (2019) 'a -Synuclein in blood cells differentiates Parkinson ' s disease from healthy controls', *Annals of Clinical and Translational Neurology*, 6(12), pp. 2426–2436. doi: 10.1002/acn3.50944.

Eliezer, D. *et al.* (2001) 'Conformational properties of α-synuclein in its free and lipid-associated states', *Journal of Molecular Biology*, 307(4), pp. 1061–1073. doi: 10.1006/jmbi.2001.4538.

Emmanouilidou, E. *et al.* (2010) 'Cell-Produced -Synuclein Is Secreted in a Calcium-Dependent Manner by Exosomes and Impacts Neuronal Survival', *Journal of Neuroscience*, 30(20), pp. 6838–6851. doi: 10.1523/JNEUROSCI.5699-09.2010.

Emmanouilidou, E., Stefanis, L. and Vekrellis, K. (2010) 'Cell-produced a-synuclein oligomers are targeted to , and impair , the 26S proteasome', *Neurobiology of Aging*. Elsevier Inc., 31(6), pp. 953–968. doi: 10.1016/j.neurobiolaging.2008.07.008.

Encinas, M. *et al.* (1999) 'Extracellular-Regulated Kinases and Phosphatidylinositol 3-Kinase

Are Involved in Brain-Derived Neurotrophic Factor-Mediated Survival and neuritogenesis of the Neuroblastoma Cell Line SH-SY5Y', *Journal of Neurochemistry*, 73(4), pp. 1409–1421. doi: 10.1046/j.1471-4159.1999.0731409.x.

Encinas, M. *et al.* (2000) 'Sequential Treatment of SH-SY5Y Cells with Retinoic Acid and Brain-Derived Neurotrophic Factor Gives Rise to Fully Differentiated , Neurotrophic Factor-Dependent ', *Journal of Neurochemistry*, 75(3), pp. 991–1003.

Evans, M. J. and Kaufman, M. H. (1981) 'Establishment in culture of pluripotenial cells from mouse embryos', *Nature*, 292, pp. 154–156.

Fagerqvist, T. *et al.* (2013) 'Off-pathway α-synuclein oligomers seem to alter α-synuclein turnover in a cell model but lack seeding capability in vivo', *Amyloid*, 20(4), pp. 233–244. doi: 10.3109/13506129.2013.835726.

Falkenburger, B. H., Saridaki, T. and Dinter, E. (2016) 'Cellular models for Parkinson's disease', *Journal of Neurochemistry*, 139, pp. 121–130. doi: 10.1111/jnc.13618.

Falker, C. *et al.* (2016) 'Exosomal cellular prion protein drives fibrillization of amyloid beta and counteracts amyloid beta-mediated neurotoxicity', *Journal of Neurochemistry*, 137(1).

Fan, Y.-G. *et al.* (2018) 'Iron and Alzheimer's Disease: From Pathogenesis to Therapeutic Implications', *Frontiers in Neuroscience*, 12(September), pp. 1–14. doi: 10.3389/fnins.2018.00632.

Fares, M.-B. *et al.* (2016) 'Induction of de novo α-synuclein fibrillization in a neuronal model for Parkinson's disease', *Proceedings of the National Academy of Sciences of the United States of America*, pp. E912–E921. doi: 10.1073/pnas.1512876113.

de Farias, C. C. *et al.* (2016) 'Highly specific changes in antioxidant levels and lipid peroxidation in Parkinson's disease and its progression: Disease and staging biomarkers and new drug targets', *Neuroscience Letters*. Elsevier Ireland Ltd, 617, pp. 66–71. doi: 10.1016/j.neulet.2016.02.011.

Farrer, M. *et al.* (2004) 'Comparison of Kindreds with Parkinsonism and α-Synuclein Genomic Multiplications', *Annals of Neurology*, 55(2), pp. 174–179. doi: 10.1002/ana.10846.

Faucheux, B. A. *et al.* (2003) 'Neuromelanin associated redox-active iron is increased in the substantia nigra of patients with Parkinson ' s disease', *Journal of Neurochemistry*, 86, pp. 1142–1148. doi: 10.1046/j.1471-4159.2003.01923.x.

Fauré, J. *et al.* (2006) 'Exosomes are released by cultured cortical neurones', *Molecular and Cellular Neuroscience*, 31(4), pp. 642–648. doi: 10.1016/j.mcn.2005.12.003.

Fauvet, B. *et al.* (2012) 'α-Synuclein in central nervous system and from erythrocytes, mammalian cells, and Escherichia coli exists predominantly as disordered monomer', *Journal of Biological Chemistry*, 287(19), pp. 15345–15364. doi: 10.1074/jbc.M111.318949.

Feany, M. B. and Bender, W. W. (2000) 'A Drosophila model of Parkinson's disease', *Nature*, 404(March), pp. 394–398.

Federico, A. *et al.* (2012) 'Mitochondria, oxidative stress and neurodegeneration', *Journal of the Neurological Sciences*. Elsevier B.V., 322(1–2), pp. 254–262. doi: 10.1016/j.jns.2012.05.030.

Feng, H. and Stockwell, B. R. (2018) 'Unsolved mysteries: How does lipid peroxidation cause ferroptosis?', *PLoS Biology*, 16(5), pp. 1–15. doi: 10.1371/journal.pbio.2006203.

Ferese, R. *et al.* (2018) 'Heterozygous PLA2G6 mutation leads to iron accumulation within basal ganglia and Parkinson's disease', *Frontiers in Neurology*, 9(JUL), pp. 1–6. doi: 10.3389/fneur.2018.00536.

Fevrier, B. *et al.* (2004) 'Cells release prions in association with exosomes', *Proceedings of the National Academy of Sciences*, 101(26), pp. 9683–9688. doi: 10.1073/pnas.0308413101.

Fink, S. L. and Cookson, B. T. (2006) 'Caspase-1-dependent pore formation during pyroptosis leads to osmotic lysis of infected host macrophages', *Cellular Microbiology*, 8(July), pp. 1812–1825. doi: 10.1111/j.1462-5822.2006.00751.x.

Finley, D. (2012) 'Recognition and Processing of Ubiquitin-Protein Conjugates by the Proteasome', *Annual review of biochemistry*, 78, pp. 477–513. doi: 10.1146/annurev.biochem.78.081507.101607.Recognition.

Flower, T. R. *et al.* (2005) 'Heat Shock Prevents Alpha-synuclein-induced Apoptosis in a Yeast Model of Parkinson's Disease', *Journal of Molecular Biology*, 351, pp. 1081–1100. doi: 10.1016/j.jmb.2005.06.060.

Flusberg, D. A. and Sorger, P. K. (2015) 'Surviving apoptosis: Life-death signaling in single cells', *Trends in Cell Biology*. Elsevier Ltd, 25(8), pp. 446–458. doi: 10.1016/j.tcb.2015.03.003.

Formation, P. S. O. and Park, E. (2013) 'Lipid Peroxidation Product 4-Hydroxy-2-Nonenal', *Antioxidants & Redox Signaling*, 18(7), pp. 770–783. doi: 10.1089/ars.2011.4429.

Forster, J. I. *et al.* (2016) 'Characterization of differentiated SH-SY5Y as neuronal screening model reveals increased oxidative vulnerability', *Journal of Biomolecular Screening*, 21(5), pp. 496–509. doi: 10.1177/1087057115625190.

Foulds, P. G. *et al.* (2011) 'Phosphorylated a-synuclein can be detected in blood plasma and is potentially a useful biomarker for Parkinson ' s disease', *The FASEB Journal*, 25, pp. 4127–4137. doi: 10.1096/fj.10-179192.

Fowler, D. M. *et al.* (2006) 'Functional amyloid formation within mammalian tissue', *PLoS Biology*, 4(1), pp. 0100–0107. doi: 10.1371/journal.pbio.0040006.

Freeman, D. *et al.* (2013) 'Alpha-Synuclein Induces Lysosomal Rupture and Cathepsin Dependent Reactive Oxygen Species Following Endocytosis', *PLoS ONE*, 8(4). doi: 10.1371/journal.pone.0062143.

Freichel, C. *et al.* (2007) 'Age-dependent cognitive decline and amygdala pathology in α-synuclein transgenic mice', *Neurobiology of Aging*, 28(9), pp. 1421–1435. doi: 10.1016/j.neurobiolaging.2006.06.013.

Friedlich, A. L., Tanzi, R. E. and Rogers, J. T. (2007) 'The 5′-untranslated region of Parkinson's disease α-synuclein messengerRNA contains a predicted iron responsive element', *Molecular Psychiatry*, 12(3), pp. 222–223. doi: 10.1038/sj.mp.4001937.

Friedmann Angeli, J. P. *et al.* (2014) 'Inactivation of the ferroptosis regulator Gpx4 triggers acute renal failure in mice', *Nature Cell Biology*, 16(12), pp. 1180–1191. doi: 10.1038/ncb3064.

Fuchs, Y. and Steller, H. (2011) 'Programmed cell death in animal development and disease', *Cell*. Elsevier Inc., 147(4), pp. 742–758. doi: 10.1016/j.cell.2011.10.033.

Fujiwara, H. *et al.* (2002) 'A-Synuclein Is Phosphorylated in Synucleinopathy Lesions', *Nature Cell Biology*, 4(2), pp. 160–164. doi: 10.1038/ncb748.

Furukawa, K. *et al.* (2006) 'Plasma membrane ion permeability induced by mutant α-synuclein contributes to the degeneration of neural cells', *Journal of Neurochemistry*, 97(4).

Fusco, G. *et al.* (2017a) 'Structural basis of membrane disruption and cellular toxicity by α-synuclein oligomers', *Science*, 1440(December), pp. 1–30. doi: 10.1126/science.aan6160.

Fusco, G. *et al.* (2017b) 'Supplementary Materials for Structural basis of membrane disruption and cellular toxicity by α-synuclein oligomers', *Science*, 1440(December), pp. 1–30. doi: 10.1126/science.aan6160.

Gagne, J. J. and Power, M. C. (2010) 'Anti-inflammatory drugs and risk of Parkinson disease A meta-analysis', *Neurology*, 74(12).

Gallegos, S. *et al.* (2015) 'Features of alpha-synuclein that could explain the progression and irreversibility of Parkinson's disease', *Frontiers in Neuroscience*, 9(FEB), pp. 1–11. doi: 10.3389/fnins.2015.00059.

Galluzzi, L. *et al.* (2015) 'Essential versus accessory aspects of cell death: Recommendations of the NCCD 2015', *Cell Death and Differentiation*, 22(1), pp. 58–73. doi: 10.1038/cdd.2014.137.

Galluzzi, L. *et al.* (2018) 'Molecular mechanisms of cell death: Recommendations of the Nomenclature Committee on Cell Death 2018', *Cell Death and Differentiation*, 25(3), pp. 486–541. doi: 10.1038/s41418-017-0012-4.

Galluzzi, L., Kepp, O. and Kroemer, G. (2016) 'Mitochondrial regulation of cell death: a phylogenetically conserved control', *Microbial Cell*, 3(3), pp. 101–108. doi: 10.15698/mic2016.03.483.

Galvin, J. E. *et al.* (2001) 'Differential Expression and Distribution of alpha-, beta- , and gamma-Synuclein in the Developing Human Substantia Nigra', *Experimental n*, 355, pp. 347–355. doi: 10.1006/exnr.2000.7615.

Gan, M. *et al.* (2015) 'Extracellular ATP induces intracellular alpha-synuclein accumulation via P2X1 receptor-mediated lysosomal dysfunction', *Neurobiology of Aging*. Elsevier Inc, 36(2), pp. 1209–1220. doi: 10.1016/j.neurobiolaging.2014.10.037.

Gao, M. *et al.* (2015) 'Glutaminolysis and Transferrin Regulate Ferroptosis', *Molecular Cell*. Elsevier Inc., 59(2), pp. 298–308. doi: 10.1016/j.molcel.2015.06.011.

Gaschler, M. M. *et al.* (2018) 'FINO2initiates ferroptosis through GPX4 inactivation and iron oxidation', *Nature Chemical Biology*. Springer US, 14(5), pp. 507–515. doi: 10.1038/s41589-018-0031-6.

Gaschler, M. M. and Stockwell, B. R. (2017) 'Lipid peroxidation in cell death', *Biochemical and Biophysical Research Communications*. Elsevier Ltd, 482(3), pp. 419–425. doi: 10.1016/j.bbrc.2016.10.086.

Gavathiotis, E. *et al.* (2010) 'BH3-Triggered Structural Reorganization Drives the Activation of Proapoptotic BAX', *Molecular Cell*. Elsevier Inc., 40(3), pp. 481–492. doi: 10.1016/j.molcel.2010.10.019.

Ge, P., Dawson, V. L. and Dawson, T. M. (2020) 'PINK1 and Parkin mitochondrial quality control : a source of regional vulnerability in Parkinson's disease', *Molecular Neurodegeneration*. Molecular Neurodegeneration, 15(20), pp. 1–18.

Geng, N. *et al.* (2018) 'Knockdown of ferroportin accelerates erastin-induced ferroptosis in neuroblastoma cells', *Eur Rev Med Pharmacol Sci*, 22(12), pp. 3826–3836. doi: 10.26355/eurrev_201806_15267.

Gerdes, J. *et al.* (1983) 'Production of a mouse monoclonal anibody reactive with a human nuclear antigen associated with cell proliferation', *International Journal of Cancer*, 31(1), pp. 13–20.

Ghaemmaghami, S. *et al.* (2007) 'Cell division modulates prion accumulation in cultured cells.', *Proceedings of the National Academy of Sciences of the United States of America*,

104(46), pp. 17971–6. doi: 10.1073/pnas.0708372104.

Ghosh, D. *et al.* (2017) 'A-Synuclein Aggregation and Its Modulation', *International Journal of Biological Macromolecules*. Elsevier B.V., 100, pp. 37–54. doi: 10.1016/j.ijbiomac.2016.10.021.

Giasson, B. I. *et al.* (2001) 'A Hydrophobic Stretch of 12 Amino Acid Residues in the Middle of a-Synuclein Is Essential for Filament Assembly', *Journal of Biological Chemistry*, 276(4), pp. 2380–2386. doi: 10.1074/jbc.M008919200.

Giguère, N., Nanni, S. B. and Trudeau, L. E. (2018) 'On cell loss and selective vulnerability of neuronal populations in Parkinson's disease', *Frontiers in Neurology*, 9(JUN). doi: 10.3389/fneur.2018.00455.

Glick, D., Barth, S. and Macleod, K. F. (2010) 'Autophagy : cellular and molecular mechanisms', *Journal of Pathology The*, 221(1), pp. 3–12. doi: 10.1002/path.2697.Autophagy.

Goedert, M. *et al.* (2013) '100 years of Lewy pathology', *Nature Reviews Neurology*. Nature, 9, pp. 13–24.

Goldie, B. J., Barnett, M. M. and Cairns, M. J. (2014) 'BDNF and the maturation of posttranscriptional regulatory networks in human SH-SY5Y neuroblast differentiation', *Frontiers in Cellular Neuroscience*, 8(October), pp. 1–7. doi: 10.3389/fncel.2014.00325.

Golts, N. *et al.* (2002) 'Magnesium Inhibits Spontaneous and Iron-induced Aggregation of alpha-Synuclein', *The Journal of Biological Chemistry*, 277(18), pp. 16116–16123. doi: 10.1074/jbc.M107866200.

Goodwill, K. E., Sabatier, C. and Stevens, R. C. (1998) 'Crystal Structure of Tyrosine Hydroxylase with Bound Cofactor Analogue and Iron at 2 . 3 Å Resolution : Self-Hydroxylation of Phe300 and the Pterin-Binding Site', *Biochemistry*, 37(39). doi: 10.1021/bi981462g.

Gorell, J. M. *et al.* (1995) 'Increased iron-related MRI contrast in the substantia nigra in Parkinson's disease', *Neurology*, 45(6), pp. 1138–1143.

Gorell, J. M. *et al.* (1997) 'Occupational exposures to metals as risk factors for Parkinson's disease.', *Neurology*, 48(3), pp. 650–658.

Gousset, K. *et al.* (2009) 'Prions hijack tunnelling nanotubes for intercellular spread', *Nature Cell Biology*, 11(3), pp. 328–336. doi: 10.1038/ncb1841.

Graham, D. G. (1978) 'Oxidative Pathways for Catecholamines in the Genesis of Neuromelanin and Cytotoxic Quinones', *Molecular Pharmacology*, 14, pp. 633–643.

Graham, F. L. *et al.* (1977) 'Charateristics of a human cell line transformed by DNA from human adenovirus type 5', *Journal of General Virology*, 36, pp. 59–72.

Grau, C. M. and Greene, L. A. (2012) 'Use of PC12 cells and rat superior cervical ganglion sympathetic neurons as models for neuroprotective assays relevant to Parkinson's disease', *Methods in Moelcular Biology*, 846, pp. 201–211. doi: 10.1017/CBO9780511544873.009.

Greenbaum, E. A. *et al.* (2005) 'The E46K mutation in ??-synuclein increases amyloid fibril formation', *Journal of Biological Chemistry*, 280(9), pp. 7800–7807. doi: 10.1074/jbc.M411638200.

Greene, L. A. (1978) 'Nerve growth factor prevents the death and stimulates the neuronal differentiation of clonal PC12 pheochromocytoma cells in serum-free medium', *Journal of Cell Biology*, (18), pp. 747–755.

Greene, L. A. and Rein, G. (1977) 'Release of [3H]norepinephrine from a clonal line of pheochromocytoma cells (PC12) by nicotinic cholinergic stimulation', *Brain Research*, 138(3), pp. 521–528.

Greene, L. A. and Tischler, A. S. (1976) 'Establishment of a noradrenergic clonal line of rat adrenal pheochromocytoma cells which respond to nerve growth factor.', *Proceedings of the National Academy of Sciences*, 73(7), pp. 2424–2428. doi: 10.1073/pnas.73.7.2424.

Gregory, A. *et al.* (2008) 'Neurodegeneration associated with genetic defects in phospholipase A2', *Neurology*, 71(18), pp. 1402–1409. doi: 10.1212/01.wnl.0000327094.67726.28.

Greten-Harrison, B. *et al.* (2010) 'aBy-Synuclein triple knockout mice reveal age-dependent neuronal dysfunction', *Proceedings of the National Academy of Sciences*, 107(45), pp. 19573–19578. doi: 10.1073/pnas.1005005107.

Griffith, L. G. and Swartz, M. A. (2006) 'Capturing complex 3D tissue physiology in vitro', *Nature Reviews Molecular Cell Biology*, 7(3), pp. 211–224. doi: 10.1038/nrm1858.

Groll, M. *et al.* (1999) 'The catalytic sites of 20S proteasomes and their role in subunit maturation : A mutational and crystallographic study', *Proceedings of the National Academy of Sciences*, 96(September), pp. 10976–10983.

Grosse, L. *et al.* (2016) 'Bax assembles into large ring-like structures remodeling the mitochondrial outer membrane in apoptosis', *The EMBO Journal*, 35(4), pp. 402–413. doi: 10.15252/embj.201592789.

Grozdanov, V. and Danzer, K. M. (2018) 'Release and uptake of pathologic alpha-synuclein', *Cell and Tissue Research*. Cell and Tissue Research, 373, pp. 175–182.

Gruschus, J. M. (2015) 'Did α -Synuclein and Glucocerebrosidase Coevolve ? Implications for Parkinson's Disease', *PLoS ONE*, 2, pp. 1–21. doi: 10.1371/journal.pone.0133863.

Guan, H. *et al.* (2017) 'Mitochondrial ferritin protects SH-SY5Y cells against H 2 O 2 - induced oxidative stress and modulates α -synuclein expression', *Experimental Neurology*. The Authors, 291, pp. 51–61. doi: 10.1016/j.expneurol.2017.02.001.

Guiney, S. J. *et al.* (2017) 'Ferroptosis and cell death mechanisms in Parkinson's disease', *Neurochemistry International*. Elsevier Ltd, 104, pp. 34–48. doi: 10.1016/j.neuint.2017.01.004.

Guo, B. B., Bellingham, S. A. and Hill, A. F. (2015) 'The neutral sphingomyelinase pathway regulates packaging of the prion protein into exosomes', *Journal of Biological Chemistry*, 290(6), pp. 3455–3467. doi: 10.1074/jbc.M114.605253.

Guo, B. B., Bellingham, S. A. and Hill, A. F. (2016) 'Stimulating the release of exosomes increases the intercellular transfer of prions', *Journal of Biological Chemistry*, 291(10), pp. 5128–5137. doi: 10.1074/jbc.M115.684258.

Guo, J. T. *et al.* (2008) 'Inhibition of Vesicular Monoamine Transporter-2 Activity in alpha-Synuclein Stably Transfected SH-SY5Y Cells', *Cellular and Molecular Neurobiology*, 28, pp. 35–47. doi: 10.1007/s10571-007-9227-0.

Guzman, J. N. *et al.* (2018) 'Systemic isradipine treatment diminishes calcium-dependent mitochondrial oxidant stress', *Journal of Clinical Investigation*, 128(6), pp. 2266–2280. doi: 10.1172/JCI95898.

Haberman, A. *et al.* (2012) 'The synaptic vesicle SNARE neuronal Synaptobrevin promotes endolysosomal degradation and prevents neurodegeneration', *The Journal of Cell Biology*, 196(2), pp. 261–276. doi: 10.1083/jcb.201108088.

Hague, S. *et al.* (2003) 'Early-Onset Parkinson's Disease Caused by a Compound Heterozygous DJ-1 Mutation', *Annals of Neurology*, 54(2), pp. 271–274.

Halliday, G. M. and McCann, H. (2008) 'Human-based studies on α-synuclein deposition and relationship to Parkinson's disease symptoms', *Experimental Neurology*, 209(1), pp. 12–21. doi: 10.1016/j.expneurol.2007.07.006.

Han, J. Y., Choi, T. S. and Kim, H. I. (2018) 'Molecular Role of Ca 2 + and Hard Divalent Metal Cations on Accelerated Fibrillation and Interfibrillar Aggregation of α -Synuclein', *Scientific Reports*. Springer US, (September 2017), pp. 1–11. doi: 10.1038/s41598-018-20320-5.

Hanahan, D. and Weinberg, R. A. (2011) 'Hallmarks of Cancer: The Next Generation', *Cell*. Elsevier Inc., 144. doi: 10.1016/j.cell.2011.02.013.

Hansson, O. *et al.* (2014) 'Levels of cerebrospinal fluid α-synuclein oligomers are increased in Parkinson's disease with dementia and dementia with Lewy bodies compared to Alzheimer's disease', *Alzheimer's Research and Therapy*, 6(1), pp. 4–9. doi: 10.1186/alzrt255.

Harbi, D. and Harrison, P. M. (2014) 'Classifying prion and prion-like phenomena', *Prion*, 8(2), pp. 1–5. doi: 10.4161/pri.27960.

Harding, C., Heuser, J. and Stahl, P. (1983) 'Receptor-mediated Endocytosis of Transferrin and of the Transferrin Receptor in Rat Reticulocytes Recycling', *J. Cell. Biol.*, 97, pp. 329–339. doi: 10.1038/nrm973.

Harris, G. *et al.* (2018) 'Toxicity, recovery, and resilience in a 3D dopaminergic neuronal in vitro model exposed to rotenone', *Archives of Toxicology*. Springer Berlin Heidelberg, 92(8), pp. 2587–2606. doi: 10.1007/s00204-018-2250-8.

Hartmann, A. *et al.* (2001) 'Caspase-8 Is an Effector in Apoptotic Death of Dopaminergic Neurons in Parkinson ' s Disease , But Pathway Inhibition Results in Neuronal Necrosis', *The Journal of Neuroscience*, 21(7), pp. 2247–2255.

Hashemi, S. H. *et al.* (2003) 'SSR2(a) Receptor Expression and Adrenergic/Cholinergic Characteristics in Differentiated SH-SY5Y Cells *', *Neurochemical Research*, 28(April), pp. 449–460.

Hashimoto, M. *et al.* (1999) 'Oxidative stress induces amyloid-like aggregate formation of NACP/alpha-synuclein in vitro.', *Neuroreport*, 10(4), pp. 717–721.

Hawkes, C. H. and Braak, H. (2007) 'Parkinson's disease: A dual hit hypothesis', *Journal of Neurobiology Neurosurgery and Psychiatry*, 78(9), pp. 1032–1032.

He, L. *et al.* (2017) 'Antioxidants Maintain Cellular Redox Homeostasis by Elimination of Reactive Oxygen Species', *Cellular Physiology and Biochemistry*, 44, pp. 532–553. doi: 10.1159/000485089.

He, Q. *et al.* (2011) 'Alpha-synuclein aggregation is involved in the toxicity induced by ferric iron to SK-N-SH neuroblastoma cells.', *Journal of Neural Transmission*, 118(3), pp. 397–406. doi: 10.1007/s00702-010-0453-0.

He, Y. *et al.* (1996) 'Increased iron in the substantia nigra of 6-OHDA induced parkinsonian rats : a nuclear microscopy study', *Brain Research*, 735, pp. 149–153.

Heeman, B. *et al.* (2009) 'Depletion of PINK1 affects mitochondrial metabolism , calcium homeostasis and energy maintenance', *Journal lof Cell Science*, 124(7), pp. 1115–1125. doi: 10.1242/jcs.078303.

Hejjaoui, M. *et al.* (2011) 'Towards elucidation of the role of ubiquitination in the

pathogenesis of parkinson's disease with semisynthetic ubiquitinated α-synuclein', *Angewandte Chemie - International Edition*, 50(2), pp. 405–409. doi: 10.1002/anie.201005546.

Hendrickson, M. L. *et al.* (2011) 'Expression of nestin by neural cells in the adult rat and human brain', *PLoS ONE*, 6(4). doi: 10.1371/journal.pone.0018535.

Hinz, M., Stein, A. and Uncini, T. (2011) 'Amino acid management of Parkinson's disease : a case study', *International Journal of General Medicine*, 4, pp. 165–174. doi: 10.2147/IJGM.S16621.

Ho, P. W. *et al.* (2020) 'Age-dependent accumulation of oligomeric SNCA / α -synuclein from impaired degradation in mutant LRRK2 knockin mouse model of Parkinson disease : role for therapeutic activation of chaperone-mediated autophagy (CMA)', *Autophagy*. Taylor & Francis, 16(2), pp. 347–370. doi: 10.1080/15548627.2019.1603545.

Hoarau-Véchot, J. *et al.* (2018) 'Halfway between 2D and animal models: Are 3D cultures the ideal tool to study cancer-microenvironment interactions?', *International Journal of Molecular Sciences*, 19(1). doi: 10.3390/ijms19010181.

Hoenen, C. *et al.* (2016) 'Alpha-synuclein proteins promote pro-inflammatory cascades in microglia: Stronger effects of the a53t mutant', *PLoS ONE*, 11(9), pp. 1–24. doi: 10.1371/journal.pone.0162717.

Hong, D.-P., Fink, A. L. and Uversky, V. N. (2015) 'Smoking and Parkinson's disease: Does nicotine affect a-synuclein fibrillation?', *Biochimica et Biophysica Acta*, 25(8), pp. 713–724. doi: 10.1097/MCA.0000000000000178.Endothelial.

Hoshimaru, M. *et al.* (1996) 'Differentiation of the immortalized adult neuronal progenitor cell line HC2S2 into neurons by regulatable suppression of the v-myc oncogene.', *Proceedings of the National Academy of Sciences*, 93(February), pp. 1518–1523. doi: 10.1073/pnas.93.4.1518.

Howie, A. J. and Brewer, D. B. (2009) 'Optical properties of amyloid stained by Congo red: History and mechanisms', *Micron*. Elsevier Ltd, 40(3), pp. 285–301. doi: 10.1016/j.micron.2008.10.002.

Hruska, K. S. *et al.* (2008) 'Gaucher Disease : Mutation and Polymorphism Spectrum in the Glucocerebrosidase Gene (GBA)', *Human Mutation*, 29(March). doi: 10.1002/humu.20676.

Huang, M. *et al.* (2019) 'α -Synuclein : A Multifunctional Player in Exocytosis , Endocytosis , and Vesicle Recycling', *Frontiers in Neuroscience*, 13(January), pp. 1–8. doi: 10.3389/fnins.2019.00028.

Hughes, C. S., Postovit, L. M. and Lajoie, G. A. (2010) 'Matrigel: a complex protein mixture required for optimal growth of cell culture.', *Proteomics*, 10(9), pp. 1886–1890. doi: 10.1002/pmic.200900758.

Ichim, G. and Tait, S. W. G. (2016) 'A fate worse than death: Apoptosis as an oncogenic process', *Nature Reviews Cancer*. Nature Publishing Group, 16(8), pp. 539–548. doi: 10.1038/nrc.2016.58.

Iljina, M. *et al.* (2016) 'Kinetic model of the aggregation of alpha-synuclein provides insights into prion-like spreading', *Proceedings of the National Academy of Sciences*, 113(9), pp. E1206–E1215. doi: 10.1073/pnas.1524128113.

Illes-Toth, E. *et al.* (2015) 'Distinct higher-order α-synuclein oligomers induce intracellular aggregation', *Biochemical Journal*, 468(3), pp. 485–493. doi: 10.1042/BJ20150159.

Imai, H. *et al.* (2017) 'Lipid Peroxidation-Dependent Cell Death Regulated by GPX4 and

Ferroptosis', *Apoptotic and Non-Apoptotic Cell Death*, 403, pp. 143–170.

Inestrosa, N. C., Marzolo, M. P. and Bonnefont, A. B. (1998) 'Cellular and molecular basis of estrogen's neuroprotection - Potential relevance for Alzheimer's disease [Review]', *Molecular Neurobiology*, 17(1–3), pp. 73–86. doi: 10.1007/BF02802025.

Ingelsson, M. (2016) 'Alpha-synuclein oligomers-neurotoxic molecules in Parkinson's disease and other lewy body disorders', *Frontiers in Neuroscience*, 10(SEP), pp. 1–10. doi: 10.3389/fnins.2016.00408.

Ioannidis, J. P. A. (2012) 'Extrapolating from Animals to Humans', *Science Translational Medicine*, 4(151), pp. 151ps15-151ps15. doi: 10.1126/scitranslmed.3004631.

Ishizawa, T. *et al.* (2003) 'Colocalization of Tau and Alpha-Synuclein Epitopes in Lewy Bodies', *Journal of Neuropathology and Experimental Neurology*, 62(4), pp. 389–397.

Ito, K. *et al.* (2017) 'MPP+ induces necrostatin-1- and ferrostatin-1-sensitive necrotic death of neuronal SH-SY5Y cells', *Cell Death Discovery*. The Author(s), 3(December 2016), p. 17013. doi: 10.1038/cddiscovery.2017.13.

Iwai, A. *et al.* (1995) 'The precursor protein of non-Aβ component of Alzheimer's disease amyloid is a presynaptic protein of the central nervous system', *Neuron*, 14(2), pp. 467–475. doi: 10.1016/0896-6273(95)90302-X.

Izumi, Y. *et al.* (2005) 'Iron Accelerates the Conversion of Dopamine-Oxidized Intermediates Into Melanin And Provides Protection in SH-SY5Y Cells', *Journal of Neuroscience Research*, 137(August), pp. 126–137. doi: 10.1002/jnr.20595.

Jana, N. R. (2012) 'Protein homeostasis and aging: Role of ubiquitin protein ligases', *Neurochemistry International*, 60(5), pp. 443–447.

Jang, A. *et al.* (2010) 'Non-classical exocytosis of α-synuclein is sensitive to folding states and promoted under stress conditions', *Journal of Neurochemistry*, 113(5), pp. 1263–1274. doi: 10.1111/j.1471-4159.2010.06695.x.

Jankovic, J. (2005) 'Searching for a relationship between manganese and welding and Parkinson's disease', *Neurology*, 64(12), pp. 2021–2028. doi: 10.1212/01.WNL.0000166916.40902.63.

Jarrett, J. T. and Lansbury, P. T. (1993) 'Seeding "one-dimensional crystallisation" of amyloid: A pathogenic mechanism in Alzheimer's disease and scrapie?', *Cell*, 73(6), pp. 1055–1058.

Jaunmuktane, Z. *et al.* (2015) 'Evidence for human transmission of amyloid-β pathology and cerebral amyloid angiopathy', *Nature*, 525(7568), pp. 247–250. doi: 10.1038/nature15369.

Jellinger, K. A. (2009) 'A critical evaluation of current staging of α-synuclein pathology in Lewy body disorders', *Biochimica et Biophysica Acta - Molecular Basis of Disease*. Elsevier B.V., 1792(7), pp. 730–740. doi: 10.1016/j.bbadis.2008.07.006.

Jellinger, K. A. (2019) 'Is Braak staging valid for all types of Parkinson's disease?', *Journal of Neural Transmission*. Springer Vienna, 126(4), pp. 423–431. doi: 10.1007/s00702-018-1898-9.

Jellinger, K. A. and Korczyn, A. D. (2018) 'Are dementia with Lewy bodies and Parkinson's disease dementia the same disease?', *BMC Medicine*. BMC Medicine, 16(1), pp. 1–16. doi: 10.1186/s12916-018-1016-8.

Jenkins, A. *et al.* (2014) 'Ferrous iron formation following the co-aggregation of ferric iron and the Alzheimer's disease peptide b-amyloid (1 –42)', *J. R. Soc. Interface*.

Jenner, P. *et al.* (1992) 'Oxidative stress as a cause of nigral cell death in Parkinon's disease and incidental Lewy body pathology disease', *Annals of Neurology*, 32, pp. S82-87.

Jensen, L. M. (1987) 'Phenotypic differentiation of aphidicolin-selected human neuroblastoma cultures after long-term exposure to nerve growth facotr', *Developmental Biology*, 120(1), pp. 56–64.

Jiang, L. *et al.* (2015) 'Ferroptosis as a p53-mediated activity during tumour suppression', *Nature*, 520(7545), pp. 57–62. doi: 10.1038/nature14344.

Jiang, P. *et al.* (2017) 'Impaired endo-lysosomal membrane integrity accelerates the seeding progression of α-synuclein aggregates', *Scientific Reports*. Springer US, 7(1), pp. 1–13. doi: 10.1038/s41598-017-08149-w.

Jing, X. *et al.* (2014) 'Rifampicin protects PC12 cells from rotenone-induced cytotoxicity by activating GRP78 via PERK-eIF2α-ATF4 pathway', *PLoS ONE*, 9(3), pp. 1–9. doi: 10.1371/journal.pone.0092110.

Jo, J. *et al.* (2016) 'Midbrain-like Organoids from Human Pluripotent Stem Cells Contain Functional Dopaminergic and Neuromelanin-Producing Neurons', *Cell Stem Cell*, 19(2), pp. 248–257. doi: 10.1016/j.stem.2016.07.005.

Johansen, J. L. *et al.* (2010) 'HIF prolyl hydroxylase inhibition increases cell viability and potentiates dopamine release in dopaminergic cells', *Journal of Neurochemistry*, 115(1), pp. 209–219. doi: 10.1111/j.1471-4159.2010.06917.x.

Johnstone, R. M. *et al.* (1987) 'Vesicle Formation during Reticulocyte Maturation: Association of plasma membrane activities with released vesicles (exosomes)', *Journal of Biological Chemistry*, 262(1), pp. 9412–9420.

Jorgensen, I. and Miao, E. A. (2016) 'Pyroptotic cell death defends against intracellular pathogens', *Immunology Reviews*, 265(1), pp. 130–142. doi: 10.1111/imr.12287.Pyroptotic.

Kagan, V. E. *et al.* (2017) 'Oxidised arachidonic and adrenic PEs navigate cells to ferroptosis', *Nature Chemical Biology*, 13(November 2016). doi: 10.1038/nchembio.2238.

Kahle, P. J. *et al.* (2000) 'Subcellular localization of wild-type and Parkinson's disease-associated mutant alpha -synuclein in human and transgenic mouse brain.', *The Journal of neuroscience : the official journal of the Society for Neuroscience*, 20(17), pp. 6365–6373. doi: 20/17/6365 [pii].

Kakhlon, O. and Cabantchik, Z. I. (2002) 'The Labile Iron Pool: Characterisation, Measurement, and Participation in Cellular Processes', *Free Radical Biology & Medicine*, 33(8), pp. 457–463.

Kandinov, B., Giladi, N. and Korczyn, A. D. (2007) 'The effect of cigarette smoking, tea, and coffee consumption on the progression of Parkinson's disease', *Parkinsonism and Related Disorders*, 13(4), pp. 243–245. doi: 10.1016/j.parkreldis.2006.11.004.

Kandinov, B., Giladi, N. and Korczyn, A. D. (2009) 'Smoking and tea consumption delay onset of Parkinson's disease', *Parkinsonism and Related Disorders*. Elsevier Ltd, 15(1), pp. 41–46. doi: 10.1016/j.parkreldis.2008.02.011.

Kanu, N. *et al.* (2002) 'Transfer of scrapie prion infectivity by cell contact in culture', *Current Biology*, 12(7), pp. 523–530. doi: 10.1016/S0960-9822(02)00722-4.

Kaplan, D. R. *et al.* (1993) 'Induction of TrkB by retinoic acid mediates biologic responsiveness to BDNF and differentiation of human neuroblastoma cells', *Neuron*, 11(2), pp. 321–331.

Kara, E. *et al.* (2015) 'A 6 . 4MB duplication of the alpha-synuclein locus causing fronto-

temporal dementia and parkinsonism - phenotype-genotype correlations', *JAMA Neurology*, 71(9), pp. 1162–1171. doi: 10.1001/jamaneurol.2014.994.A.

Karpinar, D. P. *et al.* (2009) 'Pre-fibrillar α-synuclein variants with impaired B-structure increase neurotoxicity in parkinson's disease models', *EMBO Journal*, 28(20), pp. 3256–3268. doi: 10.1038/emboj.2009.257.

Kaushik, S. and Cuervo, A. M. (2018) 'The coming of age of chaperone-mediated autophagy', *Nature Reviews Molecular Cell Biology*. Springer US, 19(6), pp. 365–381. doi: 10.1038/s41580-018-0001-6.

Khan, A. U. *et al.* (2019) 'Awareness and current knowledge of Parkinson's disease: a neurodegenerative disorder', *International Journal of Neuroscience*. Taylor & Francis, 129(1), pp. 55–93. doi: 10.1080/00207454.2018.1486837.

Killinger, B. A. *et al.* (2019) 'Endogenous alpha-synuclein monomers , oligomers and resulting pathology : let ' s talk about the lipids in the room', *npj Parkinson's Disease*. Springer US, pp. 37–40. doi: 10.1038/s41531-019-0095-3.

Killinger, B. and Kordower, J. H. (2019) 'Spreading of alpha-synuclein – relevant or epiphenomenon?', *Journal of Neurochemistry*, p. jnc.14779. doi: 10.1111/jnc.14779.

Kim, S. *et al.* (2018) 'GBA1 deficiency negatively affects physiological α -synuclein tetramers and related multimers', *Proceedings of the National Academy of Sciences of the United States of America*, 115(4), pp. 4–9. doi: 10.1073/pnas.1700465115.

Kim, Y. H. *et al.* (2016) 'A 3D human neural cell culture system for modeling Alzheimer's disease', *Nature Protocols*, 10(7), pp. 985–1006. doi: 10.1038/nprot.2015.065.A.

Kirchner, P. *et al.* (2019) 'Proteome-wide analysis of chaperone- mediated autophagy targeting motifs', *PLoS Biology*, pp. 1–27.

Kirik, D. *et al.* (2002) 'Parkinson-Like Neurodegeneration Induced by Targeted Overexpression of α-Synuclein in the Nigrostriatal System', *The Journal of Neuroscience*, 22(7), pp. 2780–2791. doi: 10.1523/jneurosci.22-07-02780.2002.

Klatzo, I., Gajusek, D. C. and Zigas, V. (1959) *Evaluation of pathological findings in twelve cases of kuru.* Edited by L. Van Boagert et al. Amsterdam, The Netherlands: Elsevier Publishing Company.

Knowles, T. P. J. *et al.* (2009) 'An Analytical Solution to the Kinetics of Breakable Filament Assembly', *Science*, 1533(2009), pp. 1533–1537. doi: 10.1126/science.1178250.

Kojima, N. *et al.* (1994) 'Induction of cholinergic differentiation with neurite sprouting by de novo biosynthesis and expression of GD3 and b-series gangliosides in Neuro2a cells', *Journal of Biological Chemistry*, 269(48), pp. 30451–30456.

Konno, T. *et al.* (2016) 'Autosomal dominant Parkinson's disease caused by SNCA duplications', *Parkinsonism and Related Disorders*, 22(Suppl 1), pp. S1–S6. doi: 10.1016/j.parkreldis.2015.09.007.

Koprich, J. B., Kalia, L. V and Brotchie, J. M. (2017) 'Animal models of α-synucleinopathy for Parkinson disease drug development', *Nature Reviews Neuroscience*. Nature Publishing Group, 18(9), pp. 515–529. doi: 10.1038/nrn.2017.75.

Korczyn, A. D. *et al.* (1999) 'A 3-year randomized trial of ropinirole and bromocriptine in early Parkinson's disease', *Neurology*, 53(2).

Kordower, Jeffrey H *et al.* (2008) 'Lewy body–like pathology in long-term embryonic nigral transplants in Parkinson's disease', *Nature Medicine*, 14(5), pp. 504–506. doi: 10.1038/nm1747.

Kordower, Jeffrey H. *et al.* (2008) 'Transplanted dopaminergic neurons develop PD pathologic changes: A second case report', *Movement Disorders*, 23(16), pp. 2303–2306. doi: 10.1002/mds.22369.

Kordower, J. H. *et al.* (2013) 'Disease duration and the integrity of the nigrostriatal system in Parkinson's disease', *Brain*, 136(8), pp. 2419–2431. doi: 10.1093/brain/awt192.

Korecka, J. A. *et al.* (2013) 'Phenotypic Characterization of Retinoic Acid Differentiated SH-SY5Y Cells by Transcriptional Profiling', *PLoS One*, 8(5), p. e63862. doi: 10.1371/journal.pone.0063862.

Kovalevich, J. *et al.* (2013) *Considerations for the Use of SH-SY5Y Neuroblastoma Cells in Neurobiology Chapter 2 Considerations for the Use of SH - SY5Y Neuroblastoma Cells in Neurobiology*. doi: 10.1007/978-1-62703-640-5.

Kramer, M. L. and Schulz-Schaeffer, W. J. (2007) 'Presynaptic a-Synuclein Aggregates, Not Lewy Bodies, Cause Neurodegeneration in Dementia with Lewy Bodies', *Journal of Neuroscience*, 27(6), pp. 1405–1410. doi: 10.1523/jneurosci.4564-06.2007.

Krishna, A. *et al.* (2014) 'Systems genomics evaluation of the SH-SY5Y neuroblastoma cell line as a model for Parkinson's disease', *BMC Genomics*, 15(1), p. 1154. doi: 10.1186/1471-2164-15-1154.

Krug, A. K. *et al.* (2014) 'Transcriptional and metabolic adaptation of human neurons to the mitochondrial toxicant MPP +', *Cell Death and Disease*, 5(5), pp. 1–15. doi: 10.1038/cddis.2014.166.

Kruger, R. *et al.* (1998) 'Ala30Pro mutation in the gene encoding alpha-synlein in Parkinson's disease', *Nature Genetics*, 18, pp. 106–108.

Kuczius, T. and Groschup, M. H. (1999) 'Differences in proteinase K resistance and neuronal deposition of abnormal prion proteins characterize bovine spongiform encephalopathy (BSE) and scrapie strains', *Molecular medicine*, 5(6), pp. 406–418. doi: 0144 [pii].

Kunjappu, M. J., Hochstrasser, M. and Wolf, D. H. (2014) 'Assembly of the 20S proteasome', *BBA - Molecular Cell Research*. Elsevier B.V., 1843(1), pp. 2–12. doi: 10.1016/j.bbamcr.2013.03.008.

Kuwana, T. *et al.* (2002) 'Bid, Bax, and lipids cooperate to form supramolecular openings in the outer mitochondrial membrane', *Cell*, 111(3), pp. 331–342. doi: 10.1016/S0092-8674(02)01036-X.

Kwan, J. Y. *et al.* (2012) 'Iron accumulation in deep cortical layers accounts for MRI signal abnormalities in ALS: Correlating 7 tesla MRI and pathology', *PLoS ONE*, 7(4). doi: 10.1371/journal.pone.0035241.

Lahiri, V. and Klionsky, D. J. (2017) 'Functional impairment in RHOT1/Miro1 degradation and mitophagy is a shared feature in familial and sporadic Parkinson disease', *Autophagy*, 13(8), pp. 1259–1261. doi: 10.1080/15548627.2017.1327512.

Lai, B. C. L. *et al.* (2002) 'Occupational and environmental risk factors for Parkinson's disease', *Parkinsonism and Related Disorders*, 8, pp. 297–309. doi: 10.1136/oem.2006.027003.

Lan, A. P. *et al.* (2016) 'The neurotoxicity of iron, copper and cobalt in Parkinson's disease through ROS-mediated mechanisms', *BioMetals*, 29(4), pp. 665–678. doi: 10.1007/s10534-016-9942-4.

Lan, D. *et al.* (2015) 'Proteasome inhibitor-induced autophagy in PC12 cells overexpressing

A53T mutant α -synuclein', *Molecular Medicine Reports*, 11, pp. 1655–1660. doi: 10.3892/mmr.2014.3011.

Lander, G. C. *et al.* (2012) 'Complete subunit architecture of the proteasome regulatory particle', *Nature*. Nature Publishing Group, 482(7384), pp. 186–191. doi: 10.1038/nature10774.

Langston, J. *et al.* (1983) 'Chronic Parkinsonism in humans due to a product of meperidine-analog synthesis', *Science*, 219(4587), pp. 979–980. doi: 10.1126/science.6823561.

Langston, J. W. *et al.* (1984) 'Selective nigral toxicity after systemic administration of 1-methyl-4-phenyl-1, 2, 5, 6-tetrahydropyrine (MPTP) in the squirrel monkey', *Brain Research*, 292(2), pp. 390–394.

Langston, J. W. *et al.* (1999) 'Evidence of Active Nerve Cell Degeneration in the Substantia Nigra of Humans Years', *Annals of Neurology*, 46, pp. 598–605.

Langston, J. W. *et al.* (2015) 'Multisystem Lewy body disease and the other parkinsonian disorders', *Nature Genetics*, 47(12), pp. 1378–1384. doi: 10.1038/ng.3454.

Lashuel, H. A. *et al.* (2002) 'A-Synuclein, Especially the Parkinson'S Disease-Associated Mutants, Forms Pore-Like Annular and Tubular Protofibrils', *Journal of Molecular Biology*, 322(5), pp. 1089–1102. doi: 10.1016/S0022-2836(02)00735-0.

Lashuel, H. A., Overk, C. R., Oueslati, A., *et al.* (2013) 'The many faces of alpha-synuclein: from structure and toxicity to therapeutic target', *Nature Reviews Neuroscience*, 70(4), pp. 646–656. doi: 10.1002/ana.22528.Toll-like.

Lashuel, H. A., Overk, C. R., Oueslati, Abid, *et al.* (2013) 'The Many Faces of α-Synuclein-From Structure and Toxicity to Therapeutic Target', *Nature Reviews Neuroscience*, 13(2), pp. 83–96. doi: 10.1002/ana.22528.Toll-like.

Latham, M. P., Sekhar, A. and Kay, L. E. (2014) 'Understanding the mechanism of proteasome 20S core particle gating', *Proceedings of the National Academy of Sciences*, 111(15), pp. 5532–5537. doi: 10.1073/pnas.1322079111.

Lautenschläger, J., Kaminski, C. F. and Schierle, S. K. (2017) 'a -Synuclein – Regulator of Exocytosis , Endocytosis , or Both ?', *Trends in Cell Biology*. Elsevier Ltd, 27(7), pp. 468–479. doi: 10.1016/j.tcb.2017.02.002.

Lawrence, R. E. and Zoncu, R. (2019) 'The lysosome as a cellular centre for signalling, metabolism and quality control', *Nature Cell Biology*. Springer US, 21(February). doi: 10.1038/s41556-018-0244-7.

Lázaro, D. F. *et al.* (2014) 'Systematic Comparison of the Effects of Alpha-synuclein Mutations on Its Oligomerization and Aggregation', *PLoS Genetics*, 10(11). doi: 10.1371/journal.pgen.1004741.

Lee, B. R. and Kamitani, T. (2011) 'Improved immunodetection of endogenous α-synuclein', *PLoS ONE*, 6(8). doi: 10.1371/journal.pone.0023939.

Lee, C. M. and Reddy, E. P. (1999) 'The v- myc oncogene', *Oncogene*, 18, pp. 2997–3003.

Lee, H.-J. (2005) 'Intravesicular Localization and Exocytosis of -Synuclein and its Aggregates', *Journal of Neuroscience*, 25(25), pp. 6016–6024. doi: 10.1523/JNEUROSCI.0692-05.2005.

Lee, M. K. *et al.* (2002) 'Human alpha-synuclein-harboring familial Parkinson's disease-linked Ala-53 to Thr mutation causes neurodegenerative disease with alpha-synuclein aggregation in transgenic mice', *Proceedings of the National Academy of Sciences of the United States of America*, 99(13), pp. 8968–8973.

Lee, S. H. *et al.* (2017) 'Brain regional iron contents in progressive supranuclear palsy', *Parkinsonism and Related Disorders*. Elsevier Ltd, 45, pp. 28–32. doi: 10.1016/j.parkreldis.2017.09.020.

Lees, A. J., Hardy, J. and Revesz, T. (2009) 'Parkinson's disease', *The Lancet*. Elsevier Ltd, 373(9680), pp. 2055–2066. doi: 10.1016/S0140-6736(09)60492-X.

Lehmensiek, V. *et al.* (2006) 'Dopamine transporter-mediated cytoxicity of 6-OHDA in vitro depends on expression of mutant a-synucleins related to PD', *Neurochemistry International*, 48(5), pp. 329–340.

Lendahl, U., Zimmerman, L. B. and McKay, R. D. G. (1990) 'CNS stem cells express a new class of intermediate filament protein', *Cell*, 60(4), pp. 585–595.

Lesage, S. *et al.* (2013) 'G51D α-synuclein mutation causes a novel parkinsonian-pyramidal syndrome', *Annals of Neurology*, 73(4).

Lesage, S. and Brice, A. (2009) 'Parkinson's disease: From monogenic forms to genetic susceptibility factors', *Human Molecular Genetics*, 18(R1), pp. 48–59. doi: 10.1093/hmg/ddp012.

Lev, N. *et al.* (2013) 'DJ-1 Protects Against Dopamine Toxicity : Implications for Parkinson ' s Disease and Aging', *Journals of Gerontology: Biological Sciences*, 68(3), pp. 215–225. doi: 10.1093/gerona/gls147.

Lewerenz, J. *et al.* (2018) 'Oxytosis / Ferroptosis —(Re-) Emerging Roles for Oxidative Cell Death in Diseases of the Central Nervous System', *Frontiers in Neuroscience*, 12(April). doi: 10.3389/fnins.2018.00214.

Li, J.-Y. *et al.* (2010) 'Characterisation of Lewy Body Pathology in 12- and 16-Year-Old Intrastriatal Mesencephalic Grafts Surviving in a Patient with Parkinson's disease', *Movement Disorders*, 25(8), pp. 1091–1096. doi: 10.1002/mds.22794.

Li, J. *et al.* (2008) 'Lewy bodies in grafted neurons in subjects with Parkinson's disease suggest host-to-graft disease propagation', *Nature Medicine*, 14(5), pp. 501–503. doi: 10.1038/nm1746.

Li, J. *et al.* (2012) 'The RIP1/RIP3 necrosome forms a functional amyloid signaling complex required for programmed necrosis', *Cell*, 150(2), pp. 339–350. doi: 10.1016/j.cell.2012.06.019.

Li, J., Tan, L. and Yu, J. (2014) 'The role of the LRRK2 gene in Parkinsonism', *Molecular Neurodegeneration*, 9(47), pp. 1–17.

Li, J., Uversky, V. N. and Fink, A. L. (2001) 'Effect of familial Parkinson's disease point mutations A30P and A53T on the structural properties, aggregation, and fibrillation of human α-synuclein', *Biochemistry*, 40(38), pp. 11604–11613. doi: 10.1021/bi010616g.

Li, W. *et al.* (2007) 'Localization of α-synuclein to mitochondria within midbrain of mice', *Neuroreport*, 18, pp. 1543–1546.

Li, W. J. *et al.* (2010) 'Dose- and time-dependent α-synuclein aggregation induced by ferric iron in SK-N-SH cells', *Neuroscience Bulletin*, 26(3), pp. 205–210. doi: 10.1007/s12264-010-1117-7.

Li, Y. *et al.* (2017) 'Biometal Dyshomeostasis and Toxic Metal Accumulations in the Development of Alzheimer's Disease', *Frontiers in Molecular Neuroscience*, 10(October), pp. 1–18. doi: 10.3389/fnmol.2017.00339.

Lieberman, A. (1996) 'Adolf Hitler had Post-encephalitic Parkinsonism', *Parkinsonism and Related Disorders*, 2(2), pp. 95–103. doi: 10.1016/1353-8020(96)00005-3.

Liebman, S. W. and Chernoff, Y. O. (2012) 'Prions in yeast', *Genetics*, 191(4), pp. 1041–1072. doi: 10.1534/genetics.111.137760.

Lim F. and Sun A.M. (1980) 'Microencapsulated Islets as Bioartificial Endocrine Pancreas', *Science*, 210(4472), pp. 908–910.

Lindersson, E. *et al.* (2004) 'Proteasomal Inhibition by α-Synuclein Filaments and Oligomers', *Journal of Biological Chemistry*, 279(13), pp. 12924–12934. doi: 10.1074/jbc.M306390200.

Linert, W. *et al.* (1996) 'Dopamine, 6-hydroxydopamine, iron, and dioxygen- their mutual interactions and possible implication in the development of Parkinson's disease', *Biochimica et Biophysica Acta*, 1316, pp. 160–168.

Linkermann, A. *et al.* (2014) 'Synchronized renal tubular cell death involves ferroptosis', *Proceedings of the National Academy of Sciences*, 111(47), pp. 16836–16841. doi: 10.1073/pnas.1415518111.

Lippa, C. F. *et al.* (2007) 'DLB and PDD boundary issues: diagnosis, treatment, molecular pathology, and biomarkers.', *Neurology*, 68(11).

Liu, S. *et al.* (2007) 'α-synuclein involvement in hippocampal synaptic plasticity: role of NO, cGMP, cGK and CaMKII', *European Journal of Neuroscience*, 25(12), pp. 3583–3596.

Liu, Y. and Schubert, D. R. (2009) 'The specificity of neuroprotection by antioxidants', *Journal of Biomedical Science*, 14(Figure 1), pp. 1–14. doi: 10.1186/1423-0127-16-98.

Logroscino, G. *et al.* (2008) 'Dietary Iron Intake and Risk of Parkinson's Disease', *American Journal of Epidemiology*, 168(12), pp. 1381–1388. doi: 10.1093/aje/kwn273.

Lopert, P. and Patel, M. (2014) 'Redox Biology Brain mitochondria from DJ-1 knockout mice show increased respiration-dependent hydrogen peroxide consumption', *Redox Biology*. Elsevier Ltd., 2, pp. 667–672. doi: 10.1016/j.redox.2014.04.010.

Lopes, F. M. *et al.* (2010) 'Comparison between proliferative and neuron-like SH-SY5Y cells as an in vitro model for Parkinson disease studies', *Brain Research*. Elsevier B.V., 1337, pp. 85–94. doi: 10.1016/j.brainres.2010.03.102.

Lőrincz, T. *et al.* (2015) 'Ferroptosis is Involved in Acetaminophen Induced Cell Death', *Pathology and Oncology Research*, 21(4), pp. 1115–1121. doi: 10.1007/s12253-015-9946-3.

Lotharius, J. *et al.* (2002) 'Effect of mutant α-synuclein on dopamine homeostasis in a new human mesencephalic cell line', *Journal of Biological Chemistry*, 277(41), pp. 38884–38894. doi: 10.1074/jbc.M205518200.

Lotharius, J. (2005) 'Progressive Degeneration of Human Mesencephalic Neuron-Derived Cells Triggered by Dopamine-Dependent Oxidative Stress Is Dependent on the Mixed-Lineage Kinase Pathway', *Journal of Neuroscience*, 25(27), pp. 6329–6342. doi: 10.1523/JNEUROSCI.1746-05.2005.

Louis, N., Evelegh, C. and Graham, F. L. (1997) 'Cloning and sequencing of the cellular-viral junctions from the human adenovirus type 5 transformed 293 cell line', *Virology*, 233(2), pp. 423–429. doi: 10.1006/viro.1997.8597.

Lu, Y. *et al.* (2011) 'Phosphorylation of α-Synuclein at Y125 and S129 Alters Its Metal Binding Properties: Implications for Understanding the Role of α-Synuclein in the Pathogenesis of Parkinson's Disease and Related Disorders', *ACS Chemical Neuroscience*, 2(11), pp. 667–675. doi: 10.1021/cn200074d.

Ludtmann, M. H. R. *et al.* (2018) 'α-synuclein oligomers interact with ATP synthase and open the permeability transition pore in Parkinson's disease', *Nature Communications*.

Springer US, 9(1). doi: 10.1038/s41467-018-04422-2.

Luk, K. C. *et al.* (2009) 'Exogenous alpha-synuclein fibrils seed the formation of Lewy body-like intracellular inclusions in cultured cells', *Proceedings of the National Academy of Sciences*, 106(47), pp. 20051–20056. doi: 10.1073/pnas.0908005106.

Macdonald, M. E. *et al.* (1993) 'A novel gene containing a trinucleotide repeat that is expanded and unstable on Huntington's disease chromosomes', *Cell*, 72(6), pp. 971–983.

Machiya, Y. *et al.* (2010) 'Phosphorylated α-Synuclein at Ser-129 is targeted to the proteasome pathway in a ubiquitin-independent manner', *Journal of Biological Chemistry*, 285(52), pp. 40732–40744. doi: 10.1074/jbc.M110.141952.

Mackenzie, I. R. A. (2001) 'The Pathology of Parkinson's disease', *BCMJ*, 43(3), pp. 142–147.

Madison, M. N. and Okeoma, C. M. (2015) 'Exosomes: Implications in HIV-1 pathogenesis', *Viruses*, 7(7), pp. 4093–4118. doi: 10.3390/v7072810.

Magtanong, L. and Dixon, S. J. (2020) 'Ferroptosis and Brain Injury', *Developmental Neuroscience*, 40, pp. 382–395. doi: 10.1159/000496922.Ferroptosis.

Di Maio, R. *et al.* (2016) 'alpha-Synuclein bindss to TOM20 and inhibits mitochondrial protein import in Parkinson's disease', *Science translational medicine*, 8(342), p. 342ra78. doi: 10.1126/scitranslmed.aaf3634.

Mak, S. K. *et al.* (2010) 'Lysosomal Degradation of a-Synuclein in Vivo', *The Journal of Biological Chemistry*, 285(18), pp. 13621–13629. doi: 10.1074/jbc.M109.074617.

Maker, H. S. *et al.* (1981) 'Coupling of Dopamine Oxidation (Monoamine Oxidase Activity) to Glutathine Oxidation Via the Generation of Hydrogen Peroxide in Rat Brain Homogenates', *Journal of Neurochemistry*, 36(2).

Malgieri, G. and Eliezer, D. (2008) 'Structural effects of Parkinson's disease linked DJ-1 mutations', *Protein Science*, 17, pp. 855–868. doi: 10.1110/ps.073411608.et.

Man, W. K. *et al.* (2020) 'A Role of Cholesterol in Modulating the Binding of α -Synuclein to Synaptic-Like Vesicles', *Frontiers in Neuroscience*, 14(January), pp. 1–11. doi: 10.3389/fnins.2020.00018.

Manfredsson, F. P. *et al.* (2018) 'Induction of alpha-synuclein pathology in the enteric nervous system of the rat and non-human primate results in gastrointestinal dysmotility and transient CNS pathology', *Neurobiology of Disease*, 112(January), pp. 106–118. doi: 10.1016/j.nbd.2018.01.008.

Mao, X. *et al.* (2016) 'Pathological α-synuclein transmission initiated by binding lymphocyte-activation gene 3', *Science*, 353(6307). doi: 10.1126/science.aah3374.

Marchini, A. *et al.* (2019) 'Multifunctionalized hydrogels foster hNSC maturation in 3D cultures and neural regeneration in spinal cord injuries', *Proceedings of the National Academy of Sciences*, 116(15), pp. 7483–7492. doi: 10.1073/pnas.1818392116.

Maria, E., Patrick, M. and Muqit, M. M. K. (2004) 'Hereditary Early-Onset Parkinson ' s Disease Caused by Mutations in PINK1', *Science*, 304(5674), pp. 1158–1160.

Marie, G. *et al.* (2015) 'Acceleration of α-synuclein aggregation by exosomes', *Journal of Biological Chemistry*, 290(5), pp. 2969–2982. doi: 10.1074/jbc.M114.585703.

Marijanovic, Z. *et al.* (2009) 'Identification of an intracellular site of prion conversion', *PLoS Pathogens*, 5(5). doi: 10.1371/journal.ppat.1000426.

van der Mark, M. *et al.* (2015) 'Occupational exposure to solvents, metals and welding fumes and risk of Parkinson's disease', *Parkinsonism and Related Disorders*. Elsevier Ltd, 21(6), pp. 635–639. doi: 10.1016/j.parkreldis.2015.03.025.

Marras *et al.* (2018) 'Prevalence of Parkinson's disease across North America', *npj Parkinson's Disease*. Springer US, 4(1), pp. 1–7. doi: 10.1038/s41531-018-0058-0.

Martín-Clemente, B. *et al.* (2004) 'Alpha-Synuclein expression levels do not significantly affect proteasome function and expression in mice and stably transfected PC12 Cell Lines', *The Journal of Biological Chemistry*.

Martin-Sanchez, D. *et al.* (2017) 'Ferroptosis, but Not Necroptosis, Is Important in Nephrotoxic Folic Acid–Induced AKI', *Journal of the American Society of Nephrology*, 28(1), pp. 218–229. doi: 10.1681/ASN.2015121376.

Martin, L. J. (2006) 'Parkinson's Disease -Synuclein Transgenic Mice Develop Neuronal Mitochondrial Degeneration and Cell Death', *Journal of Neuroscience*, 26(1), pp. 41–50. doi: 10.1523/jneurosci.4308-05.2006.

Martin, L. J. *et al.* (2014) 'The mitochondrial permeability transition pore regulates Parkinson's disease development in mutant α-synuclein transgenic mice', *Neurobiology of Aging*. Elsevier Ltd, 35(5), pp. 1132–1152. doi: 10.1016/j.neurobiolaging.2013.11.008.

Martinez-vicente, M. *et al.* (2008) 'Dopamine-modified α -synuclein blocks chaperone-mediated autophagy', *The Journal of Clinical Investigation*, 118(2), pp. 777–788. doi: 10.1172/JCI32806DS1.

Martínez, J. H. *et al.* (2018) 'Alpha-synuclein mitochondrial interaction leads to irreversible translocation and complex I impairment', *Archives of Biochemistry and Biophysics*. Elsevier, 651(April), pp. 1–12. doi: 10.1016/j.abb.2018.04.018.

Mason, R. J. *et al.* (2016) 'Copper Binding and Subsequent Aggregation of α-Synuclein Are Modulated by N-Terminal Acetylation and Ablated by the H50Q Missense Mutation', *Biochemistry*, 55, pp. 4737–4741. doi: 10.1021/acs.biochem.6b00708.

Mason, R. J. (2018) *Conformational Changes and the Self-Assembly of Alpha-Synuclein*. Sheffield Hallam University.

Masters, S. C. and Fu, H. (2001) '14-3-3 Proteins Mediate an Essential Anti-apoptotic Signal', *Journal of Biological Chemistry*, 276(48), pp. 45193–45200. doi: 10.1074/jbc.M105971200.

Mastroeni, D. *et al.* (2009) 'Microglial responses to dopamine in a cell culture model of Parkinson's disease.', *Neurobiology Aging*, 30(11), pp. 1805–1817. doi: 10.1016/j.neurobiolaging.2008.01.001.Microglial.

Mathivanan, S. *et al.* (2012) 'ExoCarta 2012: Database of exosomal proteins, RNA and lipids', *Nucleic Acids Research*, 40(D1), pp. 1241–1244. doi: 10.1093/nar/gkr828.

Matsushita, M. *et al.* (2015) 'T cell lipid peroxidation induces ferroptosis and prevents immunity to infection', *The Journal of Experimental Medicine*, 212(4), pp. 555–568. doi: 10.1084/jem.20140857.

Mazzio, E. and Soliman, K. F. A. (2003) 'D-(+)-glucose rescue against 1-methyl-4-phenylpyridinium toxicity through anaerobic glycolysis in neuroblastoma cells', *Brain Research*, 962(1–2), pp. 48–60. doi: 10.1016/S0006-8993(02)03695-8.

Mazzulli, J. R. *et al.* (2011) 'Gaucher Disease Glucocerebrosidase and a -Synuclein Form a Bidirectional Pathogenic Loop in Synucleinopathies', *Cell*. Elsevier Inc., 146(1), pp. 37–52. doi: 10.1016/j.cell.2011.06.001.

Mazzulli, J. R. *et al.* (2016) 'α-Synuclein-induced lysosomal dysfunction occurs through disruptions in protein trafficking in human midbrain synucleinopathy models', *Proceedings of the National Academy of Sciences of the United States of America*, 113(7), pp. 1931–1936. doi: 10.1073/pnas.1520335113.

McCann, H., Cartwright, H. and Halliday, G. M. (2016) 'Neuropathology of α-synuclein propagation and braak hypothesis', *Movement Disorders*, 31(2), pp. 152–160. doi: 10.1002/mds.26421.

McCulloch, C. C. *et al.* (2008) 'Exploring gene-environment interactions in Parkinson's disease', *Human Genetics*, 123(3), pp. 257–265. doi: 10.1007/s00439-008-0466-z.

McCulloch, L. *et al.* (2011) 'Follicular dendritic cell-specific prion protein (PrPc) expression alone is sufficient to sustain prion infection in the spleen', *PLoS Pathogens*, 7(12). doi: 10.1371/journal.ppat.1002402.

Mcdowall, J. S. *et al.* (2017) 'Steady-State Kinetics of α - Synuclein Ferrireductase Activity Identifies the Catalytically Competent Species', *Biochemistry*, 56, pp. 2497–2505. doi: 10.1021/acs.biochem.7b00257.

McDowall, J. S. *et al.* (2017) 'Alph-synuclein ferrireductase activity is detectible in vivo, is altered in Parkinson's disease and increases the neurotoxicity of DOPAL', *Molecular and Cellular Neuroscience*, 85, pp. 1–11.

McKinley, M. P. *et al.* (1991) 'Ultrastructural localization of scrapie prion proteins in cytoplasmic vesicles of infected cultured cells', *Lab Investigations*, 65(6), pp. 622–630.

Mclean, P. J., Kawamata, H. and Hyman, B. T. (2001) 'a-Synuclein enhanced green fluorescene protein fusion proteins form proteasome sensitive inclusions in primary neurons', *Neuroscience*, 104(3), pp. 901–912.

McNaught, K. S. P. *et al.* (2003) 'Altered Proteasomal Function in Sporadic Parkinson's Disease', *Experimental Neurology*, 179(1), pp. 38–46.

McNaught, K. S. P. and Jenner, P. (2001) 'Proteasomal function is impaired in substantia nigra in Parkinson's disease', *Neuroscience Letters*, 297(3), p. 2001.

Meier, F. *et al.* (2012) 'Semi-Synthetic, Site-Specific Ubiquitin Modification of α- Synuclein Reveals Differential Effects on Aggregation', *Journal of the American Chemical Society*, 134(12), pp. 5468–5471. doi: 10.1038/jid.2014.371.

Milber, J. M. *et al.* (2012) 'Lewy pathology is not the first sign of degeneration in vulnerable neurons in Parkinson disease', *Neurology*, 79(24).

Miraglia, F. *et al.* (2018) 'Subcellular localization of alpha-synuclein aggregates and their interaction with membranes', *Neural Regeneration Research*, 13(7), pp. 1136–1144.

Mirzaei, H. *et al.* (2006) 'Identification of rotenone-induced modifications in α-synuclein using affinity pull-down and tandem mass spectrometry', *Analytical Chemistry*, 78(7), pp. 2422–2431. doi: 10.1021/ac051978n.

Mo, J. S. *et al.* (2012) 'Phosphorylation of nicastrin by SGK1 leads to its degradation through lysosomal and proteasomal pathways', *PLoS ONE*, 7(5). doi: 10.1371/journal.pone.0037111.

Moccia, M. *et al.* (2016) 'Caffeine consumption and the 4-year progression of de novo Parkinson's disease', *Parkinsonism and Related Disorders*. Elsevier Ltd, 32, pp. 116–119. doi: 10.1016/j.parkreldis.2016.08.005.

Mochizuki, H. *et al.* (1996) 'Histochemical detection of apoptosis in Parkinson's disease', *Journal of the Neurological Sciences*, 137(2), pp. 120–123. doi: 10.1016/0022-510X(95)00336-Z.

Moisan, F. *et al.* (2016) 'Parkinson disease male-to-female ratios increase with age: French nationwide study and meta-analysis', *Journal of Neurology, Neurosurgery and Psychiatry*, 87(9), pp. 952–957. doi: 10.1136/jnnp-2015-312283.

Molinoff, P. B. and Axelrod, J. (1971) 'Biochemistry of catecholamines', *Annual review of biochemistry*, 40, pp. 465–500.

Muddapu, V. R. *et al.* (2020) 'Neurodegenerative Diseases – Is Metabolic Deficiency the Root Cause ?', *Frontiers in Neuroscience*, 14(March), pp. 1–19. doi: 10.3389/fnins.2020.00213.

Muhoberac, B. B. and Vidal, R. (2019) 'Iron , Ferritin , Hereditary Ferritinopathy , and Neurodegeneration', *Frontiers in Neuroscience*, 13(December). doi: 10.3389/fnins.2019.01195.

Muntané, G., Ferrer, I. and Martinez-Vicente, M. (2012) 'A-Synuclein Phosphorylation and Truncation Are Normal Events in the Adult Human Brain', *Neuroscience*. Elsevier Inc., 200, pp. 106–119. doi: 10.1016/j.neuroscience.2011.10.042.

Murphy, D. D. *et al.* (2000) 'Synucleins are developmentally expressed, and alpha-synuclein regulates the size of the presynaptic vesicular pool in primary hippocampal neurons.', *The Journal of neuroscience : the official journal of the Society for Neuroscience*, 20(9), pp. 3214–3220. doi: 10.1016/S0165-3806(96)00210-6.

Murray, I. V. J. *et al.* (2003) 'Role of a-synuclein carboxy-terminus on fibril formation in vitro', *Biochemistry*, 42(28), pp. 8530–8540. doi: 10.1021/bi027363r.

Nagata, S. and Tanaka, M. (2017) 'Programmed Cell Death and the Immune System', *Cell Death and Immunity*, 17, pp. 333–340. doi: 10.1016/S0065-2776(08)60822-6.

Nakamura, K. *et al.* (2008) 'Optical Reporters for the Conformation of -Synuclein Reveal a Specific Interaction with Mitochondria', *Journal of Neuroscience*, 28(47), pp. 12305–12317. doi: 10.1523/jneurosci.3088-08.2008.

Nakamura, K. *et al.* (2011) 'Direct membrane association drives mitochondrial fission by the Parkinson disease-associated protein α-synuclein', *Journal of Biological Chemistry*, 286(23), pp. 20710–20726. doi: 10.1074/jbc.M110.213538.

Nakamura, S. and Yoshimori, T. (2017) 'New insights into autophagosome – lysosome fusion', *Journal of Cell Science*, 130, pp. 1209–1216. doi: 10.1242/jcs.196352.

Nalls, M. A. *et al.* (2015) 'Large-scale meta-analysis of genome-wide association data identifies six new risk loci for Parkinson's disease', *Nature Genetics*, 46(9), pp. 989–993. doi: 10.1038/ng.3043.Large-scale.

Narendra, D. *et al.* (2008) 'Parkin is recruited selectively to impaired mitochondria and promotes their autophagy', *The Journal of Cell Biology*, 183(5), pp. 795–803. doi: 10.1083/jcb.200809125.

Nath, S. *et al.* (2012) 'Spreading of Neurodegenerative Pathology via Neuron-to-Neuron Transmission of -Amyloid', *Journal of Neuroscience*, 32(26), pp. 8767–8777. doi: 10.1523/JNEUROSCI.0615-12.2012.

Nazli, Y. *et al.* (2016) 'Expression changes of genes associated with apoptosis and survival processes in Parkinson ' s disease', *Neuroscience Letters*, 615, pp. 72–77. doi: 10.1016/j.neulet.2016.01.029.

Nemani, V. M. *et al.* (2010) 'Increased Expression of α-Synuclein Reduces Neurotransmitter Release by Inhibiting Synaptic Vesicle Reclustering after Endocytosis', *Neuron*. Elsevier Ltd, 65(1), pp. 66–79. doi: 10.1016/j.neuron.2009.12.023.

Nevrly, M. *et al.* (2010) 'Effect of entacapone on plasma homocysteine levels in Parkinson's disease patients', *Neurological Sciences*, 31, pp. 565–569.

Ninkina, N. *et al.* (2012) 'Contrasting Effects of a-Synuclein and y-Synuclein on the Phenotype of Cysteine String Protein a (CSP a) Null Mutant Mice Suggest Distinct Function of these Proteins in Neuronal', *The Journal of Biological Chemistry*, 287(53), pp. 44471–44477. doi: 10.1074/jbc.M112.422402.

Nishida, Y. *et al.* (2008) 'Identification and classification of genes regulated by phosphatidylinositol 3-kinase- and TRKB-mediated signalling pathways during neuronal differentiation in two subtypes of the humna neuroblastoma cell line SH-SY5Y', *BMC Research Notes*, 11, pp. 1–11. doi: 10.1186/1756-0500-1-95.

Nishina, K. A. *et al.* (2006) 'The stoichiometry of host PrPC glycoforms modulates the efficiency of PrPSc formation in vitro', *Biochemistry*, 45(47), pp. 14129–14139. doi: 10.1021/bi061526k.

Nonaka, T. *et al.* (2010) 'Seeded Aggregation and Toxicity of a-Synuclein and Tau', *The Journal of Biological Chemistry*, 285(45), pp. 34885–34898. doi: 10.1074/jbc.M110.148460.

Nübling, G. S. *et al.* (2014) 'Modelling Ser129 phosphorylation inhibits membrane binding of pore-forming alpha-synuclein oligomers', *PLoS ONE*, 9(6), pp. 1–7. doi: 10.1371/journal.pone.0098906.

Nuñez, G. *et al.* (1990) 'Deregulated Bcl-2 gene expression selectively prolongs survival of growth factor-deprived hemopoietic cell lines', *The Journal of Immunology*, 144(9), pp. 3602–3610.

Nyholm, D., Klangemo, K. and Johansson, A. (2012) 'Levodopa / carbidopa intestinal gel infusion long-term therapy in advanced Parkinson's disease', *European Journal of Neurology*, (January 1991), pp. 1079–1085. doi: 10.1111/j.1468-1331.2012.03679.x.

O'Keeffe, G. W. and Sullivan, A. M. (2018) 'Evidence for dopaminergic axonal degeneration as an early pathological process in Parkinson's disease', *Parkinsonism and Related Disorders*, 56(May), pp. 9–15. doi: 10.1016/j.parkreldis.2018.06.025.

Oaks, A. W. *et al.* (2013) 'Age-Dependent Effects of A53T Alpha-Synuclein on Behavior and Dopaminergic Function', *PLoS ONE*, 8(4). doi: 10.1371/journal.pone.0060378.

Oertel, W. and Schulz, J. B. (2016) 'Current and experimental treatments of Parkinson disease: a guide for neuroscientists', *Journal of Neurochemistry*, 139(S1).

Ogen-Shtern, N., Ben David, T. and Lederkremer, G. Z. (2016) 'Protein aggregation and ER stress', *Brain Research*. Elsevier, 1648, pp. 658–666. doi: 10.1016/j.brainres.2016.03.044.

Ohgami, R. S. *et al.* (2005) 'Identification of a ferrireductase required for efficient transferrin-dependent iron uptake in erythroid cells', *Nature Genetics*, 37(11), pp. 1264–1269.

de Oliveira, R. M. *et al.* (2017) 'The mechanism of sirtuin 2–mediated exacerbation of alpha-synuclein toxicity in models of Parkinson disease', *PLoS Biology*, 15(3), pp. 1–27. doi: 10.1371/journal.pbio.2000374.

Oppenheim, R. W. *et al.* (1991) 'Control of Embryonic Motoneuron Survival in Vivo by Ciliary Neurotrophic Factor', *Science*, 251, pp. 1616–1619.

Orenstein, S. J. *et al.* (2013) 'Interplay of LRRK2 with chaperone-mediated autophagy', *Nature Publishing Group*. Nature Publishing Group, 16(4), pp. 394–406. doi: 10.1038/nn.3350.

Ostrerova-Golts, N. *et al.* (2000) 'The A53T a-Synuclein Mutation Increases Iron-Dependent Aggregation and Toxicity', *The Journal of Neuroscience*, 20(16), pp. 6048–6054.

Ostrerova, N. *et al.* (1999) ‘a-Synuclein Shares Physical and Functional Homology with 14-3-3 Proteins’, *The Journal of Neuroscience*, 19(14), pp. 5782–5791.

Oueslati, A. *et al.* (2013) ‘Polo-like kinase 2 regulates selective autophagic -synuclein clearance and suppresses its toxicity in vivo’, *Proceedings of the National Academy of Sciences*, 110(41), pp. E3945–E3954. doi: 10.1073/pnas.1309991110.

Oueslati, A. (2016) ‘Implication of Alpha-Synuclein Phosphorylation at S129 in Synucleinopathies: What Have We Learned in the Last Decade?’, *Journal of Parkinson’s Disease*, 6(1), pp. 39–51. doi: 10.3233/JPD-160779.

Oueslati, A., Fournier, M. and Lashuel, H. A. (2010) ‘Role of post-translational modifications in modulating thestructure, function and toxicity of alpha-synuclein: Impli-cations for Parkinson’s disease pathogenesis and therapies.’, *Progress in Brain Research*, 183(115–145).

Outeiro, T. F. *et al.* (2008) ‘Formation of toxic oligomeric α-synuclein species in living cells’, *PLoS ONE*, 3(4), pp. 1–9. doi: 10.1371/journal.pone.0001867.

PAIK, S. R. *et al.* (1999) ‘Copper(II)-induced self-oligomerization of α-synuclein’, *Biochemical Journal*, 340(3), pp. 821–828.

Paillusson, S. *et al.* (2017) ‘α-Synuclein binds to the ER–mitochondria tethering protein VAPB to disrupt Ca2+ homeostasis and mitochondrial ATP production’, *Acta Neuropathologica*. Springer Berlin Heidelberg, 134(1), pp. 129–149. doi: 10.1007/s00401-017-1704-z.

Paleologou, K. E. *et al.* (2009) ‘Detection of elevated levels of soluble α-synuclein oligomers in post-mortem brain extracts from patients with dementia with Lewy bodies’, *Brain*, 132(4), pp. 1093–1101. doi: 10.1093/brain/awn349.

Pan, K. *et al.* (1993) ‘Conversion of a-helices into B-sheets features in the formation of scrapie prion proteins’, *Biochemistry*, 90(December), pp. 10962–10966. doi: VL - 90.

Panicker, N. *et al.* (2015) ‘Fyn Kinase Regulates Microglial Neuroinflammatory Responses in Cell Culture and Animal Models of Parkinson’s Disease’, *Journal of Neuroscience*, 35(27), pp. 10058–10077. doi: 10.1523/JNEUROSCI.0302-15.2015.

Pant, S., Hilton, H. and Burczynski, M. E. (2012) ‘The multifaceted exosome: Biogenesis, role in normal and aberrant cellular function, and frontiers for pharmacological and biomarker opportunities’, *Biochemical Pharmacology*. Elsevier Inc., 83(11), pp. 1484–1494. doi: 10.1016/j.bcp.2011.12.037.

Paquet, S. *et al.* (2007) ‘Efficient dissemination of prions through preferential transmission to nearby cells’, *Journal of General Virology*, 88(2), pp. 706–713.

Parihar, M. S. *et al.* (2009) ‘Alpha-synuclein overexpression and aggregation exacerbates impairment of mitochondrial functions by augmenting oxidative stress in human neuroblastoma cells’, *International Journal of Biochemistry and Cell Biology*, 41(10), pp. 2015–2024. doi: 10.1016/j.biocel.2009.05.008.

Park, I.-H. *et al.* (2008) ‘Reprogramming of human somatic cells to pluripotency with defined factors.’, *Nature*, 451(7175), pp. 141–6. doi: 10.1038/nature06534.

Parkinson’s UK (2018) *The incidence and prevalence of Parkinson’s disease in the UK*. Available at: https://www.parkinsons.org.uk/professionals/resources/incidence-and-prevalence-parkinsons-uk-report.

Pastrana, M. A. *et al.* (2006) ‘Isolation and characterization of a proteinase K-sensitive PrPSc fraction’, *Biochemistry*, 45(51), pp. 15710–15717. doi: 10.1021/bi0615442.

Pattison, I. H. (1965) ‘Resistance of the Scrapie Agent to Formalin’, *Journal of Comparative Pathology*, 75(2), pp. 159–164.

Paxinou, E. *et al.* (2001a) ‘Induction of alpha-synuclein aggregation by intracellular nitrative insult.’, *The Journal of neuroscience : the official journal of the Society for Neuroscience*, 21(20), pp. 8053–61.

Paxinou, E. *et al.* (2001b) ‘Induction of alpha-synuclein aggregation by intracellular nitrative insult.’, *The Journal of Neuroscience*, 21(20), pp. 8053–61. Available at: http://www.ncbi.nlm.nih.gov/pubmed/11588178.

Pchelina, S. N., Emel’ianov, A. K. and Usenko, T. S. (2014) ‘Molecular basis of Parkinson’s disease linked with mutations in the LRRK2 gene.’, *Molecular Biology*, 48(1), pp. 3–14. doi: 10.1134/S0026893314010117.

Peng, Y. *et al.* (2010) ‘Binding of α-synuclein with Fe(III) and with Fe(II) and biological implications of the resultant complexes’, *Journal of Inorganic Biochemistry*. Elsevier Inc., 104(4), pp. 365–370. doi: 10.1016/j.jinorgbio.2009.11.005.

Perez-lloret, S. and Barrantes, F. J. (2016) ‘Deficits in cholinergic neurotransmission and their clinical correlates in Parkinson ’ s disease’, *Nature Publishing Group*. Nature Publishing Group, (September 2015). doi: 10.1038/npjparkd.2016.1.

Perez, R. G. *et al.* (2002) ‘A Role for a-Synuclein in the Regulation of Dopamine Biosynthesis’, *The Journal of Neuroscience*, 22(8), pp. 3090–3099.

Perier, C. and Vila, M. (2012) ‘Mitochondrial Biology and Parkinson’s Disease’, *Cold Spring Harbor Perspectives in Medicine*, 4(a009332), pp. 1–19. doi: 10.1101/cshperspect.a009332.

Phan, J. A. *et al.* (2017a) ‘Early synaptic dysfunction induced by α-synuclein in a rat model of Parkinson’s disease’, *Scientific Reports*. Springer US, 7(1), pp. 1–17. doi: 10.1038/s41598-017-06724-9.

Phan, J. A. *et al.* (2017b) ‘Early synaptic dysfunction induced by α-synuclein in a rat model of Parkinson’s disease’, *Scientific Reports*. Springer US, 7(1), pp. 1–17. doi: 10.1038/s41598-017-06724-9.

Phu, A. *et al.* (2018) ‘G2019S LRRK2 enhances the neuronal transmission of tau in the mouse brain’, *Human Molecular Genetics*, 27(1), pp. 120–134. doi: 10.1093/hmg/ddx389.

Pickrell, A. M. and Youle, R. J. (2015) ‘Review The Roles of PINK1 , Parkin , and Mitochondrial Fidelity in Parkinson ’ s Disease’, *Neuron*. Elsevier Inc., 85(2), pp. 257–273. doi: 10.1016/j.neuron.2014.12.007.

Pihán, P., Carreras-Sureda, A. and Hetz, C. (2017) ‘BCL-2 family: Integrating stress responses at the ER to control cell demise’, *Cell Death and Differentiation*. Nature Publishing Group, 24(9), pp. 1478–1487. doi: 10.1038/cdd.2017.82.

Pitts, M. W. *et al.* (2014) ‘Selenoproteins in Nervous System Development and Function’, *Biological Trace Element Research*, 161(3), pp. 231–245. doi: 10.1007/s12011-014-0060-2.

Plotegher, N. *et al.* (2014) ‘Biophysical groundwork as a hinge to unravel the biology of α-synuclein aggregation and toxicity’, *Quarterly Review of Biophysics*, 47(1), pp. 1–48.

Pochapsky, T. C. (2015) ‘From intrinsically disordered protein to context-dependent folding : The α -synuclein tetramer is teased out of hiding’, *Proceedings of the National Academy of Sciences of the United States of America*, 112(31), pp. 9502–9503. doi: 10.1073/pnas.1512077112.

Pöltl, D. *et al.* (2012) ‘Uncoupling of ATP-depletion and cell death in human dopaminergic neurons’, *NeuroToxicology*, 33(4), pp. 769–779. doi: 10.1016/j.neuro.2011.12.007.

Poluha, W. *et al.* (1996) 'The cyclin-dependent kinase inhibitor p21 (WAF1) is required for survival of differentiating neuroblastoma cells.', *Molecular and Cellular Biology*, 16(4), pp. 1335–1341. doi: 10.1128/mcb.16.4.1335.

Polymeropoulos, M. H. *et al.* (1997) 'Mutation in the alpha-Synuclein Gene Identified in Families with Parkinson's Disease', *Science*, 276(June), pp. 2045–2048.

Porcari, R. *et al.* (2015) 'The H50Q Mutation Induces a 10-fold Decrease in the Solubility of a-Synuclein', *The Journal of Biological Chemistry*, 290(4), pp. 2395–2404. doi: 10.1074/jbc.M114.610527.

Pound, P. and Bracken, M. B. (2014) 'Is animal research sufficiently evidence based to be a cornerstone of biomedical research?', *Bmj*, 348(may30 1), pp. g3387–g3387. doi: 10.1136/bmj.g3387.

Prakash, S. *et al.* (2004) 'An unstructured initiation site is required for efficient proteasome-mediated degradation', *Nature Structural & Molecular Biology*, 11, pp. 830–837.

Pranke, I. M. *et al.* (2011) 'a-Synuclein and ALPS motifs are membrane curvature sensors whose contrasting chemistry mediates selective vesicle binding', *Journal of Biological Chemistry*, 194(1), pp. 89–103. doi: 10.1083/jcb.201011118.

Presgraves, S. P. *et al.* (2004) 'Terminally differentiated SH-SY5Y cells provide a model system for studying neuroprotective effects of dopamine agonists', *Neurotox.Res.*, 5(8), pp. 579–598.

Properzi, F. *et al.* (2015) 'Detection of exosomal prions in blood by immunochemistry techniques', *Journal of General Virology*, 96(7), pp. 1969–1974.

Proukakis, C. *et al.* (2013) 'A novel alpha-synuclein missense mutation in PD', *Neurology*, 80, pp. 1062–1064. doi: 10.1212/WNL.0b013e31828727ba.

Prusiner, S. (1982) 'Novel proteinaceous infectious particles cause scrapie', *Science*, 216(4542), pp. 136–144. doi: 10.1126/science.6801762.

Prusiner, S. B. *et al.* (1982) 'Further Purification and Characterization of Scrapie Prions', *Biochemistry*, 21(26), pp. 6942–6950. doi: 10.1021/bi00269a050.

Przedborski, S. and Jackson-Lewis, V. (1998) 'Mechanisms of MPTP toxicity', *Movement Disorders*, 13(S1), pp. 35–38.

Qing, H. *et al.* (2009) 'Lrrk2 interaction with α-synuclein in diffuse Lewy body disease', *Biochemical and Biophysical Research Communications*. Elsevier Inc., 390(4), pp. 1229–1234. doi: 10.1016/j.bbrc.2009.10.126.

Ransohoff, R. M. (2016) 'How neuroinflammation contributes to neurodegeneration', *Science*, 353(6301), pp. 777–783. doi: 10.1126/science.aag2590.

Rasia, R. M. *et al.* (2005) 'Structural characterization of copper(II) binding to -synuclein: Insights into the bioinorganic chemistry of Parkinson's disease', *Proceedings of the National Academy of Sciences*, 102(12), pp. 4294–4299. doi: 10.1073/pnas.0407881102.

Recasens, A. *et al.* (2014) 'Lewy Body Extracts from Parkinson Disease Brains Trigger a-Synuclein Pathology and Neurodegeneration in Mice and Monkeys', *Annals of Neurology*, 75(3), pp. 351–362. doi: 10.1002/ana.24066.

Redza-dutordoir, M. and Averill-bates, D. A. (2016) 'Activation of apoptosis signalling pathways by reactive oxygen species', *BBA - Molecular Cell Research*. Elsevier B.V., 1863(12), pp. 2977–2992. doi: 10.1016/j.bbamcr.2016.09.012.

Reeve, A. K. *et al.* (2015a) 'Aggregated α-synuclein and complex I deficiency: Exploration of

their relationship in differentiated neurons', *Cell Death and Disease*. Nature Publishing Group, 6(7), pp. e1820-10. doi: 10.1038/cddis.2015.166.

Reeve, A. K. *et al.* (2015b) 'Aggregated α-synuclein and complex I deficiency: Exploration of their relationship in differentiated neurons', *Cell Death and Disease*. Nature Publishing Group, 6(7), pp. e1820-10. doi: 10.1038/cddis.2015.166.

Reeve, A., Simcox, E. and Turnbull, D. (2014) 'Ageing and Parkinson's disease: why is advancing age the biggest risk factor?', *Ageing Research Reviews*, 14(100), pp. 19–30.

Reinert, A. *et al.* (2019) 'Iron concentrations in neurons and glial cells with estimates on ferritin concentrations', *BMC Neuroscience*. BioMed Central, pp. 1–14. doi: 10.1186/s12868-019-0507-7.

Repetto, M. G., Ferrarotti, N. F. and Boveris, A. (2010) 'The involvement of transition metal ions on iron-dependent lipid peroxidation', *Archives of Toxicology*, 84, pp. 255–262. doi: 10.1007/s00204-009-0487-y.

Rey, N. L. *et al.* (2013) 'Transfer of human α-synuclein from the olfactory bulb to interconnected brain regions in mice', *Acta Neuropathologica*, 126(4), pp. 555–573. doi: 10.1007/s00401-013-1160-3.

Reyes, J. F. *et al.* (2015) 'A cell culture model for monitoring α-synuclein cell-to-cell transfer', *Neurobiology of Disease*. Elsevier B.V., 77, pp. 266–275. doi: 10.1016/j.nbd.2014.07.003.

Rhodes, S. L. and Ritz, B. (2013) 'Genetics of iron regulation and the possible role of iron in Parkinson's disease', *Neurobiology of Disease*, 32(2), pp. 183–195. doi: 10.1016/j.nbd.2008.07.001.Rhodes.

Richardson, D. R. *et al.* (2010) 'Mitochondrial iron trafficking and the integration of iron metabolism between the mitochondrion and cytosol', *Proceedings of the National Academy of Sciences of the United States of America*, 107(24). doi: 10.1073/pnas.0912925107.

Richarme, G. *et al.* (2015) 'Parkinsonism-associated Protein DJ-1 / Park7 Is a Major Protein Deglycase That Repairs Methylglyoxal- and Glyoxal-glycated Cysteine , Arginine , and Lysine Residues', *The Journal of Biological Chemistry*, 290(3), pp. 1885–1897. doi: 10.1074/jbc.M114.597815.

Riederer, P. and Laux, G. (2011) 'MAO-inhibitors in Parkinson ' s Disease', *Experimental Neurobiology*, 20(March), pp. 1–17. doi: 10.5607/en.2011.20.1.1.

Riek, R. *et al.* (1996) 'NMR structure of the mouse prion protein PrP (121-231)', *Nature Letter*, 382, pp. 180–182.

Robert, G. *et al.* (2012) 'The caspase 6 derived N-terminal fragment of DJ-1 promotes apoptosis via increased ROS production', *Cell Death and Differentiation*. Nature Publishing Group, 19(11), pp. 1769–1778. doi: 10.1038/cdd.2012.55.

Robertson, C. *et al.* (2006) 'Cellular prion protein is released on exosomes from activated platelets Cellular prion protein is released on exosomes from activated platelets', *Hematology*, 107(10), pp. 3907–3911. doi: 10.1182/blood-2005-02-0802.

Ronai, Z. A. (2016) 'Monoubiquitination in proteasomal degradation', *Proceedings of the National Academy of Sciences*, 113(32), pp. 8894–8896. doi: 10.1073/pnas.1610186113.

Ronzitti, G. *et al.* (2014) 'Exogenous -Synuclein Decreases Raft Partitioning of Cav2.2 Channels Inducing Dopamine Release', *Journal of Neuroscience*, 34(32), pp. 10603–10615. doi: 10.1523/jneurosci.0608-14.2014.

Rospigliosi, C. C. *et al.* (2009) 'The E46K Parkinson's-linked mutation enhances C- to N-terminal contacts in α-synuclein', *Journal of Molecular Biology*, 388(5), pp. 1022–1032. doi:

10.1002/ana.22528.Toll-like.

Rott, R. *et al.* (2008) ‘Monoubiquitylation of α-Synuclein by seven in absentia homolog (SIAH) promotes its aggregation in dopaminergic cells’, *Journal of Biological Chemistry*, 283(6), pp. 3316–3328. doi: 10.1074/jbc.M704809200.

Rouault, T. A. (2013) ‘Iron metabolism in the CNS : implications for neurodegenerative diseases’, *Nature Publishing Group*. Nature Publishing Group, (14), pp. 551–564. doi: 10.1038/nrn3453.

Rousseau, A. and Bertolotti, A. (2018) ‘Regulation of proteasome assembly and activity in health and disease’, *Nature Reviews Molecular Cell Biology*. Springer US, 19, pp. 697–712. doi: 10.1038/s41580-018-0040-z.

Rout, A. K. *et al.* (2014) ‘Structure of Transmembrane Domain of Lysosome-associated Membrane Protein Type 2a (LAMP-2A) Reveals Key Features for Substrate Specificity in Chaperone-mediated Autophagy’, *The Journal of Biological Chemistry*, 289(51), pp. 35111–35123. doi: 10.1074/jbc.M114.609446.

Rowe, C. C. *et al.* (2014) ‘Predicting Alzheimer Disease with b -Amyloid Imaging : Results from the Australian Imaging , Biomarkers , and Lifestyle Study of Ageing’, *Annals of Neurology*, 74, pp. 905–913. doi: 10.1002/ana.24040.

Rubinsztein, D. C., Mariño, G. and Kroemer, G. (2011) ‘Autophagy and aging’, *Cell*, 146(5), pp. 682–695. doi: 10.1016/j.cell.2011.07.030.

Rudge, P. *et al.* (2015) ‘Iatrogenic CJD due to pituitary-derived growth hormone with genetically determined incubation times of up to 40 years’, *Brain*, 138(11), pp. 3386–3399. doi: 10.1093/brain/awv235.

Rustom, A. *et al.* (2004) ‘Nanotubular Highways for Intercellular Organelle Transport’, *Science*, 303(5660), pp. 1007–1010. doi: 10.1126/science.1093133.

Ryan, B. J. *et al.* (2015) ‘Mitochondrial dysfunction and mitophagy in Parkinson ’ s : from familial to sporadic disease’, *Trends in Biochemical Sciences*. Elsevier Ltd, 40(4), pp. 200–210. doi: 10.1016/j.tibs.2015.02.003.

Ryu, E. J. *et al.* (2002) ‘Endoplasmic reticulum stress and the unfolded protein response in cellular models of Parkinson’s disease’, *The Journal of Neuroscience*, 22(24), pp. 10690–10698.

Ryu, M. Y. *et al.* (2008) ‘Localization of CKII β subunits in Lewy bodies of Parkinson’s disease’, *Journal of the Neurological Sciences*, 266(1–2), pp. 9–12. doi: 10.1016/j.jns.2007.08.027.

Saá, P. *et al.* (2014) ‘First demonstration of transmissible spongiform encephalopathy-associated prion protein (PrPTSE) in extracellular vesicles from plasma of mice infected with mouse-adapted variant creutzfeldt-jakob disease by in vitro amplification’, *Journal of Biological Chemistry*, 289(42), pp. 29247–29260. doi: 10.1074/jbc.M114.589564.

Saborio, G. P., Permanne, B. and Soto, C. (2001) ‘Sensitive detection of pathological prion protein by cyclic amplification of protein misfolding’, *Nature*, 411(6839), pp. 810–813.

Sacino, A. N. *et al.* (2013) ‘Conformational templating of α-synuclein aggregates in neuronal-glial cultures’, *Molecular Neurodegeneration*. Molecular Neurodegeneration, 8(1), p. 1. doi: 10.1186/1750-1326-8-17.

Sacino, A. N. *et al.* (2014) ‘Amyloidogenic α-synuclein seeds do not invariably induce rapid, widespread pathology in mice’, *Acta Neuropathologica*, 127, pp. 645–665. doi: 10.1007/s00401-014-1268-0.

Saha, A. R. *et al.* (2000) 'SHORT COMMUNICATION Induction of neuronal death by a -synuclein', *European Journal of Neuroscience*, 12(September 1999), pp. 3073–3077.

Sala, G. *et al.* (2016) 'Rotenone down-regulates HSPA8/hsc70 chaperone protein in vitro: A new possible toxic mechanism contributing to Parkinson's disease', *NeuroToxicology*. Elsevier B.V., 54, pp. 161–169. doi: 10.1016/j.neuro.2016.04.018.

Sampathu, D. M. *et al.* (2003) 'Ubiquitination of α-synuclein is not required for formation of pathological inclusions in α-synucleinopathies', *American Journal of Pathology*, 163(1), pp. 91–100. doi: 10.1016/S0002-9440(10)63633-4.

Sanders, L. H. *et al.* (2014) 'LRRK2 mutations cause mitochondrial DNA damage in iPSC-derived neural cells from Parkinson's disease patients: Reversal by gene correction', *Neurobiology of Disease*, 62, pp. 1–13. doi: 10.1016/j.nbd.2013.10.013.LRRK2.

Sardi, S. P., Cheng, S. H. and Shihabuddin, L. S. (2015) 'Gaucher-related synucleinopathies: The examination of sporadic neurodegeneration from a rare (disease) angle', *Progress in Neurobiology*. Elsevier Ltd, 125, pp. 47–62. doi: 10.1016/j.pneurobio.2014.12.001.

Saric, T., Graef, C. I. and Goldberg, A. L. (2004) 'Pathway for Degradation of Peptides Generated by Proteasomes', *The Journal of Biological Chemistry*, 279(45), pp. 46723–46732. doi: 10.1074/jbc.M406537200.

Sasaki, A. *et al.* (2015) 'Sensitive western blotting for detection of endogenous Ser129-phosphorylated α-synuclein in intracellular and extracellular spaces', *Scientific Reports*. Nature Publishing Group, 5(May), pp. 1–15. doi: 10.1038/srep14211.

Sato, M. *et al.* (2018) 'The ferroptosis inducer erastin irreversibly inhibits system x c − and synergizes with cisplatin to increase cisplatin's cytotoxicity in cancer cells', *Scientific Reports*. Springer US, (June 2017), pp. 1–9. doi: 10.1038/s41598-018-19213-4.

Sattler, T. and Mayer, A. (2000) 'Cell-free Reconstitution of Microautophagic Vacuole Invagination and Vesicle Formation', *The Journal of Cell*, 151(3), pp. 529–538.

Sborgi, L. *et al.* (2016) 'GSDMD membrane pore formation constitutes the mechanism of pyroptotic cell death', *The EMBO Journal*, 35(16), pp. 1766–1778.

Schafer, B. *et al.* (2009) 'Mitochondrial Outer Membrane Proteins Assist Bid in Bax-mediated Lipidic Pore Formation', *Molecular Biology of the Cell*, 20, pp. 2276–2285. doi: 10.1091/mbc.E08.

Schapira, A. H. V. (2015) 'Glucocerebrosidase and Parkinson disease : Recent advances', *Molecular and Cellular Neuroscienceo*, 66(0 0), pp. 37–42. doi: 10.1016/j.mcn.2015.03.013.Glucocerebrosidase.

Schildknecht, S. *et al.* (2009) 'Requirement of a dopaminergic neuronal phenotype for toxicity of low concentrations of 1-methyl-4-phenylpyridinium to human cells', *Toxicology and Applied Pharmacology*. Elsevier Inc., 241(1), pp. 23–35. doi: 10.1016/j.taap.2009.07.027.

Schmidt, F. *et al.* (2012) 'Single-channel electrophysiology reveals a distinct and uniform pore complex formed by α-synuclein oligomers in lipid membranes', *PLoS ONE*, 7(8), pp. 1–7. doi: 10.1371/journal.pone.0042545.

Schmittgen, T. D. and Livak, K. J. (2008) 'Analyzing real-time PCR data by the comparative CT method', *Nature Protocols*, 3(6), pp. 1101–1108. doi: 10.1038/nprot.2008.73.

Schneider, J. L., Suh, Y. and Cuervo, A. M. (2014) 'Deficient Chaperone-Mediated Autophagy in Liver Leads to Metabolic Dysregulation', *Cell Metabolism*. Elsevier Inc., 20(3), pp. 417–432. doi: 10.1016/j.cmet.2014.06.009.

Scholz, D. *et al.* (2011) 'Rapid, complete and large-scale generation of post-mitotic neurons from the human LUHMES cell line', *Journal of Neurochemistry*, 119(5), pp. 957–971. doi: 10.1111/j.1471-4159.2011.07255.x.

Schöndorf, D. C. *et al.* (2014) 'IPSC-derived neurons from GBA1-associated Parkinson's disease patients show autophagic defects and impaired calcium homeostasis', *Nature Communications*, 5(May). doi: 10.1038/ncomms5028.

Schüle, B., Pera, R. A. R. and Langston, J. W. (2009) 'Can cellular models revolutionize drug discovery in Parkinson's disease?', *Biochimica et Biophysica Acta - Molecular Basis of Disease*. Elsevier B.V., 1792(11), pp. 1043–1051. doi: 10.1016/j.bbadis.2009.08.014.

Schulman, B. A. and Harper, J. W. (2009) 'Ubiquitin-like protein activation by E1 enzymes: the apex for downstream signaling pathways', *Nature Reviews Molecular Cell Biology*, 10(5), pp. 319–331. doi: 10.1038/nrm2673.Ubiquitin-like.

Scott, D. A. *et al.* (2010) 'A Pathologic Cascade Leading to Synaptic Dysfunction in -Synuclein-Induced Neurodegeneration', *Journal of Neuroscience*, 30(24), pp. 8083–8095. doi: 10.1523/jneurosci.1091-10.2010.

Shabek, N. *et al.* (2012) 'The Size of the Proteasomal Substrate Determines Whether Its Degradation Will Be Mediated by Mono- or Polyubiquitylation', *Molecular Cell*. Elsevier Inc., 48(1), pp. 87–97. doi: 10.1016/j.molcel.2012.07.011.

Shan, Z. *et al.* (2016) 'Establishment of a simple cell-based ELISA for the direct detection of abnormal isoform of prion protein from prion-infected cells without cell lysis and proteinase K treatment', *Prion*, 10(4), pp. 305–318. doi: 10.1080/19336896.2016.1189053.

Shavali, S. *et al.* (2008) 'Mitochondrial localization of alpha-synuclein protein in alpha-synuclein overexpressing cells', *Neuroscience Letters*, 439(2), pp. 125–128. doi: 10.1016/j.neulet.2008.05.005.

Shaw, G. *et al.* (2002) 'Preferential transformation of human neuronal cells by human adenoviruses and the origin of HEK293', *The FASEB Journal*, 16(8).

Sheelakumari, R. *et al.* (2017) 'Assessment of iron deposition in the brain in frontotemporal dementia and its correlation with behavioral traits', *American Journal of Neuroradiology*, 38(10), pp. 1953–1958. doi: 10.3174/ajnr.A5339.

Shendelman, S. *et al.* (2004) 'DJ-1 Is a Redox-Dependent Molecular Chaperone That Inhibits a -Synuclein Aggregate Formation', *PLoS Biology*, 2(11). doi: 10.1371/journal.pbio.0020362.

Shim, H. J. *et al.* (2014) 'High-Dose Irradiation Induces Cell Cycle Arrest, Apoptosis, and Developmental Defects during Drosophila Oogenesis', *PLoS ONE*, 9(2), p. e89009. doi: 10.1371/journal.pone.0089009.

Shimoji, M. *et al.* (2005) 'Absence of inclusion body formation in the MPTP mouse model of Parkinson's disease', *Molecular Brain Research*, 134(1), pp. 103–108. doi: 10.1016/j.molbrainres.2005.01.012.

Shrivastava, A. N. *et al.* (2015) 'K + -ATPase and impair Na + gradient', *The EMBO Journal*, 34(19), pp. 2408–2423.

Shrivastava, A. N. *et al.* (2020) 'Differential Membrane Binding and Seeding of Distinct a -Synuclein Fibrillar Polymorphs', *Biophysical Journal*. Biophysical Society, 118(5), pp. 1301–1320. doi: 10.1016/j.bpj.2020.01.022.

Shults, C. W. (2006) 'Lewy bodies', *Proceedings of the National Academy of Sciences*, 103(6), pp. 1661–1668. doi: 10.1073/pnas.0509567103.

Sian, J. *et al.* (1994) 'Alterations in glutathione levels in Parkinson's disease and other neurodegenerative disorders affecting basal ganglia', *Annals of Neurology*, 36(3), pp. 348–355.

Sian, J. and Peter, H. (2020) 'The role of alpha - synuclein as ferrireductase in neurodegeneration associated with Parkinson ' s disease', *Journal of Neural Transmission*. Springer Vienna, (0123456789). doi: 10.1007/s00702-020-02192-0.

Sidransky, E. *et al.* (2009) 'Multicenter Analysis of Glucocerebrosidase Mutations in Parkinson's disease', *New England Journal of Medicine*, 361, pp. 1651–1661.

Silveira, J. R. *et al.* (2005) 'The most infectious prion protein particles', *Nature*, 437(7056), pp. 257–261. doi: 10.1016/S0140-6736(02)11602-3.Association.

Singh, P. K. *et al.* (2013) 'Curcumin Modulates α - Synuclein Aggregation and Toxicity', *ACS Chemical Neuroscience*, 4, pp. 393–407. doi: 10.1021/cn3001203.

Singleton, A. B. *et al.* (2003) 'alpha-Synuclein Locus Triplication Causes Parkinson's Disease', *Science*, 302(October). doi: 10.1126/science.1090278.

Sipe, J. C., Lee, P. and Beutler, E. (2002) 'Brain Iron Metabolism and Neurodegenerative Disorders', *Developmental Neuroscience*, 24, pp. 188–196.

Sipe, J. D. *et al.* (2014) 'Nomenclature 2014: Amyloid fibril proteins and clinical classification of the amyloidosis', *Amyloid*, 21(4), pp. 221–224. doi: 10.3109/13506129.2014.964858.

Sipe, J. D. *et al.* (2016) 'Amyloid fibril proteins and amyloidosis: chemical identification and clinical classification International Society of Amyloidosis 2016 Nomenclature Guidelines', *Amyloid*, 23(4), pp. 209–213. doi: 10.1080/13506129.2016.1257986.

Smidt, M. P. and Burbach, J. P. H. (2007) 'How to make a mesodiencephalic dopaminergic neuron', *Nature Reviews Neuroscience*, 8(January), pp. 21–32. doi: 10.1038/nrn2039.

Smirnova, L. *et al.* (2016) 'A LUHMES 3D dopaminergic neuronal model for neurotoxicity testing allowing long-term exposure and cellular resilience analysis', *Archives of Toxicology*. Springer Berlin Heidelberg, 90(11), pp. 2725–2743. doi: 10.1007/s00204-015-1637-z.

Smith, D. M. *et al.* (2005) 'ATP Binding to PAN or the 26S ATPases Causes Association with the 20S Proteasome , Gate Opening , and Translocation of Unfolded Proteins', *Molecular Cell*, 20, pp. 687–698. doi: 10.1016/j.molcel.2005.10.019.

Smith, D. P. *et al.* (2008) 'Formation of a high affinity lipid-binding intermediate during the early aggregation phase of α-synuclein', *Biochemistry*, 47(5), pp. 1425–1434. doi: 10.1021/bi701522m.

Smith, R. A. S. *et al.* (2015) 'Analysis of toxic amyloid fibril interactions at natively derived membranes by ellipsometry', *PLoS ONE*, 10(7), pp. 1–15. doi: 10.1371/journal.pone.0132309.

Smith, W. W. *et al.* (2005) 'Endoplasmic reticulum stress and mitochondrial cell death pathways mediate A53T mutant alpha-synuclein-induced toxicity', *Human Molecular Genetics*, 14(24), pp. 3801–3811. doi: 10.1093/hmg/ddi396.

Smith, Y. *et al.* (2012) 'Parkinson's disease therapeutics: New developments and challenges since the introduction of levodopa', *Neuropsychopharmacology*. Nature Publishing Group, 37(1), pp. 213–246. doi: 10.1038/npp.2011.212.

Sofic, E. *et al.* (1988) 'Increased iron (III) and total iron content in post mortem substantia nigra of parkinsonian brain.', *Journal of Neural Transmission*, 74(3).

Soldner, F. *et al.* (1999) 'MPP+ inhibits proliferation of PC12 cells by a p21(WAF1/Cip1)-

dependent pathway and induces cell death in cells lacking p21(WAF1/Cip1)', *Experimental Cell Research*, 250(1), pp. 75–85. doi: 10.1006/excr.1999.4504.

Soliman, Y. *et al.* (2009) 'The effects of piroxicam in the attenuation of MPP+/MPTP toxicity in vitro and in vivo', *Neurochemical Research*, 34(2), pp. 304–310. doi: 10.1007/s11064-008-9779-5.

Spillantini, M. *et al.* (1997) 'alpha-Synuclein in Lewy bodies', *Nature*, 388, pp. 839–841.

Spillantini, M. G., Divane, A. and Goedert, M. (1995) 'Assignment of human alpha-synuclein (SNCA) and beta-synuclein (SNCB) genes to chromosomes 4q21 and 5q35.', *Genomics*, pp. 379–81. doi: 10.1006/geno.1995.1063.

Spinelli, K. J. *et al.* (2014) 'Presynaptic Alpha-Synuclein Aggregation in a Mouse Model of Parkinson's Disease', *Journal of Neuroscience*, 34(6), pp. 2037–2050. doi: 10.1523/jneurosci.2581-13.2014.

Srivastava, S. *et al.* (2015) 'Post-conversion sialylation of prions in lymphoid tissues', *Proceedings of the National Academy of Sciences*, 112(48), pp. E6654–E6662. doi: 10.1073/pnas.1517993112.

Srivastava, S. and Baskakov, I. V. (2015) 'Contrasting effects of two lipid cofactors of prion replication on the conformation of the prion protein', *PLoS ONE*, 10(6), pp. 1–16. doi: 10.1371/journal.pone.0130283.

Stahl, N. *et al.* (1987) 'Scrapie prion protein contains a phosphatidylinositol glycolipid', *Cell*, 51(2), pp. 229–240.

Stefanis, L. *et al.* (2019) 'How is alpha-synuclein cleared from the cell?', *Journal of Neurochemistry*, pp. 1–14. doi: 10.1111/jnc.14704.

Stefanova, N. *et al.* (2001) 'Glial Cell Death Induced by Overexpression of a-Synuclein', *Journal of Neuroscience Research*, 65(February), pp. 432–438.

Stelzmann, R. a., Schnitzlein, H. N. and Murtagh, F. R. (1995) 'An English translation of Alzheimer's 1907 Paper "Uber eine eigenartige Erlranliung der Hirnrinde"', *Clinical Anatomy*, 8, pp. 429–431. doi: 10.1068/p5028.

Stuendl, A. *et al.* (2016) 'Induction of α-synuclein aggregate formation by CSF exosomes from patients with Parkinson's disease and dementia with Lewy bodies', *Brain*, 139(2), pp. 481–494. doi: 10.1093/brain/awv346.

Sun, J. *et al.* (2019) 'Functional cooperation of α -synuclein and VAMP2 in synaptic vesicle recycling', *Proceedings of the National Academy of Sciences of the United States of Americao*, 116(23). doi: 10.1073/pnas.1903049116.

Sun, L. *et al.* (2018) 'Lack of PINK1 alters glia innate immune responses and enhances mediated neuron death', *Scientific Reports*, 8(December 2017), pp. 1–16. doi: 10.1038/s41598-017-18786-w.

Sun, Y. *et al.* (2012) 'Voltage-dependent anion channels (VDACs) recruit parkin to defective mitochondria to promote mitochondrial autophagy', *Journal of Biological Chemistry*, 287(48), pp. 40652–40660. doi: 10.1074/jbc.M112.419721.

Supattapone, S. (2004) 'Prion protein conversion in vitro', *Journal of Molecular Medicine*, 82(6), pp. 348–356. doi: 10.1007/s00109-004-0534-3.

Suraweera, A. *et al.* (2012) 'Failure of Amino Acid Homeostasis Causes Cell Death following Proteasome Inhibition', *Molecular Cell*, 6, pp. 242–253. doi: 10.1016/j.molcel.2012.08.003.

Surmeier, D. J., Obeso, J. A. and Halliday, G. M. (2017) 'Selective neuronal vulnerability in

Parkinson disease', *Nature Reviews Neuroscience*, 18(2), pp. 101–113. doi: 10.1038/nrn.2016.178.

Surmeier, D. J. and Schumacker, P. T. (2013) 'Calcium, bioenergetics, and neuronal vulnerability in Parkinson's disease', *Journal of Biological Chemistry*, 288(15), pp. 10736–10741. doi: 10.1074/jbc.R112.410530.

Suzanne, M. and Steller, H. (2013) 'Shaping organisms with apoptosis', *Cell Death and Differentiation*. Nature Publishing Group, 20(5), pp. 669–675. doi: 10.1038/cdd.2013.11.

Sveinbjornsdottir, S. (2016) 'The clinical symptoms of Parkinson's disease', *Journal of Neurochemistry*, 139(S1), pp. 318–324.

Swatek, K. N. and Komander, D. (2016) 'Ubiquitin modifications', *Cell Research*. Nature Publishing Group, 26(4), pp. 399–422. doi: 10.1038/cr.2016.39.

Taguchi, K. *et al.* (2016) 'Brain Region-Dependent Differential Expression of alpha-Synuclein', *The Journal of Comparative Neurology*, 1258, pp. 1236–1258. doi: 10.1002/cne.23901.

Takahashi, K. *et al.* (2007) 'Induction of pluripotent stem cells from adult human fibroblasts by defined factors', *Cell*, 131, pp. 861–872. doi: 10.1097/01.ogx.0000305204.97355.0d.

Takahashi, K. and Yamanaka, S. (2006) 'Induction of pluripotent stem cells from mouse embryonic and adult fibroblast cultures by defined factors.', *Cell*, 126(4), pp. 663–76. doi: 10.1016/j.cell.2006.07.024.

Takahashi, M. *et al.* (2007) 'Oxidative stress-induced phosphorylation, degradation and aggregation of α-synuclein are linked to upregulated CK2 and cathepsin D', *European Journal of Neuroscience*, 26(4), pp. 863–874. doi: 10.1111/j.1460-9568.2007.05736.x.

Takeda, A. *et al.* (1998) 'Abnormal Accumulation of NACP/alpha-Synuclein in Neurodegenerative Disorders', *American Journal of Pathology*, 152(2), pp. 367–372.

Tan, S., Schubert, D. and Maher, P. (2001) 'Oxytosis: a novel form of programmed cell death', *Current Tpoics in Medicinal Chemistry*, 1(6), pp. 497–506.

Tanaka, Y. *et al.* (2001) 'Inducible expression of mutant alpha-synuclein decreases proteasome activity and increases senstivity to mitochondria-dependent apoptosis', *Human Molecular Genetics*, 10(9), pp. 919–926.

Tang-Schomer, M. D. *et al.* (2014) 'Bioengineered functional brain-like cortical tissue', *Proceedings of the National Academy of Sciences*, 111(38), pp. 13811–13816. doi: 10.1073/pnas.1324214111.

Tatton, N. A. (2000) 'Increased Caspase 3 and Bax Immunoreactivity Accompany Nuclear GAPDH Translocation and Neuronal Apoptosis in Parkinson ' s Disease', *Experimental Neurology*, 166, pp. 29–43. doi: 10.1006/exnr.2000.7489.

Tatton, N. A. and Kish, S. J. (1997) 'IN SITU DETECTION OF APOPTOTIC NUCLEI IN THE SUBSTANTIA NIGRA COMPACTA OF MICE USING TERMINAL DEOXYNUCLEOTIDYL TRANSFERASE LABELLING AND ACRIDINE ORANGE STAINING', *Neuroscience*, 77(4), pp. 1037–1048.

Tavassoly, O. *et al.* (2014) 'Cu (II) and dopamine bind to α-synuclein and cause large conformational changes', *FEBS Journal*, 281(12), pp. 2738–2753.

Taylor-Whiteley, T. R. *et al.* (2019) 'Recapitulating Parkinson's disease pathology in a three-dimensional human neural cell culture model', *Disease Models & Mechanisms*, 12(4), p. dmm038042. doi: 10.1242/dmm.038042.

Taylor, D. R. and Hooper, N. M. (2006) 'The prion protein and lipid rafts (Review)', *Molecular Membrane Biology*, 23(1), pp. 89–99. doi: 10.1080/09687860500449994.

Tekirdag, K. and Cuervo, A. M. (2018) 'Chaperone-mediated autophagy and endosomal microautophagy : Jointed by a chaperone', *The Journal of Biological Chemistry*, 293(10), pp. 5414–5424. doi: 10.1074/jbc.R117.818237.

Teppola, H. *et al.* (2016) 'Morphological Differentiation Towards Neuronal Phenotype of SH-SY5Y Neuroblastoma Cells by Estradiol, Retinoic Acid and Cholesterol', *Neurochemical Research*. Springer US, 41(4), pp. 731–747. doi: 10.1007/s11064-015-1743-6.

Theillet, F.-X. *et al.* (2016) 'Structural disorder of monomeric α-synuclein persists in mammalian cells', *Nature*. Nature Publishing Group, 530(7588), pp. 45–50. doi: 10.1038/nature16531.

Thomas, J. P. *et al.* (1990) 'Enzymatic reduction of phospholipid and cholesterol hydroperoxides in artificial bilayers and lipoproteins', *Biochimica et Biophysica Acta*, 1045(3), pp. 252–260.

Thomas, P. and Smart, T. G. (2005) 'HEK293 cell line: A vehicle for the expression of recombinant proteins', *Journal of Pharmacological and Toxicological Methods*, 51(3 SPEC. ISS.), pp. 187–200. doi: 10.1016/j.vascn.2004.08.014.

Todde, V., Veenhuis, M. and Klei, I. J. Van Der (2009) 'Autophagy: Principles and significance in health and disease', *Biochimica et Biophysica Acta*, 1792, pp. 3–13. doi: 10.1016/j.bbadis.2008.10.016.

De Toro, J. *et al.* (2015) 'Emerging roles of exosomes in normal and pathological conditions: new insights for diagnosis and therapeutic applications', *Frontiers in Immunology*.

Totterdell, S., Hanger, D. and Meredith, G. E. (2004) 'The ultrastructural distribution of alpha-synuclein-like protein in normal mouse brain', *Brain Research*, 1004(1–2), pp. 61–72. doi: 10.1016/j.brainres.2003.10.072.

Del Tredici, K. *et al.* (2002) 'Where does parkinson disease pathology begin in the brain?', *Journal of Neuropathology and Experimental Neurology*, 61(5), pp. 413–426.

Tremblay, R. G. *et al.* (2009) 'Differentiation of mouse Neuro 2A cells into dopamine neurons', *Journal of Neuroscience Methods*, 186(1), pp. 60–67. doi: 10.1016/j.jneumeth.2009.11.004.

Triplett, J. C. *et al.* (2015) 'Quantitative expression proteomics and phosphoproteomics profile of brain from PINK1 knockout mice: insights into mechanisms of familial Parkinson's disease', *Journal of Neurochemistry*, 133(5), pp. 750–765. doi: 10.1111/jnc.13039.

Tsigelny, I. F. *et al.* (2012) 'Role of a-synuclein penetration into the membrane in the mechanisms of oligomer pore formation', *FEBS Journal*, 279(6), pp. 1000–1013. doi: 10.1002/ana.22528.Toll-like.

Tuite, M. F. and Cox, B. S. (2003) 'Propagation of yeast prions', *Nature Reviews Molecular Cell Biology*, 4(11), pp. 878–889. doi: 10.1038/nrm1247.

Tyson, T., Steiner, J. A. and Brundin, P. (2016) 'Sorting out release, uptake and processing of alpha-synuclein during prion-like spread of pathology', *Journal of Neurochemistry*, 139, pp. 275–289. doi: 10.1111/jnc.13449.

Ueda, K. *et al.* (1993a) 'Molecular cloning of cDNA encoding an unrecognized component of amyloid in Alzheimer disease.', *Proceedings of the National Academy of Sciences*, 90(23), pp. 11282–11286. doi: 10.1073/pnas.90.23.11282.

Ueda, K. *et al.* (1993b) 'Molecular cloning of cDNA encoding an unrecognized component of

amyloid in Alzheimer disease.', *Proceedings of the National Academy of Sciences*, 90(23), pp. 11282–11286. doi: 10.1073/pnas.90.23.11282.

Uemura, N. *et al.* (2018) 'Inoculation of α-synuclein preformed fibrils into the mouse gastrointestinal tract induces Lewy body-like aggregates in the brainstem via the vagus nerve', *Molecular Neurodegeneration*. Molecular Neurodegeneration, 13(1), pp. 1–11. doi: 10.1186/s13024-018-0257-5.

Ulmer, T. S. and Bax, A. (2005) 'Comparison of structure and dynamics of micelle-bound human α-synuclein and Parkinson disease variants', *Journal of Biological Chemistry*, 280(52), pp. 43179–43187. doi: 10.1074/jbc.M507624200.

Ulusoy, A. *et al.* (2015) 'Neuron-to-neuron α-synuclein propagation in vivo is independent of neuronal injury', *Acta neuropathologica communications*, 3, p. 13. doi: 10.1186/s40478-015-0198-y.

Umek, N. *et al.* (2018) 'Dopamine Autoxidation Is Controlled by Acidic pH', *Frontiers in Molecular Neuroscience*, 11(December), pp. 1–8. doi: 10.3389/fnmol.2018.00467.

Unno, M. *et al.* (2002) 'The Structure of the Mammalian 20S ˚ Resolution Proteasome at 2 . 75 A', *Structure*, 10(02), pp. 609–618.

Upton, J. W. and Chan, F. K. M. (2014) 'Staying alive: Cell death in antiviral immunity', *Molecular Cell*, 54(2), pp. 273–280. doi: 10.1016/j.molcel.2014.01.027.

Uversky, V. N. *et al.* (2002) 'Biophysical Properties of the Synucleins and Their Propensities to Fibrillate', *Journal of Biological Chemistry*, 277(14), pp. 11970–11978. doi: 10.1074/jbc.M109541200.

Uversky, V. N., Li, J. and Fink, A. L. (2001) 'Metal-triggered Structural Transformations , Aggregation , and Fibrillation of Human a-Synuclein', *The Journal of Biological Chemistry*, 276(47), pp. 44284–44296. doi: 10.1074/jbc.M105343200.

Valente, E. Ma. *et al.* (2004) 'Hereditary Early-Onset Parkinson ' s Disease Caused by Mutations in PINK1', *Science*, 304(5674), pp. 1158–1160.

Do Van, B. *et al.* (2016) 'Ferroptosis, a newly characterized form of cell death in Parkinson's disease that is regulated by PKC', *Neurobiology of Disease*. Elsevier Inc., 94, pp. 169–178. doi: 10.1016/j.nbd.2016.05.011.

Vandenabeele, P. *et al.* (2010) 'Molecular mechanisms of necroptosis: An ordered cellular explosion', *Nature Reviews Molecular Cell Biology*. Nature Publishing Group, 11(10), pp. 700–714. doi: 10.1038/nrm2970.

Vázquez-Fernández, E. *et al.* (2016) 'The Structural Architecture of an Infectious Mammalian Prion Using Electron Cryomicroscopy', *PLoS Pathogens*, 12(9), pp. 1–21. doi: 10.1371/journal.ppat.1005835.

Veith, N. M. *et al.* (2009) 'Immunolocalisation of PrPSc in scrapie-infected N2a mouse neuroblastoma cells by light and electron microscopy', *European Journal of Cell Biology*, 88(1), pp. 45–63. doi: 10.1016/j.ejcb.2008.08.001.

Vella, L. J. *et al.* (2007) 'Packaging of prions into exosomes is associated with a novel pathway of PrP processing', *The Journal of Pathology*, 211(5).

Viceconte, N. *et al.* (2015) 'Neuromelanin activates proinflammatory microglia through a caspase-8-dependent mechanism', *Journal of Neuroinflammation*, 12(5), pp. 1–15. doi: 10.1186/s12974-014-0228-x.

Victoria, G. S. *et al.* (2016) 'Astrocyte-to-neuron intercellular prion transfer is mediated by cell-cell contact', *Scientific Reports*. Nature Publishing Group, 6(January), pp. 25–28. doi:

10.1038/srep20762.

Victoria, G. S. and Zurzolo, C. (2015) 'Trafficking and degradation pathways in pathogenic conversion of prions and prion-like proteins in neurodegenerative diseases', *Virus Research*. Elsevier B.V., 207, pp. 146–154. doi: 10.1016/j.virusres.2015.01.019.

Vila, M. *et al.* (2001) 'Bax ablation prevents dopaminergic neurodegeneration in the 1-methyl- mouse model of Parkinson's disease', *Proceedings of the National Academy of Sciences of the United States of America*, 98(5), pp. 2837–2842.

Vinci, M. *et al.* (2012) 'Advances in establishment and analysis of three- dimensional tumor spheroid-based functional assays for target validation and drug evaluation Advances in establishment and analysis of three- dimensional tumor spheroid-based functional assays for target va', *BMC Biology*. BioMed Central Ltd, 10(1), p. 29. doi: 10.1186/1741-7007-10-29.

Visanji, N. P. *et al.* (2008) 'PYM50028, a novel, orally active, nonpeptide neurotrophic factor inducer, prevents and reverses neuronal damage induced by MPP+ in mesencephalic neurons and by MPTP in a mouse model of Parkinson's disease', *The FASEB Journal*, 22(7), pp. 2488–2497.

Visanji, N. P. *et al.* (2011) 'Effect of Ser-129 Phosphorylation on Interaction of α-Synuclein with Synaptic and Cellular Membranes', *Journal of Biological Chemistry*, 286(41), pp. 35863–35873. doi: 10.1074/jbc.m111.253450.

Viswanath, V. *et al.* (2001) 'Caspase-9 Activation Results in Downstream Caspase-8 Activation and Bid Cleavage in 1-Methyl-4-Phenyl-1 , 2 , 3 , 6-Tetrahydropyridine- Induced Parkinson ' s Disease', *The Journal of Neuroscience*, 21(24), pp. 9519–9528.

Vives-bauza, C. *et al.* (2009) 'PINK1-dependent recruitment of Parkin to mitochondria in mitophagy', *Proceedings of the National Academy of Sciences of the United States of Americao*, 107(1), pp. 1–6. doi: 10.1073/pnas.0911187107.

Vogiatzi, T. *et al.* (2008) 'Wild Type a-Synuclein Is Degraded by Chaperone-mediated Autophagy and Macroautophagy in Neuronal Cells', *The Journal of Biological Chemistry*, 283(35), pp. 23542–23556. doi: 10.1074/jbc.M801992200.

Volles, M. J. *et al.* (2001) 'Vesicle permeabilization by protofibrillar α-synuclein: Implications for the pathogenesis and treatment of Parkinson's disease', *Biochemistry*, 40(26), pp. 7812–7819. doi: 10.1021/bi0102398.

Volpicelli-Daley, L. A. *et al.* (2011) 'Exogenous alpha-Synuclein Fibrils Induce Lewy Body Pathology Leading to Synaptic Dysfunction and Neuron Death', *Neuron*. Elsevier Inc., 72(1), pp. 57–71. doi: 10.1016/j.neuron.2011.08.033.

Wakamatsu, K. *et al.* (2003) 'The structure of neuromelanin as studied by chemical degradative methods', *Journal of Neurochemistry*, 86, pp. 1015–1023. doi: 10.1046/j.1471-4159.2003.01917.x.

Walden, H. and Muqit, M. M. K. (2017) 'Ubiquitin and Parkinson's disease through the looking glass of genetics', *Biochemical Journal*, 474(9), pp. 1439–1451. doi: 10.1042/bcj20160498.

Walker, D. G. *et al.* (2013) 'Changes in Properties of Serine 129 Phosphorylated α-Synuclein with Progression of Lewy Type Histopathology in Human Brains', *Experimental Neurology*, 240, pp. 190–204. doi: 10.1016/j.expneurol.2012.11.020.Changes.

Walkinshaw, G. and Waters, C. M. (1994) 'Neurotoxin-induced cell death in neuronal PC12 cells is mediated by induction of apoptosis', *NeuroscienceNeuroscience*, 63(4), pp. 975–987.

Wallings, R. L. *et al.* (2019) 'Lysosomal Dysfunction at the Centre of Parkinson ' s Disease

and Frontotemporal Dementia / Amyotrophic Lateral Sclerosis', *Trends in Neurosciences*. Elsevier Inc., 42(12), pp. 899–912. doi: 10.1016/j.tins.2019.10.002.

Wan, W. *et al.* (2017) 'Iron Deposition Leads to Neuronal α-Synuclein Pathology by Inducing Autophagy Dysfunction', *Frontiers in Neurology*, 8(January), pp. 2–11. doi: 10.3389/fneur.2017.00001.

Wang, F. *et al.* (2007) 'Lipid interaction converts prion protein to a PrPSc-like proteinase k-resistant conformation under physiological conditions', *Biochemistry*, 46(23), pp. 7045–7053. doi: 10.1021/bi700299h.

Wang, F. *et al.* (2010) 'Generating a Prion with Bacterially Expressed Recombinant Prion Protein', *Science*, 327(5969), pp. 1132–1135. doi: 10.1126/science.1183748.Generating.

Wang, G. *et al.* (2013) 'Mapping of the N-linked glycoproteome of human spermatozoa', *Journal of Proteome Research*, 12(12), pp. 5750–5759. doi: 10.1021/pr400753f.

Wang, J. *et al.* (2016) 'Meta-analysis of brain iron levels of Parkinson ' s disease patients determined by postmortem and MRI measurements', *Nature Publishing Group*. Nature Publishing Group, (October), pp. 1–13. doi: 10.1038/srep36669.

Wang, L. *et al.* (2009) 'Receptor Interacting Protein Kinase-3 Determines Cellular Necrotic Response to TNF- a', *Cell*. Elsevier Inc., 137(6), pp. 1100–1111. doi: 10.1016/j.cell.2009.05.021.

Wang, R. *et al.* (2015) 'Effect of lysosomal and ubiquitin-proteasome system dysfunction on the abnormal aggregation of α-synuclein in PC12 cells', *Experimental and Therapeutic Medicine*, 9(6), pp. 2088–2094. doi: 10.3892/etm.2015.2432.

Wang, R. *et al.* (2019) 'Iron-induced oxidative stress contributes to α-synuclein phosphorylation and up-regulation via polo-like kinase 2 and casein kinase 2', *Neurochemistry International*, 125(February), pp. 127–135. doi: 10.1016/j.neuint.2019.02.016.

Wang, S. and El-Deiry, W. S. (2003) 'TRAIL and apoptosis induction by TNF-family death receptors', *Oncogene*, 22(53 REV. ISS. 7), pp. 8628–8633. doi: 10.1038/sj.onc.1207232.

Wang, W. *et al.* (2011) 'A soluble -synuclein construct forms a dynamic tetramer', *Proceedings of the National Academy of Sciences*, 108(43), pp. 17797–17802. doi: 10.1073/pnas.1113260108.

Wang, Wei *et al.* (2011) 'A soluble α -synuclein construct forms a dynamic tetramer', 108(43), pp. 17797–17802. doi: 10.1073/pnas.1113260108.

Wang, X. *et al.* (2019) 'Pathogenic alpha-synuclein aggregates preferentially bind to mitochondria and affect cellular respiration', *Acta neuropathologica communications*. Acta Neuropathologica Communications, 7(1), p. 41. doi: 10.1186/s40478-019-0696-4.

Wang, X. and Gerdes, H. H. (2015) 'Transfer of mitochondria via tunneling nanotubes rescues apoptotic PC12 cells', *Cell Death and Differentiation*. Nature Publishing Group, 22(7), pp. 1181–1191. doi: 10.1038/cdd.2014.211.

Watson, G. S. and Leverenz, J. B. (2010) 'Profile of Cognitive Impairment in Parkinson Disease', *Brain Pathologyn*, 20(3), pp. 640–645. doi: 10.1111/j.1750-3639.2010.00373.x.Profile.

Waxman, E. A. and Giasson, B. I. (2011) 'Characterization of kinases involved in the phosphorylation of aggregated α-synuclein', *Journal of Neuroscience Research*, 89(2), pp. 231–247. doi: 10.1002/jnr.22537.

Webb, J. L. *et al.* (2003) 'a-Synuclein Is Degraded by Both Autophagy and the Proteasome',

The Journal of Biological Chemistry, 278(27), pp. 25009–25013. doi: 10.1074/jbc.M300227200.

Weber, P. *et al.* (2006) 'Cell-free formation of misfolded prion protein with authentic prion infectivity', *Proceedings of the National Academy of Sciences*, 103(43), pp. 15818–15823. doi: 10.1073/pnas.0605608103.

Wechalekar, A. D., Gillmore, J. D. and Hawkins, P. N. (2016) 'Systemic amyloidosis', *The Lancet*. Elsevier Ltd, 387(10038), pp. 2641–2654. doi: 10.1016/S0140-6736(15)01274-X.

Weinreb, O. *et al.* (2013) 'Targeting dysregulation of brain iron homeostasis in Parkinson's disease by iron chelators', *Free Radical Biology and Medicine*. Elsevier, 62, pp. 52–64. doi: 10.1016/j.freeradbiomed.2013.01.017.

Weissmann, C. (2004) 'The state of the prion', *Nature Reviews Microbiology*, 2(11), pp. 861–871. doi: 10.1038/nrmicro1025.

Westphal, C. H. and Chandra, S. S. (2013) 'Monomeric Synucleins Generate Membrane Curvature', *The Journal of Biological Chemistry*, 288(3), pp. 1829–1840. doi: 10.1074/jbc.M112.418871.

Wickner, R. (1994) '[URE3] as an altered URE2 protein: evidence for a prion analog in Saccharomyces cerevisiae', *Science*, 264(5158), pp. 566–569. doi: 10.1126/science.7909170.

Wik, L. *et al.* (2012) 'Separate mechanisms act concurrently to shed and release the prion protein from the cell', *Prion*, 6(5), pp. 498–509. doi: 10.4161/pri.22588.

Wilson, M. A. *et al.* (2004) 'The Parkinson ' s disease protein DJ-1 is neuroprotective due to cysteine-sulfinic acid-driven mitochondrial localization', *Proceedings of the National Academy of Sciences of the United States of America*, 101(24), pp. 9103–9108.

Winner, B. *et al.* (2011) 'In vivo demonstration that alpha-synuclein oligomers are toxic.', *Proceedings of the National Academy of Sciences of the United States of America*, 108(10), pp. 4194–9. doi: 10.1073/pnas.1100976108.

Winslow, A. R. *et al.* (2010) 'a-Synuclein impairs macroautophagy: implications for Parkinson's disease', *The Journal of Cell Biology*, 190(6), pp. 1023–1037. doi: 10.1083/jcb.201003122.

Winslow, A. R. and Rubinsztein, D. C. (2011) 'The Parkinson disease protein α -synuclein inhibits autophagy', *Autophagy*, 7(4), pp. 429–431. doi: 10.4161/auto.7.4.14393.

Wirdefeldt, K. *et al.* (2011) 'Epidemiology and etiology of Parkinson ' s disease : a review of the evidence', *European Journal of Epidemiology*, 26, pp. S1–S58. doi: 10.1007/s10654-011-9581-6.

Wolters, E. C. and Braak, H. (2006) 'Parkinson's disease: premotor clinico-pathological correlations', *Journal of Neural Transmission*, 70, pp. 309–319.

Wong, Y. C. and Krainc, D. (2016) 'Lysosomal trafficking defects link Parkinson's disease with Gaucher's disease', *Movement Disorders*, 31(11), pp. 1610–1618.

Wong, Y. C. and Krainc, D. (2017) 'α -synuclein toxicity in neurodegeneration : mechanism and therapeutic strategies', *Nature Publishing Group*. Nature Publishing Group, 23(2). doi: 10.1038/nm.4269.

Wood, S. J. *et al.* (1999) 'a-Synuclein Fibrillogenesis is Nucleation-dependent', *Biochemistry*, pp. 19509–19512. doi: 10.1074/jbc.274.28.19509.

Wooten, G. F. *et al.* (2004) 'Are men at greater risk for Parkinson's disease than women?',

Journal of Neurology, Neurosurgery and Psychiatry, 75(4), pp. 637–639. doi: 10.1136/jnnp.2003.020982.

Wördehoff, M. and Hoyer, W. (2018) 'α-Synuclein Aggregation Monitored by Thioflavin T Fluorescence Assay', *Bio-Protocol*, 8(14). doi: 10.21769/bioprotoc.2941.

Wu, B. *et al.* (2011) 'Phosphorylation of a -synuclein upregulates tyrosine hydroxylase activity in', *Acta Histochemica*, 113, pp. 32–35. doi: 10.1016/j.acthis.2009.07.007.

Wu, G. *et al.* (1998) 'Induction of axon-like and dendrite-like processes in neuroblastoma cells', *Journal of Neurocytology*, 27(1), pp. 1–14.

Wu, Y. Y. *et al.* (2019) 'Opportunities and challenges for the use of induced pluripotent stem cells in modelling neurodegenerative disease', *Open Biology*, 9(1). doi: 10.1098/rsob.180177.

Xiang, W. *et al.* (2013) 'Oxidative stress-induced posttranslational modifications of alpha-synuclein: Specific modification of alpha-synuclein by 4-hydroxy-2-nonenal increases dopaminergic toxicity', *Molecular and Cellular Neuroscience*. Elsevier Inc., 54, pp. 71–83. doi: 10.1016/j.mcn.2013.01.004.

Xiao, Y. *et al.* (2018) 'Iron promotes a-synuclein aggregation and transmission by inhibiting TFEB-mediated autophagosome-lysosome fusion', *Journal of Neurochemistry*, 145, pp. 34–50. doi: 10.1111/jnc.14312.

Xicoy, H., Wieringa, B. and Martens, G. J. M. (2017) 'The SH-SY5Y cell line in Parkinson's disease research: a systematic review', *Molecular Neurodegeneration*. Molecular Neurodegeneration, 12(10), pp. 1–11. doi: 10.1186/s13024-017-0149-0.

Xie, W. and Chung, K. K. K. (2012) 'Alpha-synuclein impairs normal dynamics of mitochondria in cell and animal models of Parkinson's disease', *Journal of Neurochemistry*, 122(2), pp. 404–414. doi: 10.1111/j.1471-4159.2012.07769.x.

Xie, Y. *et al.* (2016) 'Ferroptosis: Process and function', *Cell Death and Differentiation*, 23(3), pp. 369–379. doi: 10.1038/cdd.2015.158.

Xilouri, M. *et al.* (2009) 'Abberant a -Synuclein Confers Toxicity to Neurons in Part through Inhibition of Chaperone-Mediated Autophagy', *PLoS One*, 4(5), pp. 16–20. doi: 10.1371/journal.pone.0005515.

Xu, C. *et al.* (2017) 'DJ-1 Inhibits α -Synuclein Aggregation by Regulating Chaperone-Mediated Autophagy', *Frontiers in Aging Neuroscience*, 9(September), pp. 1–13. doi: 10.3389/fnagi.2017.00308.

Xu, C. *et al.* (2018) 'A versatile three-dimensional foam fabrication strategy for soft and hard tissue engineering', *Biomedical Materials (Bristol)*. IOP Publishing, 13(2), p. 25018. doi: 10.1088/1748-605X/aaa1f6.

Xu, J. *et al.* (2002) 'Dopamine-dependent neurotoxicity of α -synuclein : A mechanism for selective neurodegeneration in Parkinson disease', *Nature Medicine*, 8(6).

Xu, Y. *et al.* (2015) 'Unraveling the role of hydrogen peroxide in α-synuclein aggregation using an ultrasensitive nanoplasmonic probe', *Analytical Chemistry*, 87(3), pp. 1968–1973. doi: 10.1021/ac5043895.

Yagoda, N. *et al.* (2007) 'RAS-RAF-MEK-dependent oxidative cell death involving voltage-dependent anion channels', *Nature Letters*, 447(June). doi: 10.1038/nature05859.

Yamaguchi, Y. and Miura, M. (2015) 'Programmed cell death in neurodevelopment', *Developmental Cell*. Elsevier Inc., 32(4), pp. 478–490. doi: 10.1016/j.devcel.2015.01.019.

Yang, L. *et al.* (2004) 'A novel systemically active caspase inhibitor attenuates the toxicities of MPTP, malonate, and 3NP in vivo', *Neurobiology of Disease*, 17(2), pp. 250–259. doi: 10.1016/j.nbd.2004.07.021.

Yang, W. L. and Sun, A. Y. (1998) 'Paraquat-induced cell death in PC12 cells', *Neurochemical Research*, 23(11), pp. 1387–1394.

Yang, W. S. *et al.* (2014) 'Regulation of Ferroptotic Cancer Cell Death by GPX4', *Cell*, 156(0), pp. 317–331. doi: 10.1016/j.cell.2013.12.010.Regulation.

Yang, W. S. and Stockwell, B. R. (2008) 'Synthetic Lethal Screening Identifies Compounds Activating Iron-Dependent, Nonapoptotic Cell Death in Oncogenic-RAS-Harboring Cancer Cells', *Chemistry and Biology*, 15(3), pp. 234–245. doi: 10.1016/j.chembiol.2008.02.010.

Yasuda, T. *et al.* (2013) 'Neurodegenerative changes initiated by presynaptic dysfunction', *Translational Neurodegeneration*, 2(1), pp. 1–5. doi: 10.1186/2047-9158-2-16.

Yavich, L., Tanila, H. and Vepsa, S. (2004) 'Role of a -Synuclein in Presynaptic Dopamine Recruitment', *Neurobiology of Disease*, 24(49), pp. 11165–11170. doi: 10.1523/JNEUROSCI.2559-04.2004.

Ye, Y. and Rape, M. (2009) 'Building ubiquitin chains: E2 enzymes at work', *Nature Reviews Molecular Cell Biology*. Nature Publishing Group, 10(11), pp. 755–764. doi: 10.1038/nrm2780.

Yim, W. W. and Mizushima, N. (2020) 'Lysosome biology in autophagy', *Cell Discovery*. Springer US, 6(6). doi: 10.1038/s41421-020-0141-7.

Yoshimura, T. *et al.* (1993) 'Molecular characterisation of the "26S" proteasome complex from rat liver', *Journal of Structural Biology*, 111, pp. 200–211.

Yu, H. and Matouschek, A. (2017) 'Recognition of Client Proteins by the Proteasome', *Annual Review of Biophysics*, 46, pp. 146–173.

Yu, S. *et al.* (2002) 'Mediation of Poly (ADP-Ribose) Polymerase-1 – Dependent Cell Death by Apoptosis-Inducing Factor', *Science Reports*, 297(July), pp. 259–264.

Yuan Aidong, Rao Mala V. , Veeranna, and N. R. A. (2017) 'Neurofilaments and Neurofilament Proteins in Health and Disease', *Cold Spring Harbor Perspectives in Biology*, 25(3), pp. 289–313. doi: 10.1007/s11065-015-9294-9.Functional.

Yuen, E. C. *et al.* (1996) 'Nerve growth factor and the neurotrophic factor hypothesis', *Brain and Development*, 18(5), pp. 362–368. doi: 10.1016/0387-7604(96)00051-4.

Zaccai, J. *et al.* (2008) 'Patterns and stages of α-synucleinopathy Relevance in a population-based cohort', *Neurology*, 70(13).

Zaltieri, M. *et al.* (2015) 'α-synuclein and synapsin III cooperatively regulate synaptic function in dopamine neurons', *Journal of Cell Science*, 128(13), pp. 2231–2243. doi: 10.1242/jcs.157867.

Zarranz, J. J. *et al.* (2003) 'The New Mutation, E46K, of alpha -Synuclein Causes Parkinson and Lewy Body Dementia', *Annals of Neurology*, 55, pp. 164–173.

Zecca, L. *et al.* (2001) 'Iron , neuromelanin and ferritin content in the substantia nigra of normal subjects at different ages : consequences for iron storage and neurodegenerative processes', *Journal of Neurochemistry*, 76, pp. 1766–1773.

Zecca, Luigi *et al.* (2004) 'Iron, brain ageing and neurodegenerative disorders', *Nature Reviews Neuroscience*, 5(11), pp. 863–873. doi: 10.1038/nrn1537.

Zecca, L. *et al.* (2004) 'The role of iron and copper molecules in the neuronal vulnerability of locus coeruleus and substantia nigra during aging', *Proceedings of the National Academy of Sciences*, 101(26), pp. 9843–9848. doi: 10.1073/pnas.0403495101.

Zecca, L., Wilms, H., *et al.* (2008) 'Human neuromelanin induces neuroinflammation and neurodegeneration in the rat substantia nigra : implications for Parkinson ' s disease', *Acta Neuropathologica*, 116, pp. 47–55. doi: 10.1007/s00401-008-0361-7.

Zecca, L., Casella, A. A., *et al.* (2008) 'Neuromelanin can protect against iron-mediated oxidative damage in system modeling iron overload of brain aging and Parkinson's disease', *Journal of Neurochemistry*, 106, pp. 1866–1875. doi: 10.1111/j.1471-4159.2008.05541.x.

Zhang, J., Li, X. and Li, J.-D. (2019) 'The Roles of Post-translational Modifications on α-Synuclein in the Pathogenesis of Parkinson's Diseases', *Frontiers in Neuroscience*, 13(April), pp. 1–11. doi: 10.3389/fnins.2019.00381.

Zhang, X. *et al.* (2015) 'Exosomes in cancer: Small particle, big player', *Journal of Hematology and Oncology*. Journal of Hematology & Oncology, 8(1), pp. 1–13. doi: 10.1186/s13045-015-0181-x.

Zhang, Y. *et al.* (2014) 'A lifespan observation of a novel mouse model: In vivo evidence supports Aβ oligomer hypothesis', *PLoS ONE*, 9(1). doi: 10.1371/journal.pone.0085885.

Zhang, Z. *et al.* (2016) 'BH3-in-groove dimerization initiates and helix 9 dimerization expands Bax pore assembly in membranes', *The EMBO Journal*, 35(2), pp. 208–236. doi: 10.15252/embj.201591552.

Zhao, J. (2003) 'Parkin is recruited to the centrosome in response to inhibition of proteasomes', *Journal of Cell Science*, 116(19), pp. 4011–4019. doi: 10.1242/jcs.00700.

Zhu, S. *et al.* (2015) 'Prion aggregates transfer through tunneling nanotubes in endocytic vesicles', *Prion*, 9(2), pp. 125–135. doi: 10.1080/19336896.2015.1025189.

Zilka, O. *et al.* (2017) 'On the Mechanism of Cytoprotection by Ferrostatin-1 and Liproxstatin-1 and the Role of Lipid Peroxidation in Ferroptotic Cell Death', *ACS Central Science*, 3(3), pp. 232–243. doi: 10.1021/acscentsci.7b00028.

Zille, M. *et al.* (2019) 'Ferroptosis in neurons and cancer cells is similar but differentially regulated by histone deacetylase inhibitors', *Eneuro*, 6(1), p. ENEURO.0263-18.2019. doi: 10.1523/eneuro.0263-18.2019.

Zondler, L. *et al.* (2014) 'DJ-1 interactions with a-synuclein attenuate aggregation and cellular toxicity in models of Parkinson's disease', *Cell Death and Diseasel*, 5(e1350), pp. 1–10. doi: 10.1038/cddis.2014.307.

Zondler, L. *et al.* (2017) 'Proteasome impairment by α-synuclein', *PloS one*, 12(9), p. e0184040. doi: 10.1371/journal.pone.0184040.

Zucca, F. A. *et al.* (2015) 'Interactions of iron , dopamine and neuromelanin pathways in brain aging and Parkinson ' s disease', *Progress in Neurobiology*, 155, pp. 96–119. doi: 10.1016/j.pneurobio.2015.09.012.

© 2019. Published by The Company of Biologists Ltd | Disease Models & Mechanisms (2019) 12, dmm038042. doi:10.1242/dmm.038042

RESOURCE ARTICLE

Recapitulating Parkinson's disease pathology in a three-dimensional human neural cell culture model

Teresa R. Taylor-Whiteley[1], Christine L. Le Maitre[1], James A. Duce[2,3], Caroline F. Dalton[1] and David P. Smith[1,*]

ABSTRACT

Extensive loss of dopaminergic neurons and aggregation of the protein α-synuclein into ubiquitin-positive Lewy bodies represents a major neuropathological hallmark of Parkinson's disease (PD). At present, the generation of large nuclear-associated Lewy bodies from endogenous wild-type α-synuclein, translationally regulated under its own promoter in human cell culture models, requires costly and time-consuming protocols. Here, we demonstrate that fully differentiated human SH-SY5Y neuroblastoma cells grown in three-dimensional cell culture develop Lewy-body-like pathology upon exposure to exogenous α-synuclein species. In contrast to most cell- and rodent-based PD models, which exhibit multiple diffuse α-synuclein aggregates throughout the cytoplasm, a single large nuclear inclusion that is immunopositive for α-synuclein and ubiquitin is rapidly obtained in our model. This was achieved without the need for overexpression of α-synuclein or genetic modification of the cell line. However, phosphorylation of α-synuclein within these inclusions was not observed. The system described here provides an ideal tool to screen compounds to therapeutically intervene in Lewy body formation, and to investigate the mechanisms involved in disease progression in synucleinopathies.

KEY WORDS: 3D cell culture, Amyloid, Lewy body, Oligomer, Parkinson's, Synuclein

INTRODUCTION

The presence of large cell-associated protein aggregates is the key pathological hallmark commonly associated with many neurodegenerative disorders (Poewe et al., 2017). In Parkinson's disease (PD) and other synucleinopathies, the intrinsically disordered protein α-synuclein (α-syn) undergoes misfolding into amyloid fibrils (Poewe et al., 2017). These fibrils form the major protein component of intracellular deposits associated with Lewy bodies (LBs) in the cell soma, and Lewy neurites (LNs) in axons of surviving neurons (Theillet et al., 2016; Spillantini et al., 1997; Langston et al., 2015). The association of α-syn with pre-synaptic terminals from *in vitro* and *in vivo* models suggests a normal physiological role in the regulation of neurotransmitter release and synaptic function, but its role in disease remains poorly understood (Iwai et al., 1995; Kahle et al., 2000; Murphy et al., 2000; Nemani et al., 2010). Familial early-onset forms of PD are associated with mutations in the *SNCA* gene, encoding α-syn (Polymeropoulos et al., 1997; Singleton et al., 2003). Genomic duplications, triplications and missense mutations (e.g. A53T, A30P, E46K and H50Q) all implicate α-syn in the pathogenesis of PD (Spatola and Wider, 2014). However, only 10% of cases are linked to a genetic basis of the disease, with the majority of cases having an unknown aetiology (Mcculloch et al., 2008; Wirdefeldt et al., 2011). Insights from *in vitro* and *in vivo* models suggest that α-syn acts as a 'prion-like' protein, with a propensity to misfold and form aggregates that promote cell-to-cell propagation, which assists in the spread of pathology (Braak et al., 2003; Li et al., 2008; Kordower et al., 2008; Danzer et al., 2009; Aulić et al., 2014; Hawkes et al., 2007).

The mechanisms underlying LB formation and the influence of α-syn pathology on disease pathogenesis remain poorly understood, largely due to the lack of whole-animal or cell-based models that recapitulate the development of these inclusions. One of the significant barriers in PD research surrounds the difficulty in obtaining cultures of the A9-subtype dopaminergic neuronal population that are specifically affected in the disease (Arenas et al., 2015). Several cell culture models have been used for studying PD, and to investigate the role of α-syn aggregation. These models include: non-patient-specific human cell lines (SH-SY5Y, HEK293, LUHMES); animal-derived cell lines (rat PC12, mouse N2a cells); stem cells, including induced pluripotent cell lines (iPSCs) and human mesenchymal (MSCs)/embryonic stem cells (ESCs); and primary animal-derived midbrain neuron cultures (Falkenburger et al., 2016; Smidt and Burbach, 2007). Each of these cell types has its own strengths and limitations; for example, the use of iPSCs that differentiate into dopaminergic neurons *in vitro* overcomes the ethical issues associated with using ESCs. However, culturing these cells is expensive and labour-intensive (as long as 75 days in culture), meaning that their use is inevitably out of reach for many research groups (Smirnova et al., 2016; D'Antonio et al., 2017). The cost incurred, time constraints and ethical framework required for animal-based research are again inhibitory for many laboratories.

To address the experimental and ethical issues of ESCs and animal models, alternative systems have been developed to model the complex pathogenesis of the disorder. Relatively few studies have observed the development of LB pathology without overexpressing high levels of human versions of α-syn (Volpicelli-Daley et al., 2011; Falkenburger et al., 2016). In addition, a predominant number of studies rely on the introduction of a familial mutation into α-syn (e.g. A53T) to increase aggregation propensity (Li et al., 2001; Koprich et al., 2017). Recombinant expression of wild-type (WT) human

[1]Biomedical Sciences Research Centre, Department of Bioscience and Chemistry, Sheffield Hallam University, Sheffield, South Yorkshire S1 1WB, UK. [2]School of Biomedical Sciences, The Faculty of Biological Sciences, University of Leeds, Leeds, West Yorkshire LS2 9JT, UK. [3]The ALBORADA Drug Discovery Institute, University of Cambridge, Cambridge Biomedical Campus, Hills Road, Cambridge CB2 0AH, UK.

*Author for correspondence (d.p.smith@shu.ac.uk)

C.L.L., 0000-0003-4489-7107; J.A.D., 0000-0002-8762-2245; C.F.D., 0000-0002-1404-873X; D.P.S., 0000-0001-5177-8574

Received 11 November 2018; Accepted 21 March 2019

Disease Models & Mechanisms (2019) 12, dmm038042. doi:10.1242/dmm.038042

α-syn in *Drosophila* mirrors the formation of LB-like structures and neuronal loss, but this has unfortunately not been replicated in higher-order organisms or human-cell-based models (Feany and Bender, 2000). Interestingly, rodent models of PD that overexpress human α-syn by mutations in the *SNCA* gene (e.g. the M83 strain, overexpressing mutant human A53T α-syn) do develop inclusions but the anatomical distribution is widely variable among animals and often coincides with areas of substantial neuroinflammation (Sacino et al., 2014; Lee et al., 2002; Dawson et al., 2011; Fares et al., 2016). Importantly, impaired human α-syn fibrillisation can occur in rodent models due to an interaction with endogenously expressed mouse α-syn. Such interactions highlight a fundamental experimental caveat when investigating LB formation in mouse models or rodent-derived primary neuronal cultures (Fares et al., 2016). Species differences between rodent models (including primary rodent cell culture systems) make it difficult to model and extrapolate findings to human subjects (Goldie et al., 2014; Ioannidis, 2012; Pound and Bracken, 2014).

In previous human-cell-based models, limitations have also arisen from the use of traditional two-dimensional (2D) monolayers. Intracellular α-syn aggregates are often observed as multiple cytoplasmic punctate inclusions rather than recapitulating the typical large singular inclusions associated with human pathology (Danzer et al., 2009; Desplats et al., 2009; Aulić et al., 2014). Formation of LB-like pathology in human cell culture models has only been achieved through overexpression of α-syn, either driven from viral promoters or in cell lines not associated with the disease, such as those from human embryonic kidney lines (HEK-293) (Volpicelli-Daley et al., 2011; Luk et al., 2009; Sacino et al., 2013). Such viral promotors do not allow the study of transcriptional and translational modulations brought about during the disease state. To address these issues, *in vitro* 3D culture systems are increasingly being utilised for a multitude of disease models, with the aim of more closely mimicking an *in vivo* environment with tissue-like cell density and cell-to-cell as well as cell-to-extracellular-matrix contacts (Griffith and Swartz, 2006; Tang-Schomer et al., 2014; Choi et al., 2014; Smirnova et al., 2016). Taken together, the limitations of both *in vitro* and *in vivo* models demonstrate a greater need to develop a human-relevant culture system to model LB pathology.

The use of human-derived neuroblastoma cell lines, such as the SH-SY5Y catecholaminergic neuroblastoma cell line, remains a popular choice in PD research (Xicoy et al., 2017). Although the SH-SY5Y cell line does display genetic anomalies, it is important to note that nearly all pathways dysregulated in PD remain intact in this line (Krishna et al., 2014) and punctate intracellular inclusions can be induced by exposure to preformed amyloid material (Illes-Toth et al., 2015). In addition, upon differentiation, this proliferative immature neuroblast expresses the characteristic proteins associated with dopaminergic neurons, including tyrosine hydroxylase (TH) and dopamine transporter (DAT), making it a comparable model of the cell type affected in the disease state (Presgraves et al., 2004; Lopes et al., 2010; Kovalevich and Langford, 2013).

Differentiation to a fully mature neuronal phenotype can be achieved using all-trans retinoic acid (RA), followed by treatment with brain-derived neurotrophic factor (BDNF) (Encinas et al., 2000). This procedure yields a preferentially homogenous population of cells compared to other differentiation protocols, including short- or long-term treatment with RA alone (Encinas et al., 2000). Although the importance of using differentiated SH-SY5Y in PD research is becoming increasingly apparent, a large number of publications still either use the undifferentiated line, do not report their differentiation protocol or employ a differentiation protocol that solely utilises RA. These procedures then do not fully provide a mature neuronal phenotype (Goldie et al., 2014; Xicoy et al., 2017).

Here, we developed an easily replicable cell culture methodology that recapitulates the formation of LB-like inclusions. The Encinas et al. (2000) protocol was adapted to generate neuron-like cells in a 2D cell culture format that could subsequently be maintained within a 3D matrix. By incorporating the RA+BDNF-differentiated cells into a 3D matrix, we have been able to induce the formation of nuclear-associated ubiquitinated LB-like α-syn aggregates upon treatment with preformed α-syn oligomers. The formation of these LB-like aggregates was achieved without the need for overexpression of α-syn or modification of the genomic material.

RESULTS

Differentiated SH-SY5Y in 2D culture express markers of dopaminergic neurons

Controversy remains as to whether RA or RA+BDNF promotes SH-SY5Y cell differentiation and the development of a terminal neural dopaminergic phenotype (Korecka et al., 2013; Xicoy et al., 2017; Lopes et al., 2010). Thus, transcriptional and translational analysis of key neuronal markers was carried out to limit assumptions regarding the phenotypic state of the SH-SY5Y cell line used here. Undifferentiated SH-SY5Y cells display a characteristic morphology of two distinct phenotypes: neuroblastic ('N-type'; Fig. 1A, arrow); and substrate adherent ('S-type'; Fig. 1A, asterisk). In agreement with others (Korecka et al., 2013; Forster et al., 2015; Ito et al., 2017), upon treatment with RA or RA+BDNF, the neuroblastic SH-SY5Y cells differentiated to a more neuron-like phenotype. Average neurite lengths and standard deviations of 51.22±22.87 µm (undifferentiated), 64.91±33.07 µm (RA) and 130.50±77.91 µm (RA+BDNF) were observed (Fig. 1A), with interquartile ranges of 34.43-62.53, 40.83-80.85 and 74.83-164.8 µm, respectively. Significantly longer neurite length was observed in both RA and RA+BDNF groups compared to undifferentiated cells, with increased network complexity in the RA+BDNF group (Fig. 1A). Following treatment with RA, the non-differentiating 'S-type' population was increasingly visible at day 5 and, if continuously cultured up to 14 days, under these conditions, progressively overgrew the cultures (data not shown). The addition of BDNF and withdrawal of RA promoted the development of a homogenous population of cells with a negligible amount of 'S-type' cells surviving (Encinas et al., 2000).

Key to the development of an effective cell culture model of PD is the expression of relevant neuronal markers. Cells at all stages of differentiation were stained with antibodies for the neuron markers neurofilament 200 (NF200) (Fig. 1B) and βIII-tubulin (encoded by *TUBB3*) (data not shown). NF200 staining was reduced following differentiation with RA (7±3%) compared to undifferentiated SH-SY5Y (43±21%), potentially relating to an increased population of 'S-type' cells within the culture. NF200 immunopositivity was increased in RA+BDNF (64±17%) compared to undifferentiated and RA groups. Ki67 is a protein associated with cell proliferation that is present in the G_1, S and G_2 phases of cell cycling and mitosis but absent in the G_0 resting state. Undifferentiated neuroblastoma cultures expressed this marker [591,943±171,477 corrected total cell fluorescence (CTCF)/cell]. A significant reduction in expression seen in the RA (193,629±160,908 CTCF/cell) and RA+BDNF (180,465±105,445 CTCF/cell) cells indicate that they are terminally differentiated (Fig. 1C). Tyrosine hydroxylase (TH) is a key enzyme in the production and homeostasis of dopamine (DA) within catecholamine neuronal cell

Disease Models & Mechanisms (2019) 12, dmm038042. doi:10.1242/dmm.038042

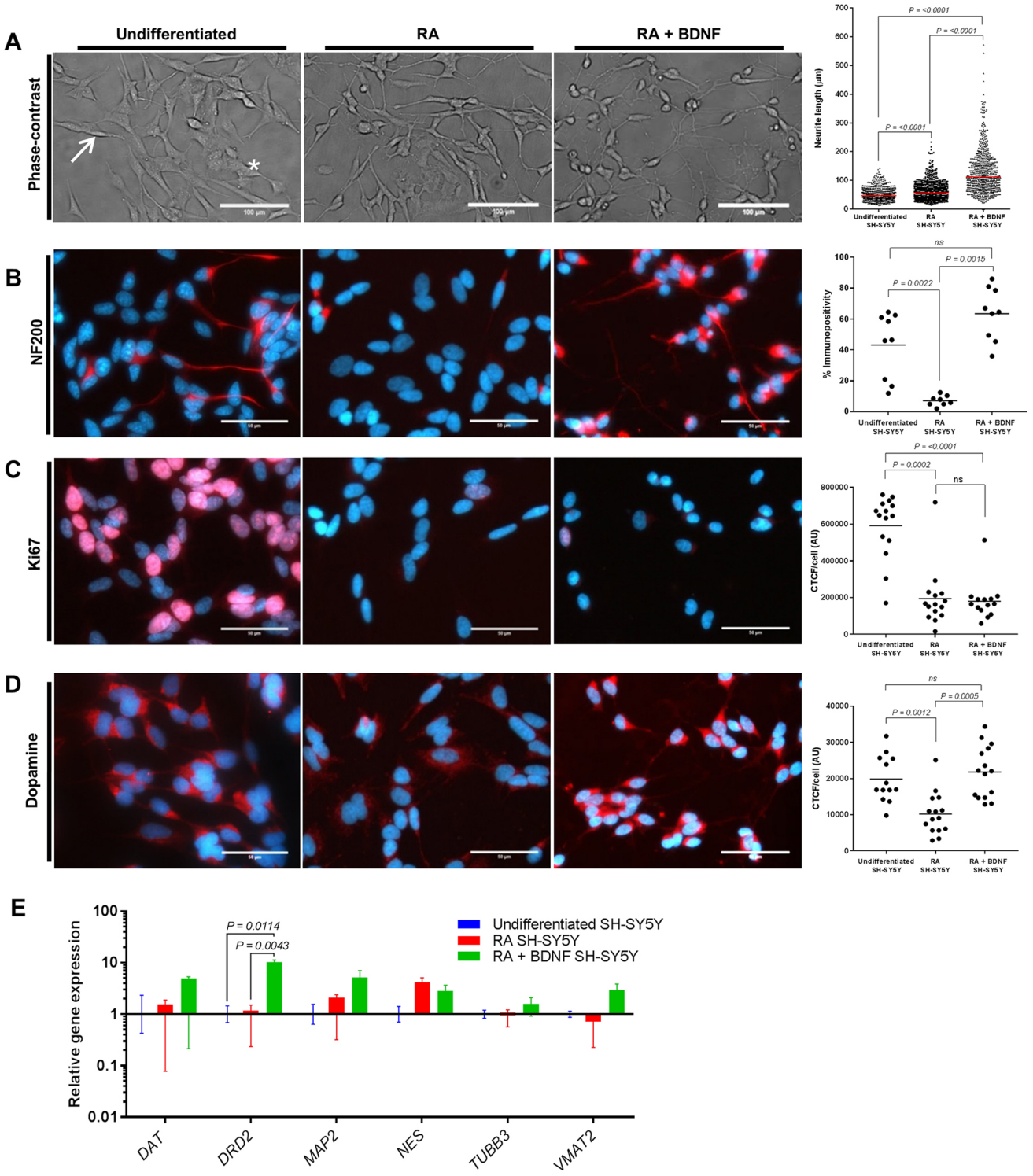

Fig. 1. Characterisation of SH-SY5Y cells following differentiation with RA alone or sequential treatment with RA+BDNF. (A) Representative phase-contrast images of SH-SY5Y differentiated with RA alone and sequential treatment with RA+BDNF. Neurite length measurements were determined by measuring 200 neurites per treatment group, with three independent biological repeats. All data points are presented, with the mean shown as a straight line. Neuroblastic ('N-type'; arrow) and substrate adherent ('S-type'; asterisk) cells are shown. (B-D) Immunocytochemistry analysis of differentiated cultures stained for NF200, Ki67 and dopamine (DA) (red). Nuclei were visualised using DAPI staining (blue). Individual data points presented with mean (straight line) for % immunopositivity (B) and CTCF/cell data (C,D) of three independent biological repeats. (E) mRNA levels of genes specifically associated with dopaminergic neurons were evaluated by qPCR. Undifferentiated cells (blue), RA treatment group (red) and RA+BDNF treatment group (green). Relative gene expression normalised to reference genes (*ACTB* and *YWHAZ*) and undifferentiated SH-SY5Y. Neuronal (*TUBB3* and *MAP2*) and dopaminergic (*DAT*, *DRD2* and *VMAT2*) markers showed increased expression in the RA+BDNF group (green) relative to the undifferentiated cells (blue). Immature neuronal marker (*NES*) expression was not significantly changed following differentiation with RA or RA+BDNF. Data presented as mean±s.e.m. of at least three independent experiments. (A-E) Differences between treatments were tested for significance using the Kruskal–Wallis test with *post hoc* Dwass-Steel-Chritchlow-Fligner for >6 data points and Conover-Inman for <6 data points. *P*-values are displayed in the figures. Scale bars: 100 µm (A); 50 µm (B-D).

Disease Models & Mechanisms (2019) 12, dmm038042. doi:10.1242/dmm.038042

types (Daubner et al., 2011) and is expressed in all three cell types (Fig. S1). An anti-DA antibody that has been demonstrated to be specific for DA through cross-reactivity studies (Banks et al., 2017) was used to determine the presence of this neurotransmitter. These terminally differentiated SH-SY5Y cells were also shown to retain a dopaminergic phenotype, whereby DA immunoreactivity was significantly increased in RA+BDNF (21,800±7126 CTCF/cell)-treated cultures compared to undifferentiated cells (19,884±6371 CTCF/cell) or those treated with RA (10,216±5823 CTCF/cell) (Fig. 1D).

Evaluation of the mRNA levels after each differentiation protocol by quantitative real-time PCR (qPCR) was used to determine the transcriptional levels of genes specifically associated with dopaminergic neurons (Fig. 1E). Increased expression of the neuronal markers βIII-tubulin (*TUBB3*) and microtubule-associated protein 2 (*MAP2*) upon RA+BDNF treatment confirmed the development of a more neuronal phenotype than observed with RA-treated or undifferentiated SH-SY5Y cells. Nestin (*NES*), an immature neuronal marker, was not significantly changed by differentiation with either RA alone or RA+BDNF treatment. A greater dopaminergic phenotype in RA-BDNF differentiated cultures was observed, indicated by elevated expression levels of DAT, DA receptor D2 and vesicular monoamine transporter member 2 when compared to the other two cell populations (Fig. 1E). Overall, these observations are in line with previously published work on differentiated SH-SY5Y cell lines in which RA+BDNF treatment was utilised, and demonstrate that these conditions result in terminally differentiated cells expressing many of the key markers of a dopaminergic neuron (Ito et al., 2017; Agholme et al., 2010; Xicoy et al., 2017).

Exogenous α-syn oligomers induce intracellular aggregation

Within the PD brain, LB pathology is only observed in a discrete cell population within *ex vivo* material (Braak et al., 2003). Here, we wanted to determine whether the extent of cellular differentiation resulted in alterations in the intracellular aggregation propensity of the cell line. Previous studies by us and others have shown that a distinct subtype of soluble oligomeric α-syn can seed intracellular aggregation of endogenous α-syn in undifferentiated SH-SY5Y lines (Danzer et al., 2009; Illes-Toth et al., 2015). Following addition of oligomeric α-syn to undifferentiated SH-SY5Y cells, the presence of multiple punctate α-syn-positive cytoplasmic inclusions with an average inclusion size of 0.28 μm^2 was confirmed in our model (Fig. 2A,B). The addition of the same oligomer treatment on RA-differentiated cultures also produced several small cytoplasmic inclusions within each cell, but the average inclusion size was significantly larger (0.82 μm^2) than in the undifferentiated SH-SY5Y cells (Fig. 2A,B). In both undifferentiated and RA-differentiated SH-SY5Y cells, all surviving cells developed the punctate inclusions (Fig. 2C).

In contrast, the addition of the same soluble oligomeric α-syn preparation to RA+BDNF-differentiated culture media demonstrated the development of a single perinuclear inclusion, consistent with a large LB-like aggregate (Fig. 2A, asterisks and arrows), with an average inclusion size of 8.95 μm^2. Cellular inclusions could be detected 24 h after treatment, but only 31% of

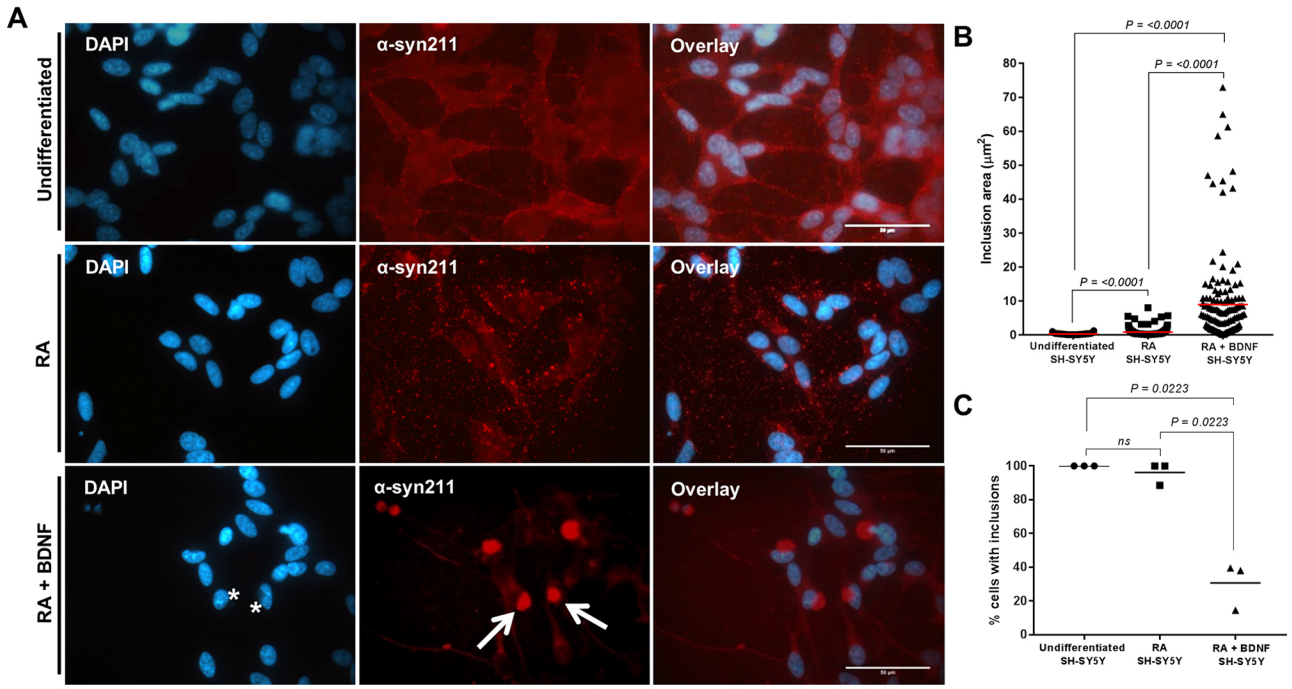

Fig. 2. Exogenous addition of α-syn oligomers induces the intracellular aggregation of α-syn in 2D SH-SY5Y cultures. (A) Double immunostaining of undifferentiated and differentiated SH-SY5Y cells reveals intracellular aggregation of α-syn following 24 h incubation with seeding oligomers. α-Syn inclusions in undifferentiated cells display several distinct, punctate accumulations dispersed throughout the cytoplasm, consistent with aggregates. In contrast, the RA+BDNF cell lines show a single prominent accumulation (red; arrows) and obscure the nucleus (asterisks). Scale bars: 50 μm. (B) Quantification of inclusion area (reflected as μm^2) shows inclusions that are present in differentiated cells to be much larger than those in undifferentiated cells (measurements obtained from three independent experiments; n=50). All data points are present, with mean shown as a straight line. (C) The percentage of cells containing inclusions was determined by counting 100 cells per repeat. Cells were deemed to contain inclusions if aggregation matched that in reference images when compared to controls. Data points are presented from three independent biological repeats. (B,C) Differences between treatments were tested for significance using Kruskal–Wallis test with post-hoc Dwass-Steel-Chritchlow-Fligner for >6 data points and Conover-Inman for <6 data points. *P*-values are displayed in the figures.

Disease Models & Mechanisms (2019) 12, dmm038042. doi:10.1242/dmm.038042

the cell population developed these structures (Fig. 2C). To our knowledge, this is the first observation of single large inclusions within a genetically unmodified cell culture model.

SH-SY5Y differentiation in 3D culture retains a dopaminergic phenotype

Despite the promising initial phenotypic outcomes from the RA+BDNF-differentiated cells cultured in a 2D format, the protocol was not robust. These cells tended to detach from the culture vessel before the end of BDNF treatment and as such presented a wide variation in inclusion size (Fig. 2B) and viability (Fig. S2A). This detachment from the culture vessel meant that, although images could be produced of cells containing LB-like inclusions, the experiment itself was not repeatable enough for future investigations. We, therefore, sought to adapt our culturing procedure to allow for greater retention of cells after RA+BDNF differentiation. It was hoped that differentiation of these cells in a 3D matrix would stabilise the cell population during the development of LB-like inclusions and allow more robust handling methods during processing and analysis.

A variety of cell densities were used to evaluate the optimal cell conditions for differentiation in 3D. In 300 µl matrix volumes (in 24-well inserts), incremental increases in densities from 1×10^6 cells/ml to 1.25×10^7 cells/ml steadily decreased the viability of cells within the matrix (~17%) as measured by lactate dehydrogenase (LDH) concentration (Fig. 3A). Upon differentiation in the 3D matrix, gene expression of *DRD2*, *MAP2* and *VMAT2* were increased (compared to undifferentiated SH-SY5Y) (Fig. 3B). A substantial increase in *VMAT2* expression within the same cells differentiated in 3D compared to 2D indicated the development of a more neuronal phenotype.

Based on these observations, a cell density of 7.5×10^6 cells/ml was selected for further studies. At this cell density, the expression levels of *DAT*, *DRD2*, *MAP2*, *TUBB3* and *VMAT2* were all increased in relative abundance to the undifferentiated cells, and *NES* expression was decreased in comparison to other cell densities. Cells displayed a homogenous distribution within the matrix, in contrast to lower densities where clusters of cells were observed (Fig. S2B). In addition, this was the highest cell density at which cell viability was unaffected. Hence, 7.5×10^6 cells/ml was the optimal balance between viability and homogeneity within the matrix. To demonstrate comparable differentiation of SH-SY5Y cultures after 7 days of treatment with RA+BDNF in 2D or 3D, all cells were confirmed to be immunonegative for Ki67 and immunopositive for NF200 and DA (Fig. 3C).

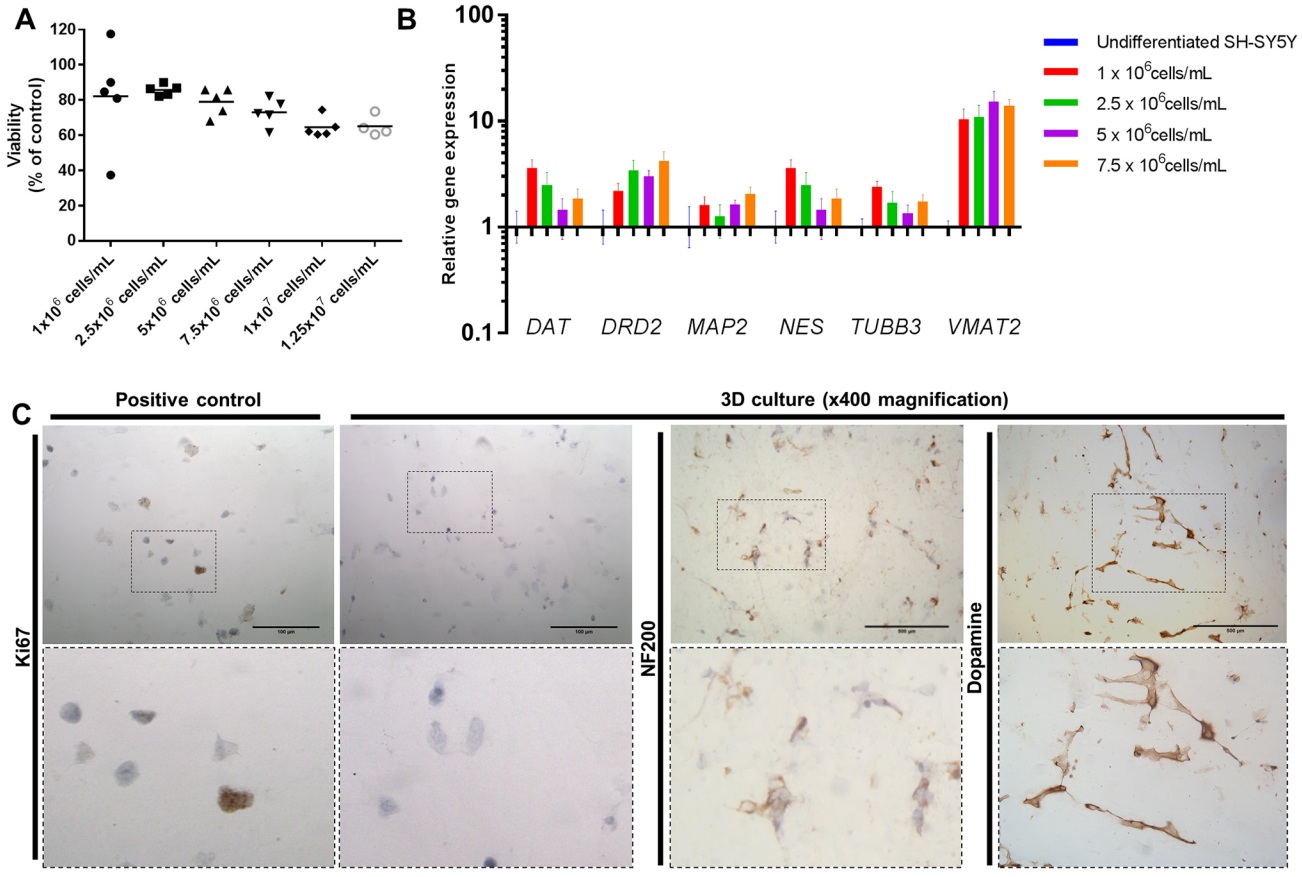

Fig. 3. Neuron-like cells cultured in 3D retain a dopaminergic phenotype. (A) Cell number optimisation of 3D-differentiated SH-SY5Y using LDH cell viability assay. An incremental increase in cell density is associated with decreased cell viability (~17% decrease from 1×10^6 cells/ml to 1.25×10^7 cells/ml). LDH cell viability assay was normalised to cell-density-matched positive controls. All data points are present, with mean shown as a straight line of at least four independent repeats. (B) mRNA levels of genes specifically associated with dopaminergic neurons were evaluated by qPCR in different cell densities. Relative gene expression normalised to reference genes (*ACTB* and *YWHAZ*) and undifferentiated SH-SY5Y. Expression of neuronal (*TUBB3*, *MAP2* and *NES*) and dopaminergic (*DAT*, *DRD2* and *VMAT2*) markers was evaluated in cell densities. A density of 7.5×10^6 cells/ml demonstrated increased expression of *DRD2*, *MAP2* and *VMAT2*, and was chosen for further experiments. Data presented as mean±s.e.m. of at least three independent experiments. (C) 3D-differentiated SH-SY5Y cultures retain a post-mitotic neuronal dopaminergic phenotype in 3D as determined by the absence of Ki67 staining and positive staining for NF200 and dopamine. Positive control for Ki67 staining is undifferentiated SH-SY5Y cultured in 3D. Scale bars: 100 µm.

Disease Models & Mechanisms (2019) 12, dmm038042. doi:10.1242/dmm.038042

Seeded inclusions in 3D cultures are reminiscent of human Lewy bodies

In vivo LBs are phenotypically more complex than the punctate aggregates of α-syn seen in 2D cell culture models. To determine the morphological changes in intracellular aggregates in 3D culture, fully differentiated cells within the matrix were treated with preformed α-syn oligomers. Similar to our observations in 2D cultures (Fig. 2), inclusions in our 3D cell culture model were detectable 24 h after α-syn oligomer treatment (Figs 4 and 5). Immunostaining of these nuclear-associated inclusions in our 3D model confirmed that they were α-syn positive (Fig. 4A) and an equivalent size to those seen *in vivo* (Fig. 5A). Fig. 4B shows the percentage of α-syn immunopositivity in 3D cultures treated for 24 h with media, solvent or α-syn in monomeric or oligomeric preparations. The data demonstrate that oligomer-treated cells develop significantly more inclusions than control cells. The percentage of cells containing observable inclusions also significantly increased relative to controls (Fig. 4C). Immunostaining for ubiquitin in the oligomer-treated 3D cell cultures demonstrated diffuse nuclear-associated staining that colocalised with the LB-like aggregates (Fig. 5B). Co-staining using both anti-α-syn and anti-ubiquitin antibodies demonstrates colocalisation of both proteins within the same inclusion (Fig. 5C). These inclusions are highly reminiscent of *in vivo* material (Shults, 2006), and completely absent in the isotype controls and untreated cultures (Fig. S3). Immunohistochemical detection of phosphorylated α-syn at S129 using a selective antibody was not able to show evidence of phosphorylation following 24 h treatment. This would indicate that the aggregates have either formed without the requirement for phosphorylation or that the S129 epitope is protected within these aggregates (Walker et al., 2013). The lack of observable phosphorylation within the inclusions would suggest that this post-translational modification may not be required for aggregate formation within this model, or occurs within a timeframe exceeding that used here. If so, then the LB-like inclusions observed here could represent an early aggregated morphology. Overall, the 3D differentiated SH-SY5Y culture model presented here can produce LB-like aggregates when treated with preformed oligomeric material that recapitulates characteristic *in vivo* LB.

DISCUSSION

Previously, our group (Illes-Toth et al., 2015) and others (Danzer et al., 2007, 2009) have reported the induction of punctate

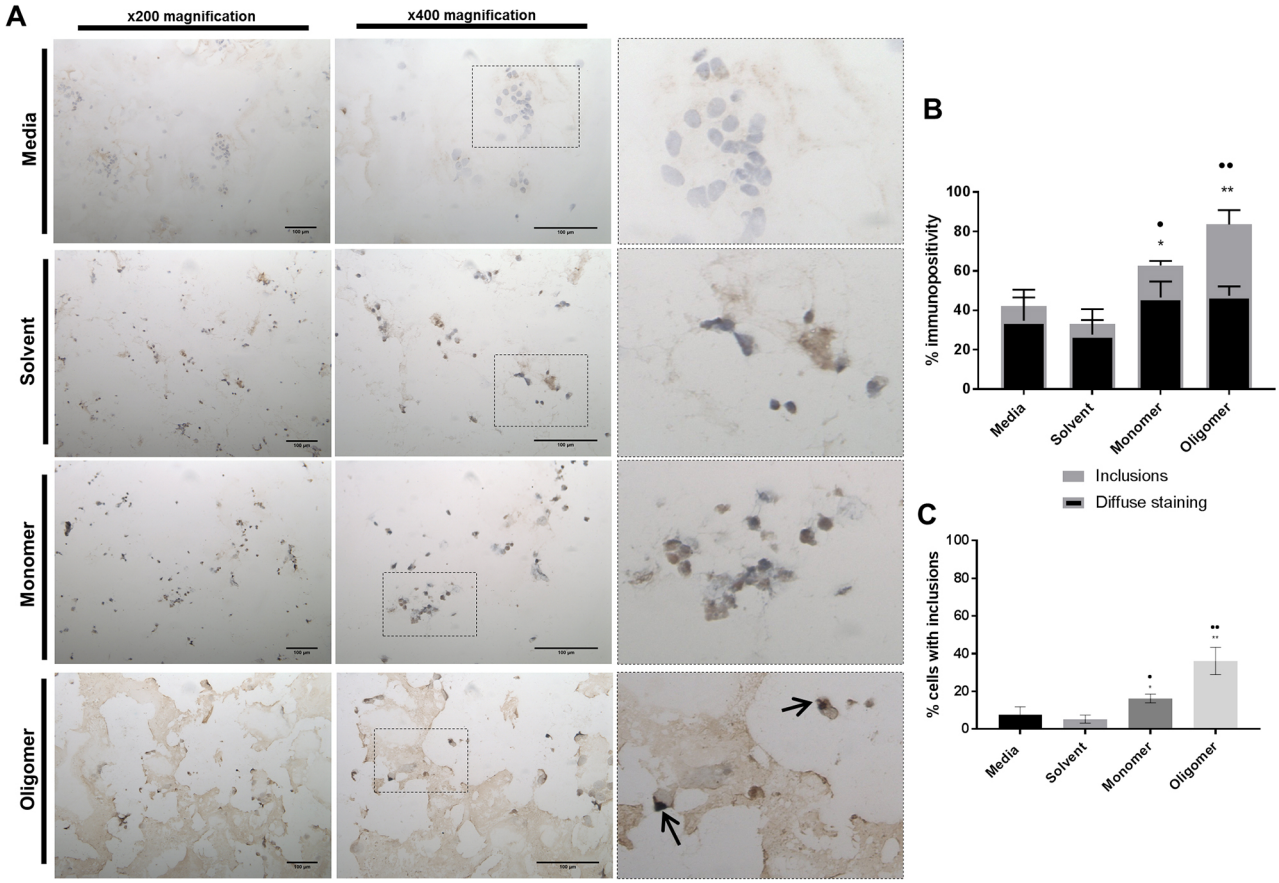

Fig. 4. Exogenous α-syn oligomers seed the development of intracellular inclusions in 3D SH-SY5Y cultures. (A) Representative images of α-syn staining with syn211 monoclonal antibody (brown) with nuclei visualised using DAPI staining (blue/purple). α-syn oligomer treatment to cells leads to strong immunoreactivity for α-syn compared to isotype controls (Fig. S2), media only, or treatment with solvent or α-syn monomer. Arrows indicate the location of the intracellular inclusions. Scale bars: 100 µm. (B) Percentage of α-syn immunopositivity in 3D cultures treated for 24 h with media, solvent or α-syn in monomeric or oligomeric preparations. Cells were deemed to contain inclusions if aggregation matched that in reference images when compared to controls. Data presented as mean±s.e.m. of three independent experiments. (C) Monomeric and oligomeric α-syn treatments resulted in an increase in the percentage of cells with inclusions. Statistical significance in the oligomer-treated cultures related to the increase in large inclusions compared with media and solvent controls. Data presented as mean±s.e.m. of three independent experiments. (*, compared to media; •, compared to solvent). Evaluation of immunohistochemical staining was performed by counting 200 cells per slide, with ten slides counted per repeat (2000 cells counted in each treatment group for three independent experiments). (B,C) Statistical differences were determined using the Kruskal–Wallis test with *post hoc* Conover-Inman ($^{*/\bullet}P \leq 0.05$, $^{**/\bullet\bullet}P \leq 0.01$).

Disease Models & Mechanisms (2019) 12, dmm038042. doi:10.1242/dmm.038042

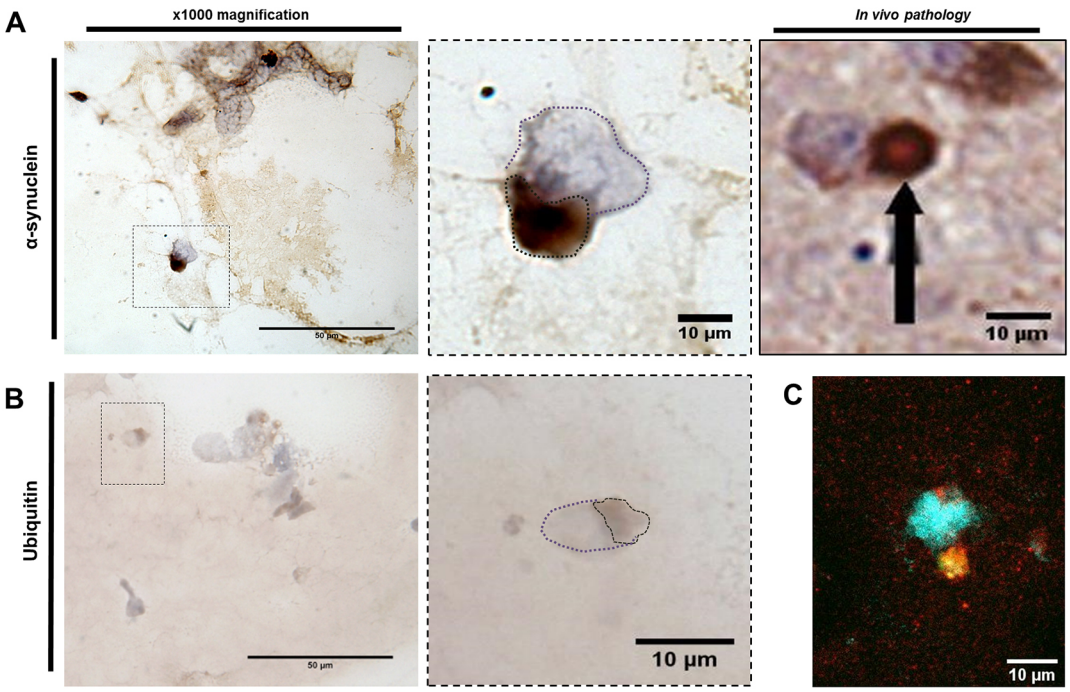

Fig. 5. α-Syn-seeded inclusions in 3D are indicative of *in vivo* Lewy body inclusions. α-Syn oligomer treatments to 3D-differentiated cultures develop α-syn-positive inclusions that demonstrate the same morphology as *in vivo* Lewy bodies (LBs; A) and are positive for the marker ubiquitin (B). Dotted line in purple highlights cell nuclei, whereas brown dotted line highlights stained area. (C) Immunofluorescence shows colocalisation of α-syn (red) and ubiquitin (green) staining. Nuclei were visualised using DAPI staining (blue). Scale bars: 50 µm (left) and 10 µm (right). *In vivo* pathology image displayed with permission from Springer Nature. This image is not published under the terms of the CC-BY license of this article. For permission to reuse, please see Chesselet et al. (2012).

intracellular aggregates in 2D undifferentiated cells when specific preparations of oligomeric α-syn are added to the media. Findings presented here describe a human 3D cell culture model that recapitulates LB-like formation. Inclusions are initiated by oligomeric α-syn preparations when introduced to terminally differentiated post-mitotic, neuron-like SH-SY5Y cells within a 3D matrix. Elevated expression of *TUBB3* and *MAP2* upon differentiation indicated stronger neuronal characteristics than when undifferentiated, and the detection of *DAT*, *DRD2* and *DA* confirmed a dopaminergic phenotype. Importantly, although the LB-like structures present in our model do not show evidence of phosphorylation, they are positive for α-syn and ubiquitin, closely resembling the morphology of inclusions found within the human pathology (Goedert et al., 2013).

Certain forms of α-syn located in the extracellular environment have recently been shown to be internalised by neurons through several receptor-mediated mechanisms and induce self-aggregation of endogenous α-syn (Bieri et al., 2018). The oligomers used in this study have previously been shown to induce the intracellular aggregation of α-syn by providing a nucleation site that recruits endogenous α-syn in the development of cell-associated aggregates (Danzer et al., 2009). This prion-like propagation has been proposed to explain the spread of the disease through the neuronal network and justify the post-mortem observations of α-syn aggregates in a PD patient that had undergone midbrain embryonic neuronal transplants (Braak et al., 2003; Kordower et al., 2008). Following internalisation, the ability of α-syn to trigger oligomerisation of endogenous α-syn potentially occurs through the oxidative or other stress responses (Deas et al., 2016; Di Maio et al., 2016). Although the precise series of events surrounding the development of these inclusions remains to be established, a model system such as the one described here opens the opportunity to investigate these mechanisms within a controlled environment and without the need to genetic modify or overexpress α-syn.

In multifactorial disorders such as PD, dissecting the complex pathological processes into simpler molecular events may allow us to better interpret disease progression. Using the 3D cell culture model described here may allow us to identify therapeutic interventions and the pathways leading to LB development before translating them to more complex models of the brain (e.g. transgenic mouse models) in which confounders such as neuroinflammation and innate immunity could mask the pathways required to be studied.

MATERIALS AND METHODS

Expression and purification of recombinant wild-type α-syn

Human WT α-syn was prepared as described previously (Smith et al., 2008). Briefly, α-syn was expressed in *Escherichia coli* BL21 (DE3) cells (New England Biolabs, Ipswich, MA, USA). Expression was induced using autoinduction media (Formedium, Norfolk, UK) at 37°C for 24 h. Bacterial cells were harvested by centrifugation at 4°C, 10,000 ***g*** and resuspended in lysis buffer [10 mM Tris-HCl (pH 8.0), 100 µg/ml lysozyme (Sigma-Aldrich, Poole, UK), 1 mM phenylmethylsulphonyl fluoride (PMSF; Sigma-Aldrich), 20 µg/ml DNase (Sigma-Aldrich), 20 µg/ml RNase (Sigma-Aldrich) and protease inhibitor cocktail (Life Technologies, Paisley, UK)]. The protein pellet was subjected to anion exchange followed by size exclusion chromatography. Lyophilised purified α-syn was stored at −20°C. Protein concentration was measured using a UV/vis spectrophotometer (CECIL 1000) at absorbance 280 nm with an extinction coefficient of 5960 M^{-1} cm^{-1}.

Preparation of seeding oligomers

Seeding oligomers were prepared as previously described by Danzer et al. (2009), omitting the addition of 10 µM $FeCl_2$. Briefly, lyophilised α-syn was dissolved in 50 mM sodium phosphate buffer (pH 7.0) containing 20% ethanol to a final concentration of 7 µM. Following overnight incubation at 21°C with continuous shaking, oligomers were concentrated 1:14 using

ultracentrifugation (VivaSpin 500 columns, MWCO 30 kDa, GE Healthcare, Buckinghamshire, UK), allowing the separation of oligomeric species from monomeric protein. Each batch of oligomers was used for experiments straight away.

Cell culture, media and reagents

SH-SY5Y human neuroblastoma cells were purchased from the European Collection of Authenticated Cell Cultures (cat. no. 94030304; Public Health England, Salisbury, UK). All cell lines were confirmed to be mycoplasma free at 3-month intervals. Cell cultures were maintained at 37°C, 5% CO_2 in DMEM high glucose with L-glutamine media (Lonza, Slough, UK) supplemented with 10% (v/v) foetal bovine serum (FBS; Life Technologies) and 1% (v/v) penicillin/streptomycin (P/S; Life Technologies); all experiments were completed within ten passages. For treatment with seeding oligomers, undifferentiated SH-SY5Y cells were allowed to adhere and expand to 70% confluence before treatment with monomeric α-syn, oligomeric α-syn or appropriate solvent controls for 24 h. For 2D differentiation into neuronal-like cells, cells were pre-differentiated in DMEM high glucose with L-glutamine supplemented with 10% (v/v) FBS, 1% (v/v) P/S and 10 µM all-trans-RA (Sigma-Aldrich). After 5 days in the presence of RA, cells were washed with serum-free DMEM and media changed to 50 ng/ml BDNF-supplemented (BDNF; cat. no. 450-02; PeproTech, London, UK) serum-free DMEM for 7 days. Following incubation, differentiated SH-SY5Y cells were treated with monomeric α-syn, oligomeric α-syn or appropriate solvent controls for 24 h at 10% v/v (0.01 mg/ml concentration referring to the monomer's concentration) (Illes-Toth et al., 2015; Danzer et al., 2007). Phase-contrast images of differentiated cells were captured using an Olympus Inverted microscope. Neurite length was measured using the free open source software, ImageJ 1.50i, whereby 200 neurites per treatment were measured, in three independent experiments.

Immunofluorescence staining

For immunofluorescence staining, 2D cultures were fixed with ice-cold methanol for 15 min at −20°C followed by washing with phosphate buffered saline (PBS) solution containing 0.1% (v/v) Tween-20 (PBS-T; Sigma-Aldrich). After washing, unspecific binding sites were blocked with a solution containing PBS and 1% (w/v) bovine serum albumin (BSA; Sigma-Aldrich) for 1 h at room temperature under gentle continuous shaking. After blocking, cells were washed in PBS-T before incubation with primary antibody in blocking solution for 1 h at room temperature under gentle continuous shaking. The following antibody dilutions were used in this study: anti-α-synuclein (syn211; 1:2000 dilution; cat. no. 32-8100; Invitrogen, ThermoFisher Scientific, Loughborough, UK), anti-DA (1:200; ab6427; Abcam, Cambridge, UK), anti-hypophosphorylated NF200 (1:100; ab82259; Abcam) and anti-Ki67 (1:200; ab16667; Abcam). Following primary-antibody incubation, cells were washed with PBS-T and incubated with secondary antibody [Texas Red™ goat anti-mouse IgG (H+L); cat. no. 100125662; ThermoFisher Scientific] for 1 h at room temperature in the dark. Nuclei were counterstained with 0.1 µg/ml 4′,6-diamidino-2-phenylindole, dihydrochloride (DAPI; Sigma-Aldrich) for 5 min. Slides were mounted with immersion oil, sealed with nail varnish and left to cure overnight at 4°C in the dark prior to image capture using an Olympus BX60 brightfield/fluorescence microscope. Evaluation of immunofluorescence staining was performed by counting 200 cells per repeat, with immunopositive cells expressed as a percentage of total count. To quantify total fluorescence per cell, fluorescent images were analysed using the image analysis software ImageJ 1.50i using the CTCF calculation, in which the background fluorescence in a selected area is subtracted from the fluorescence value of a measured area, using the calculation: CTCF=[Integrated density−(Mean fluorescence reading of background×Fluorescence of area of selection)]/Cell number. Three independent biological repeats were performed in total.

3D cell culture and differentiation

Cells were pre-differentiated with RA in uncoated T75 flasks for 5 days prior to seeding into 3D Matrigel™ cultures. Matrigel™ was diluted to 6 mg/ml total protein with ice-cold serum-free DMEM and vortexed with cell pellets for 10 s, to a final cell concentration of approximately 7.5×10^6 cells per ml of diluted Matrigel™. Using pre-chilled pipettes, Matrigel™/cell mixtures were transferred to either pre-warmed 8-well chamber slides or tissue culture inserts (ThinCerts; 0.4 µm pore size, Greiner Bio-One, Gloucestershire, UK), at 100 µl and 300 µl volumes, respectively, and incubated at 37°C for 1 h to form a colloidal gel. Following solidification of the 3D gels, pre-warmed serum-free DMEM supplemented with 50 ng/ml BDNF was added to the cultures and cells differentiated for a further 7 days. Media was changed every 3-4 days. After 7 days in 3D, cultures were treated with monomeric α-syn, oligomeric α-syn or appropriate solvent controls for 24 h at 10% v/v (0.01 mg/ml concentration referring to the monomer's concentration) (Illes-Toth et al., 2015; Danzer et al., 2007).

Cryostat sectioning and histological staining of 3D cultures

For cryostat sectioning, 3D cultures grown in tissue inserts were frozen and stored at −80°C before sectioning. The frozen samples were cut into 10 µm sections (Leica CM3050 S Research Cryostat, Leica Microsystems, Newcastle upon Tyne, UK) at −25°C and mounted on X-tra® adhesive glass slides (Leica Microsystems) and stored at −80°C prior to staining. For immunohistochemistry, 10 µm frozen sections from 3D thick-layer cultures were fixed with ice-cold 1:1 methanol and acetone, and endogenous peroxidases blocked. Staining with anti-α-synuclein monoclonal antibody (syn211; 1:100 dilution; Invitrogen) was performed using the Mouse on Mouse Polymer IHC Kit according to the manufacturer's protocols (ab127055; Abcam, Cambridge, UK). Staining with anti-ubiquitin (1:50 dilution; cat. no. ab7780; Abcam) rabbit primary antibodies was performed using the following method. Following Tris-buffered saline (TBS) washes, non-specific binding sites were blocked at room temperature for 2 h with 25% (v/v) normal goat serum (cat. no. 11819220; ThermoFisher Scientific, Loughborough, UK) and 1% (w/v) BSA in TBS. Sections were incubated with primary antibody overnight at 4°C. Slides were washed in TBS, and a 1:500 dilution of biotinylated goat anti-rabbit secondary antibody (cat. no. ab6720; Abcam) in 1% (w/v) BSA/TBS was applied for 30 min at room temperature. Binding of the secondary antibody was detected using a streptavidin-biotin complex (Vector Laboratories, Peterborough, UK) technique with 0.08% (v/v) hydrogen peroxide in 0.65 mg/ml 3,3-diaminobenzidine tetrahydrochloride (DAB; Sigma-Aldrich) in TBS. Sections were counterstained with Mayer's Haematoxylin (Leica Microsystems), dehydrated, cleared and mounted with Pertex mounting medium (Leica Microsystems). Evaluation of immunohistochemical staining was performed by counting 200 cells per slide, with ten slides counted per repeat (2000 cells counted in each treatment group for three independent experiments); immunopositive cell values are expressed as a percentage of the total count.

Immunofluorescence of 3D cultures

For immunofluorescence of 3D cultures, frozen sections were fixed with 1:1 ice-cold methanol:acetone. Blocking was performed using the Mouse on Mouse Polymer IHC Kit according to the manufacturer's protocols (ab127055; Abcam). Slides were incubated with anti-α-syn (syn211; 1:100 dilution; Invitrogen) and anti-ubiquitin (1:1000; cat. no. ab7780; Abcam) primary antibodies for 1 h at room temperature. Following PBS-T washes, secondary antibodies [Alexa Fluor® 488 goat anti-rabbit IgG (H+L) cat. no. ab150077, Abcam, and Texas Red™ goat anti-mouse IgG (H+L) cat. no. 100125662, ThermoFisher Scientific] were incubated at 1:1000 dilution for 1 h at room temperature. Nuclei were counterstained with 0.1 µg/ml DAPI (Sigma-Aldrich) for 5 min. Slides were mounted with immersion oil, sealed with nail varnish and left to cure overnight at 4°C in the dark before image capture using a Leica LSM 800 confocal microscope.

RNA extraction, cDNA synthesis and qPCR

Total RNA was extracted using either TRIzol® Reagent (Life Technologies) or the ReliaPrep™ RNA Cell Miniprep System (Promega, Southampton, UK) according to the manufacturers' protocols. Complementary DNAs (cDNAs) were synthesised by the nanoScript 2 Reverse Transcriptase kit (Primerdesign, Chandler's Ford, UK) from equal amounts of purified RNA (1 µg). Target genes were investigated using qPCR conducted on either undifferentiated or differentiated SH-SY5Y populations using pre-validated primer sets (Primerdesign). Reaction volumes of 20 µl were prepared using PrecisionPLUS 2× Real-Time PCR MasterMix premixed with ROX and SYBR green (Primerdesign). The amplification was performed under the

following conditions: 2 min at 95°C and then 40 cycles at 95°C for 15 s and 60°C for 60 s followed by a post-PCR melt-curve analysis performed on a StepOnePlus™ Real-Time PCR System (Applied Biosystems, Lutterworth, UK). The sizes of PCR products were confirmed using agarose gel electrophoresis. Reference gene analysis was undertaken using the geNormPLUS kit (Primerdesign) and Qbase+ software (Primerdesign) to identify inherently stable reference genes between different treatment groups. Gene expression levels were normalised against reference genes *ACTB* (β-actin) and *YWHAZ* (tyrosine 3-monooxygenase/tryptophan 5-monooxygenase activation protein zeta polypeptide) for each sample and fold changes were calculated using the $2^{-\Delta\Delta Ct}$ method (Schmittgen and Livak, 2008) by setting the expression levels of each gene in undifferentiated SH-SY5Y cells as 1. Data collected from at least three independent biological replicates was calculated and plotted as mean $\log_{10}$-fold changes ±s.e.m.

Cell viability

Cell viability of 2D or 3D cultures was analysed with either resazurin (mitochondrial activity) or lactate dehydrogenase (LDH; cell membrane integrity) levels. For the resazurin reduction assay, a 3 mg/ml stock solution of resazurin was prepared in cell culture media and further diluted to 10 µg/ml. Following treatment with oligomeric or monomeric species and appropriate solvent controls, media was removed and 100 µl of culture media with 10 µg/ml resazurin was incubated with the cells for 2 h. Fluorescence (Ex_{530nm}/Em_{590nm}) was measured on a CLARIOstar® plate reader (BMG LABTECH, Buckinghamshire, UK). Culture media was incubated with resazurin in parallel as a blank control. As a positive control, cells were incubated with 1% (v/v) Triton X-100. Cell viability was calculated as a percentage of live cells normalised to negative controls minus relative fluorescence intensity (RFU) of blank wells. For LDH assay, the Pierce LDH Cytotoxicity Assay Kit was used according to the manufacturer's instructions (cat. no. 88953; ThermoFisher Scientific). Briefly, 50 µl of medium from each well was transferred to a 96-well plate, followed by addition of 50 µl of reaction mixture, and incubated for 30 min at room temperature in the dark. Cell culture media was included in parallel as a blank control. After addition of 50 µl stop solution, absorbance measurements at 490 nm and 680 nm were recorded on a CLARIOstar® plate reader (BMG LABTECH). The A_{680nm} (background signal from the instrument) was subtracted from the A_{490nm} followed by subtraction of blanks. Percentages of live cells were determined by normalisation of the absorbance values from the test sample to positive controls.

Statistical analysis

Statistical analysis was undertaken using StatsDirect version 3.0.126. Data was unpaired and determined to be non-parametric following the Shapiro–Wilk test of normality; therefore, a Kruskal–Wallis test was undertaken with *post hoc* analysis. *Post hoc* analysis was only undertaken if the initial significance test was at $P<0.05$. Dwass-Steel-Chritchlow-Fligner was used for data points >6 and Conover-Inman *post hoc* analysis for <6 data points. *P*-values are denoted on the graphs. Results of all statistical analysis performed are shown in Table S1.

Acknowledgements

We thank the Biomolecular Sciences Research Centre, Sheffield Hallam University for funding the PhD studentship that has supported the work performed in this study.

Competing interests

The authors declare no competing or financial interests.

Author contributions

Conceptualization: T.R.T.-W., D.P.S.; Methodology: T.R.T.-W.; Validation: T.R.T.-W.; Formal analysis: T.R.T.-W.; Investigation: T.R.T.-W.; Writing - original draft: T.R.T.-W., C.L.L.M., J.A.D., C.F.D., D.P.S.; Writing - review & editing: T.R.T.-W., C.L.L.M., J.A.D., C.F.D., D.P.S.; Supervision: C.L.L.M., J.A.D., C.F.D., D.P.S.; Project administration: D.P.S.; Funding acquisition: D.P.S.

Funding

Sheffield Hallam University funded the PhD studentship that has supported the work performed in this study.

Data availability

qPCR and image analysis data have been deposited online at https://figshare.com/articles/_/7791314.

Supplementary information

Supplementary information available online at http://dmm.biologists.org/lookup/doi/10.1242/dmm.038042.supplemental

References

Agholme, L., Lindström, T., Kågedal, K., Marcusson, J. and Hallbeck, M. (2010). An in vitro model for neuroscience: differentiation of SH-SY5Y cells into cells with morphological and biochemical characteristics of mature neurons. *J. Alzheimer's Dis.* **4**, 1069-1082. doi:10.3233/JAD-2010-091363

Arenas, E., Denham, M. and Villaescusa, J. C. (2015). How to make a midbrain dopaminergic neuron. *Development* **142**, 1918-1936. doi:10.1242/dev.097394

Aulić, S., Le, T. T., Moda, F., Abounit, S., Corvaglia, S., Casalis, L., Gustincich, S., Zurzolo, C., Tagliavini, F. and Legname, G. (2014). Defined alpha-synuclein prion-like molecular assemblies spreading in cell culture. *BMC Neurosci.* **15**, 1-12. doi:10.1186/1471-2202-15-69

Banks, D. A., Dahal, A., Mcfarland, A. G., Flowers, B. M., Stephens, C. A., Swack, B., Gugssa, A., Anderson, W. A. and Hinton, S. D. (2017). MK-STYX alters the morphology of primary neurons, and outgrowths in MK-STYX overexpressing PC-12 cells develop a neuronal phenotype. *Front. Mol. Biosci.* **4**, 1-17. doi:10.3389/fmolb.2017.00076

Bieri, G., Gitler, A. D. and Brahic, M. (2018). Internalization, axonal transport and release of fibrillar forms of alpha-synuclein. *Neurobiol. Dis.* **109**, 219-225. doi:10.1016/j.nbd.2017.03.007

Braak, H., Del Tredici, K., Rüb, U., de Vos, R. A. I., Jansen Steur, E. N. H. and Braak, E. (2003). Staging of brain pathology related to sporadic Parkinson's disease. *Neurobiol. Aging* **24**, 197-211. doi:10.1016/S0197-4580(02)00065-9

Chesselet, M. F., Richter, F., Zhu, C., Magen, I., Watson, M. B. and Subramaniam, S. R. (2012). A progressive mouse model of Parkinson's disease: the Thy1-aSyn ("Line 61") mice. *Neurotherapeutics* **9**, 297-314. doi:10.1007/s13311-012-0104-2

Choi, S. H., Kim, Y. H., Hebisch, M., Sliwinski, C., Lee, S., D'Avanzo, C., Chen, H., Hooli, B., Asselin, C., Muffat, J. et al. (2014). A three-dimensional human neural cell culture model of Alzheimer's disease. *Nature* **515**, 274-278. doi:10.1038/nature13800

D'Antonio, M., Woodruff, G., Nathanson, J. L., D'Antonio-Chronowska, A., Arias, A., Matsui, H., Williams, R., Herrera, C., Reyna, S. M., Yeo, G. W. et al. (2017). High-throughput and cost-effective characterization of induced pluripotent stem cells. *Stem Cell Rep.* **8**, 1101-1111. doi:10.1016/j.stemcr.2017.03.011

Danzer, K. M., Haasen, D., Karow, A. R., Moussaud, S., Habeck, M., Giese, A., Kretzschmar, H., Hengerer, B. and Kostka, M. (2007). Different species of α-synuclein oligomers induce calcium influx and seeding. *J. Neurosci.* **27**, 9220-9232. doi:10.1523/JNEUROSCI.2617-07.2007

Danzer, K. M., Krebs, S. K., Wolff, M., Birk, G. and Hengerer, B. (2009). Seeding induced by alpha-synuclein oligomers provides evidence for spreading of alpha-synuclein. *J. Neurochem.* **111**, 192-203. doi:10.1111/j.1471-4159.2009.06324.x

Daubner, S. C., Le, T. and Wang, S. (2011). Tyrosine hydroxylase and regulation of dopamine synthesis. *Arch. Biochem. Biophys.* **508**, 1-12. doi:10.1016/j.abb.2010.12.017

Dawson, T. M., Ko, H. S. and Dawson, V. L. (2011). Genetic animal models of Parkinson's disease. *Neuron.* **66**, 646-661. doi:10.1016/j.neuron.2010.04.034

Deas, E., Cremades, N., Angelova, P. R., Ludtmann, M. H. R., Yao, Z., Chen, S., Horrocks, M. H., Banushi, B., Little, D., Devine, M. J. et al. (2016). Alpha-synuclein oligomers interact with metal ions to induce oxidative stress and neuronal death in Parkinson's disease. *Antioxid. Redox Signal.* **24**, 376-391. doi:10.1089/ars.2015.6343

Desplats, P., Lee, H.-J., Bae, E.-J., Patrick, C., Rockenstein, E., Crews, L., Spencer, B., Masliah, E. and Lee, S.-J. (2009). Inclusion formation and neuronal cell death through neuron-to-neuron transmission of alpha-synuclein. *Proc. Natl. Acad. Sci. USA* **106**, 13213-13218. doi:10.1073/pnas.0903691106

Di Maio, R., Barrett, P. J., Hoffman, E. K., Barrett, C. W., Zharikov, A., Bora, A., Hu, X., McCoy, J., Chu, C. T., Burton, E. A. et al. (2016). alpha-Synuclein bindss to TOM20 and inhibits mitochondrial protein import in Parkinson's disease. *Sci. Transl. Med.* **8**, 342ra78. doi:10.1126/scitranslmed.aaf3634

Encinas, M., Iglesias, M., Liu, Y., Wang, H., Muhaisen, A., Ceña, V., Gallego, C. and Comella, J. X. (2000). Sequential treatment of SH-SY5Y cells with retinoic acid and brain-derived neurotrophic factor gives rise to fully differentiated, neurotrophic factor-dependent, Human Neuron-Like Cells. *J. Neurochem.* **75**, 991-1003. doi:10.1046/j.1471-4159.2000.0750991.x

Falkenburger, B. H., Saridaki, T. and Dinter, E. (2016). Cellular models for Parkinson's disease. *J. Neurochem.* **139**, 121-130. doi:10.1111/jnc.13618

Fares, M.-B., Maco, B., Oueslati, A., Rockenstein, E., Ninkina, N., Buchman, V. L., Masliah, E. and Lashuel, H. A. (2016). Induction of de novo α-synuclein fibrillization in a neuronal model for Parkinson's disease. *Proc. Natl. Acad. Sci. USA* **113**, E912-E921. doi:10.1073/pnas.1512876113

Feany, M. B. and Bender, W. W. (2000). A Drosophila model of Parkinson's disease. *Nature.* **404**, 394-398. doi:10.1038/35006074

Forster, J. I., Köglsberger, S., Trefois, C., Boyd, O., Baumuratov, A. S., Buck, L., Balling, R. and Antony, P. M. A. (2015). Characterization of differentiated SH-SY5Y as neuronal screening model reveals increased oxidative vulnerability. *J. Biomol. Screen.* **21**, 496-509. doi:10.1177/1087057115625190

Goedert, M., Spillantini, M. G., Del Tredici, K. and Braak, H. (2013). 100 years of Lewy pathology. *Nat. Rev. Neurol.* **9**, 13-24. doi:10.1038/nrneurol.2012.242

Goldie, B. J., Barnett, M. M. and Cairns, M. J. (2014). BDNF and the maturation of posttranscriptional regulatory networks in human SH-SY5Y neuroblast differentiation. *Front. Cell. Neurosci.* **8**, 1-7. doi:10.3389/fncel.2014.00325

Griffith, L. G. and Swartz, M. A. (2006). Capturing complex 3D tissue physiology in vitro. *Nat. Rev. Mol. Cell Biol.* **7**, 211-224. doi:10.1038/nrm1858

Hawkes, C. H., Del Tredici, K. and Braak, H. (2007). Parkinson's disease: a dual-hit hypothesis. *Neuropathol. Appl. Neurobiol.* **33**, 599-614. doi:10.1111/j.1365-2990.2007.00874.x

Illes-Toth, E., Ramos, M. R., Cappai, R., Dalton, C. and Smith, D. P. (2015). Distinct higher-order α-synuclein oligomers induce intracellular aggregation. *Biochem. J.* **468**, 485-493. doi:10.1042/BJ20150159

Ioannidis, J. P. A. (2012). Extrapolating from animals to humans. *Sci. Transl. Med.* **4**, 151ps15. doi:10.1126/scitranslmed.3004631

Ito, K., Eguchi, Y., Imagawa, Y., Akai, S., Mochizuki, H. and Tsujimoto, Y. (2017). MPP+ induces necrostatin-1- and ferrostatin-1-sensitive necrotic death of neuronal SH-SY5Y cells. *Cell Death Discov.* **3**, 17013. doi:10.1038/cddiscovery.2017.13

Iwai, A., Masliah, E., Yoshimoto, M., Ge, N., Flanagan, L., Rohan de Silva, H. A., Kittel, A. and Saitoh, T. (1995). The precursor protein of non-Aβ component of Alzheimer's disease amyloid is a presynaptic protein of the central nervous system. *Neuron* **14**, 467-475. doi:10.1016/0896-6273(95)90302-X

Kahle, P. J., Neumann, M., Ozmen, L., Müller, V., Jacobsen, H., Schindzielorz, A., Okochi, M., Leimer, U., van Der Putten, H., Probst, A. et al. (2000). Subcellular localization of wild-type and Parkinson's disease-associated mutant alpha -synuclein in human and transgenic mouse brain. *J. Neurosci.* **20**, 6365-6373. doi:10.1523/JNEUROSCI.20-17-06365.2000

Koprich, J. B., Kalia, L. V. and Brotchie, J. M. (2017). Animal models of α-synucleinopathy for Parkinson disease drug development. *Nat. Rev. Neurosci.* **18**, 515-529. doi:10.1038/nrn.2017.75

Kordower, J. H., Chu, Y., Hauser, R. A., Freeman, T. B. and Olanow, C. W. (2008). Lewy body–like pathology in long-term embryonic nigral transplants in Parkinson's disease. *Nat. Med.* **14**, 504-506. doi:10.1038/nm1747

Korecka, J. A., Van Kesteren, R. E., Blaas, E., Spitzer, S. O., Kamstra, J. H., Smit, A. B., Swaab, D. F., Verhaagen, J. and Bossers, K. (2013). Phenotypic characterization of retinoic acid differentiated SH-SY5Y cells by transcriptional profiling. *PLoS ONE* **8**, e63862. doi:10.1371/journal.pone.0063862

Kovalevich, J. and Langford, D. (2013). Considerations for the use of SH-SY5Y neuroblastoma cells in neurobiology. *Methods Mol. Biol.* **1078**, 9-21. doi:10.1007/978-1-62703-640-5_2

Krishna, A., Biryukov, M., Trefois, C., Antony, P. M. A., Hussong, R., Lin, J., Heinäniemi, M., Glusman, G., Köglsberger, S., Boyd, O. et al. (2014). Systems genomics evaluation of the SH-SY5Y neuroblastoma cell line as a model for Parkinson's disease. *BMC Genomics* **15**, 1154. doi:10.1186/1471-2164-15-1154

Langston, J. W., Schüle, B., Rees, L., Nichols, R. J. and Barlow, C. (2015). Multisystem Lewy body disease and the other parkinsonian disorders. *Nat. Genet.* **47**, 1378-1384. doi:10.1038/ng.3454

Lee, M. K., Stirling, W., Xu, Y., Xu, X., Qui, D., Mandir, A. S., Dawson, T. M., Copeland, N. G., Jenkins, N. A. and Price, D. L. (2002). Human alpha-synuclein-harboring familial Parkinson's disease-linked Ala-53 to Thr mutation causes neurodegenerative disease with alpha-synuclein aggregation in transgenic mice. *Proc. Natl. Acad. Sci. USA* **99**, 8968-8973. doi:10.1073/pnas.132197599

Li, J., Uversky, V. N. and Fink, A. L. (2001). Effect of familial Parkinson's disease point mutations A30P and A53T on the structural properties, aggregation, and fibrillation of human α-synuclein. *Biochemistry* **40**, 11604-11613. doi:10.1021/bi010616g

Li, J.-Y., Englund, E., Holton, J. L., Soulet, D., Hagell, P., Lees, A. J., Lashley, T., Quinn, N. P., Rehncrona, S., Björklund, A. et al. (2008). Lewy bodies in grafted neurons in subjects with Parkinson's disease suggest host-to-graft disease propagation. *Nat. Med.* **14**, 501-503. doi:10.1038/nm1746

Lopes, F. M., Schröder, R., da F. Júnior, M. L. C. F., Zanotto-Filho, A., Müller, C. B., Pires, A. S., Meurer, R. T., Colpo, G. D., Gelain, D. P., Kapczinski, F. et al. (2010). Comparison between proliferative and neuron-like SH-SY5Y cells as an in vitro model for Parkinson disease studies. *Brain Res.* **1337**, 85-94. doi:10.1016/j.brainres.2010.03.102

Luk, K. C., Song, C., O'Brien, P., Stieber, A., Branch, J. R., Brunden, K. R., Trojanowski, J. Q. and Lee, V. M.-Y. (2009). Exogenous alpha-synuclein fibrils seed the formation of Lewy body-like intracellular inclusions in cultured cells. *Proc. Natl. Acad. Sci. USA* **106**, 20051-20056. doi:10.1073/pnas.0908005106

Mcculloch, C. C., Kay, D. M., Factor, S. A., Samii, A., Nutt, J. G., Higgins, D. S., Griffith, A., Roberts, J. W., Leis, B. C., Montimurro, J. S. et al. (2008). Exploring gene-environment interactions in Parkinson's disease. *Hum. Genet.* **123**, 257-265. doi:10.1007/s00439-008-0466-z

Murphy, D. D., Rueter, S. M., Trojanowski, J. Q. and Lee, V. M.-Y. (2000). Synucleins are developmentally expressed, and alpha-synuclein regulates the size of the presynaptic vesicular pool in primary hippocampal neurons. *J. Neurosci.* **20**, 3214-3220. doi:10.1523/JNEUROSCI.20-09-03214.2000

Nemani, V. M., Lu, W., Berge, V., Nakamura, K., Onoa, B., Lee, M. K., Chaudhry, F. A., Nicoll, R. A. and Edwards, R. H. (2010). Increased expression of α-synuclein reduces neurotransmitter release by inhibiting synaptic vesicle reclustering after endocytosis. *Neuron* **65**, 66-79. doi:10.1016/j.neuron.2009.12.023

Poewe, W., Seppi, K., Tanner, C. M., Halliday, G. M., Brundin, P., Volkmann, J., Schrag, A.-E. and Lang, A. E. (2017). Parkinson disease. *Nat. Rev. Dis. Prim.* **3**, 1-21. doi:10.1038/nrdp.2017.13

Polymeropoulos, M. H., Lavedan, C., Leroy, E., Ide, S. E., Dehejia, A., Dutra, A., Pike, B., Root, H., Rubenstein, J., Boyer, R. et al. (1997). Mutation in the α-synuclein gene identified in families with Parkinson's disease mutation in the α-synuclein gene identified in families with Parkinson's disease. *Science* **276**, 2045-2047. doi:10.1126/science.276.5321.2045

Pound, P. and Bracken, M. B. (2014). Is animal research sufficiently evidence based to be a cornerstone of biomedical research? *BMJ* **348**, g3387-g3387. doi:10.1136/bmj.g3387

Presgraves, S. P., Ahmed, T., Borwege, S. and Joyce, J. N. (2004). Terminally differentiated SH-SY5Y cells provide a model system for studying neuroprotective effects of dopamine agonists. *Neurotox. Res.* **5**, 579-598. doi:10.1007/BF03033178

Sacino, A. N., Thomas, M. A., Ceballos-Diaz, C., Cruz, P. E., Rosario, A. M., Lewis, J., Giasson, B. I. and Golde, T. E. (2013). Conformational templating of α-synuclein aggregates in neuronal-glial cultures. *Mol. Neurodegener.* **8**, 1. doi:10.1186/1750-1326-8-17

Sacino, A. N., Brooks, M., Thomas, M. A., McKinney, A. B., McGarvey, N. H., Rutherford, N. J., Ceballos-Diaz, C., Robertson, J., Golde, T. E. and Giasson, B. I. (2014). Amyloidogenic α-synuclein seeds do not invariably induce rapid, widespread pathology in mice. *Acta Neuropathol.* **127**, 645-665. doi:10.1007/s00401-014-1268-0

Schmittgen, T. D. and Livak, K. J. (2008). Analyzing real-time PCR data by the comparative CT method. *Nat. Protoc.* **3**, 1101-1108. doi:10.1038/nprot.2008.73

Shults, C. W. (2006). Lewy bodies. *Proc. Natl. Acad. Sci. USA* **103**, 1661-1668. doi:10.1073/pnas.0509567103

Singleton, A. B., Farrer, M., Johnson, J., Singleton, A., Hague, S., Kachergus, J., Hulihan, M., Peuralinna, T., Dutra, A., Nussbaum, R. et al. (2003). alpha-synuclein locus triplication causes Parkinson's disease. *Science* **302**, 841. doi:10.1126/science.1090278

Smidt, M. P. and Burbach, J. P. H. (2007). How to make a mesodiencephalic dopaminergic neuron. *Nat. Rev. Neurosci.* **8**, 21-32. doi:10.1038/nrn2039

Smirnova, L., Harris, G., Delp, J., Valadares, M., Pamies, D., Hogberg, H. T., Waldmann, T., Leist, M. and Hartung, T. (2016). A LUHMES 3D dopaminergic neuronal model for neurotoxicity testing allowing long-term exposure and cellular resilience analysis. *Arch. Toxicol.* **90**, 2725-2743. doi:10.1007/s00204-015-1637-z

Smith, D. P., Tew, D. J., Hill, A. F., Bottomley, S. P., Masters, C. L., Barnham, K. J. and Cappai, R. (2008). Formation of a high affinity lipid-binding intermediate during the early aggregation phase of α-synuclein. *Biochemistry* **47**, 1425-1434. doi:10.1021/bi701522m

Spatola, M. and Wider, C. (2014). Genetics of Parkinson's disease. *Park. Relat. Disord.*, S35-S38.

Spillantini, M. G., Schmidt, M. L., Lee, V. M.-Y., Trojanowski, J. Q., Jakes, R. and Goedert, M. (1997). alpha-Synuclein in Lewy bodies. *Nature* **388**, 839-841. doi:10.1038/42166

Tang-Schomer, M. D., White, J. D., Tien, L. W., Schmitt, L. I., Valentin, T. M., Graziano, D. J., Hopkins, A. M., Omenetto, F. G., Haydon, P. G. and Kaplan, D. L. (2014). Bioengineered functional brain-like cortical tissue. *Proc. Natl. Acad. Sci. USA* **111**, 13811-13816. doi:10.1073/pnas.1324214111

Theillet, F.-X., Binolfi, A., Bekei, B., Martorana, A., Rose, H. M., Stuiver, M., Verzini, S., Lorenz, D., van Rossum, M., Goldfarb, D. et al. (2016). Structural disorder of monomeric α-synuclein persists in mammalian cells. *Nature* **530**, 45-50. doi:10.1038/nature16531

Volpicelli-Daley, L. A., Luk, K. C., Patel, T. P., Tanik, S. A., Riddle, D. M., Stieber, A., Meaney, D. F., Trojanowski, J. Q. and Lee, V. M.-Y. (2011). Exogenous alpha-synuclein fibrils induce lewy body pathology leading to synaptic dysfunction and neuron death. *Neuron* **72**, 57-71. doi:10.1016/j.neuron.2011.08.033

Walker, D. G., Lue, L.-F., Adler, C. H., Shill, H. A., Caviness, J. N., Sabbagh, M. N., Akiyama, H., Serrano, G. E., Sue, L. I. and Beach, T. G. and Arizona Parkinson Disease Consortium. (2013). Changes in properties of Serine 129 phosphorylated α-synuclein with progression of lewy-type histopathology in human brains. *Exp. Neurol.* **240**, 190-204. doi:10.1016/j.expneurol.2012.11.020

Wirdefeldt, K., Adami, H.-O., Cole, P., Trichopoulos, D. and Mandel, J. (2011). Epidemiology and etiology of Parkinson's disease: a review of the evidence. *Eur. J. Epidemiol.* **26**, S1-S58. doi:10.1007/s10654-011-9581-6

Xicoy, H., Wieringa, B. and Martens, G. J. M. (2017). The SH-SY5Y cell line in Parkinson's disease research: a systematic review. *Mol. Neurodegener.* **12**, 1-11. doi:10.1186/s13024-017-0149-0